LABORATORY INVESTIGATION OF PERMEABILITY UPSCALING

by

Vincent C. Tidwell

Submitted in Partial Fulfillment

of the Requirements for a

Doctorate of Philosophy in Hydrology

New Mexico Institute of Mining and Technology

Department of Earth and Environmental Sciences

Socorro, New Mexico

January 1999

ABSTRACT

Parameterization of flow and transport models is often complicated by the inability to make measurements at the desired scale of analysis. This disparity in scale necessitates the use of some averaging or upscaling model to compute the effective media properties from the measured data. Although numerous theoretical models have been proposed, physical data with which to test these upscaling models are sparse and limited in scope. Here, we develop and employ a novel minipermeameter test system, which we call the Multi-Support Permeameter (MSP), to physically investigate permeability upscaling. The MSP allows precise, rapid, non-destructive measurement of permeability over a range of different sample supports (i.e., sample volumes). Measurements are made over different sample supports, subject to consistent boundary conditions and flow geometries, by simply varying the size of the minipermeameter tip seal. Experiments progress by collecting thousands of measurements from each face of meter-scale blocks of rock with each of five different tip seals (0.15, 0.31, 0.63, 1.27, and 2.54 cm radius), plus a single large (7.62 cm) tip seal designed to integrate over the entire sampling domain. Upscaling is manifest in the acquired data by changes in key permeability statistics with increasing sample support.

Permeability upscaling experiments are conducted on four blocks of rock, each exhibiting differing physical attributes: (1) Berea Sandstone, a faintly laminated fluvial-deltaic sandstone, (2) Massillon Sandstone, a conspicuously cross-stratified sandstone from a high-energy fluvial or near-shore environment, (3) Topopah Spring Tuff, a densely-welded devitrified tuff, and (4) Tiva Canyon Tuff, a poorly-welded tuff. Over 150,000 permeability measurements corresponding to six different sample supports have been collected from these four rock samples.

By comparing and contrasting results, we explore how traits distinguishing each rock sample influence the statistical and upscaling characteristics of the permeability. Results indicate that differences in the physical attributes of each rock sample give rise to measurable differences in the spatial permeability patterns, permeability distributions, and semivariograms. Results also yield clear evidence of permeability upscaling for each rock sample and each statistic investigated. Specifically, as the sample support increases the sample variance always decreases according to a power-law relation, the semivariogram range increases linearly, while small-scale (i.e., smaller than the minipermeameter tip seal) structural features are sequentially filtered from the permeability maps and semivariograms. Although each of the samples exhibit qualitatively similar upscaling trends, distinct differences are also evident. Differences between samples are manifest in the rate at which a given statistic upscales, the absolute change in the value of the statistic, and in the sense (i.e., increasing versus decreasing) of the mean upscaling. These differences are most evident between samples of differing genetic origin (e.g., sandstones versus tuffs).

To aid in the interpretation of the permeability upscaling, comparisons are made with a series of published theoretical models. The selected models differ according to the assumptions made about the nature of the permeability distribution, spatial structure, and uniformity/non-uniformity of the imposed flow field. Results suggest that the differences in upscaling exhibited by the four rock samples can be explained on the basis the spatial patterns distinguishing each; particularly, the spatial correlation of the higher permeability fraction. We also find the permeability upscaling to be strongly influenced by the non-uniform flow conditions imposed by the minipermeameter measurements. As such, this data clearly demonstrates that permeability upscaling is not an intrinsic property of a porous medium; but rather, depends on the characteristics of its measurement. In an effort to empirically quantify the measurement characteristics of the MSP, spatial weighting functions are calculated from the multi-support permeability data via linear filter theory.

ACKNOWLEDGMENTS

and if you call out for insight
and cry aloud for understanding,
and if you look for it as for silver
and search for it as for hidden treasure,
then you will understand the fear of the Lord
and find the knowledge of God.
For the Lord gives wisdom,
and from his mouth come knowledge and understanding. *Proverbs 2: 3-6*

First and foremost I owe my deepest gratitude to my Lord and Savior. It is only through His divine providence that this endeavor was accomplished. His presence has strengthened me and His guidance has directed me toward opportunity. However, even in my accomplishment I am ever humbled by the ultimate price He paid on the cross in my behalf. It is this gift that demands my life and my all.

Throughout this endeavor my family has faithfully supported me. I am particularly grateful to my wife, Penny, who has been there every step of the way. Were it not for her continual words of encouragement, my confidence would have faltered. She helped me keep work in perspective and to sharpen my focus on those things most important in life. However, it is the unselfish love which she shows me each day that gives true meaning to my life. To my children, Austin and Eric, I am grateful for the wonderful diversion from work that they provided and their vehement complaints when daddy was not showing them enough attention. And to my parents and sister, I owe so much for their guidance, example, support, and love.

To John Wilson I extend my most sincere thanks. John's ideas and insight never cease to amaze me. Undoubtedly this work has greatly benefited by his technical guidance. However, John has been much more than an advisor, he has been a mentor. Although John has provided instruction and direction, he has never forced me into a mold but rather allowed me to develop along a path unique to my abilities and personality. Most important, by his example he has set a high professional standard for me to aspire.

I count myself fortunate for the strong support I received from the other members of my research committee. Peter Mozley was of great help with describing and interpreting the geological characteristics of each rock sample. Fred Phillips contributed toward our understanding of minipermeametry and kept our meetings upbeat with his unique style of humor. Allan Gutjahr has been of great help in analyzing and interpreting the data. His instruction, insights, and encouragement have proved invaluable to me throughout this effort. To Bob Glass I owe a special debt of gratitude. For the past eight years I have had the privilege to work with a gifted scientist and experimentalist. Bob's example and encouragement has opened my eyes to science and directed me down the path of research. Were it not for his efforts in developing the Flow Visualization Laboratory, I fear that my aspirations for this advanced degree would have gone unfulfilled.

I am indebted to many members of the Flow Visualization Laboratory who have made the experimental aspects of this work a reality. In particular, I am grateful to Justin Von Doemming for his considerable help in constructing and automating the multisupport permeameter. To Lee Orear and Will Peplinski I extend my gratitude for their help with belligerent computers and data acquisition systems. Finally, I thank the student interns, Kerim Martinez, Mark Bailey, and Nick Teske for their help in collecting, organizing, and analyzing the permeability data used in this study.

This dissertation has received full and partial reviews by a wide number of people. These reviews have challenged our methodology and interpretations of the data, thereby improving the quality of this work. I extend my thanks for the internal (within Sandia National Laboratories) reviews provided by Peter Davies, Chris Rautman, Sean McKenna, Steve Conrad, and Bob Holt. I also gratefully acknowledge the help of associate editors and the peer reviews provided by Scott Tyler, Jean Behr, Alexander Desbarats, Matt Davis, and Clayton Deutsch, along with other anonymous individuals.

Finally, I gratefully acknowledge the support of Sandia National Laboratories and the Department of Energy. To Sandia National Laboratories I extend my appreciation for tuition assistance and financial support (University Part-Time Program) for two semesters while I completed course requirements. Funding for the research contained herein was provided by the Department of Energy through two sources. Experiments were initiated under the support of the U.S. Department of Energy, Office of Civilian Radioactive Waste Management, Yucca Mountain Site Characterization Project Office, under contract DE-AC04-94AL85000. This research was later extended, beginning in October of 1994, by the U.S. Department of Energy, Office of Basic Energy Science, Geoscience Research Program, under contracts DE-AC04-94AL85000 and DE-F303-96ER14589/A000. To both funding sources I express my gratitude, for without their financial support this work would not have been possible.

TABLE OF CONTENTS

LIST OF TABLES

LIST OF FIGURES

APPROVAL PAGE

This dissertation is accepted on behalf of the faculty of the Institute by the following committee:

John L Wilson

Adviser

1/19/99

Date

I release this document to New Mexico Institute of Mining and Technology

Vincent C. Tidwell

Student's Signature

1/18/99

Date

CHAPTER 1: INTRODUCTION

There is an extensive body of evidence acquired through physical and numerical experimentation (see section 7.2 for details) demonstrating the dependence of permeability on its corresponding sample support (i.e., sample volume). The change in permeability accompanying an increase in sample support is commonly referred to as upscaling. Upscaling becomes important when predicting the "effective permeability" of a heterogeneous volume of rock from permeability data measured over some smaller sample support. Also, upscaling of key summary statistics (e.g., mean, semivariogram), as used in the numerical simulations of heterogeneous random fields, may be necessitated when the scale of measurement differs from the computational grid block scale. Permeability upscaling is not an intrinsic property of a porous medium; that is, it does not solely depend on the characteristics of the porous medium. Rather, the conditions under which the permeability is measured can significantly influence upscaling.

1.1. Background

The continuum hypothesis of rational mechanics forms the basis of most subsurface flow and transport models. In this approach, the time-and-space dependence of state variables is expressed in the form of differential balance equations formulated on the principles of mass, momentum, and energy conservation. To achieve tractable solutions for the resulting balance equations, simplifying assumptions are used that typically introduce

constitutive properties into the flow/transport equations. Thus, constitutive properties (e.g., porosity, permeability) account for the integrated effects of heterogeneities and physical processes that occur at scales much smaller than the desired scale of analysis. Constitutive properties are related not to a discrete point within the porous media but to a control volume or sample support and are assumed to vary smoothly enough in time and space so that the resulting balance equations can be solved by standard analytical/numerical methods of differential equations.

Because of technological and computational constraints, it is rarely possible to measure constitutive properties at the desired scale of analysis. For this reason, some averaging or upscaling model is required to transfer information from the scale of measurement to the desired scale of analysis. If the averaging process of the particular property under study were known the problem would be alleviated. For example, the average porosity of a volume is simply the arithmetic average of the porosities of all the samples that constitute it. The simple arithmetic averaging process holds true for additive variables such as porosity and ore grade. Unfortunately, many other constitutive properties (e.g., permeability) are not additive; that is, the upscaling process not only depends on the volume fraction of the phase present but other factors as well. It is the nature of this non-additive averaging process or upscaling that is of interest here, and we use permeability to study it.

As the issue of permeability upscaling is almost universally encountered in the modeling of porous media flow and transport, significant attention has been paid to this problem (see introductory sections to Chapters 2-7). Numerous models have been proposed for upscaling permeability (see Chapters 4 and 6); however, physical data to support these theoretical models are sparse (see Chapter 2). Where physical upscaling data are available their utility is often suspect because the measurement precision, sample

integrity, spatial sampling density, and/or the method of measurement vary from one measurement scale to another (see Chapter 2). This inconsistency ultimately introduces errors and uncertainties that impair or preclude unique quantification of upscaling. Yet another problem with existing data is that the physical experiments are limited to one or, at most, two geologic media and hence lack the scope necessary to challenge the basic assumptions concerning upscaling. Supporting physical data is needed to improve confidence in existing upscaling models, bound their range of applicability relative to limiting assumptions, and, where necessary, suggest alternative models.

1.2. Objective

The primary objective of this work is to enhance fundamental understanding of permeability upscaling through systematic physical experimentation. Toward this goal, we focus our attention on three fundamental questions:

1) Do our measured permeability data upscale in a predictable and quantifiable manner; if so, what is the nature of the upscaling behavior?
2) Is the measured permeability upscaling influenced by the physical attributes of the porous media, and if so, how?
3) Are there controls beyond the characteristics of the porous media governing the measured upscaling, and if so, what?

1.3. Approach

Physical investigation of permeability upscaling is pursued through the collection of exhaustive permeability data sets, measured over a range of different sample supports (i.e., sample volumes), from a series of different blocks of rock. To make these measurements we design, construct, and test a computer automated minipermeameter that we call the

Multi-Support Permeameter (MSP). These studies are conducted in the laboratory because of the experimental control afforded; specifically, consistency in measurement across all sample supports, consistency in the physical sample (i.e., non-destructive sampling), low measurement error, and high spatial resolution in the measured data. In this way we limit the experimental variables influencing permeability upscaling to the "heterogeneity" of the rock sample, for which we have detailed information, and the characteristics of the sampling instrument, which we can quantify by empirical means (i.e., linear filter analysis).

Permeability measurements are made with the MSP by compressing a tip seal against a flat, fresh rock surface while injecting gas at a constant pressure. Using information on the seal geometry, gas flow rate, gas injection pressure, and barometric pressure, the permeability is calculated using a modified form of Darcy's Law. By simply varying the size of the minipermeameter tip seal, measurements are made over different sample supports, subject to consistent boundary conditions and flow geometry. Experiments progress by collecting thousands of measurements on multiple faces of meter-scale blocks of rock with each of five different tip seals (0.15, 0.31, 0.63, 1.27, and 2.54 cm radius), plus a single large-scale (7.62 cm) measurement designed to integrate over the entire sampling domain. We repeat this process for multiple rock samples each exhibiting different textural and structural characteristics owing to their unique depositional and diagenetic histories.

The multi-support permeability data sets acquired from the different rock samples are compared and contrasted on the basis of the physical attributes of the rock samples, statistical permeability characteristics, and permeability upscaling. To aid in the interpretation of the data, we draw comparisons between the measured permeability upscaling and theoretical upscaling models predicated on different limiting assumptions.

We make these comparisons to identify the basic controls on the measured permeability upscaling.

1.4. Organization

The body of this dissertation is organized according to six chapters, each of which is written as a separate journal article. To establish a sense of cohesion, an introduction and conclusion are included that provide details on the collective goals and results/implications of this work. Below is a brief synopsis for each of the six primary chapters.

Chapter Two: Published in Water Resources Research [vol. 33(7), pages 1607-1616, 1997]. This chapter provides a detailed description of the Multi-Support Permeameter (MSP), which we developed specifically for physically investigating permeability upscaling. Included are the results of tests conducted to evaluate the precision, accuracy, and consistency (between tip seals) of the MSP measurements. Also, data from the Berea Sandstone are given to demonstrate the MSP's ability to investigate permeability upscaling.

Chapter Three: In press, Water Resources Research. We apply linear filter theory to calculate the empirical spatial weighting functions characterizing our MSP measurements. The calculated weighting functions provide insight into how the effective radius of measurement varies with changing tip seal size and also how the MSP measurement non-uniformly weights the heterogeneities comprising the sample support.

Chapter Four: In press, Mathematical Geology. We present and analyze results for permeability upscaling experiments conducted on the Berea Sandstone sample. The Berea Sandstone is the most uniform sample investigated, exhibiting only faint subhorizontal lamination. In our analysis we compare upscaling of the mean permeability with that predicted by theoretical upscaling models predicated on both uniform and non-uniform

flow conditions. Results of the comparisons are interpreted to identify the basic controls on the measured upscaling.

Chapter Five: To be submitted to Water Resources Research or another journal. We present and analyze results for permeability upscaling experiments conducted on the Massillon Sandstone sample. The Massillon Sandstone is characterized by conspicuous cross-bedding that forms two distinct nested scales of heterogeneity. These include a large-scale structure associated with the bounding surfaces delineating individual cross-bedded sets and a small-scale structure corresponding to the planar and low-angle cross stratification occurring within each set. In this paper we investigate differences in the measured permeability upscaling between the two nested scales of heterogeneity. Also, we compare and contrast the permeability upscaling between the individual cross-bedded sets and the integrated coset (i.e., entire sampling domain).

Chapter Six: Submitted to Water Resources Research. We present and analyze results for permeability upscaling experiments conducted on the Topopah Spring Tuff sample. The tuff sample is distinguished by its bimodal permeability distribution resulting from highly-porous pumice fragments isolated in an otherwise tight rock matrix. Analysis of results is pursued according to two very different points of view; one concerns upscaling of the ensemble statistics (i.e., integrated over the entire sampling domain), while the second concerns upscaling from a local or point-wise perspective.

Chapter Seven: To be submitted to Water Resources Research. Here we compare and contrast permeability data collected from the three aforementioned rock samples along with data from an additional sample, the Tiva Canyon Tuff. With this data we relate measured differences in the statistical and upscaling characteristics of the permeability with the physical attributes distinguishing (visually) each rock sample. In this way, we explore the

control the porous medium exerts on the measured permeability and the corresponding permeability upscaling.

CHAPTER 2: LABORATORY METHOD FOR INVESTIGATING PERMEABILITY UPSCALING[1]

2.1. Abstract

Our purpose here is to describe, evaluate, and demonstrate a laboratory-based method for physically investigating permeability upscaling. The method makes use of a simple instrument, the minipermeameter, to acquire rapid, precise, non-destructive permeability measurements from heterogeneous blocks of dry rock. Critical to investigating permeability upscaling is the ability to acquire data at multiple sample supports (i.e., sample volumes) subject to consistent boundary conditions and flow geometry. Such measurements, spanning almost four-orders of magnitude on a per-volume basis, are made with the minipermeameter by simply varying the size of the minipermeameter tip seal. The precision and consistency of measurements made in this way are evaluated using a suite of data collected from blocks of three relatively homogeneous materials: Berea Sandstone and two synthetic rocks. Results suggest that measurement error is small (approximately ±1% of the measured permeability) and consistent, and measurements made at different sample supports are free from systematic bias. To demonstrate the ability of this method to measure and quantify permeability upscaling, limited data sets were collected with four different-sized tip seals from the Berea Sandstone block. Analysis reveals distinct and consistent trends diagnostic of permeability upscaling relating the sample mean (increased), variance (decreased), and semivariogram to increasing sample support.

[1] Tidwell, V.C. and J.L. Wilson, Water Resources Research, 33(7),1607-1616, 1997.

2.2. Introduction

Predictions concerning the nature and extent of contaminant migration, the effectiveness of groundwater remediation, and the efficiency of enhanced gas/oil recovery strategies depend on an understanding of the spatial characteristics of the subsurface environment. Aquifer/reservoir characterization and the subsequent integration of acquired spatial information into predictive flow and transport models face two basic problems. First, the quantity of porous media observed and/or sampled is generally a minute faction of the site under investigation. This gives rise to the need for models to predict material characteristics at unsampled locations. The second problem, which is of concern here, stems from technological constraints that limit the measurement of material properties to sample supports (volume of porous media sampled) much smaller than can be accommodated in current predictive models. This disparity in support requires measured data be averaged or upscaled to yield effective properties at the computational grid block scale. Unfortunately, many material properties, like permeability, cannot be assumed to upscale according to simple spatial averaging rules. For this reason, numerous upscaling theories, representing a wide diversity of approaches, have been proposed [e.g., Dagan, 1981; Gelhar and Axness, 1983; Cushman, 1984; Rubin and Gomez-Hernandez, 1990; Neuman, 1994].

A number of field and laboratory studies have been performed to challenge current conceptual and theoretical models of permeability upscaling. These studies differ according to the measurement techniques employed, the range in sample support investigated, and the geologic media interrogated. Laboratory-based studies conducted by Henriette et al. [1989] attempted to reconstruct the effective permeability of two 15 x 15 x 50 cm blocks of rock, one a sandstone and the other a limestone, from permeability measurements made on 15 x

15 x 15 cm intermediate-scale blocks and core samples cut from them. Parker and Albrecht [1987] performed field investigations involving the collection of permeability data from soil cores of three different volumes (92, 471, and 1770 cm^3) taken from two different soil layers. A number of other studies have investigated permeability upscaling through integrated field and laboratory measurement. In each case, permeability data were collected over a range of sample supports using a variety of different sampling techniques including core tests, single well flow meter tests, single well packer tests, large scale tracer/pump tests, and analysis of seasonal groundwater fluctuations. Such upscaling studies have been conducted in low permeability fluvial-deltaic clays [Hanor, 1993], glacial tills [Keller et al., 1989], fractured crystalline rock from a variety of depositional environments [Clauser, 1992; Brace 1984], glacial outwash sand and gravel deposits [Hess et al., 1991], fluvial sand deposits [Killey and Moltyaner, 1988], and fluvial inter-bedded sands and clays [Molz et al., 1990]. In each of these studies, measurement precision, sample integrity, spatial sampling density, and/or the method of measurement varied with sample support. This inconsistency ultimately introduced errors and uncertainties that impaired or precluded unique interpretation of the measured permeability upscaling. Furthermore, each of these studies focused on one or, at most, two geologic media and hence lack the breadth of scope necessary to challenge our basic assumptions concerning permeability upscaling.

The purpose of this technical note is to introduce a laboratory-based method for physically investigating permeability upscaling that avoids many of the problems noted in the studies above. The approach makes use of a minipermeameter that has been specially adapted for acquiring permeability data over a range of discrete sample supports. In the following we describe the method and strategy to be employed in future studies of permeability upscaling. We also evaluate and demonstrate this method though a series of tests performed on a block of Berea Sandstone and two synthetic porous rocks. The relatively homogeneous qualities of these samples provide a unique basis for testing the

experimental method as their low characteristic variability does not mask the subtle measurement errors and inconsistencies capable of rendering this experimental approach ineffective in quantifying permeability upscaling.

2.3. Method

The ultimate reason for developing the laboratory method described herein is to investigate permeability upscaling. This requires a means of measuring permeability at multiple, discrete sample supports. For this work to be quantitative, measurements made at different supports must be consistent in four basic ways. First, multi-support permeability data must be collected from the same physical sample, thus requiring the measurement technique to be non-destructive. Second, near exhaustive sampling is required at each support to avoid errors induced by sparse data effects. For this reason, large suites of data must be collected at each sample support requiring measurements to be rapid and inexpensive. Third, measurements must be sensitive to slight changes in permeability at all sample supports; thus, measurement error must be small and consistent. Fourth, measurements must be consistent in terms of flow geometry, boundary conditions, and calculational techniques so as to provide a uniform basis for comparison. Finally, as upscaling studies will need to be performed on a wide variety of geologic media, the adopted technique must have a large dynamic permeability range and the ability to discern heterogeneities occurring at different length scales.

The minipermeameter meets these basic criteria. Originally developed in the petroleum industry [Dykstra and Parsons, 1950; Eijpe and Weber, 1971] for rapid field and laboratory acquisition of permeability data, the minipermeameter has found wide-spread use in characterizing the spatial distribution of permeability in outcrops as well as rock cores and slabs. Studies have been performed on a wide range of geologic media including eolian sandstones [Chandler et al., 1989], fluvial sandstones [Dreyer et al., 1990; Davis et

al., 1993], carbonates [Kittridge et al., 1990], and volcanic tuffs [Fuller and Sharp, 1992]. Three basic minipermeameter designs exist: a non-steady or pressure decay minipermeameter [Jones, 1992], a high volume steady-state minipermeameter [e.g., Sharp et al., 1993], and a low volume steady-state minipermeameter [Davis et al., 1994]. Basic minipermeameter operation involves the compression of a tip seal against the test media through which gas is injected into the sample. Information on the gas flow rate and injection pressure is then used to calculate the permeability. Characteristics of the resulting flow field and sample support are dictated by the dimensions of the tip seal. To date, most minipermeameter studies have been performed using a single, small (~0.31 cm inner radius) tip seal, and hence single sample support.

In the following section we describe in detail how the basic minipermeameter concept has been adapted to meet the special needs of our upscaling studies. We refer to this modified minipermeameter system as the Multi-Support Permeameter (MSP).

Multi-Support Permeameter (MSP)

The MSP (Figure 2.1) has been carefully designed according to the basic criteria established above. The unique feature of the MSP is the use of different sized tip seals for investigating permeability upscaling. By simply changing the tip seal size, permeability data are acquired in a completely consistent manner over a range of discrete sample supports. The MSP is patterned after the high volume steady-state minipermeameter to allow flexibility in the measured permeability ($1x10^{-15}$ to $1x10^{-10}$ m^2) and volumetric gas supply. Automation of the minipermeameter system is achieved by integrating a computer-controlled electronic minipermeameter with an x-y positioning system to facilitate acquisition of large data sets subject to nominal measurement error. The MSP is designed for laboratory use to protect its delicate electronic equipment and to take advantage of controlled environmental conditions. As such, samples are brought to the laboratory in the

form of meter-scale blocks of rock that provide both a continuous and extensive three-dimensional medium for testing.

The MSP is composed of five basic components, an electronic minipermeameter, a tip seal, an x-y positioning system, a pneumatic system for compressing the tip seal, and a computer control system. The primary function of the electronic minipermeameter is to regulate and measure the flow of gas into the rock sample (Figure 2.1a). The minipermeameter operates by prescribing the gas injection pressure while measuring the resulting steady-state gas flow rate, gas temperature, and barometric pressure. To insure gas purity and low humidity, compressed laboratory grade nitrogen is used as the test fluid. The gas injection pressure is controlled with a two-stage pressure regulator (Victor® Model GPT 270A) and measured independently at the tip seal with a 0-100 kPa differential pressure transducer (Sensotec Model WD-TJE-18690-02). Four mass-flow meters (Sierra Instruments Model 822-S1-L-1) of varying sensitivity (0-50, 0-500, 0-2000, and 0-20,000 cm^3/min. at standard conditions) are used to measure the gas flow rate. The mass flow meters are configured in parallel with associated solenoid valves to direct gas flow to the appropriate meter. Concurrent measurement of the gas temperature is achieved with an in-line thermocouple while the ambient pressure is measured with a barometer (Sensotec Model EB/8942-01). Plumbing for the minipermeameter consists of 0.63 cm ID copper tubing and Swagelok® fittings.

Gas is directed into the rock sample via the tip seal. A series of specially designed tip seals, the diameter of which defines the sample support, are used to establish a known boundary condition on the rock surface. Tip seal sizes in current use have inner radii (r_i) of 0.15, 0.31, 0.63, 1.27, and 2.54 cm, and an outer radii (r_o) measuring twice the inner. Critical to precise measurement is a consistent and known tip seal geometry under compressed conditions. For this reason, each of the tip seals is equipped with an internal

spring-driven guide to maintain a constant inner seal diameter (Figure 2.2). Beyond this characteristic, slight variations in design among the five tip seals is necessitated because the degree of tip seal deformation increases with decreasing tip seal width ($r_o - r_i$). Specifically, an immobile outer guide is required by the 0.15, 0.31, and 0.63 cm r_i tip seals but not for the larger two seals. Tip seal thickness and hardness must also be varied. For the 0.63, 1.27, and 2.54 cm tip seals, silicone rubber (Dow Corning HS III RTV) molded into a 1.6 cm thick ring is used to establish the seal between the injection nozzle and the rock surface, while a thinner (0.5 cm) seal made of a harder silicone rubber (Dow Corning HS 630) is used for the 0.15 and 0.31 cm tip seals.

To allow unattended operation of the MSP, the electronic minipermeameter has been integrated with an x-y positioning system that is composed of two stepper motors (Compumotors Model SX83-62) and three belt drives (Daedal Model 008-7178). The system has a bi-directional repeatability of ±0.1 mm over a 1.5 by 1.5 m sampling area. The positioning system is affixed to a rigid table supported by a unistrut frame (Figure 2.1b). Rock samples are placed under the positioning system and by virtue of their weight remain stationary during sampling. The height of the positioning table can be adjusted over a 1.5 m distance to accommodate different sized samples.

A pneumatic piston is attached to the positioning system carriage for compressing the minipermeameter tip seal against the rock sample. The piston is powered by a regulated source of compressed air and controlled by means of a 3-way solenoid valve. The compression system allows each measurement to be made with the tip seal compressed squarely against the sampling surface at a consistent pressure; thus, limiting measurement error. However, to achieve a good seal proper preparation of the sampling surface, as detailed in the next section, is required. The pressures used to compress the different-sized tip seals are discussed later in this paper.

Operation of the electronic minipermeameter and x-y positioning system is controlled by a 386/25 MHz personal computer via LABTECH NOTEBOOK (Laboratories Technologies Corp.). Normal operation of the MSP begins with positioning and compressing the tip seal against the rock sample according to a pre-defined grid. Following a 10 second pause, the solenoid to the 0-2000 sccm flow meter is opened allowing gas to flow into the sample. The gas flow rate is monitored and then directed to the meter with the appropriate range. The gas flow rate, injection pressure, barometric pressure, and gas temperature averaged over a five second interval are recorded in the data file once steady gas flow is achieved. "Steady gas flow" is defined to occur at a prescribed interval of time after the mass flow meter reading has stabilized (determined from the slope of the gas flow rate/time profile). This interval of time is determined from the results of independent tests conducted prior to sampling. A discussion of the time dependency of the permeability measurements is given later. Once the data are collected the solenoid valve is closed and the tip seal raised. The positioning system moves the tip seal to the next location and the process is repeated.

Sample Acquisition and Preparation

Identification of rock samples for use in upscaling studies is a continuous process. To date, four samples, two sandstones and two volcanic tuffs, from different quarries spread across the United States have been acquired and prepared for testing. One of these is the Berea Sandstone block used in the method evaluation/demonstration studies given in this paper. In general, samples are selected according to depositional environment, diagenetic history, correlation scale and nature of exhibited heterogeneity, and permeability range inherent to the rock. The selected boulders are shipped to a quarry and cut into

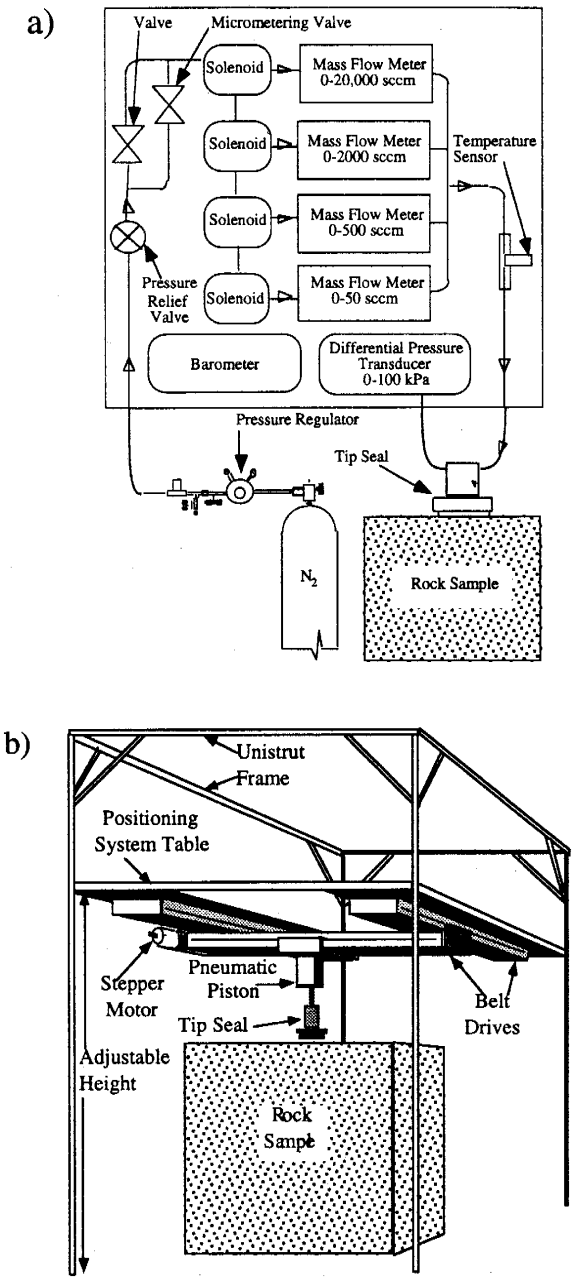

Figure 2.1. Schematic of the Multi-Support Permeameter (MSP). The MSP is specially designed for measuring permeability over a range of discrete sample supports. This system has the advantage that all measurements, regardless of sample support, are made with consistent boundary conditions and flow geometry. Automation of the MSP is achieved by the integration of an a) electronic minipermeameter and b) x-y positioner with a computer control system.

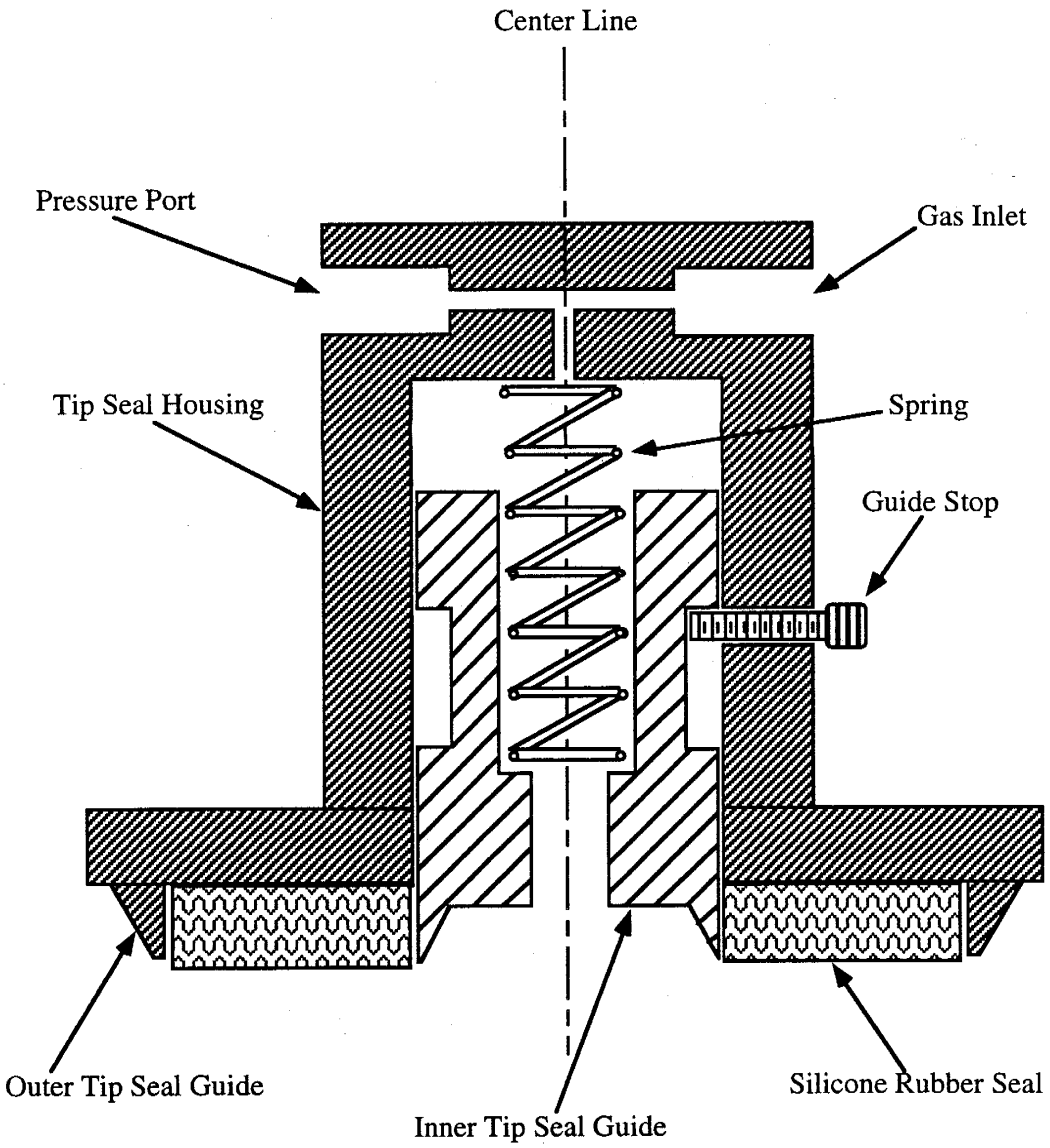

Figure 2.2. Schematic of an MSP tip seal. A molded ring of silicone rubber is used to form the seal with the rock surface while a spring loaded inner guide and immobile outer guide (0.63 cm r_t and smaller) constrain the shape of the seal under compression. A similar design is employed for each of the five tip seals.

blocks. The final block must be large enough to provide the spatial data required by the study, yet small enough to be transported and handled in the laboratory. In general, this limits blocks to a maximum size of 1.3 to 1.6 m per side. Blocks are preferred over slabs because they provide a 3-D sampling domain and a medium that is thick relative to the depth of penetration of the minipermeameter measurement.

Shaping of boulders into blocks is necessary to provide a fresh, flat surface for making measurements. We define "flat" as a surface free from abrupt surface irregularities (< 1.5 mm) that may impede the sealing of the tip on the rock surface. At the quarry the selected boulders are cut along inferred principal permeability axes into a rectangular/cubic shape using a diamond-impregnated wireline saw. Fresh water is used to lubricate and cool the wireline during cutting as well as to pressure wash the sawn surfaces. The blocks are then shipped to the lab for analysis. Prior to testing the blocks are allowed to air dry in the laboratory for a minimum of six months. This interval should provide sufficient time for the outer 15 cm of the block to equilibrate with the low ambient humidity conditions (~40%) in the laboratory and resulting in an insignificant water saturation in the rock sample. Periodically, a limited suite of repeated measurements are made on each block to substantiate this assumption.

Permeability Calculation

Permeability is calculated directly from information on seal geometry, and the measured gas flow rate, injection pressure, barometric pressure, and gas temperature (measured only to verify isothermal conditions and make slight adjustments to the fluid viscosity). These calculations are accomplished by means of a modified form of Darcy's Law developed by Goggin et al. [1988].

$$k(Q_1, P_1, P_o, r_I, r_o) = \frac{Q_1 P_1 \mu(T)}{0.5 r_I G_o\left(\frac{r_o}{r_I}\right)\left[P_1^2 - P_o^2\right]} \tag{2.1}$$

where $k\,(Q_1, P_1, P_o, r_I, r_o)$ is permeability, Q_1 is gas-flow rate, P_O is atmospheric pressure, P_1 is gas injection pressure, $\mu(T)$ is gas viscosity a function of temperature T, and $G_o(r_o/r_I)$ is a geometric factor that varies according to the ratio of the outer tip seal radius r_o to the inner tip seal radius r_I. In this model, complexities associated with the flow-field geometry are summarized by a single, analytically derived, dimensionless function, $G_o(r_o/r_I)$, given in Figure 2.3. For our geometry $G_o(r_o/r_I) = G_o(2) = 5.03$. In part, an r_o/r_I ratio of 2 is employed because it falls within a less steeply varying region of the $G_o(r_o/r_I)$ curve.

For minipermeameter measurements subject to a homogeneous, isotropic, semi-infinite half-space, the bounding surface of the resultant gas flow field is approximated as a

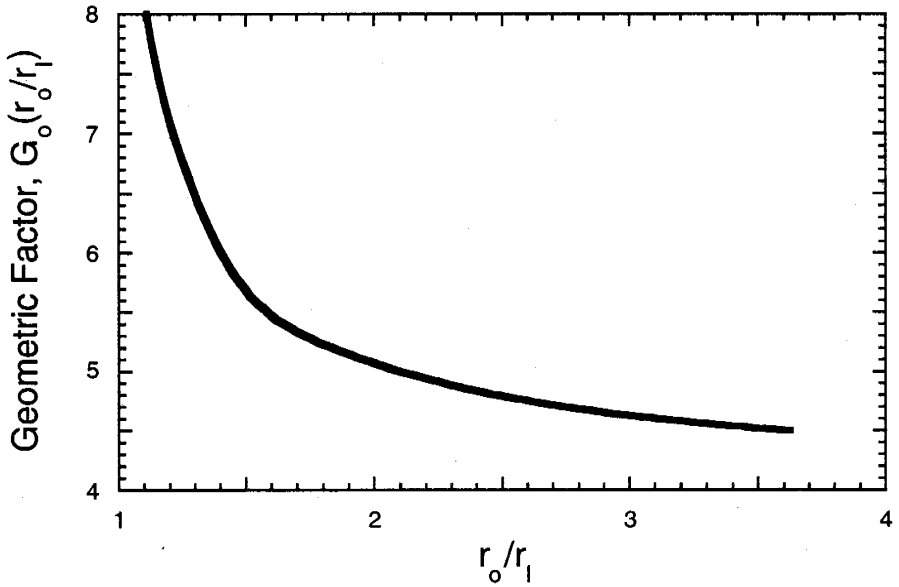

Figure 2.3. Plot of the geometric factor G_o as a function of tip seal geometry (i.e., r_o/r_I) (after Figure 5, half space solution curve, of Goggin et al. [1988]).

hemisphere [Goggin et al., 1988; Winterbottom, 1990]. The effective radius r_{eff} of the bounding surface is governed primarily by the size of the tip seal, which we define by r_1. The geometry of the diverging flow paths beneath the tip seal is controlled by the ratio r_o/r_1, thus variations in tip seal geometry (i.e., r_o/r_1 ratio) may lead to quite different permeability statistics even when r_1 is maintained constant. To preserve a consistent flow geometry across different sample supports we employ a constant r_o/r_1 ratio in the design of each tip seal. In this way, multi-support sampling subject to consistent flow-field geometry is accomplished by simply changing r_1. As a matter of convenience we have scaled the tip seal sizes so that r_1 increases by a factor of 2, and therefore the support volume by a factor of $2^3=8$.

The calculated permeability may be adversely influenced by gas slippage effects, high velocity (inertial) effects, instrument drift, and head loss in the tip seal. As such, appropriate corrections to the collected data may be required. Where necessary, the Klinkenberg factor b [Klinkenberg, 1941] is measured independently on core samples. These data are then used to establish a functional relationship between b and k_a, the absolute permeability, which is used to correct the MSP measured k data for gas slippage effects. Prior to the investigation of any rock sample the mass flux as a function of the applied pressure gradient (P_1^2-P_o^2) is measured and plotted for each of the tip seals. To avoid inertial effects, the gas injection pressure employed in upscaling studies is selected such that it falls within the linear region of the mass flux/pressure gradient curve. Instrument drift is controlled by following an annual, certified instrument calibration routine and periodic measurement of standards that span the dynamic range of the minipermeameter. Head loss is known to be a problem for the smaller tip seals at large mass flux rates. To correct for this effect, an empirical head loss factor is subtracted from the measured injection pressure. The head loss factor is determined by measuring

unrestricted gas flow from each tip seal to determine the pressure drop in the connecting hose and tip seal as a function of flow rate.

Sample Support

Important to these upscaling studies is the need to determine the sample support associated with each tip seal. In theory each measurement, regardless of tip seal size, interrogates the entire block of rock. In reality, the measurement is only influenced by the volume of rock in the direct vicinity of the tip seal. It is this "effective" volume of rock, which we term the sample support, we wish to define as a function of tip seal size.

Given the associated hemispherical flow geometry, the sample support can be quantified with knowledge of the effective radius r_{eff}. In general, r_{eff} is defined in terms of the radial distance at which minipermeameter response is no longer sensitive to porous media heterogeneities. Numerical experiments conducted by Winterbottom [1990] and Goggin et al. [1988] concluded that r_{eff} can vary from $2.5r_1$ to $4r_1$ depending on whether a 10% or 5% change in minipermeameter response, respectively, is used as the defining criteria. Laboratory experiments of Suboor and Heller [1995] found r_{eff} to equal $2.8r_1$ for a tip seal with a r_o/r_1 ratio of 2 and an undetectable change in minipermeameter response as the defining criteria. Considering the strongly divergent nature of the gas flow-field, which imparts a non-uniform weighting [e.g., Desbarats, 1994] to heterogeneities comprising the sample volume, these calculated and measured r_{eff} values are consistent with a spherical weighting of between $1/r^2$ to $1/r^3$.

In addition to the geometric controls noted above, porous media heterogeneities will influence r_{eff}. Of particular interest is the effect of media anisotropy on r_{eff} [Young, 1989]. Given the difficulties in predicting r_{eff} according to theoretical arguments, efforts have been made to quantify r_{eff} from measured MSP data. Results are given in Chapter 3.

2.4. Results and Discussion

As previously noted, our purpose is to develop a laboratory-based method for physically investigating permeability upscaling. Key to this development is a thorough evaluation of the MSP with respect to the basic design criteria stated above and its demonstration on a natural rock sample. In this section we document the results of system evaluations conducted to investigate the consistency of measurements made at different sample supports, explore the transient/steady nature of the MSP measurements, and quantify the measurement error inherent to the MSP. We then turn our attention to the demonstration of the MSP by collecting a limited set of multi-scale permeability data from a relatively homogeneous block of Berea Sandstone to determine whether the information gathered may be diagnostic of permeability upscaling. But first, we provide a brief description of the rock samples used in these studies.

Test Media

In this paper three rocks are employed to evaluate and demonstrate the MSP. We constructed two synthetic, "homogeneous" rock samples (25 cm dia. by 20 cm thick), one made of plaster and the other of mortar sieved with a 30 mesh screen. The synthetic rocks were made by mixing powdered plaster/mortar with tap water, de-airing the mixture, then allowing the mixture to cure under ambient room temperature. The third rock is a small block (0.3 by 0.3 by 0.3 m) of Berea Sandstone, acquired from Cleveland Quarries in Amherst, Ohio. This sample is characterized as a very fine grained, well sorted, thinly laminated, quartz sandstone with a very narrow permeability distribution (coefficient of variation [CV] of ~0.2). The Berea Sandstone was selected because of its widespread use in laboratory studies and its relatively uniform permeability characteristics which are unlikely to mask subtle measurement errors inherent to the MSP.

Measurement Bias

Prior to employing the MSP to investigate permeability upscaling, we must demonstrate that permeability measurements made with different sized tip seals (different sample supports) are free from any systematic bias. Given the efforts made to maintain a consistent basis of measurement across different sample supports, potential sources of systematic bias are greatly reduced. However, one potential source of bias that requires investigation is the normal stress used to compress the tip seal against the rock surface. In this section we investigate the role of tip seal compression stress on measured permeability, identify an appropriate compression stress for use with each tip seal, and demonstrate that measurements made using these compression stresses yield multi-support data free of systematic bias.

To demonstrate the relationship between compression stress and permeability a series of measurements were made with each of the five tip seals on the Berea Sandstone sample. Each measurement was made at the same location and same gas injection pressure; only the tip seal compression stress was varied. In each case an exponential decrease in permeability with increasing tip seal compression stress was found. An example is shown in Figure 2.4 for the 0.31 cm r_i tip seal. The primary cause of the decreasing permeability/compression stress trend is believed to be the extent to which the seal conforms itself to the contours of the rock surface. As compression stress is increased the seal deforms into surface irregularities preventing gas flow from short-circuiting between the rock/seal interface. Because minipermeameter measurements are particularly sensitive to the rock directly beneath the tip seal, short-circuiting gas flow does not have to span the entire tip seal width ($r_o - r_i$) to cause perceptible differences in the measured permeability.

All five tip seals exhibit an exponential permeability/compression stress relationship; however, the point where the permeability becomes effectively independent of compression stress, which we designate by σ_e, differs from one tip seal to another. Here, we define σ_e as the point where the permeability changes by less than 2% for a corresponding change in compression force of 63 N. These limits represent the resolution of the minipermeameter and pneumatic piston control system, respectively. This difference in σ_e is caused by differences in tip seal width ($r_o - r_i$), thickness, and rubber hardness. Because of these differences, an independent compression stress must be determined for each tip seal.

Two criteria have been adopted for guiding the selection of compression stresses for each of the tip seals. The first criterion requires that the compression stress be selected such that it is greater-than σ_e. Meeting this criterion alone does not assure that

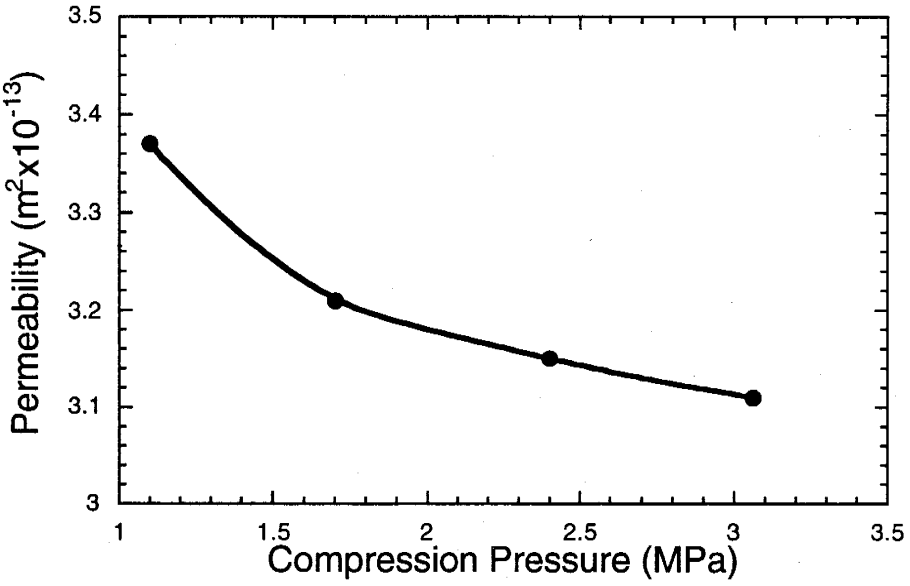

Figure 2.4. Data demonstrating the relationship between permeability and tip seal compression stress. Data were collected from a single point on the Berea Sandstone sample using the 0.31 cm tip seal. The decreasing permeability results from continued deformation of the tip seal into rock surface irregularities and/or surface pores with increasing compression stress.

measurements made at different scales will be unbiased. The necessary second criterion is that the compression stresses must be selected such that measurements made with different tip seals will yield equivalent permeability values when sampling is conducted on a homogeneous porous medium.

To determine the tip seal compression stresses that meet these two criteria, "homogeneous" porous media that are larger than the effective measurement volume of the largest tip seal (the radius and depth must be at least four times r_t [Goggin et al., 1988]) had to be identified for testing. By inspection of a wide range of porous materials we identified plaster and mortar as providing the most uniform media at the scale required. Blocks of both materials were constructed to provide two independent and different samples for testing. The permeability of these two blocks differ by more than an order of magnitude (9.80×10^{-15} and 1.45×10^{-13} m^2 respectively). Surface characteristics of the blocks also differ, with the plaster exhibiting a very flat and smooth surface while the mortar block surface was grainy, characteristic of the 30 mesh screen used to sieve the mortar.

As the synthetic rock samples were not perfectly homogeneous, we took a series of measurements on a square 3 by 3 grid on one end of each block. Grid spacing was decreased with increasing tip seal size, 1.5, 1.5, 1.25, 1.0, and 0.5 cm, respectively, to maximize coverage of the block face for each tip seal. Testing involved performing multiple samplings of the same 3 by 3 grid with each tip seal, using different compression stresses, to identify the point at which the measured permeability becomes effectively independent of compression stress (i.e., σ_e). From these data, a compression stress was then selected for each tip seal that minimized the difference in measured permeability between the five tip seals for both the plaster and mortar samples. The compression stresses found to meet

these criteria were 1.7, 1.55, 0.68, 0.52, and 0.24 MPa (absolute) for increasing tip seal size, respectively.

The permeability data collected from the mortar and plaster blocks at these compression stresses were then used to evaluate the consistency of measurements made at different sample supports. The evaluation was based on the results of a two-way analysis of variance (ANOVA) without replication. The two null hypotheses tested include: 1) the mean permeabilities measured by each of the five tip seals are equal and 2) the mean permeabilities measured at different locations are equal. Results for each block indicate that the null hypothesis that the mean permeabilities measured by each of the five different tip seals are equal cannot be rejected at a level of significance of 5% (Table 2.1). This means that differences in the permeability measured by the five different tip seals on both the mortar and plaster blocks are statistically insignificant. Conversely, the null hypothesis that the mean permeabilities at different locations are equal cannot be rejected in the case of the mortar block but can be rejected for the plaster block at a 5% significance level. That is, neither of the blocks is perfectly homogeneous and in the case of the plaster block the inhomogeneity is statistically significant.

We conclude that there is no systematic bias between measurements made at different sample supports. Given the range of permeabilities and surface conditions tested such consistency will be realized for other rock samples with similarly smooth surfaces (see discussion on sample preparation). However, an independent check is performed on any new rock sample prior to initiating upscaling studies. The check involves making measurements over a range of compression stresses to verify that the tip seal compression stress is greater than σ_e.

Table 2.1. A two-way ANOVA without replication was performed to evaluate the consistency of permeability measurements made with different sized tip seals on "homogeneous" blocks of mortar and plaster. On each block a 3 by 3 grid of data was collected with each tip seal and subjected to a two-way ANOVA. Results indicate that measurements made at different sample supports on these "homogeneous" rocks are statistically indistinguishable.

Mortar Block

	SS	df	MS	F statistic	F critical
Sample Location	2.59E-31	8	3.23E-32	1.10	2.24
Tip Seal Size	5.21E-32	4	1.30E-32	0.44	2.67
Error	9.42E-31	32	2.94E-32		
Total	1.25E-30	44			

Plaster Block

	SS	df	MS	F statistic	F critical
Sample Location	1.09E-27	8	1.36E-28	2.67	2.24
Tip Seal Size	4.58E-28	4	1.15E-28	2.25	2.67
Error	1.63E-27	32	5.10E-29		
Total	3.18E-27	44			

Steady Gas Flow

Permeability calculations based on Equation 2.1 assume steady-state gas flow. To test this assumption, experiments were performed on the Berea Sandstone sample by compressing each tip seal against the sample and continuously measuring the gas flow rate at a constant injection pressure. The permeability was calculated at one minute intervals and the percent difference with respect to the initial measurement was plotted (Figure 2.5). Time zero is taken to be the time when the flow rate stabilizes as defined by the slope of the gas flow rate/time profile reaching a pre-defined lower limit. From these data the

permeability is noted to decrease with time; however, the trend is small with respect to the measured permeability. Given that the trend is most pronounced for the smaller tip seals and differs between the two types of seal materials used, this behavior is attributed to slow relaxation of the seal into surface irregularities. In selecting the optimal measurement time, the error caused by this effect is weighted against the time necessary to completely investigate a given rock sample involving thousands of measurements. In this case, a measurement time of 2 minutes following the initial stabilization of flow (~1 min.) was adopted for the studies performed on the Berea Sandstone sample.

Measurement Error

Measurement error associated with the MSP was evaluated by means of a one-way ANOVA performed on a set of repeated permeability data collected from the Berea Sandstone sample. For each tip seal, nine groups of four replicate measurements were collected using a 3 by 3 grid on 10 cm centers. At this spacing, the data are spatially correlated (see next section); however, this lack of independence is not expected to change the conclusions of this test given the definitive results. Results of the ANOVA (Table 2.2) indicate that the null hypothesis, the means of the 9 groups of four permeability measurements are equal, is rejected at a significance level of 5%. This suggests that the measurement error is statistically insignificant in relation to the inherent variability of the sample.

Analysis of the repeated data also reveals that instrument error is very small in absolute terms. For each tip seal and each of the nine sampled locations, the coefficient of variation (CV) of the four repeated measurements was calculated. The average CV was calculated to be 0.006 with a standard deviation of 0.006. Also calculated was the average CV for each of the five tip seals which was found to range from 0.014 (0.15 cm tip) to 0.002 (1.27 cm tip). From this analysis we see that measurement error is small, generally

less than ±1% and consistent for the different sized tip seals. Also, the measured error is consistent with the results of a propagation of errors analysis [Doebelin, 1966], which predicts the measurement precision to be ±2% of the measured permeability, based on the precision of the electronic instruments comprising the minipermeameter.

Spatial Measurements

A suite of spatial permeability data was collected from the Berea Sandstone sample using four different-sized tip seals to investigate the precision and accuracy of the test system with respect to key statistical measures of upscaling (i.e., sample mean and variance), and to determine whether the gathered data provide information diagnostic of upscaling behavior. The purpose here is not to investigate the permeability upscaling of the Berea Sandstone itself, but to evaluate and demonstrate the measurement technique. A complete analysis of this sample's upscaling behavior is reserved for a future publication.

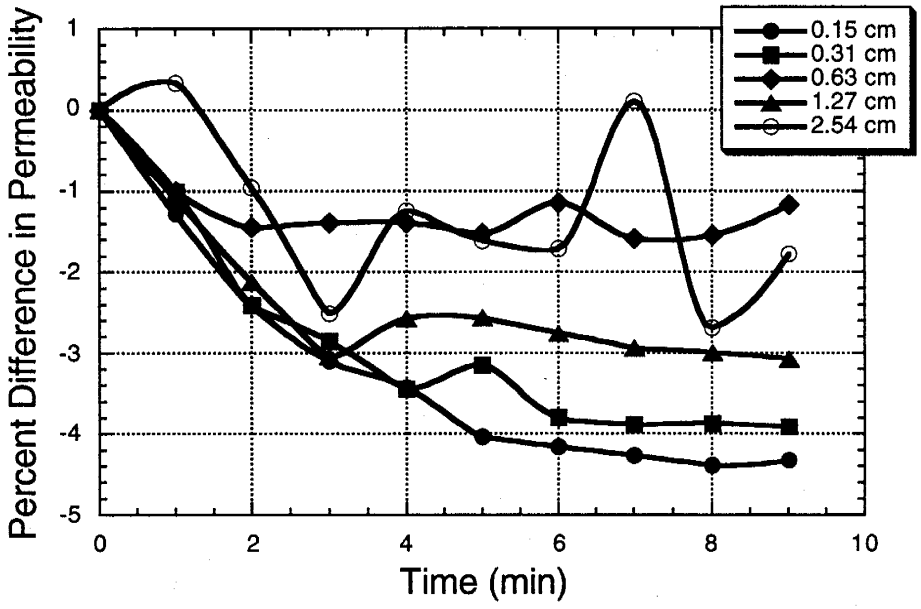

Figure 2.5. MSP permeability measurements as a function of time. Data were acquired with each tip seal at a fixed location on the Berea Sandstone sample. Measurements were collected with the tip seal continuously compressed and permeability calculated at one minute intervals. Percent difference values were calculated with respect to the permeability measured at t=0. Similar results were found at other locations on the Berea sample.

Table 2.2. To evaluate MSP measurement error, a one-way ANOVA was performed on a series of repeated data sets. Nine groups of four repeated permeability measurements were made on the Berea Sandstone block with each of the five tip seals. The data were then subjected to an ANOVA which revealed that measurement error is insignificant with respect to the spatial variability of the sample. To facilitate presentation the ANOVA results have been collapsed into a single table. For each tip seal F critical is 2.31 (at a 5% significance level) while the degrees of freedom between groups is 8 and within groups is 27.

Tip Seal Inner Radius (cm)	Mean Square Between Groups	Mean Square Within Groups	F statistic
0.15	9.86E-27	2.65E-29	372.01
0.31	1.39E-26	6.81E-30	2041.01
0.63	6.83E-27	9.94E-31	6870.96
1.27	2.84E-27	6.06E-31	4691.78
2.54	1.45E-27	8.24E-30	176.01

Exhaustive spatial permeability data were collected from a single face (we have termed Face 5) of the Berea Sandstone sample cut normal to the lamination. Measurements were made at four different sample supports using the 0.15, 0.31, 0.63, and 1.27 cm r_t tip seals. Sampling was performed within a 20 by 20 cm area using a 24 by 24 point grid (576 points) on 0.85 cm centers. At this grid spacing considerable overlap occurs between neighboring measurements for the 0.31 cm and larger tip seals. Gray-scale plots of the permeability fields for these tip seals are shown in Figure 2.6. Notable features include horizontal lamination evident in each permeability field, smoothing of the permeability fields with increasing sample support, and consistency of high- and low-permeability zones among the different fields.

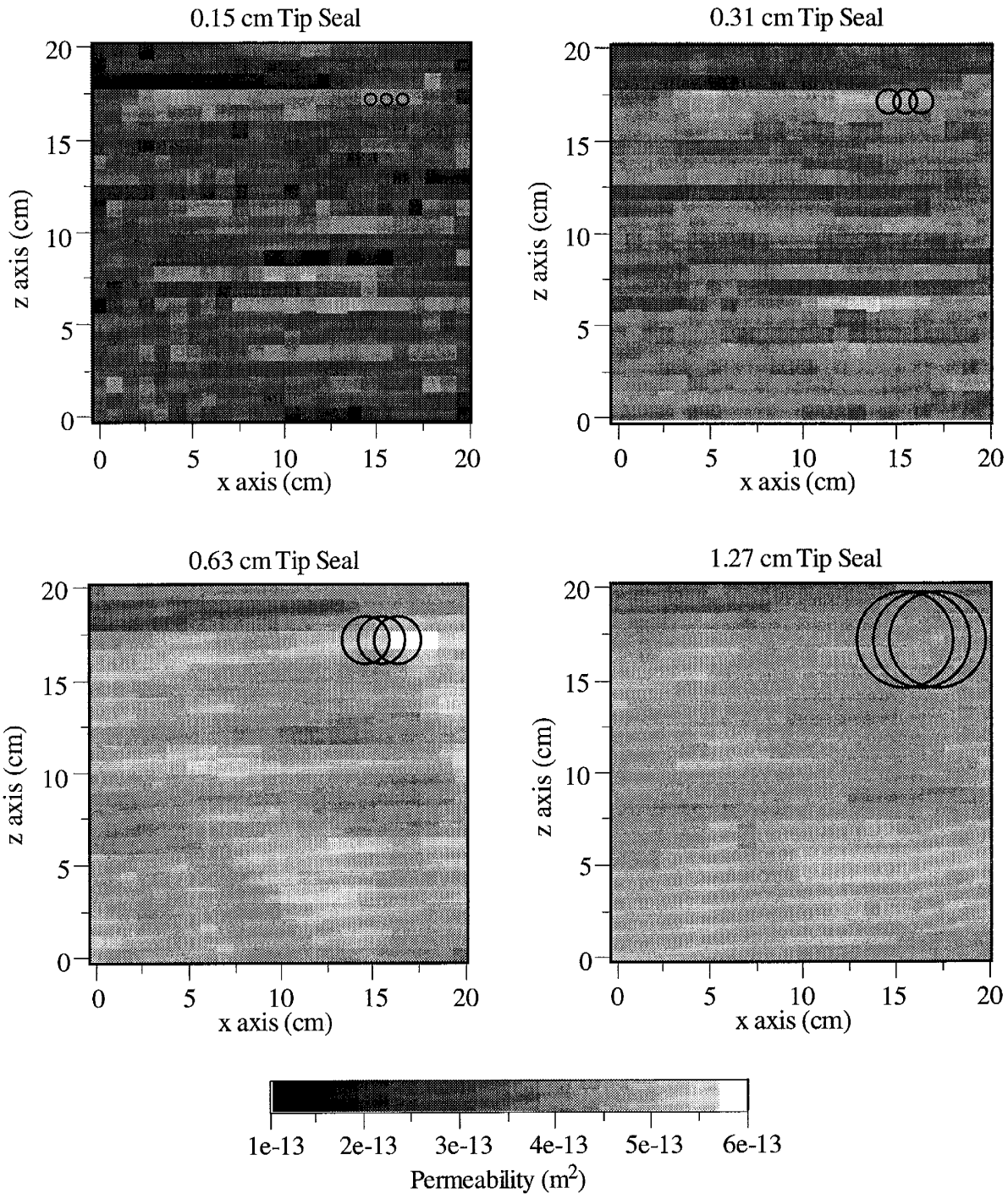

Figure 2.6. Permeability fields (m^2) measured with the a) 0.15, b) 0.31, c) 0.63, and d)1.27 cm r_I tip seals on the Berea Sandstone samle. Data were collected on a 24 x 24 grid with 0.85 cm centers. Sample domain size was 20 x 20 cm. The three black rings in each image are included to indicate the degree of overlap between neighboring measurements. The radii of the rings in each image is set equal to the corresponding outer tip seal radius.

The measured permeability fields are summarized according to their cumulative distribution functions (CDFs) and univariate summary statistics. From the shape of the CDFs shown in Figure 2.7, it is apparent that the sample mean increases with increasing sample support while the sample variance decreases. In fact, the mean and variance upscale in a very distinct and consistent manner. The trend in the sample mean (2.66, 3.43, 4.00, and 4.49 $x10^{-13}$ m^2 for increasing tip seal size) could be interpreted as an increased tendency of larger tip seals to sample the well connected, higher permeability zones within the Berea sample (see Chapters 4 and 7). The trend in the variance (5.99, 4.88, 3.60, and 1.89 $x10^{-27}$ m^4 for increasing tip seal size) results because measurements made at larger supports interrogate more rock and hence average over more spatial variability than do measurements made at smaller sample supports.

To evaluate the repeatability of the measured CDFs and summary statistics, a second identical set of spatial permeability data was collected on the same grid, but two weeks after the initial sampling. From the overlapping CDFs given in Figure 2.7, it can be seen that the repeated data sets are nearly indistinguishable from each other. The maximum deviation between any of the repeated distribution functions is 6%, which occurred along a steep portion of the 1.27 cm curve. Minimal differences between the means (<2%) and variances (<2%) of repeated data sets were also noted.

Also of interest is whether the data acquired with the minipermeameter compare favorably in absolute terms with that collected by other researchers. We first note that the block of Berea Sandstone was quarried from a zone known to yield permeabilities between $2x10^{-13}$ and $4x10^{-13}$ m^2 (Cleveland Quarries, personal communication, 10/11/94), which is the mean permeability range measured in this study. Favorable comparisons can also be drawn with minipermeameter data collected by Giordano et al. [1985] from a 0.61 x 0.61 x 1.27 m slab of Berea Sandstone taken from an unidentified quarry. Using a tip seal with a

0.75 cm outer seal radius r_o, they sampled the slab on a 40 by 40 grid with 1.5 cm centers. They describe their sandstone as diagonally stratified, hence we draw comparison with our Face 6 (face parallel to stratification) which exhibits very similar structure. Giordano et al. [1985] report a mean permeability of 2.45×10^{-13} m^2 and coefficient of variation of 0.28, compared to 2.73×10^{-13} m^2 and 0.27, respectively, measured with the MSP on Face 6 using the 0.31 cm r_l tip seal (i.e., 0.62 cm r_o).

The spatial continuity of the Berea Sandstone permeability data has also been analyzed. Sample semivariograms were calculated using Fourier analysis for each of the four tip seals using a search direction oriented normal to lamination (Figure 2.8). Each of the semivariograms exhibit a periodic spatial structure characteristic of the stratified structure of the Berea Sandstone (Figure 2.6). Two periodic features are evident, one with a period of approximately 3.8 cm and the other 16 cm. Although not shown, sample

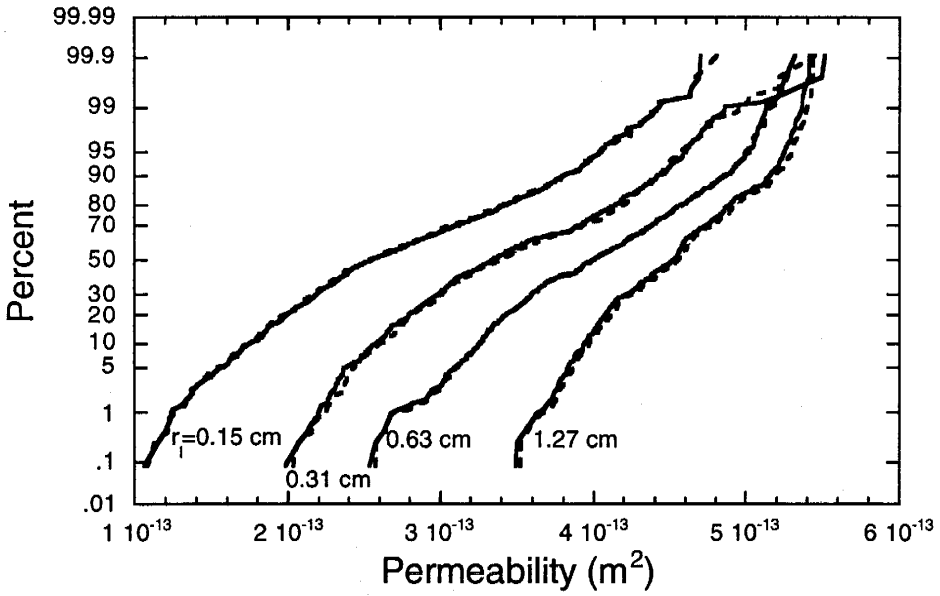

Figure 2.7. Cumulative distribution functions for the permeability data sets measured with the 0.15, 0.31, 0.63, and 1.27 cm tip seals on the Berea Sandstone sample. Measurement of these data sets was repeated approximately two weeks later yielding CDFs that are almost indistinguishable from the former (solid vs. dashed line for each tip seal).

semivariograms oriented parallel to lamination exhibit a linear trend with separation distance suggesting the correlation length is >10 cm, thus confirming the geometric anisotropy evident in the gray scale images (Figure 2.6).

As with the univariate statistics, two distinct trends relating characteristics of the semivariogram to the sample support are evident. First, we note that the magnitude of the semivariogram sill decreases with increasing support, which is consistent with the decreasing variance. Second, as the sample support increases the influence of the high frequency structural element is reduced relative to the lower frequency element. This is, as the sample support size approaches the period of the structural feature, it is effectively averaged out of the permeability field.

Analysis of the multi-support permeability data collected from the Berea Sandstone sample has revealed distinct and consistent trends between the sample support and various summary statistics. Specifically, the sample mean was noted to increase with increasing sample support while the sample variance was found to decrease. Trends in the semivariogram sill and shape were likewise found to correlate with increasing sample support. Considering the effort made to insure consistent measurement and the relatively "homogenous" qualities of the Berea Sandstone sample, we are convinced that these measured trends are not simply artifacts of the sampling program but are diagnostic of permeability upscaling.

2.5. Conclusions

We have introduced, evaluated, and demonstrated a method for physically investigating permeability upscaling. Data are acquired by means of a Multi-Support Permeameter (MSP), which is composed of an electronic minipermeameter and x-y positioner integrated with a computer control system. The MSP provides a non-destructive

means of exhaustively measuring permeability on meter-scale blocks of heterogeneous rock. The key feature of the MSP is the use of different sized tip seals to measure the permeability at different sample supports. In this way, measurements are made under consistent flow and boundary conditions regardless of sample support. Results of experiments performed to evaluate the MSP indicate that measurement error is small and consistent and that measurements made with different size tip seals are free from systematic bias.

Demonstration of the MSP was performed on a relatively homogeneous block of Berea Sandstone. Permeability measurements made at four discrete sample supports were found to exhibit strong, consistent trends in the mean, variance, and semivariogram as a function of sample support. As these basic statistical measures are the building blocks to most theoretical upscaling models, these distinct trends are seen as encouraging results indicating that such measurements provide insight into permeability upscaling. Our next

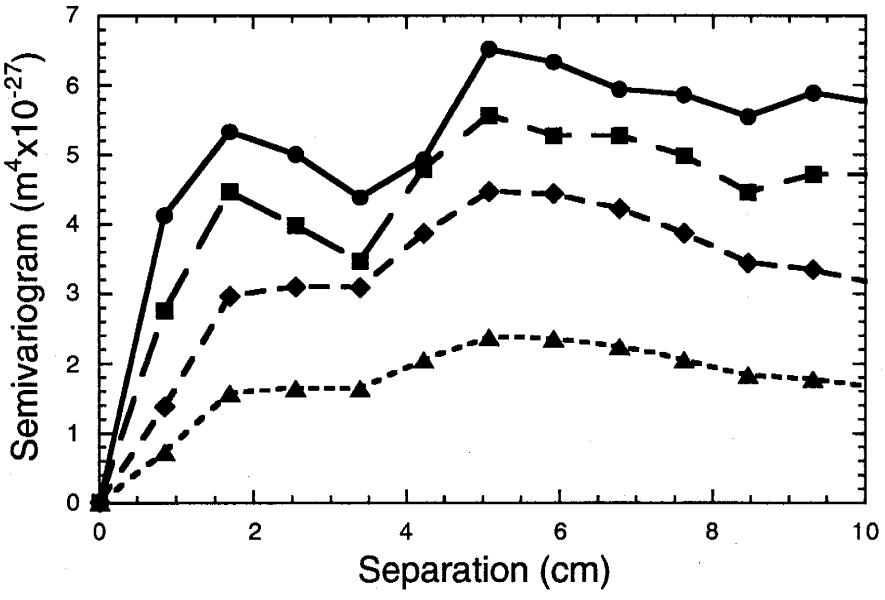

Figure 2.8. Sample semivariograms measured with the 0.15, 0.31, 0.63, and 1.27 cm tip seals (circles, squares, diamonds, and triangles, respectively) on the Berea Sandstone sample. Search direction is oriented normal to lamination.

step is to fully investigate the Berea Sandstone sample by making measurements on additional rock faces and with additional tip seals. Next, other rock samples with differing depositional and diagenetic histories, and characterized by greater permeability variation will be investigated.

Acknowledgments. Justin Von Doemming and Mark Bailey are acknowledged for their help in constructing the MSP and their help in data collection. We would like to thank Robert J. Glass for providing constructive advice throughout this effort. We also acknowledge the helpful review comments of A.J. Desbarats and two anonymous reviewers. This work was supported by the U.S. Department of Energy, Office of Basic Energy Science, Geoscience Research Program, under contract DE-AC04-94AL85000 and DE-F303-96ER14589/A000. Sandia is a multiprogram laboratory operated by Sandia Corporation, a Lockheed Martin Company, for the United States Department of Energy.

2.6. References

Brace, W.F., Permeability of crystalline rocks: New in situ measurements, *J. Geophys. Res.*, 89(B6), 4327-4330, 1984.

Chandler, M.A., G. Kocurek, D.J. Goggin, and L.W. Lake, Effects of stratigraphic heterogeneity on permeability in eolian sandstone sequence, Page Sandstone, Northern Arizona, *AAPG Bull.*, 73(5), 658-668, 1989.

Clauser, C., Permeability of crystalline rocks, *Eos. Trans. AGU*, 73(21), 233, 1992.

Cushman, J.H., On unifying the concepts of scale, instrumentation, and stochastics in the development of multiphase transport theory, *Water Resour. Res.*, 20(11), 1668-1676, 1984.

Dagan, G., Analysis of flow through heterogeneous random aquifers by the method of embedding matrix 1. Steady flow, *Water Resour. Res.*, 17(1), 107-121, 1981.

Davis, J.M., R.C. Lohmann, F.M. Phillips, J.L. Wilson, and D.W. Love, Architecture of the Sierra Ladrones Formation, Central New Mexico: Depositional controls on the permeability correlation structure, *Geol. Soc. Am. Bull.*, 105(8), 998-1007, 1993.

Davis, J.M., J.L. Wilson, and F.M. Phillips, A portable air-minipermeameter for rapid in-situ field measurements, *Ground Water*, 32(2), 258-266, 1994.

Desbarats, A.J., Spatial averaging of hydraulic conductivity under radial flow conditions, *Math. Geol.*, 26(1), 1-21, 1994.

Doebelin, E.O. , *Measurement Systems: Application and Design*, McGraw Hill, New York, 1966.

Dreyer, T., A. Scheie, and O. Walderhaug, Minipermeameter-based study of permeability trends in channel sand bodies, *AAPG Bull.*, 74(4), 359-374, 1990.

Dykstra, H., and R.L. Parsons, The prediction of oil recovery by water flood, in *Secondary Recovery of Oil in the United States*, 2nd ed., American Petroleum Institute, New York, pp. 160-174, 1950.

Eijpe, R., and K.J. Weber, Mini-permeameters for consolidated rock and unconsolidated sand, *AAPG Bull.*, 55(2), 307-309, 1971.

Fuller, C.M., and J.M. Sharp, Jr., Permeability and fracture patterns in extrusive volcanic rocks: Implication from the Welded Santana Tuff, Trans-Pecos Texas," *Geol. Soc. Am. Bull.*, 104, 1485-1496, 1992.

Gelhar, L.W., and C.L. Axness, Three-dimensional stochastic analysis of macrodispersion in aquifers, *Water Resour. Res.*, 19(1), 161-180, 1983.

Giordano, R.M., S.J. Salter, and K.K. Mohanty, The effects of permeability variations on flow in porous media, *SPE 14356*, paper presented at the 60th Annual Technical Conference, Soc. of Pet. Eng., Las Vegas, NV, Sept. 22-25, 1985.

Goggin, D. J., R. L. Thrasher, and L. W. Lake, A theoretical and experimental analysis of minipermeameter response including gas slippage and high velocity flow effects, *In Situ*, 12(1-2), 79-116, 1988.

Hanor, J.S., Effective hydraulic conductivity of fractured clay beds at a hazardous waste landfill, Louisiana Gulf Coast, *Water Resour. Res.*, 29(11), 3691-3698, 1993.

Henriette, A., C.G. Jacquin, and P.M. Adler, The effective permeability of heterogeneous porous media, *PCH PhysicoChemical Hydrodynamics*, 11(1), 61-80, 1989.

Hess, K.M., S.H. Wolf, M.A. Celia, and S.P. Garabedian, Macrodispersion and spatial variability of hydraulic conductivity in a sand and gravel aquifer, Cape Cod, Massachusetts, *EPA/600/M-91/005, Environmental Research Brief*, Environmental Protection Agency, Ada, OK, 1991.

Jones, S.C., The profile permeameter -- A new, fast, accurate minipermeameter, *SPE 24757*, paper presented at the 67th Annual Technical Conference, Soc. of Pet. Eng., Washington, DC, October 4-7, 1992.

Keller, C.K., G. van der Kamp, and J.A. Cherry, A multiscale study of the permeability of a thick clayey till, *Water Resour. Res.*, 25(11), 2299-2317, 1989.

Killey, R.W.D., and G.L. Moltyaner, Twin Lake tracer tests: Setting, methodology, and hydraulic conductivity distribution, *Water Resour. Res.*, 24(10), 1585-1612, 1988.

Kittridge, M.G., L.W. Lake, F.J. Lucia, and G.E. Fogg, Outcrop/subsurface comparisons of heterogeneity in the San Andres Formation, *SPE Form. Eval.*, 5(3), 233-240, 1990.

Klinkenberg, L.J., The permeability of porous media to liquids and gases, in *Drilling and Production Practices,* pp. 200-213, American Petroleum Institute, New York, 1941.

Molz, L.J., O. Guven, J.G. Melville, and C. Cardone, Hydraulic conductivity measurement at different scales and contaminant transport modeling, in *Dynamics of Fluids in Hierarchical Porous Media*, edited by J.H. Cushman, Academic Press, New York, pp. 37-59, 1990.

Neuman, S. P., Generalized scaling of permeabilities: Validation and effect of support scale, *Geophys. Res. Lett.*, 21(5), 349-353, 1994.

Parker, J.C., and K.A. Albrecht, Sample volume effects on solute transport predictions, *Water Resour. Res.*, 23(12), 2293-2301, 1987.

Rubin, Y., and J.J. Gomez-Hernandez, A stochastic approach to the problem of upscaling of conductivity in disordered media: Theory and unconditional numerical simulations, *Water Resour. Res.*, 26(4), 691-701, 1990.

Sharp, Jr., J.M., L. Fu, P. Cortez, and E. Wheeler, An electronic minipermeameter for use in the field and laboratory, *Ground Water*, 32(1), 41-46, 1993.

Suboor, M.A., and J.P. Heller, Minipermeameter characteristics critical to its use, *In Situ*, 19(3), 225-248, 1995.

Winterbottom, F.A., Numerical modeling of a minipermeameter, M.Eng. thesis, 120 pp., Heriot-Watt University, Edinburgh, 1990.

Young, G.R., Determining permeability anisotropy from a core plug using a minipermeameter, MS. thesis, 118 pp., Univ. of Texas, Austin, 1989.

CHAPTER 3: WHAT DOES AN INSTRUMENT MEASURE? EMPIRICAL SPATIAL WEIGHTING FUNCTIONS CALCULATED FROM PERMEABILITY DATA SETS MEASURED ON MULTIPLE SAMPLE SUPPORTS[2]

3.1. Abstract

With the aid of linear filter theory we analyze 13,824 permeability measurements to empirically address the question, "what does an instrument measure?" By measure we mean the sample support or sample volume associated with an instrument, as well as, how the instrument spatially weights the heterogeneities comprising that sample support. Although the theoretical aspects of linear filter analysis are well documented, physical data for testing the filtering behavior of an instrument, particularly in the context of porous media flow, are rare to non-existent. Our exploration makes use of permeability data measured with a minipermeameter on a block of Berea Sandstone. Data were collected according to a uniform grid that was re-sampled with tip seals of increasing size (i.e., increasing sample support). Spatial weighting (filter) functions characterizing the minipermeameter measurements were then calculated directly from the permeability data sets. In this paper we limit our presentation to one of the six rock faces, consisting of 2,304 measurements, as the general results for each rock face are similar. We found that the empirical weighting functions are consistent with the basic physics of the minipermeameter measurement. They decay as a non-linear function of radial distance from

[2] Tidwell, V.C., A.L. Gutjahr, and J.L. Wilson, Water Resources Research, 35(1), 43-54, 1999.

the center of the tip seal, consistent with the divergent flow geometry imposed by the minipermeameter. The magnitude of the weighting function decreases while its breadth increases with increasing tip seal size, reflecting the increasing sample support. We further demonstrate, both empirically and theoretically, that non-additive properties like permeability are amenable to linear filter analysis under certain limiting conditions (i.e., small variances). Specifically, the weighing function is independent of the power average employed in its calculation (e.g., arithmetic vs. harmonic average). Finally, we examine the implications of these results for other instruments commonly employed in hydraulic testing (e.g., slug and pump tests).

3.2. Introduction

Questions concerning what is actually measured by an instrument are commonly raised within the context of reservoir and aquifer characterization. For example, what is the radius of influence imposed by a pump test?; how are the results of a slug test influenced by media heterogeneities near the well bore versus those further away? Answers to such questions are rarely simple, while assumptions concerning what is measured by the instrument can significantly influence flow and transport modeling conditioned on the acquired data.

How might one quantify the measurement characteristics of an instrument? Matheron [1965] and Marle [1967] suggest the treatment of an instrument as linear filter. The mathematical development of their approach begins by assuming a field variable k_o with non-zero magnitude and point-support (infinitely small sample volume) can be defined at each point $\bar{x}$ within the spatial domain interrogated by the instrument. The corresponding macroscopic field variable k_m is then the convolution of the point-support

field variable with a weighting function (also know as a filter function) unique to the instrument, β_{mo}, over the volume V

$$k_m(\bar{x}) = \int_V \beta_{mo}\left(\bar{\xi}\right) k_o\left(\bar{x} - \bar{\xi}\right) d\bar{\xi} \tag{3.1}$$

where the integration variable, $\bar{\xi}$, is referenced to a coordinate frame whose origin is at the point $\bar{x}$. The weighting function is assumed integrable with finite support such that

$$\int_V \beta_{mo}\left(\bar{\xi}\right) d\bar{\xi} = 1 \tag{3.2}$$

In this way, the weighting function β_{mo} explicitly accounts for the influence of the measurement process on the value of k_m. Thus, the macroscopic field variable, k_m, is a function of both the characteristics of the porous medium (through the point-support field variable, k_o) and the characteristics of the instrument.

Macroscopic field variables defined in this manner have found application in generalized theories of multiscale transport and in the design of sampling networks. Baveye and Sposito [1984] recognized that the value of a macroscopic field variable and its accuracy are inherently related to the method of measurement and to the physical features of the porous media. Accordingly, they proposed the weighting function as a convenient means for relating characteristics of an instrument's measurement to the measured macroscopic field variable. Cushman [1984] exploited the filtering aspects of an instrument so as to place restrictions that make its measurement relevant to its physical environment. He defined an ideal instrument as one that filters out small-scale features (noise) while preserving the large-scale structure. Knowledge of the filtering characteristics of an instrument also provide a basis for defining those heterogeneities that can be explicitly

resolved by an instrument of given size and those that cannot be resolved [Cushman, 1986]. Beckie [1996] explores the concept of minimum resolvable scale of heterogeneity for the case of field measurements made on a regular sampling network. Additionally, Beckie et al. [1994] explore the effect of unresolved heterogeneities on explicitly resolved, large-scale groundwater flow behavior and in a later work introduce a method and framework for modeling explicitly resolved large-scale flow dynamics for a given scale of characterization [Beckie et al., 1996].

Central to the concept of linear filtering is the formulation of a weighting function β_{mo} for an instrument. To date, such efforts have relied on theoretical constructs coupled with mathematical modeling. One of the most widely recognized examples is the inverse distance squared weighting of heterogeneities by radial flow to a well [Cardwell and Parsons, 1945; Desbarats, 1992a]. Oliver [1990] used a perturbation approach to calculate the weighting function for permeability estimates derived from the semilog plot of drawdown versus time for non-steady pump test data. Weighting functions have been developed according to theoretical means for a number of other problems including: measurement of porosity by flow-through borehole tests using a radioactive tracer [Moltyaner, 1989], measurement of liquid-phase porosity by nuclear magnetic resonance imaging [Maneval et al., 1990], and measurement of soil water content by time domain reflectometry [Knight, 1992].

It is apparent that linear filter analysis has received considerable theoretical attention within the context of porous media flow and transport; however, there is a concerning lack of physical data demonstrating the filtering aspects of instruments commonly employed in hydraulic testing. Recent laboratory studies employing the Multi-Support Permeameter (MSP) (see Chapter 2) provide a unique opportunity to directly calculate weighting functions relating permeability data measured at one sample support (i.e., sample volume)

with that measured at another. The MSP is a computer automated minipermeameter with which exhaustive sets of permeability data are acquired from meter-scale blocks of rock. With this instrument permeability data are collected at different sample supports by simply changing the size of the tip seal used in the measurement. The primary goal of this study is to provide physical evidence concerning the filtering characteristics of a common hydraulic testing instrument, the minipermeameter. Of particular interest are: 1) whether weighting functions can be practically calculated from the measured permeability data, 2) whether the weighting functions behave in a manner consistent with the flow physics of the minipermeameter, 3) whether linear filtering can be applied to non-additive properties like permeability, and 4) whether results drawn from the minipermeameter analyses provide insight into the linear filtering characteristics of other instruments, like slug or well tests.

3.3. Methods

The sparse empirical evidence concerning the filtering behavior of instruments used in hydraulic testing attests to the difficulty in acquiring the necessary data. Here, we have adapted a minipermeameter test system that provides a unique opportunity to empirically address this issue. Our use of the minipermeameter stems both from its interesting measurement characteristics (i.e., divergent flow geometry) and the ease with which it is adapted to the special needs of this study. With this test system, 1) all measurements, regardless of sample support, are made subject to consistent boundary conditions and flow geometries; 2) measurements are non-destructive, allowing all data to be collected from the same physical sample; and, 3) measurements are precise, subject to small and consistent measurement error. Although other instruments (e.g., slug, well, or tracer tests) could be adapted to meet these criteria, testing would be limited to 10's of measurements. The fast, inexpensive measurements provided by the minipermeameter allow the collection of 1000's

to 10,000's of data points, a necessity of such studies. Below we describe the Multi-Support Permeameter and sampling strategy in more detail.

Multi-Support Permeameter (MSP)

Permeability data are acquired by simply compressing a tip seal against a flat, fresh rock surface while injecting gas at a constant pressure. Using information on the seal geometry, gas flow rate, gas injection pressure, and barometric pressure, the permeability is calculated using a modified form of Darcy's Law [Goggin et al., 1988]. Automation of this process is achieved with the MSP, which is comprised of a minipermeameter coupled with an x-y positioner and computer control system. The minipermeameter functions as the measurement device of the MSP and consists of four electronic mass-flow meters (0-50, 0-500, 0-2000, and 0-20,000 cm^3/min. at standard conditions), a pressure transducer (0-100 kPa gauge), a barometer, and a gas temperature sensor that are all connected to a regulated source of compressed nitrogen. Measurements are made according to a user specified sampling grid programmed into the x-y positioner. Along with locating the tip seal for sampling, the positioner also compresses the tip seal squarely against the rock surface with a consistent and constant force. The electronic permeameter and x-y positioner are configured with a computer control system to govern the data acquisition process and provide unattended operation of the MSP. A full description and analysis of the MSP is given in Chapter 2.

Gas is directed into the rock sample via the tip seal (Figure 3.1). The tip seal is comprised of a milled aluminum housing to which a disk-shaped seal of molded silicone rubber is affixed. Measurements are made at different sample supports, subject to consistent boundary conditions and flow geometries, by simply varying the radius of the tip seal. Four tip seals each of different size are employed in this study. These specially

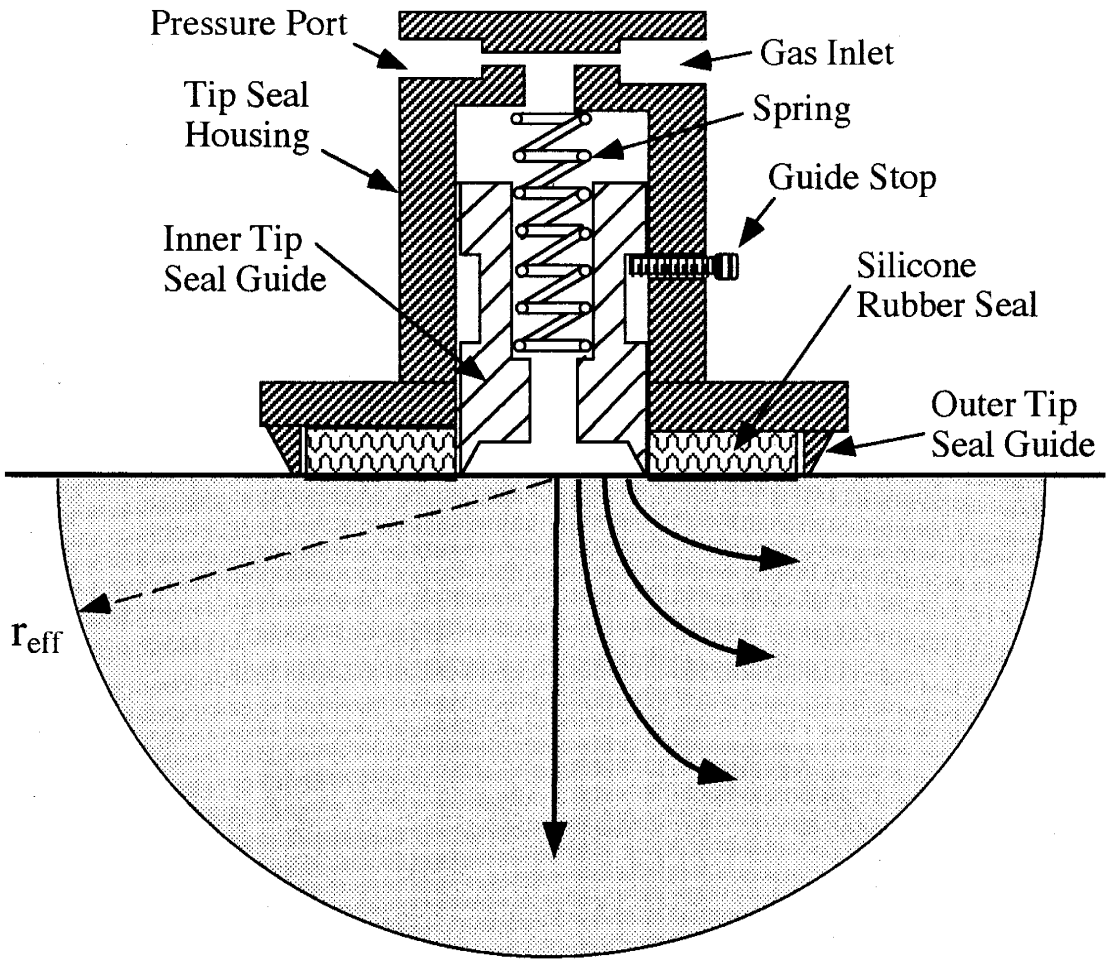

Figure 3.1. Schematic of an MSP tip seal and the corresponding gas flow field formed during measurement. Note the strongly diverging gas flow paths.

designed tip seals have inner radii r_i of 0.15, 0.31, 0.63, and 1.27 cm, while the outer radii, r_o, is $2r_i$ (twice the inner radii). In efforts to control the tip seal geometry under compression, and thus the boundary conditions under which measurements are made, each tip seal is equipped with a spring driven inner guide. In addition, the smaller tip seals (<0.63 cm), which are prone to distortion under compression, are equipped with an immobile outer guide.

The geometry of the tip seal largely dictates the nature of the resulting gas flow field in the porous medium (Figure 3.1). Where the rock sample can be characterized as a homogeneous, isotropic, semi-infinite half-space, the bounding surface of the resultant gas flow field will approximate a hemisphere [Goggin et al., 1988]. The effective radius, r_{eff}, of the bounding surface is governed primarily by the size of the tip seal, which we define by r_i, while the geometry of the flow paths beneath the tip seal is controlled by the ratio r_o/r_i, which is kept constant in this study. Probably the most important aspect of the minipermeameter flow field is the highly divergent nature of the flow paths. Beyond its effect on the shape of the weighting function, as shown below, the non-uniform flow field imparted by the MSP exerts significant influence on the manner with which the permeability upscales [e.g., Desbarats 1982a; Indelman and Abramovich, 1994].

The MSP is designed for laboratory investigation of meter-scale blocks of rock. Blocks are preferred because they provide multiple surfaces for sampling, with each oriented parallel to an inferred principal axis of permeability. Blocks also provide a test medium that is thick relative to the depth of penetration of any permeameter measurement. Sampling of a block proceeds by making measurements on a single face with each tip seal, then flipping the rock and repeating the process. Measurements are made with each tip seal according to the same regular grid. To avoid boundary effects on the measurements, the

grid is located away from the edges of the block. The grid spacing is selected so as to yield exhaustive spatial coverage of the sampling domain with the smallest tip seal while the dimensions of the grid are dictated by the scale of the heterogeneity (including 3-4 correlation length scales where possible). However, compromise in the grid spacing and dimensions is often required due to the total number of sampling points and hence the time required to sample the grid.

Test Media and Sampling Grid

For this study, permeability data were acquired from a 0.3 by 0.3 by 0.3 m block of Berea Sandstone obtained from Cleveland Quarries in Amherst, Ohio. The Berea Sandstone was selected for testing because it is commonly used in laboratory studies and, more importantly, because it is relatively homogeneous. It was our intention in this study to avoid samples exhibiting strong structural features that may significantly alter the flow geometry and hence the nature of the weighting function associated with the MSP. By visual inspection (Figure 3.2a), the sample may be characterized as a very-fine grained, well-sorted, quartz sandstone. The sample is relatively featureless except for faint, subhorizontal lamination.

Measurements were collected from all six faces of the sandstone sample. For each face, measurements were made on the exact same grid using the 0.15, 0.31, 0.63, and 1.27 cm r_t tip seals with no movement of the MSP or rock sample during the duration of sampling. The sampling grid contained 576 measurement points organized on a square 24 by 24 lattice on 0.85 cm centers. The total size of the grid was 19.5 by 19.5 cm. Sampling with the four tip seals yielded 2304 permeability measurements on each face; a total of 13,824 measurement over the entire block. Here, we limit our presentation to a single block face cut normal to the lamination, designated as Face 2, as the general results for all six faces are similar.

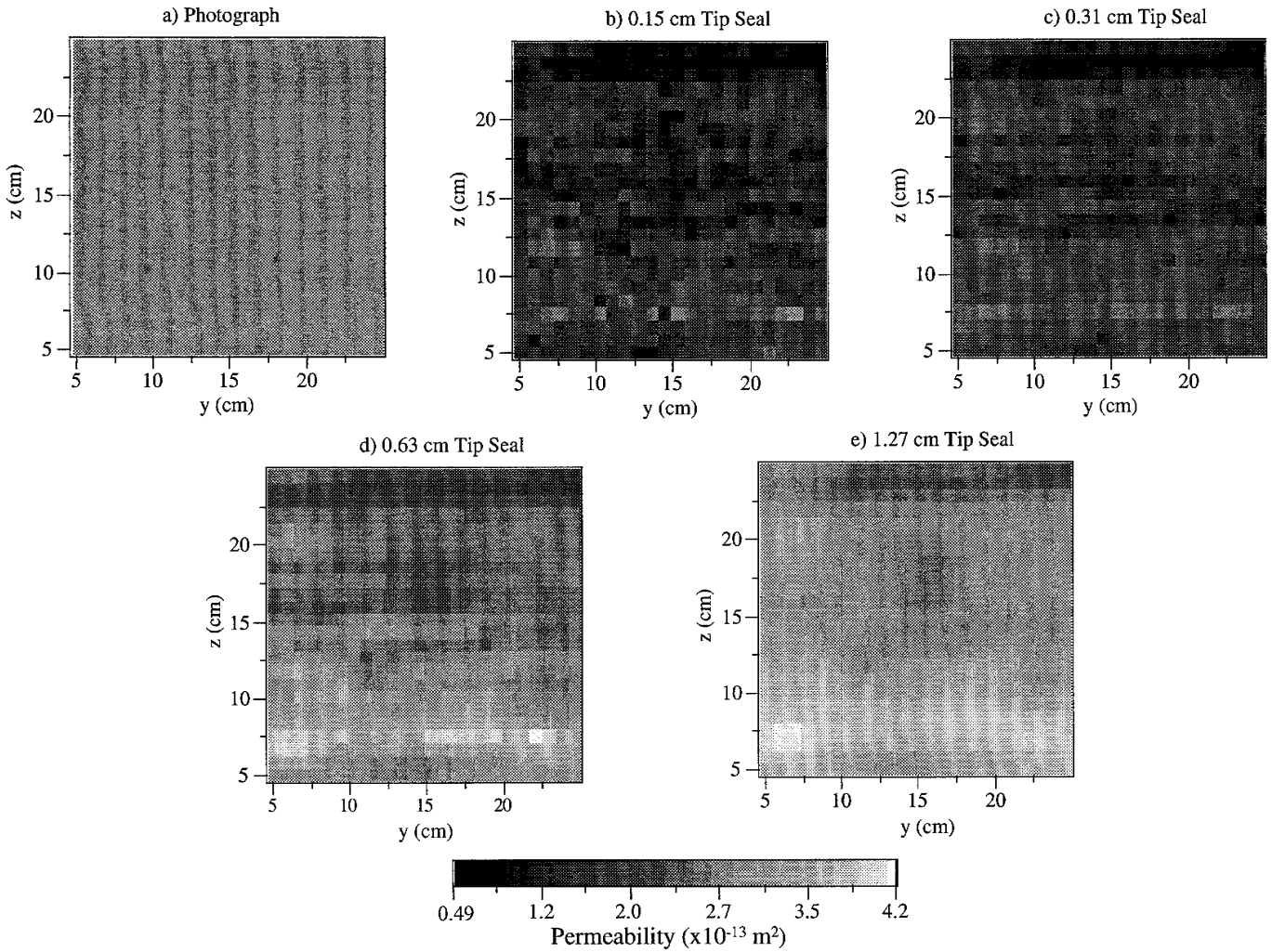

Figure 3.2. Photograph a) of Face 2 of the Berea Sandstone sample showing the area sampled with the MSP. The corresponding permeability fields (where k is in m^2) measured with the b) 0.15, c) 0.31, d) 0.63, and e) 1.27 cm r_f tip seals are also given. Data were collected on a 24 by 24 point sampling grid with 0.85 cm centers. Sample domain size was 19.5 by 19.5 cm. Note that the grid origin is located approximately 5 cm from the block edges.

Calculation of Weighting Functions

Linear filter analysis of the multi-support permeability data sets begins with the Fourier transform of Equation 3.1. If

$$\hat{k}(\bar{u}) = \int_{-\infty}^{\infty} \exp[-2\pi i \bar{u} \cdot \bar{x}] k(\bar{x}) d\bar{x} \tag{3.3}$$

denotes the Fourier transform of k (where the integral is a multiple integral) then Equation 3.1 becomes

$$\hat{k}_m(\bar{u}) = \hat{\beta}_{mo}(\bar{u}) \hat{k}_o(\bar{u}) \tag{3.4}$$

where m designates the sample support, $\bar{u}$ is the spatial frequency vector, $\bar{x}$ is the position vector, $\hat{k}_m$ is the Fourier transform of k_m, and $\hat{\beta}_{mo}$ is the Fourier transform of β_{mo}. The advantage of working in the frequency domain is that the integral in Equation 3.1 is replaced by a simple multiplicative relation. With data available at several sample supports, say m=i and j, we can find a frequency domain expression for $\hat{\beta}_{ij}$, relating the permeability measured with one sample support i with that collected at any other j, similar to that given in Equation 3.4:

$$\hat{k}_i(\bar{u}) = \hat{\beta}_{ij}(\bar{u}) \hat{k}_j(\bar{u}) \tag{3.5}$$

By making measurements with four different-sized tip seals, we have data at four different sample supports. The four data sets can be paired in six different ways thus allowing six unique weighting functions β_{ij} to be calculated.

The weighting function $\hat{\beta}_{ij}$ in the frequency domain is calculated from the permeability data sets at sample supports i and j according to the simple relation [Shumway, 1988]

$$\hat{\beta}_{ij}(\bar{u}) = \frac{f_{ij}(\bar{u})}{f_{jj}(\bar{u})} \tag{3.6}$$

where f_{jj} is the (auto-) spectral density function of the permeability data set measured with sample support j and f_{ij} is the cross-spectral density function calculated between permeability data sets measured with sample supports i and j. The auto- and cross-spectral density functions are given by

$$f_{ij}(\bar{u}) = \int_{-\infty}^{\infty} \exp[-2\pi i \bar{u} \cdot \bar{s}] C_{ij}(\bar{s}) d\bar{s} \tag{3.7}$$

where $C_{ij}(\bar{s}) = \mathrm{cov}\left[k_i(\bar{x} - \bar{s}), k_j(\bar{x})\right]$ and $\bar{s}$ is the separation vector. The spectral density is a measure of the variance of $k_j(\bar{x})$ distributed over frequency. In practice the spectral density can be estimated by multiplying the Fourier transform of the data set $\hat{k}_j$ by its complex conjugate $\hat{k}_j^*$

$$f_{jj}(\bar{u}) = \hat{k}_j(\bar{u})\hat{k}_j^*(\bar{u}) \tag{3.8}$$

Similarly, the cross-spectral density function, f_{ij} is given by

$$f_{ij}(\bar{u}) = \hat{k}_i(\bar{u})\hat{k}_j^*(\bar{u}) \tag{3.9}$$

where we have arbitrarily taken i to correspond to the data set from the larger of the two tip seals.

The spectral functions defined in Equations 3.8 and 3.9 are calculated from the measured permeability data sets after transformation into the frequency domain via the Fourier transform. Prior to taking the transform each permeability data set is normalized to mean zero. A Fast Fourier Transform (FFT) algorithm is employed and the data sets are padded with zeros to form a 32 by 32 matrix. The discrete Fourier transform is then

$$\hat{k}_i(\bar{u}) = 576^{-1/2} \sum_{x_1=0}^{31} \sum_{x_2=0}^{31} k_i(\bar{x}) \exp[-2\pi i \bar{u} \cdot \bar{x}] \tag{3.10}$$

where 576 is the number of permeability data values, $\bar{x} = (y,z)$, and $\bar{u} = (u_1,u_2)$. Because we are manipulating discrete Fourier transforms, neither the spectral density function nor the cross-spectral density function is guaranteed to converge in any statistical sense to a limiting value as the number of observations increases [Jenkins and Watts, 1968]. For this reason, the spectral functions estimated in Equations 3.8 and 3.9 must be smoothed prior to their use in Equation 3.6. In our analysis we employ a simple moving window average characterized by a circular geometry, three point radius (29 total points), and uniform weighting. The corresponding bandwidth, the ratio of window size to padded domain size, is approximately 0.03. Other window sizes and shapes were investigated and determined to have relatively minor influence on the shape and magnitude of β_{ij}.

In general the cross-spectral density, f_{ij}, is complex as is the weighting function, $\hat{\beta}_{ij}$. To simplify the presentation and interpretation of $\hat{\beta}_{ij}$, it is separated into two real parts, one corresponding to the amplitude change between the *i*th and *j*th data series and the other corresponding to the phase shift. The weighting function amplitude change or gain G_{ij} and phase shift ϕ_{ij}, respectively, are given as:

$$G_{ij}(\bar{u}) = \frac{\left(c_{ij}^2(\bar{u}) + q_{ij}^2(\bar{u})\right)^{1/2}}{f_{jj}(\bar{u})} \tag{3.11}$$

$$\phi_{ij}(\bar{u}) = \tan^{-1}\left(\frac{q_{ij}(\bar{u})}{c_{ij}(\bar{u})}\right) \tag{3.12}$$

where c_{ij} and q_{ij} correspond to the real and complex parts of the cross-spectral density function, respectively.

The final step in the procedure is to find the weighting function in the spatial domain, β_{ij}. This is accomplished by taking the inverse Fourier transform of $\hat{\beta}_{ij}$

$$\beta_{ij}(\bar{x}) = 576^{-1/2} \sum_{u_1=0}^{31} \sum_{u_2=0}^{31} \hat{\beta}_{ij}(\bar{u}) \exp[2\pi i \bar{u} \cdot \bar{x}] \tag{3.13}$$

Note that the calculated weighting function, β_{ij}, is defined in terms of two sample supports (tip seal sizes), each of finite dimension. With these exhaustive data sets it is also possible to obtain a non-unique estimate for β_{mo}, which relates the point-support permeability (associated with an infinitely small sample support) with that measured over some larger support *m*; however, such analyses are beyond the scope of this paper.

The point-support permeability k_o varies in three-dimensions, and each measurement k_m is a function of that three-dimensional distribution. However, the permeability data are collected from discrete rock faces on a two-dimensional grid and sampling of the third dimension is not possible. Consequently the estimates of β_{ij} presented below are two-dimensional. Nevertheless, our results demonstrate that the two-dimensional analyses provide useful insight into the spatial weighting characteristics of the MSP and the effective radius of measurement. Quantitative modeling of the empirical weighting functions will require a better understanding of the three-dimensionality of this problem, and hence is a subject of current investigation.

3.4. Results

Spatial Permeability Data

The two-dimensional permeability fields measured with the 0.15, 0.31, 0.63, and 1.27 cm r_l tip seals on Face 2 of the Berea Sandstone sample are given in Figure 3.2. Inspection of the fields reveals that the lamination faintly visible (to the eye) in the sampled rock face (Figure 3.2a) correlates with the modest anisotropy exhibited in each of the permeability fields (Figure 3.2b-e). Other notable features include the evident smoothing of the permeability fields with increasing sample support, and consistency of high- (e.g., z=7.5 cm) and low-permeability laminae (e.g., z=22.5-25 cm) among the different fields. In fact, the noted spatial trends can be traced across the other three block faces oriented normal to lamination (e.g., see Figures 2.6 and 4.1).

The cumulative distribution functions (CDFs) for the permeability data measured with each of the four tip seals are given in Figure 3.3. The CDFs are characterized by a small range, low variance, and essentially non-Gaussian behavior (the natural-log

permeabilities are likewise characterized by a non-Gaussian distribution). Distinct trends with changing sample support are evident. The sample mean is seen to increase with increasing sample support ($E[k_I(\bar{x})]$=1.35, 1.48, 2.71, and 3.11x10^{-13} m^2, respectively) while the sample variance fluctuates ($Var[k_I(\bar{x})]$=1.57, 1.35, 2.72, and 1.92x10^{-27} m^4, respectively). Although the permeability fields exhibit distinct "smoothing" with increasing tip seal size (Figure 3.2) the sample variance does not reflect this behavior because of the influence of the increasing mean permeability.

Spatial correlation of the permeability field was investigated by calculating the spectral density function and semivariogram for the data acquired with each tip seal. Two-dimensional spectral density functions were calculated according to Equation 3.8, while two-dimensional semivariograms were calculated by taking the inverse Fourier transform of the spectral density function then subtracting the result from the sample variance. The two-dimensional spectral density function and semivariogram calculated from the 1.27 cm

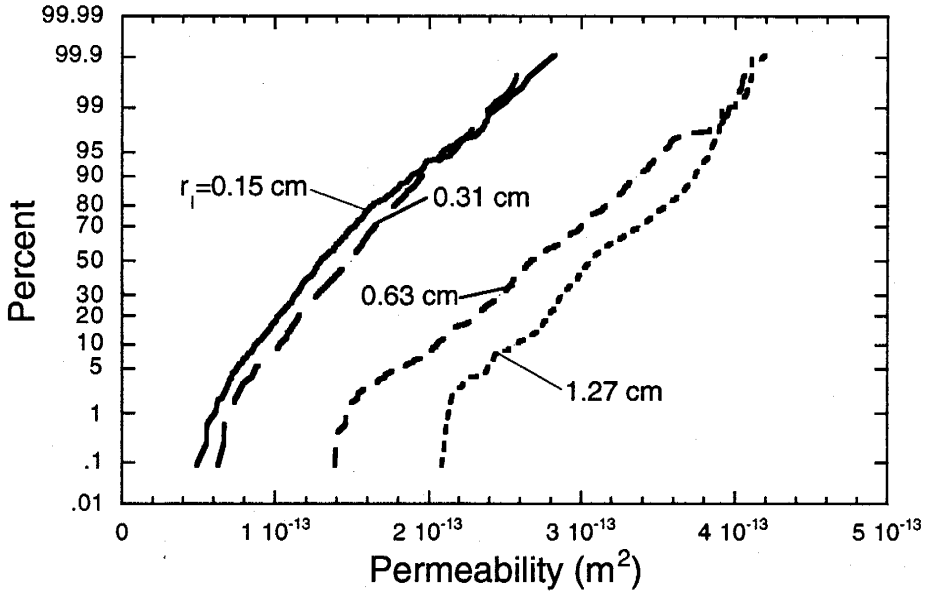

Figure 3.3. Cumulative distribution functions for the permeability data sets given in Figure 3.2. Each curve represents 576 measured permeability values.

tip seal data set are plotted in Figure 3.4. The spectral density function is anisotropic with a single peak centered at the origin. The anisotropy is evidenced by the increased energy (variance) normal to lamination compared to that parallel to lamination. Likewise, the semivariogram shows strong spatial correlation parallel to the lamination (beyond the length of the semivariogram) and weaker correlation orthogonal to lamination. Although data from all four tip seals yield similar frequency/spatial structures, distinct trends in the magnitude and continuity of the functions are evident. The central peak of the spectral density function increases in magnitude but becomes more narrow as tip seal size (sample support) is increased, while the semivariogram range increases and the sill decreases.

Linear Filtering

Weighting functions in the frequency and spatial domain have been calculated for all possible pairings of the four permeability data sets acquired from Face 2 of the Berea Sandstone. Similar analyses were conducted for the other faces of the Berea Sandstone (not shown) and the basic results and trends noted here hold for them as well.

Our analysis begins in the frequency domain where we find the calculated weighting functions to be symmetric and centered on zero frequency. This implies that the phase shift is effectively zero, and thus the gain function (Equation 3.11) fully characterizes the weighting function in the frequency domain $\hat{\beta}_{ij}$. The two-dimensional gain functions calculated between the 0.31 and 0.15 cm tip seal data sets and the 1.27 and 0.15 cm tip seal data sets (designated as the 0.31-0.15 cm filter and 1.27-0.15 cm filter, respectively) are given in Figure 3.5. These represent the cases for the least and greatest difference between tip seal size or, equivalently, sample support. To assist in the interpretation, vertical (normal to lamination) and horizontal (parallel to lamination) transects taken through the two-dimensional gain functions are plotted in Figure 3.6.

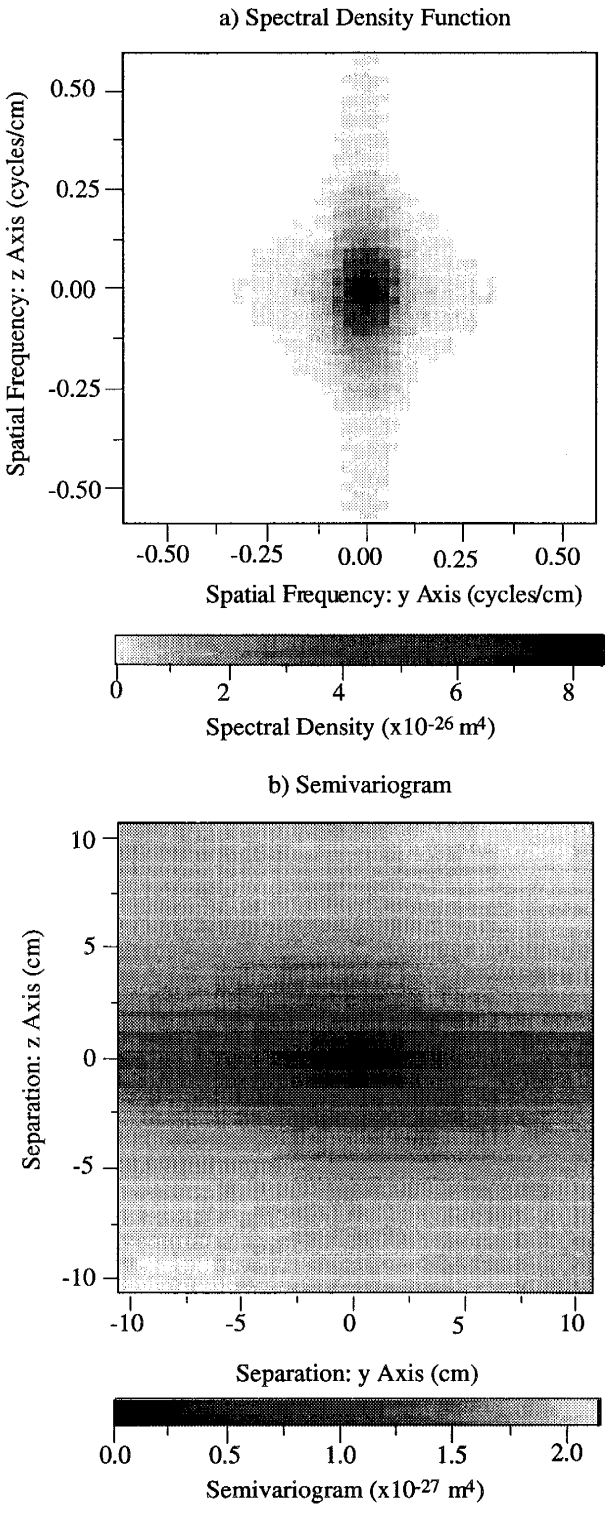

Figure 3.4. Two-dimensional a) spectral density function and b) semivariogram calculated from the permeability data collected with the 1.27 cm r_1 tip seal on Face 2 of the Berea Sandstone sample.

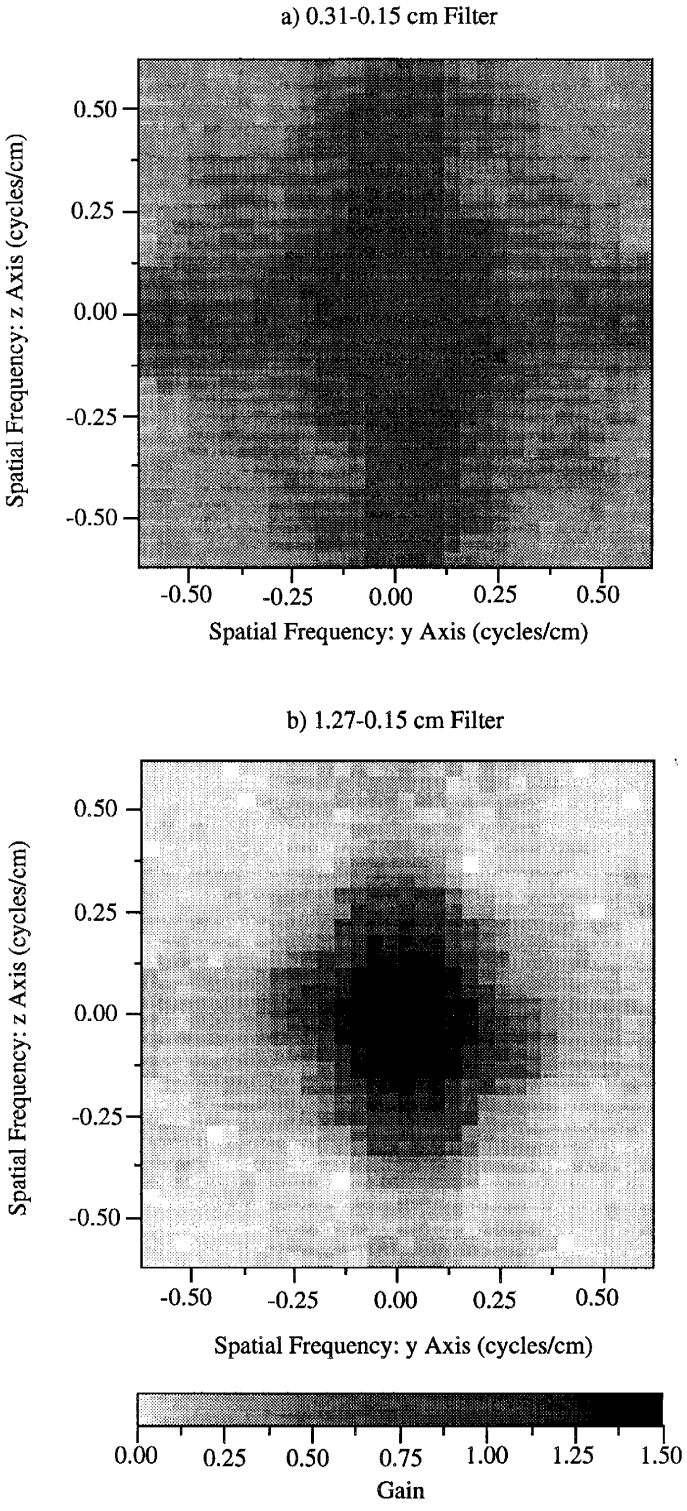

Figure 3.5. Two-dimensional gain functions (frequency domain) relating measurements made with the 0.15 cm tip seal with that measured with the a) 0.31 cm tip (0.31-0.15 cm filter) and b) the 1.27 cm tip (1.27-0.15 cm filter).

Several important features are evident in the plotted gain functions. First, both functions have a general parabolic shape centered on zero frequency. This suggests that the spatial weighting imparted by the minipermeameter is not uniform but rather decreases radially from the center of the tip seal (uniform weighting would yield a delta function response in the frequency domain). Second, the gain function also narrows as the difference in tip seal size increases. This implies that the effective radius of the measurement increases with increasing tip seal size. Third, slight anisotropy in both functions is noted as exhibited by larger gain values normal to lamination.

Another important feature is the magnitude of the gain function at zero frequency. According to the definite integral property of the Fourier transform [Bracewell, 1986], the gain should have a magnitude of one at zero frequency if the corresponding weighting

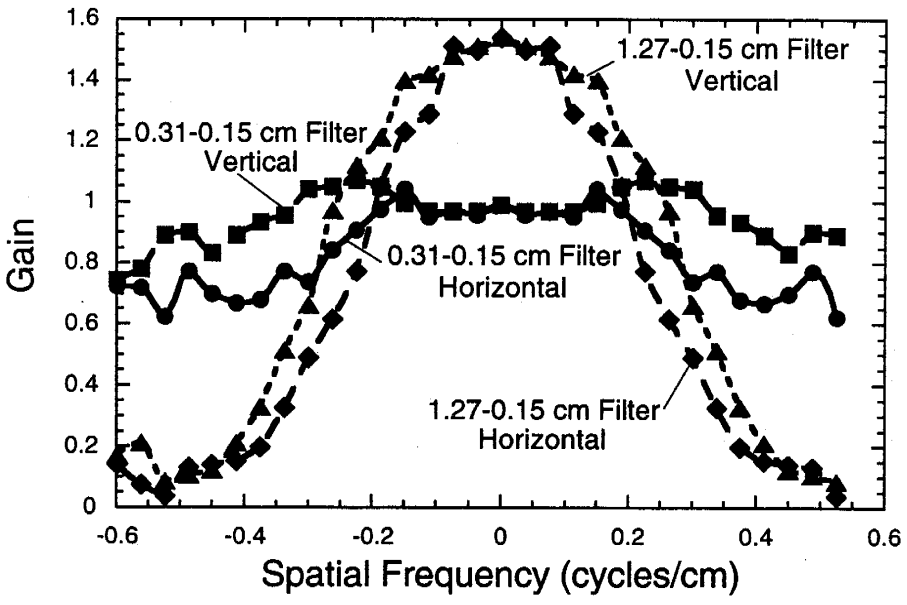

Figure 3.6. Gain function transects oriented parallel and normal to sample lamination and centered on zero frequency. Shown are transects through the 0.31-0.15 and 1.27-0.15 cm filters given in Figure 3.5.

function in the spatial domain is to integrate to one (see Equation 3.2). While the 0.31-0.15 filter meets this criterion the 1.27-0.15 cm filter has a magnitude much greater than one at zero frequency. In fact, all the calculated gain functions except the 0.31-0.15 cm filter have magnitudes exceeding one at zero frequency.

The cause of this discrepancy has its roots in the linear filter model (Equation 3.1). One important assumption of the model is that the field property being filtered upscales according to a arithmetic averaging process. The permeability data collected from the Berea Sandstone obviously do not upscale according to an arithmetic average as shown by the sample mean, which increases with increasing sample support. Although each data set is normalized to mean zero prior to analysis, the variance is not adjusted. Differences between the measured variance reduction and that modeled by an arithmetic averaging process ultimately bias the magnitude of the calculated gain function.

Two different approaches are explored to constrain the calculated weighting functions according to the criterion specified in Equation 3.2. In the first approach a consistent permeability transform that accounts for the variance upscaling is sought (e.g., log-transform). The second is an *ad hoc* approach that involves a rescaling of the gain function by its magnitude at zero frequency.

Consider a field variable, for example permeability, that upscales according to a simple linear transform. The upscaled permeability k_i can be represented as a spatial power-average [e.g., Korvin, 1981; Deutsch, 1989; Desbarats 1992b] of the permeabilities measured over a smaller support k_j subject to the spatial weighting as quantified by β_{ij}

$$k_i^{\omega}(\bar{x}) = \int_V \beta_{ij}(\bar{\xi}, \omega) k_j^{\omega}(\bar{x} - \bar{\xi}) d\bar{\xi} \quad \text{for } \omega \neq 0 \tag{3.14a}$$

$$\ln k_i(\bar{x}) = \int_V \beta_{ij}(\bar{\xi}, \omega) \ln k_j(\bar{x} - \bar{\xi}) d\bar{\xi} \quad \text{for } \omega = 0 \tag{3.14b}$$

where ω is the power exponent. Filter analysis via Equation 3.14 is accomplished by simply applying a consistent transform to each data set prior to analysis. Weighting functions for ω= -1 (harmonic average), 0 (geometric average), 1 (arithmetic average), and 2 were calculated using the Berea Sandstone permeability data sets. An example of the results is given in Figure 3.7 that shows a transect oriented parallel to lamination through the gain function of the 0.63-0.31 cm filter. Although not shown, the same general behavior and trends are found in the other coordinate directions and for the other gain functions.

There are a number of notable features evident in the gains calculated from the transformed data. First, the magnitude of the gain function decreases as ω decreases

$$\left[G_{ij}(\bar{u})\right]_{\omega=2} > \left[G_{ij}(\bar{u})\right]_{\omega=1} > \left[G_{ij}(\bar{u})\right]_{\omega=0} > \left[G_{ij}(\bar{u})\right]_{\omega=-1}$$

(see Figure 3.7). Second, the ratio between gain functions calculated with different ω's is not constant for functions associated with different tip seal pairs *i, j* (not shown):

$$\frac{\left[G_{0.31,0.15}(\bar{u})\right]_{\omega=2}}{\left[G_{0.31,0.15}(\bar{u})\right]_{\omega=1}} \neq \frac{\left[G_{1.27,0.15}(\bar{u})\right]_{\omega=2}}{\left[G_{1.27,0.15}(\bar{u})\right]_{\omega=1}} \neq \frac{\left[G_{0.63,0.31}(\bar{u})\right]_{\omega=2}}{\left[G_{0.63,0.31}(\bar{u})\right]_{\omega=1}} \cdots$$

Third, different values of ω are required to achieve $G_{ij}(0) = 1$ for different tip seal pairs. For the case of the 0.63-0.31 cm filter an ω between 0 and 1 is needed (Figure 3.7) while for the 0.31-0.15 and 1.27-0.63 cm filters an ω between 1 and 2 is required. The noted inconsistencies between gain functions largely reflects the behavior of the variance upscaling.

The difficulty involved with finding a value of ω, by trial and error, that yields $G_{ij}(0) = 1$ is obvious. For this reason, we explore an alternative approach in which we rescale the gain function by its value at zero frequency

$$\breve{G}_{ij}(\bar{u}) = \frac{G_{ij}(\bar{u})}{G_{ij}(0)} \tag{3.15}$$

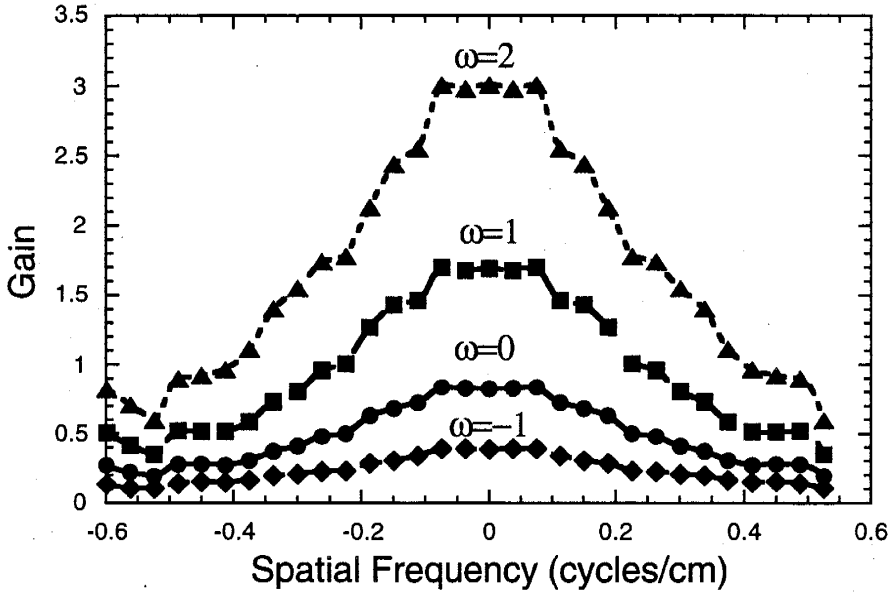

Figure 3.7. Comparison of gain functions calculated for the spatial power-average (Equation 3.14) with ω=-1, 0, 1, and 2. Shown are gain function transects oriented parallel to sample lamination for the 0.63-0.31 cm filter.

where $\breve{G}_{ij}$ is the rescaled gain function. In effect, the rescaling simply normalizes the linear filter calculations for the bias introduced by the variance (magnitude of the function) while retaining the spatial/frequency characteristics of the weighting function. While this is an *ad hoc* approach, it can be justified under certain circumstances as we show below.

To explore this approach, we employed Equation 3.15 to rescale the gain functions for the 0.63-0.31 cm filter calculated for different values of ω (Figure 3.7). Results are plotted in Figure 3.8 showing that the rescaled gain functions collapse onto a single function. Rescaling was likewise performed for each of the other tip seal pairs (not shown) yielding similar results to that given in Figure 3.8. What this means is that the calculated weighting functions are essentially independent of ω except for a simple rescaling by their magnitude at zero frequency. This result can be verified theoretically for variables that have low variance and are jointly (within and between data sets) log-normal (see Section 3.6). Thus, the physical data (Figure 3.8) combined with the theoretical analysis (Section 3.6) are consistent with our simple rescaling of the gain function.

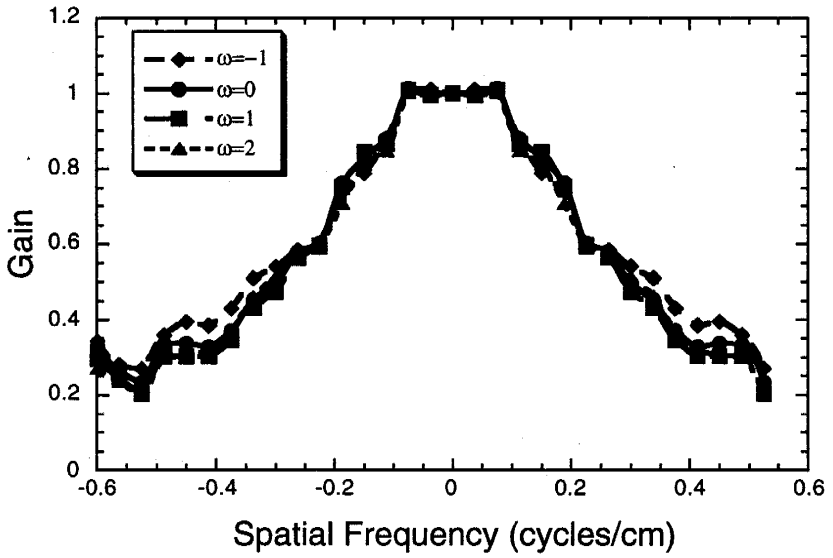

Figure 3.8. Gain function transects given in Figure 3.7 rescaled according to Equation 3.15.

Empirical weighting functions in the spatial domain (Equation 3.13) have been calculated from the rescaled gain functions associated with the Berea Sandstone data. Two-dimensional weighting functions for the 0.31-0.15 and 1.27-0.15 cm filters are given in Figure 3.9 while corresponding transects taken parallel to lamination through the 0.31-0.15, 0.63-0.31, and 1.27-0.15 cm filters are given in Figure 3.10. Inspection of the data reveals that each empirical weighting function is centered on the point of measurement (i.e., k_i) and decays according to a non-linear function of radial distance. Consistent trends between weighting functions calculated for different tip seal pairs are also evident. Specifically, as the difference in tip seal size (i.e., $\Delta r = r_i - r_j$) is increased the magnitude of the weighting function decreases while the spread of the function increases. Although anisotropy in the gain functions is evident (Figure 3.6) only a faint indication of anisotropy is found in the calculated weighting functions shown in Figure 3.9. As a check on the calculated weighting functions we integrated each over the full sampling domain and found their volumes to all equal 1, consistent with the criterion for a weighting function (Equation 3.2).

To aid in the description of the empirical weighting functions we have fit a simple model to the data. Note that the modeling is not intended to rigorously quantify weighting function behavior but simply to serve as a basis for comparison. Because the empirical weighting functions are only faintly anisotropic we use a radially symmetric, isotropic Gaussian model

$$\beta_{ij}(r) = \frac{1}{a_{ij}^2}\exp\left[-\frac{\pi r^2}{a_{ij}^2}\right] \tag{3.16}$$

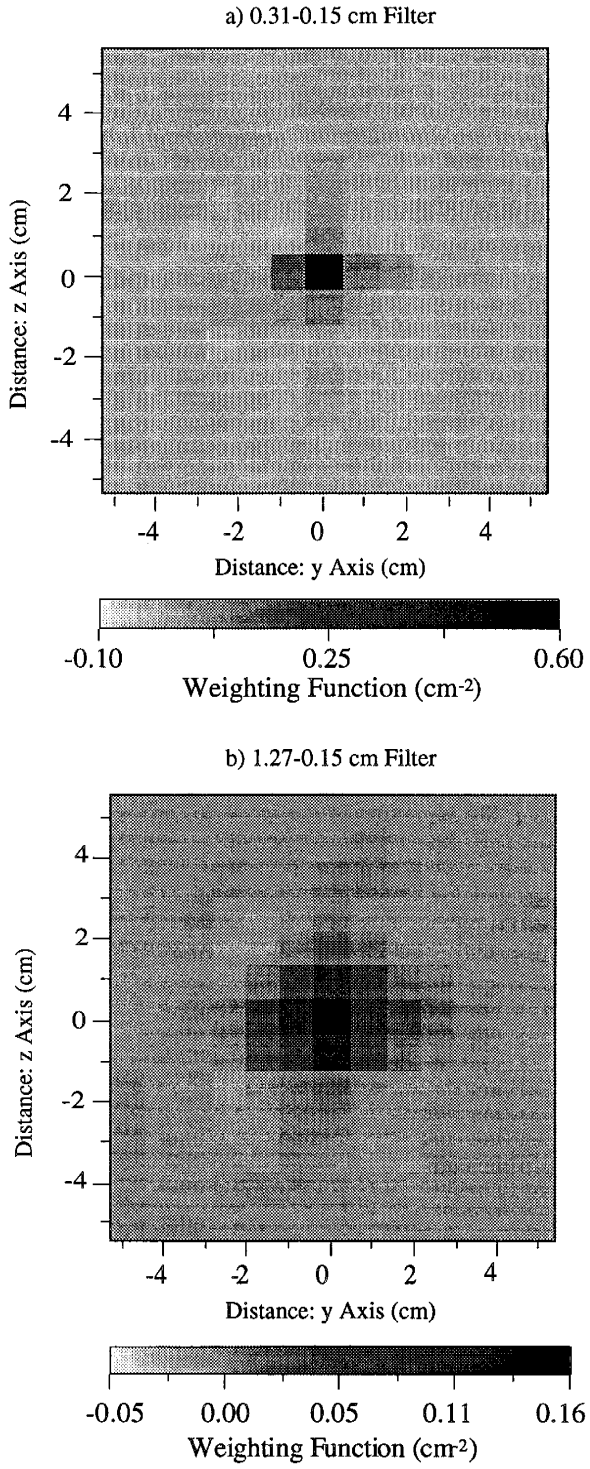

Figure 3.9. Two-dimensional weighting functions (spatial domain) relating measurements made with the 0.15 cm tip seal with that measured with the a) 0.31 cm tip (0.31-0.15 cm filter) and b) the 1.27 cm tip (1.27-0.15 cm filter). The weighting functions have been truncated at a distance of 5 cm from the center of measurement (i.e., k_i) as their magnitude is essentially zero beyond this point. Also note that different gray-scales have been employed in (a) and (b) because of the significant difference in peak values between the two weighting functions.

where a_{ij} is a model coefficient (cm) and r is radial distance (cm). Fitting of the model to the data in Figure 3.10 was accomplished by determining the value of a_{ij} from the relation $a_{ij} = \sqrt{\beta_{ij}^{-1}(0)}$. We rejected fitting an anisotropic model to the data as differences in the weighting functions along different coordinate axes were not statistically significant. The Gaussian model provides a good fit to the general shape of the calculated weighting functions; however, the model does not perfectly fit the data, particularly in the vicinity of the right shoulder.

Although it is apparent that the magnitude of the weighting function decreases as the difference in the tip seal size increases (i.e., Δr), the accompanying increase in the spread of the function is not easily discerned in the transects plotted in Figure 3.10. We investigate this point with the aid of the fitted Gaussian model. We note that the Gaussian model integrates to one (Equation 3.2) for any value of a_{ij} and the empirical weighting functions

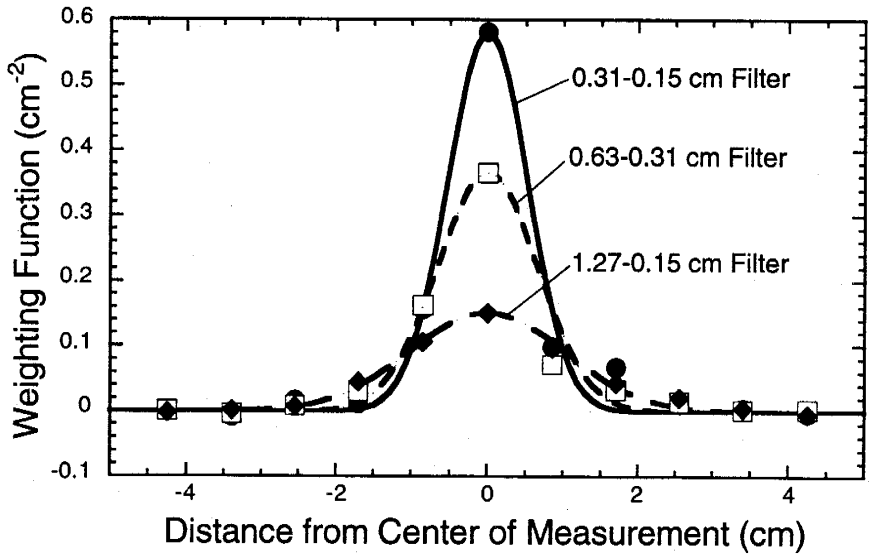

Figure 3.10. Weighting function transects (symbols) oriented parallel to sample lamination for the 0.31-0.15, 0.63-0.31, and the 1.27-0.15 cm filters. A radially symmetric, isotropic Gaussian model (Equation 3.16) has been fit to each transect (solid lines).

(Figure 3.9) also integrate to one. Thus, the reduction in the peak magnitude is accompanied by a proportional increase in the spread of the function, such that the integrated magnitude of the weighting function is preserved. As seen in Figure 3.10, this behavior leads to relatively minor changes in the magnitude of the weighing function at radial distances beyond 1 cm.

3.5. Discussion and Conclusions

We now review our results in light of the four questions raised in the introduction to this paper and end with a discussion of unresolved issues.

Calculating Spatial Weighting Functions from Physical Data

The most important aspect of this work is that the spatial weighting functions were calculated directly from physical data, not inferred from theoretical arguments or numerical simulations. In this way, the presented results provide rare physical evidence of a hydraulic instrument functioning as a linear filter. This analysis was made possible by a unique set of permeability data collected from a block of Berea Sandstone. Spatially exhaustive permeability data sets measured at four different sample supports, each subject to consistent flow geometries and boundary conditions, formed the basis of the analysis. Empirical weighting functions in both the frequency and spatial domains were calculated that relate 576 permeability data acquired at one sample support with the same number of data collected at another larger support. Arguments concerning the validity of the calculated weighting functions are given below.

Measurement Physics Versus the Empirical Weighting Function

The characteristics and behavior of the empirical weighting functions are consistent with the basic physics governing gas flow from a minipermeameter tip seal. Specifically, the weighting functions are centered on the measurement, consistent with the symmetry of the tip seal. Each of the weighting functions decay according to a nonlinear function of

radial distance (see the fitted Gaussian model in Figure 3.10). This nonlinear behavior is consistent with the strongly divergent flow geometry imparted by the minipermeameter. The data indicate that the shape of the weighting function changes in a predictable manner as tip seal size is varied. As the difference in tip seal size increases the peak magnitude of the weighting function decreases while the spread of the function increases. In physical terms this suggests that as the tip seal size becomes larger the effective radius of the measurement, and thus the sample support, increases.

Weighting Functions for Non-Additive Properties

The calculation of weighting functions for non-additive properties like permeability was verified both empirically and theoretically. We showed empirically that the calculated weighting functions were independent of the spatial averaging process (ω value) except for a rescaling of the gain function by its magnitude at zero frequency (Figure 3.8). This result was then verified theoretically for permeabilities that are jointly log normal and subject to low variance (see Section 3.6). In fact, our data suggest that the jointly log normal assumption is not a rigid constraint. Where these limiting assumptions are not met it may still be possible to employ linear filter theory by applying a consistent transform to the data prior to analysis (as was done with the power-average transform). However, difficulties in identifying an appropriate transform and the questionable utility of a weighting function specific to a "non-standard" transform renders this approach a difficult choice.

Implications for Other Instruments

Although we have focused on data collected with a minipermeameter, our results have important implications for a variety of other instruments commonly employed in hydraulic testing. Of general significance is the fact that the empirical weighting functions are consistent with that which would be predicted for a minipermeameter based on our understanding of the measurement physics of the instrument. This result suggests that considerable insight into the weighting characteristics of an instrument (e.g., slug or pump

tests) can be achieved with theoretical modeling. This also suggests that the characteristics of the weighting function are strongly influenced by the instrument; however, whether weighting functions can be formulated independent of the characteristics of the porous medium, as assumed by Cardwell and Parsons [1945], Moltyaner [1989], Maneval et al. [1990], Oliver[1990], Knight [1992], and Desbarats [1992a], needs further investigation (see below). Our analysis demonstrates that extensive data are required to empirically calculate a weighting function. The collection of such exhaustive data sets for filter analysis of slug or pump tests would be a logistical nightmare, if possible at all. Tests using surrogate instruments like the minipermeameter are thus needed to further investigate the relationship between weighting functions, measurement physics, media heterogeneity, and the spatial averaging process.

Unresolved Issues

Although this study provides important insight into the linear filtering characteristics of a instrument, several critical questions remain to be answered. One of the most important is whether media heterogeneity/anisotropy influences the characteristics and behavior of the weighting function. We selected the Berea Sandstone for this study because it is considered "relatively" homogeneous and isotropic. Nevertheless, Figure 3.2 reveals modest permeability anisotropy, for which corresponding anisotropy was noted in the gain function. However, upon transformation to the spatial domain, the anisotropy was no longer statistically distinguishable in the weighting function. Additional studies with rocks exhibiting greater heterogeneity and anisotropy are needed.

Another question concerns the quantification of the calculated weighting functions. Here, we fit a Gaussian model to the data out of convenience; however, several other models $\left(\text{e.g., } f\left(\frac{1}{r^2}\right), f\left(\frac{1}{r^3}\right)\right)$ were found to fit the data equally as well. The highly non-linear shape of the empirical weighting functions, resulting from the non-uniform flow

geometry imparted by the minipermeameter tip seal, make it difficult to distinguish between models. The non-linear shape also makes it difficult to resolve small, but potentially important, changes in the weighting function. Specifically, changes in the shape (i.e., sample support) of the weighting function due to changing tip seal size (Figure 3.10) or due to anisotropy in the permeability field. Of course, the collection of data at even higher spatial resolution would help address this problem.

Although these studies have benefited from the spatially detailed permeability maps that formed the basis of analysis, the data are limited to two dimensions. Detailed collection of data in all three dimensions is problematic in porous media flow. This raises the question of how information from the third-dimension will affect the calculated weighting functions. If the third-dimension indeed affects the calculations, can the information gap be spanned without recourse to detailed sampling of the third-dimension?

3.6. Appendix: Spatial Power-Average and the Weighting Function

Weighting functions calculated from permeability data transformed according to differing spatial power-averages (ω) were found to collapse onto a single function upon rescaling (Figure 3.8). The purpose of this appendix is to explain this behavior and to determine what conditions are required for the weighting function to be effectively independent of ω (except for a simple rescaling by its magnitude at zero frequency, Equation 3.15).

Consider the field variable k_j, which is assumed to be stationary and ergodic, measured with support j. Further consider the transform $Y_j = \ln(k_j)$ with first and second moments defined by

$$E\left[Y_j(\bar{x})\right] = \mu_j$$
$$Var\left[Y_j(\bar{x})\right] = \sigma_{jj}$$
$$Cov\left[Y_i(\bar{x}-\bar{s}), Y_j(\bar{x})\right] = C_{ij}(\bar{s})$$

where $\bar{s}$ is the separation vector. If k_i and k_j are jointly (both within and between data sets) log-normal then

$$E\left[k_j^{\omega}(\bar{x})\right] = \exp\left[\omega\mu_j + \omega^2\sigma_{jj}/2\right] \tag{A1}$$

$$E\left[k_i^{\omega}(\bar{x}-\bar{s})k_j^{\omega}(\bar{x})\right] = \exp\left[\omega(\mu_i+\mu_j) + \omega^2\left(\sigma_{ii}+\sigma_{jj}+2C_{ij}(\bar{s})\right)/2\right] \tag{A2}$$

From Equations A1 and A2

$$Cov\left[k_i^{\omega}(\bar{x}-\bar{s}), k_j^{\omega}(\bar{x})\right] = A_{ij}\left[\exp\left[\omega^2 C_{ij}(\bar{s})\right]-1\right] \tag{A3}$$

where $A_{ij} = \exp\left[\omega(\mu_i+\mu_j) + \omega^2\left(\sigma_{ii}+\sigma_{jj}\right)/2\right]$. Expanding the exponential in Equation A3

$$Cov\left[k_i^{\omega}(\bar{x}-\bar{s}), k_j^{\omega}(\bar{x})\right] = A_{ij}\left[\omega^2 C_{ij}(\bar{s}) + \frac{\omega^4}{2!}C_{ij}^2(\bar{s}) + \frac{\omega^6}{3!}C_{ij}^3(\bar{s}) + ...\right] \tag{A4}$$

and taking the Fourier transform of Equation A4 we find the corresponding spectral density function

$$f_{ij}(\bar{u}) = \omega^2 A_{ij}\left[g_{ij}(\bar{u}) + \frac{\omega^2}{2!}g_{ij}^{[2]}(\bar{u}) + \frac{\omega^4}{3!}g_{ij}^{[3]}(\bar{u}) + ...\right] \tag{A5}$$

where $g_{ij}^{[\ ]}$ is the spectral density of C_{ij} raised to the power []. $g_{ij}^{[m]}$ is also the m-fold convolution of $g_{ij}^{[1]}$. Note that $C_{ij}^{[m]}(\bar{s}) = \sigma_{ij}^m \rho_{ij}^m(\bar{s})$ where ρ_{ij}^m is the correlation coefficient between data sets measured with supports *i* and *j*. Thus, as *m* increases ρ_{ij}^m will approach 0 for s≠0. The corresponding cross-spectral density function will become constant in the frequency domain, and if $\sigma_{ij} < 1$, will also approach 0. This is illustrated below for the exponential covariance. From Equation 3.6 the weighting function in the frequency domain $\hat{\beta}_{ij}$ is calculated by

$$\hat{\beta}_{ij}(\bar{u}) = \frac{f_{ij}(\bar{u})}{f_{jj}(\bar{u})} = \frac{A_{ij}}{A_{jj}}\left[\frac{g_{ij}(\bar{u}) + \frac{\omega^2}{2!}g_{ij}^{[2]}(\bar{u}) + \frac{\omega^4}{3!}g_{ij}^{[3]}(\bar{u}) + ...}{g_{jj}(\bar{u}) + \frac{\omega^2}{2!}g_{jj}^{[2]}(\bar{u}) + \frac{\omega^4}{3!}g_{jj}^{[3]}(\bar{u}) + ...}\right]$$

$$\equiv \frac{A_{ij}}{A_{jj}}\left[\frac{g_{ij}(\bar{u}) + R_{ij}(\omega,\bar{u})}{g_{jj}(\bar{u}) + R_{jj}(\omega,\bar{u})}\right] \qquad \text{(A6)}$$

where R_{ij} represents the higher-order terms. Finally, rescaling Equation A6 by its magnitude at zero frequency

$$\frac{\hat{\beta}_{ij}(\bar{u})}{\hat{\beta}_{ij}(0)} = \left[\frac{g_{ij}(\bar{u}) + R_{ij}(\omega,\bar{u})}{g_{jj}(\bar{u}) + R_{jj}(\omega,\bar{u})}\right] \cdot \left[\frac{g_{jj}(0) + R_{jj}(\omega,0)}{g_{ij}(0) + R_{ij}(\omega,0)}\right] \qquad \text{(A7)}$$

If the R_{ij} terms are small with respect to their associated g_{ij} terms then we can neglect the higher-order terms to obtain:

$$\frac{\hat{\beta}_{ij}(\bar{u})}{\hat{\beta}_{ij}(0)} \cong \left[\frac{g_{ij}(\bar{u})}{g_{jj}(\bar{u})}\right] \cdot \left[\frac{g_{jj}(0)}{g_{ij}(0)}\right] \tag{A8}$$

and thus the weighting function is independent of ω.

For the special case of $\omega = 0$ (i.e., $k_j^0 = \ln k_j$, as defined in Equation 3.14b), the rescaled weighting function is identically equal to the first-order term given in Equation A8. Thus, employing a spatial power-average $(\omega \neq 0)$ is seen to introduce higher-order spectral terms into the weighting function. In fact, as ω is increased, the weighting on these higher-order terms likewise increases. It is apparent from Figure 3.8, by comparing the curve for $\omega = 0$ with that for the other $\omega' s$, that the higher order terms can be neglected in this case with minimal error.

To explore the conditions under which the higher-order terms might be neglected, we assume a covariance/spectral density function and substitute above. For this analysis we adopt an exponential structure for both the auto- and cross-covariance:

$$C_{ij}(\bar{s}) = \sigma_{ij} \exp\left[-\left(\frac{s_1^2}{\lambda_{1,ij}^2} + \frac{s_2^2}{\lambda_{2,ij}^2}\right)^{\frac{1}{2}}\right] \tag{A9}$$

where σ_{ij} is the modeled variance and $\lambda_{l,ij}$ is the correlation length scale vector in the direction of the principal permeability axes (l=1,2). The corresponding Fourier transform of Equation A9 is

$$g_{ij}(\bar{u}) = \frac{2\pi\sigma_{ij}\lambda_{1,ij}\lambda_{2,ij}}{\left[1+4\pi^2\left(\bar{\lambda}_{ij}^2\cdot\bar{u}^2\right)\right]^{\frac{3}{2}}} \tag{A10}$$

where $\bar{\lambda}_{ij}^2\cdot\bar{u}^2 = \left(\lambda_{1,ij}^2u_1^2+\lambda_{2,ij}^2u_2^2\right)$. The transform of $C_{ij}^{[m]}$ is

$$g_{ij}^{[m]}(\bar{u}) = \frac{2\pi\sigma_{ij}^m\lambda_{1,ij}\lambda_{2,ij}m}{\left[m^2+4\pi^2\left(\bar{\lambda}_{ij}^2\cdot\bar{u}^2\right)\right]^{\frac{3}{2}}} \tag{A11}$$

Substituting the exponential spectral density function (Equations A10 and A11) into Equation A7 we have

$$\frac{\hat{\beta}_{ij}(\bar{u})}{\hat{\beta}_{ij}(0)} = \left[\frac{\dfrac{2\pi\sigma_{ij}\lambda_{1,ij}\lambda_{2,ij}}{\left[1+4\pi^2\left(\bar{\lambda}_{ij}^2\cdot\bar{u}^2\right)\right]^{\frac{3}{2}}}+\dfrac{\omega^2}{2!}\dfrac{4\pi\sigma_{ij}^2\lambda_{1,ij}\lambda_{2,ij}}{\left[4+4\pi^2\left(\bar{\lambda}_{ij}^2\cdot\bar{u}^2\right)\right]^{\frac{3}{2}}}+.....}{\dfrac{2\pi\sigma_{jj}\lambda_{1,jj}\lambda_{2,jj}}{\left[1+4\pi^2\left(\bar{\lambda}_{jj}^2\cdot\bar{u}^2\right)\right]^{\frac{3}{2}}}+\dfrac{\omega^2}{2!}\dfrac{4\pi\sigma_{jj}^2\lambda_{1,jj}\lambda_{2,jj}}{\left[4+4\pi^2\left(\bar{\lambda}_{jj}^2\cdot\bar{u}^2\right)\right]^{\frac{3}{2}}}+.....}\right]$$

$$\cdot\left[\frac{2\pi\sigma_{jj}\lambda_{1,jj}\lambda_{2,jj}+\dfrac{\omega^2\pi\sigma_{jj}^2\lambda_{1,jj}\lambda_{2,jj}}{4}+....}{2\pi\sigma_{ij}\lambda_{1,ij}\lambda_{2,ij}+\dfrac{\omega^2\pi\sigma_{ij}^2\lambda_{1,ij}\lambda_{2,ij}}{4}+....}\right] \tag{A12}$$

To draw comparison between our model and the empirical weighting functions, statistical parameters measured on the Berea Sandstone were substituted into Equation A12. Second-order terms were found to range from 0.1-13% of that of the first-order terms, while third-order terms range from 0.1-3% of that of the second-order terms. The significance of the higher-order terms grows with increasing frequency. Thus, both the distribution and

magnitude of error (due to neglecting the higher-order terms) predicted by Equation A12 is consistent with that seen in Figure 3.8.

Unfortunately the rescaled weighting function is not dominated by a single variable. Whether the higher-order terms can be neglected depends on the variances (i.e., σ_{jj}, and σ_{ij}) and correlation length scales (i.e., $\bar{\lambda}_{jj}, \bar{\lambda}_{ij}$) for the auto- and cross-covariance processes. However, a quick review of the Berea Sandstone data suggests that low sample variance (σ_{jj}= 0.087, 0.067, 0.041, and 0.021 for the 0.15, 0.31, 0.63, and 1.27 cm tip seals, respectively) is responsible for the behavior noted in Figure 3.8. Similar conclusions (i.e., higher-order terms could be neglected under conditions of low variance) were drawn in the theoretical development of weighting functions describing the measurement of soil water content by time domain reflectometry [Knight, 1992]. Although our analysis assumes the permeability is jointly log normal, the fact that the Berea permeability data is not log-normally distributed suggests that the rescaling of the weighting functions is relatively robust with respect to the distributional assumptions.

Acknowledgments. The authors wish to acknowledge the assistance of Justin Von Doemming in constructing the multi-support permeameter and Mark Bailey for his help in data collection. We would also like to thank Robert J. Glass for providing constructive advice and Scott Tyler, Steve Conrad, and Peter Davies for their insightful reviews. This work was supported by the U.S. Department of Energy, Office of Basic Energy Science, Geoscience Research Program, under contracts DE-AC04-94AL85000 and DE-F303-96ER14589/A000. Sandia is a multiprogram laboratory operated by Sandia Corporation, a Lockheed Martin Company, for the United States Department of Energy.

3.7. References

Baveye, P. and G. Sposito, The operational significance of the continuum hypothesis in the theory of water movement through soils and aquifers, *Water Resour. Res.*, 20(5), 521-530, 1984.

Beckie, R., Measurement scale, network sampling scale, and groundwater model parameters, *Water Resour. Res.*, 32(1), 65-76, 1996.

Beckie, R., A.A. Aldama, and E.F. Wood, The universal structure of the groundwater flow equations, *Water Resour. Res.*, 30(5), 1407-1419, 1994.

Beckie, R., A.A. Aldama, and E.F. Wood, Modeling the large-scale dynamics of saturated groundwater flow using spatial-filtering theory: 1. Theoretical development, *Water Resour. Res.*, 32(5), 1269-1280, 1996.

Bracewell, R.N., *The Fourier Transform and Its Applications*, 474 pp., McGraw-Hill, New York, 1986.

Cardwell, W.T. and R.L. Parsons, Average permeabilities of heterogeneous oil sands, *Trans. Am. Inst. Min. Metall. Pet. Eng.*, 160, 34-42, 1945.

Cushman, J.H., On unifying the concepts of scale, instrumentation, and stochastics in the development of multiphase transport theory, *Water Resour. Res.*, 20(11), 1668-1676, 1984.

Cushman, J.H., On measurement, scale, and scaling, *Water Resour. Res.*, 22(2), 129-134, 1986.

Desbarats, A.J., Spatial averaging of transmissivity in heterogeneous fields with flow toward a well, *Water Resour. Res.*, 28(3), 757-767, 1992a.

Desbarats, A.J., Spatial averaging of hydraulic conductivity in three-dimensional heterogeneous porous media, *Math. Geol.*, 24(3), 249-267, 1992b.

Deutsch, C.V., Calculating effective absolute permeability in sandstone/shale sequences, *SPE Form. Eval.*, 4(3), 343-348, 1989.

Goggin, D. J., R. L. Thrasher, and L. W. Lake, A theoretical and experimental analysis of minipermeameter response including gas slippage and high velocity flow effects, *In Situ*, 12(1-2), 79-116, 1988.

Indelman, P. and B. Abramovich, Nonlocal properties of nonuniform averaged flows in heterogeneous media, *Water Resour. Res.*, 30(12), 3385-3393, 1994.

Jenkins, G.M. and D.G. Watts, *Spectral Analysis and its Applications*, 525 pp., Holden-Day, San Francisco, 1968.

Knight, J.H., Sensitivity of time domain reflectometry measurements to lateral variations in soil water content, *Water Resour. Res.*, 28(9), 2345-2352, 1992.

Korvin, G., Axiomatic characterization of the general mixture rule, *Geoexploration*, 19, 267-276, 1981.

Maneval, J.E., M.J. McCarthy, and S. Whitaker, Use of nuclear magnetic resonance as an experimental probe in multiphase systems: Determination of the instrument weight function for measurements of liquid-phase volume fractions, *Water Resour. Res.,* 26(11), 2807-2816, 1990.

Marle, C.-M., Ecoulements monophasiques en milieu poreux, *Rev. Inst. Fr. Petrol.*, 22, 1471-1509, 1967.

Matheron, G., *Les Variables Regionalisees et Leur Estimation*, Masson, Paris, 1965.

Moltyaner, G.L., Hydrodynamic dispersion at the local scale of continuum representation, *Water Resour. Res.,* 25(5), 1041-1048, 1989.

Oliver, D.S., The averaging process in permeability estimation from well-test data, *SPE Form. Eval.,* 5, 319-324, 1990.

Shumway, R.H., *Applied Statistical Time Series Analysis*, Prentice Hall, Englewood Cliffs, 1988.

CHAPTER 4: PERMEABILITY UPSCALING MEASURED ON A BLOCK OF BEREA SANDSTONE: RESULTS AND INTERPRETATION[3]

4.1. Abstract

To physically investigate permeability upscaling over 13,000 permeability values were measured with four different sample supports (i.e., sample volumes) on a block of Berea Sandstone. At each sample support spatially-exhaustive permeability data sets were measured, subject to consistent flow geometry and boundary conditions, with a specially adapted minipermeameter test system. Here, we present and analyze a subset of the data consisting of 2304 permeability values collected from a single block face oriented normal to stratification. Results reveal a number of distinct and consistent trends (i.e., upscaling) relating changes in key summary statistics to an increasing sample support. Examples include the sample mean and semivariogram range that increase with increasing sample support and the sample variance that decreases. To help interpret the measured mean upscaling we compared it to theoretical models that are only available for somewhat different flow geometries. The comparison suggests that the non-uniform flow imposed by the minipermeameter, coupled with local-scale (i.e., smallest sample support for which data is available) permeability anisotropy, are the primary causes of the measured upscaling. This work demonstrates, experimentally, that it is not always appropriate to treat the local-

[3] Tidwell, V.C. and J.L. Wilson, in press Mathematical Geology, 1999.

scale permeability as an intrinsic feature of the porous medium; that is, independent of its conditions of measurement.

4.2. Introduction

Rarely can permeability data be acquired at the desired scale of analysis. The resulting disparity between the scale at which permeability data are measured and the desired scale of analysis, which is almost always larger than the former, necessitates the application of averaging or upscaling models. Because upscaling confronts a wide range of simulation and prediction problems in the geosciences, a variety of analytical and numerical models have been developed. As a full deterministic description of natural geologic materials is impractical, upscaling is commonly approached though stochastic means with the spatially heterogeneous qualities of the porous media treated as correlated random variables. Upscaling is accomplished by spatially integrating the stochastic partial-differential equations derived from the fundamental conservation laws of continuum mechanics. The roots of permeability upscaling lie at the pore scale and hence significant effort has been made to predict the macroscopic permeability from the pore-scale characteristics of the porous medium [e.g., Marle, 1967; Cushman, 1984; Bear and Bachmat, 1990]. This level of upscaling is generally averted due to the availability of permeability data measured on some macroscopic sample support (i.e., sample volume). Upscaling of permeability values from the measurement scale to the desired scale of analysis is conditioned on the spatial statistical characteristics of the permeability. Where simplifying assumptions concerning the spatial structure of the porous medium can be made and flows are uniform, upscaled permeability estimates are derived directly through analytical solutions [e.g., Gutjahr et al., 1978, Dagan, 1981; Gelhar and Axness, 1983; Deutsch, 1989; Rubin and Gomez-Hernandez, 1990; Desbarats, 1992a]. Where non-uniform flows are encountered a single effective permeability value can no longer be defined that is dependent solely on the statistical properties of the permeability; rather,

upscaling must explicitly account for the flow conditions unique to the problem [e.g., Matheron, 1967; Ababou and Wood, 1990; Desbarats, 1992b; Neuman and Orr, 1993; Indelman and Abramovich, 1994; Sanchez-Vila, 1997]. For cases involving complicated heterogeneities and/or flows numerical solutions to the upscaling problem are necessitated [e.g., White and Horne, 1987; Kitanidis, 1990; Kossack et al., 1990; Durlofsky, 1991]. The key assumption of these stochastic theories is that the permeability is a weakly stationary or periodic, ergodic random variable. Where the permeability exhibits long-range spatial persistence, fractal [e.g., Neuman 1994] theories have been proposed for quantifying upscaling behavior. Although such theoretical and numerical studies add greatly to our understanding of permeability upscaling, physical data collected under carefully controlled conditions are needed to suggest and test models.

Laboratory upscaling experiments have recently been conducted on a block of Berea Sandstone. These studies were made possible by a unique minipermeameter test system (see Chapter 2) that we call the Multi-Support Permeameter (MSP). Here, we present 2,304 permeability values measured on a single block face of the Berea Sandstone sample. These permeability data were measured with four different sample supports spanning 2.5 orders of magnitude on a per-volume basis. Although the Berea Sandstone is known for its relatively uniform permeability characteristics, distinct and consistent upscaling trends were measured. The measured upscaling in the mean permeability is compared with that predicted by theoretical models that differ according to their assumptions concerning flow uniformity. These comparisons are used to interpret the measured upscaling and infer the governing processes.

4.3. Methods

The data presented here provide a unique opportunity to physically investigate permeability upscaling. Extensive data sets were collected over a series of discrete sample

supports. Key attributes of the data include: 1) all measurements, regardless of sample support, were made subject to consistent boundary conditions and flow geometries; 2) measurements were non-destructive thus allowing all data to be collected from the same physical sample; 3) dense sampling grids were employed to provide detailed spatial information on the permeability field; and, 4) measurements were precise, subject to small and consistent measurement error. By acquiring data in this manner, sampling artifacts that can aggravate quantification of permeability upscaling were minimized or eliminated.

Collection of such permeability data is made possible with a specially adapted minipermeameter test system, which we call the Multi-Support Permeameter (MSP). Permeability data are acquired with this system by simply compressing a tip seal against a flat, fresh rock surface while injecting gas at a constant pressure. Using information on the seal geometry, gas flow rate, gas injection pressure, and barometric pressure, the permeability is calculated using a modified form of Darcy's Law [Goggin et al., 1988]. Automation of this process is achieved by coupling a minipermeameter with an x-y positioner and computer control system. The minipermeameter functions as the measurement device of the MSP and consists of four electronic mass-flow meters (0-50, 0-500, 0-2000, and 0-20,000 cm^3/min. at standard conditions), a pressure transducer (0-100 kPa gauge), a barometer, and a gas temperature sensor that are all connected to a regulated source of compressed nitrogen. Measurements are made according to a user specified sampling grid programmed into the x-y positioner. Along with locating the tip seal for sampling, the positioner also compresses the tip seal squarely against the rock surface with a consistent and constant force. The minipermeameter and x-y positioner are configured with a computer control system to govern the data acquisition process and provide unattended operation of the MSP. A full description and analysis of the MSP is given in Chapter 2.

Measurements are made at different sample supports, subject to consistent boundary conditions and flow geometries, by simply varying the radius of the tip seal. Tip seals, specifically designed for this program, consist of a rigid aluminum housing to which a molded silicone rubber ring is affixed. A series of such tip seals have been built with inner radii r_I of 0.15, 0.31, 0.63, and 1.27 cm and an outer radii (r_o) measuring twice the inner. Critical to precise measurement is a consistent and known tip seal geometry under compressed conditions. For this reason, each of the tip seals is equipped with an internal spring-driven guide to maintain a constant inner seal diameter. For the 0.63 cm and smaller tip seals, which experience considerable deformation on compression, an immobile outer guide is also employed.

It is important to note that the ring-shaped tip seal imposes a strongly divergent flow geometry on the test medium. The resulting non-uniform flow field not only has important implications relative to the measured permeability upscaling, as we will see later, but also raises questions concerning what the MSP actually measures. To address this latter issue, we empirically investigated the measurement characteristics of the MSP by way of linear filter analysis (see Chapter 3). Results, as given by the empirical spatial weighting functions, indicate that the sample support is approximately hemispherical (even for the samples characterized by permeability anisotropy) consistent with the symmetry of the tip seal. Heterogeneities located near the center of the tip seal influence the measurement more than those located further away, consistent with the divergent flow field imposed by the MSP. Also, as the tip seal size increases the effective radius, r_{eff}, of measurement increases. Although additional work is needed to fully quantify the sample support associated with each tip seal, we and others [e.g., Goggin et al., 1988] believe that the r_{eff} is roughly proportional to r_I, hence the volumetric sample support increases by a power of 8 for each doubling of r_I.

The non-uniform flow geometry imposed by the minipermeameter tip seal also influences the measured permeability upscaling. Although many hydraulic testing methods (e.g., pump tests, tracer tests, slug tests) are subject to non-uniform flow, relatively little theoretical work has been devoted to upscaling under such conditions. In fact, no upscaling studies have been conducted to date for flow geometries consistent with that of the minipermeameter. Thus, we do not test existing theories, but rather examine the results in light of these theories.

4.4. Results

Permeability data were acquired from a 0.3 by 0.3 by 0.3 m block of Berea Sandstone obtained from Cleveland Quarries in Amherst, Ohio. The Berea Sandstone is believed to be of Mississippian Age with its origins in a low-energy, fluvial-deltaic environment [Pepper et al., 1954]. According to visual inspection (Figure 4.1a), the sample may be characterized as a very-fine grained, well sorted quartz sandstone. The sample is relatively featureless except for faint subhorizontal stratification. The Berea Sandstone was selected for testing because of its common use in laboratory studies and its relatively simple physical features. In short, it is one of the most uniform (deterministically homogeneous) rock samples we've encountered. Samples from other depositional environments, with much larger permeability variances and different spatial correlation structures, have likewise been investigated and are reported in Chapters 5 and 6.

Over 13,000 permeability measurements were collected over all six faces of the sandstone sample; however, the analyses reported here focus on 2304 data collected from a single face cut normal to the stratification (which we term Face 3). Measurements were made on the exact same grid using the 0.15, 0.31, 0.63, and 1.27 cm tip seals. Although

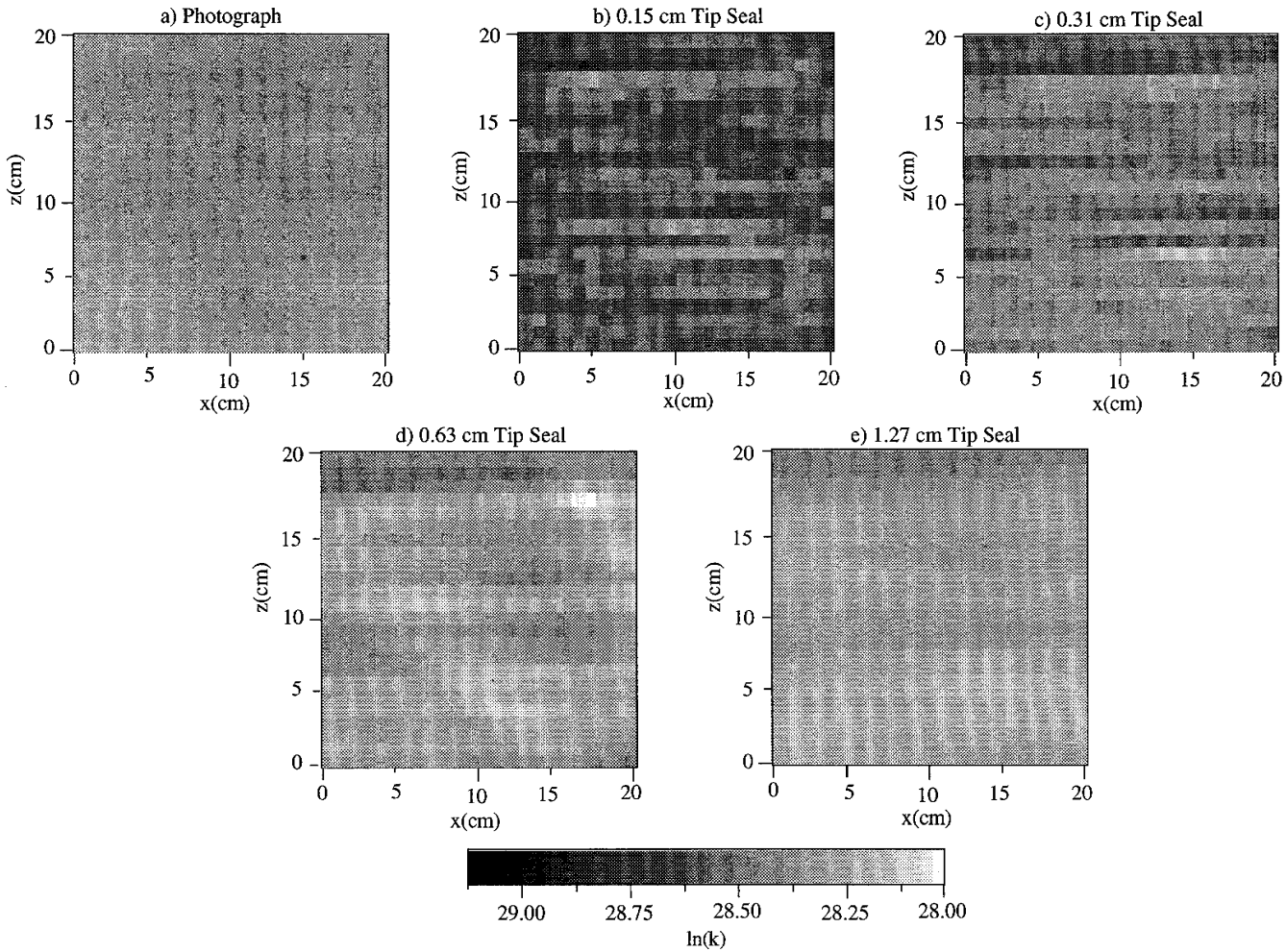

Figure 4.1. Photograph a) of Face 3 of the Berea Sandstone sample. Also shown are the natural log permeability fields measured with the b) 0.15, c) 0.31, d) 0.63, and e) 1.27 cm r_1 tip seals on this rock face. Data were collected on a 24 by 24 point grid with 0.85 cm centers.

larger tip seals are available for sampling they were not used because of the limited dimensions of the rock sample. The sampling grid contained 576 measurement points organized on a square 24 by 24 lattice on 0.85 cm centers. To avoid boundary effects on the measurements, a total grid size of 19.5 by 19.5 cm was used that provides a 5.25 cm buffer between the grid and edge of the block.

Spatial Permeability Measurements

The natural-log permeability fields (i.e., $\ln[k(x,z)]$ where k is permeability in m^2, and x and z denote the spatial location) measured with the 0.15, 0.31, 0.63, and 1.27 cm r_l tip seals are given in Figure 4.1. Three important attributes of these permeability fields should be noted. First, comparisons drawn between the photograph (Figure 4.1a) and permeability fields reveal that the stratification faintly visible to the eye in the Berea Sandstone correlates with the anisotropy exhibited by the permeability fields. Second, each of the four tip seals reproduce the same basic spatial permeability patterns. Specifically, laminae of alternating "high" and "low" permeability are located in the same position in each of the data sets (e.g., the low-permeability laminae centered at z=7.5 cm, and at 18.5 cm). In fact, these laminae can be traced across all four block faces cut normal to the stratification (Figure 2.6 and Figure 3.2). Finally, distinct smoothing of the permeability field is evident as the tip seal size increases. This smoothing occurs because measurements made at larger supports interrogate more rock and hence average over more spatial variability than do measurements made at smaller sample supports.

The cumulative distribution functions (CDFs) for the natural-log permeability data measured with each of the four tip seals are given in Figure 4.2 while the corresponding summary statistics are given in Table 4.1. The CDFs are characterized by a small range and correspondingly low variance. Data for the 0.15 cm tip seal are approximately log-normally distributed; however, as the tip seal size increases, asymmetry in the distribution becomes

more apparent. Several distinct trends with changing sample support are evident. The sample mean increases with increasing sample support while the sample variance decreases. Inspection of the CDFs reveals that upscaling influences the distribution beyond the sample mean and variance, as evidenced by the increasing asymmetry of the distribution and the distinct difference in the degree of upscaling exhibited by the upper and lower tails of the CDFs.

To investigate the spatial correlation of the permeability data, full two-dimensional semivariograms were calculated for each of the natural-log permeability data sets using Fourier analysis (via Fast Fourier Transforms, see Bracewell, 1986 and Section 3.3). The two-dimensional semivariogram calculated for the 1.27 cm data set is given in Figure 4.3 revealing anisotropy in the permeability field. Transects oriented along the major and minor permeability axes are plotted in Figure 4.4. The transects show strong spatial correlation

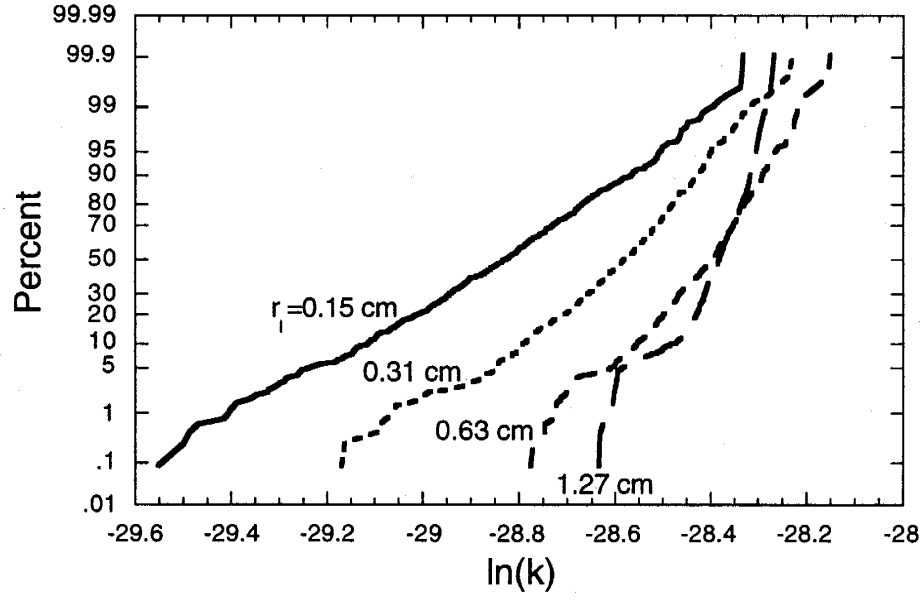

Figure 4.2. Cumulative distribution functions for the natural-log permeability data sets given in Figure 4.1. Each curve represents 576 permeability values.

Table 4.1. Summary statistics for the natural-log permeability data sets measured with different size tip seals (r_t) on Face 3 of the Berea Sandstone sample.

	0.15 cm	0.31 cm	0.63 cm	1.27 cm
Mean	-28.84	-28.60	-28.41	-28.39
Median	-28.83	-28.58	-28.39	-28.38
Standard Deviation	0.21	0.15	0.11	0.072
Variance	0.046	0.021	0.012	0.0053
Kurtosis	0.18	1.08	0.67	1.88
Skewness	-0.34	-0.75	-0.70	-1.32
Range	1.22	0.94	0.63	0.37
Minimum	-29.55	-29.17	-28.78	-28.63
Maximum	-28.33	-28.23	-28.15	-28.27
Count	576	576	576	576

parallel to the stratification, as exhibited by a range that extends beyond the length of the semivariogram (Figure 4.4a), and very weak correlation in the orthogonal direction (Figure 4.4b). A weak hole-effect is apparent normal to stratification reflecting the layered (i.e., periodic) structure of the Berea Sandstone (Figure 4.1).

The sample semivariograms calculated from the four different tip seal data sets have been fit with an exponential γ_e model

$$\gamma_e(\vec{s}) = C_o + \sigma\left(1 - \exp\left[-\left(\frac{(3\vec{s})^2}{\vec{\lambda}^2}\right)^{1/2}\right]\right) \tag{4.1}$$

where C_o is the nugget, σ the variance of the natural-log permeability, $\vec{\lambda} = (\lambda_x, \lambda_z)$ the semivariogram range (cm), and $\vec{s} = (s_x, s_z)$ the separation vector (cm) in the principal directions (see Figure 4.1). Model parameters fit to the semivariogram data are given in Table 4.2. The coefficients for the exponential model oriented parallel to stratification should be viewed with caution as the length of the sample semivariogram is insufficient to uniquely estimate the range and sill parameters. Nevertheless, a number of consistent and distinct trends are evident among the semivariograms. First, the sill of the semivariogram decreases with increasing sample support, consistent with the decreasing variance, while

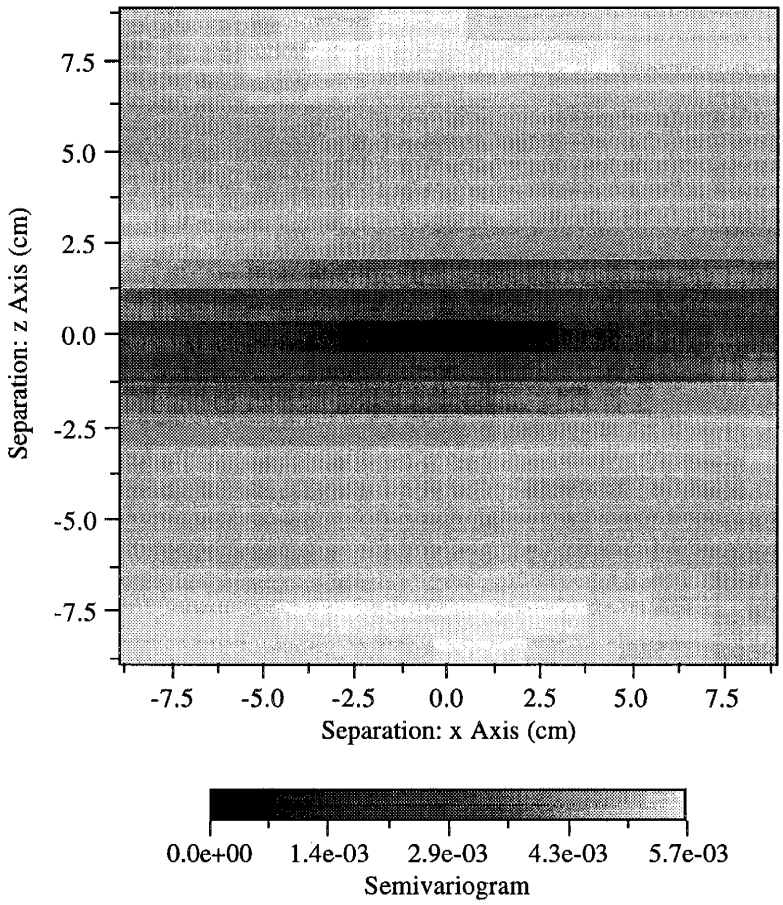

Figure 4.3. Two-dimensional semivariogram calculated from the natural-log permeability data set collected with the 1.27 cm r_1 tip seal on Face 3 of the Berea Sandstone sample.

the general shape of the semivariogram remains unchanged (except for dampening of the hole-effect in Figure 4.4b). Also, the fitted range values $\vec{\lambda}$ increase linearly with sample support reflecting the increasing characteristic length of the measurement [Clark, 1977; Journel and Huijbregts, 1978].

As noted above, all six faces of the Berea Sandstone sample have been investigated. Although there would be some advantage to presenting this data all in one place, the logistics of conveying this extensive set of information in a concise manner is a formidable task. As all six faces exhibit very similar upscaling characteristics it would be redundant for purposes of this paper to present the other faces here. However, data beyond that provided above, can be found in other references. In Chapter 2 data are presented from Face 5, which is located directly opposite of the block from Face 3 (given here), while data from Face 2, orthogonal to Faces 3 and 5 and oriented normal to stratification, can be found in Chapter 2. Each sampled block face exhibits a roughly log-normal permeability distribution with a mean that increases with increasing sample support and a variance that decreases. In each case the semivariogram exhibits an exponential structure with a range >20 cm parallel to stratification and very short range correlation (0.8-3 cm) normal to stratification. With increasing sample support, the magnitude of the semivariogram always decreases, the range increases, while the general anisotropic exponential spatial structure is maintained. The most noteworthy differences among block faces are in the absolute magnitudes of the mean and variances of the log permeabilities. Mean permeabilities may vary by a full natural-log unit (for a given tip seal size) while variances may differ by as much as a factor of 3.

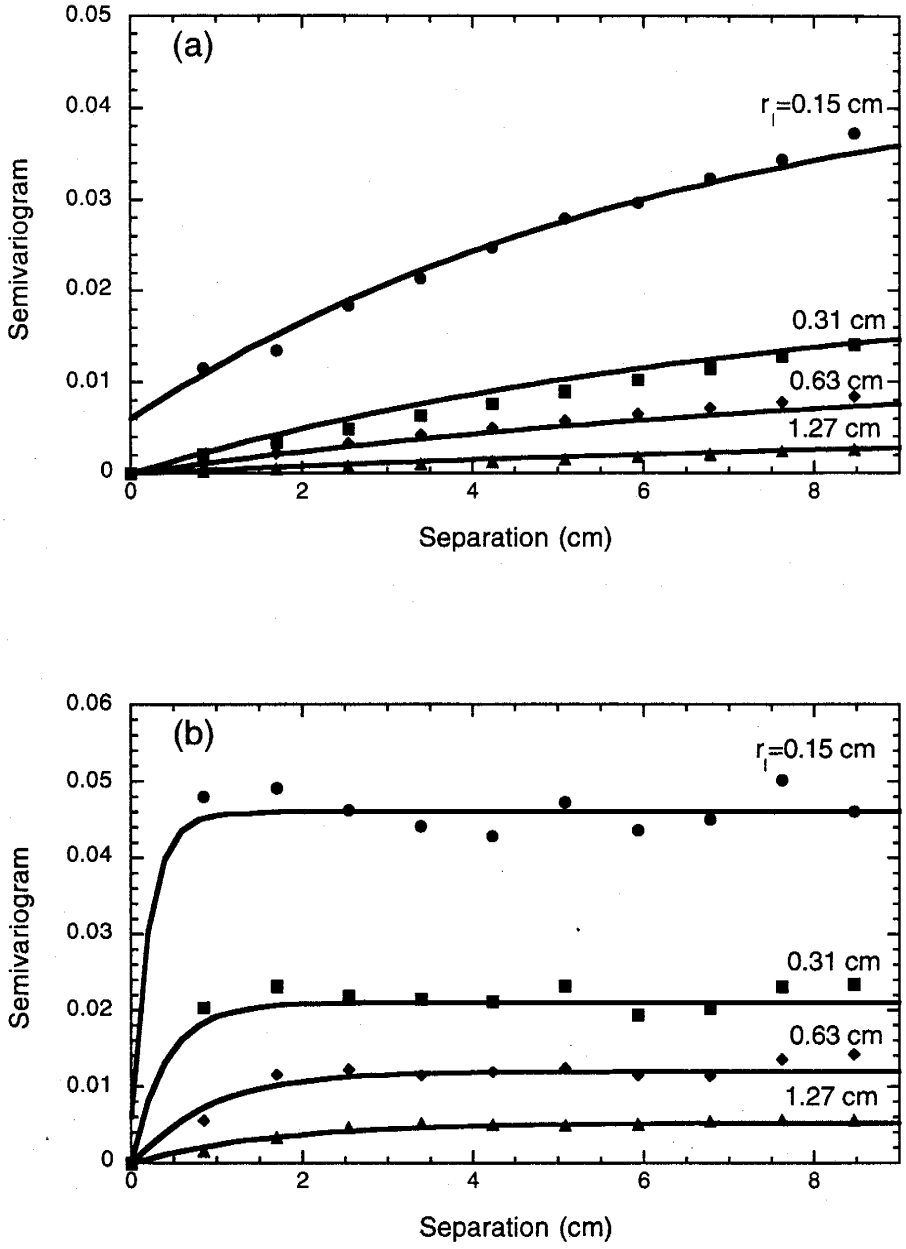

Figure 4.4. Semivariogram transects (symbols) for the natural-log permeability data sets measured with each of the four different-size tip seals on Face 3 of the Berea Sandstone sample. Transect orientations are a) parallel and b) normal to stratification. The fitted semivariogram models (Equation 4.1) are given by solid lines.

Table 4.2. Exponential model parameters fit to the semivariograms shown in Figure 4.4.

Tip	C_o	σ	λ_x	λ_z
0.15	0.006	0.040	19.5	0.63
0.31	0.0	0.021	22.5	1.20
0.63	0.0	0.012	27.0	2.70
1.27	0.0	0.0053	36.0	4.89

Model Comparison

We now interpret the measured permeability upscaling through comparison with theoretical upscaling models. Although there are a number of interesting upscaling trends evident in the data, we limit our attention to the sample mean. We draw comparison with two different analytical models, one that assumes uniform-flow conditions and another that assumes non-uniform radial flow. We recognize that these models are not fully consistent with the experimental conditions, but there are no published analytical or numerical studies that deal with permeability upscaling for hemispherical flow in an anisotropic medium. The development of such theories are well beyond the scope of the current paper. For this reason, our intent is not to test the theories but use them as limiting cases to interpret the key processes governing the measured upscaling. A careful review of the fundamental modeling assumptions in light of actual experimental conditions forms the basis of our analysis.

The sample means calculated from the Berea Sandstone data measured on Face 3 with the four different-size tip seals are plotted in Figure 4.5 as a function of the inner tip seal radius. For this analysis we have plotted the arithmetically averaged mean permeabilities ($\bar{k}_j^a = E\left[k_j(\vec{x})\right]$, where j designates tip seal size). Inspection of Figure 4.5

reveals that the sample mean follows a smooth trend, increasing by a factor of 1.5 for a 2.5 order of magnitude increase in sample support.

Our first comparison is drawn with an effective permeability model that assumes an infinite domain (i.e., domain size is much larger than the correlation length scale of the medium, λ_o) and mean uniform-flow conditions. Our permeability measurements are clearly inconsistent with the modeling assumptions; nevertheless, we perform this analysis so that we may compare results with the test case assuming non-uniform flow. We make our comparison with the spectral/perturbation model of Gelhar and Axness [1983]. Their model can be tailored to our problem by considering the MSP flow geometry and the spatial structure of the Berea Sandstone. Given the orientation of the MSP on this face of the rock, normal to stratification, we assume that flow parallel to stratification dominates. According to Gelhar and Axness, the effective permeability, $\bar{k}_{xx}$, of an infinite domain subject to uniform flow oriented parallel to stratification is

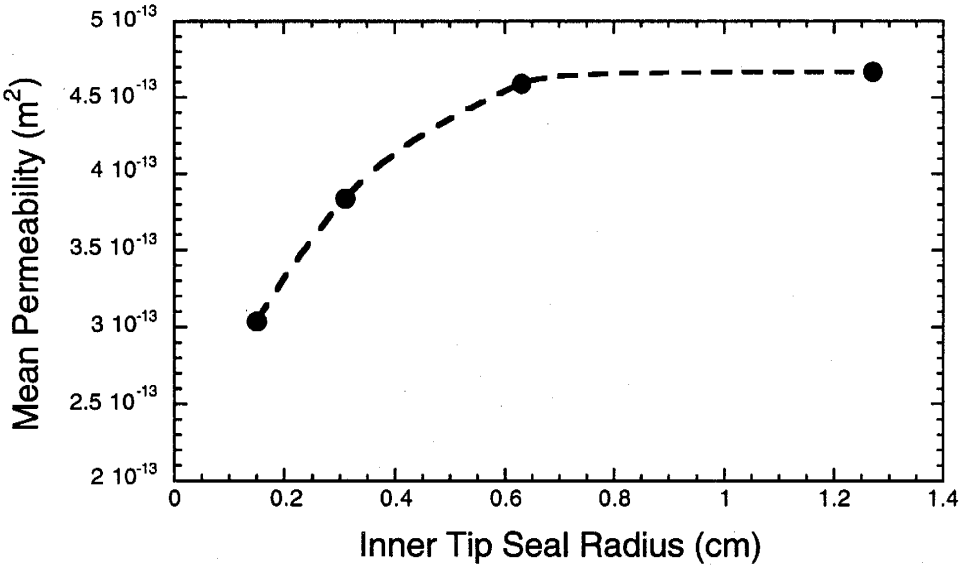

Figure 4.5. Mean upscaling (symbols) plotted as a function of the inner tip seal radius.

$$\bar{k}_{xx} = \bar{k}_o^g \exp\left[\sigma_o\left(\frac{1}{2} - g_{xx}\right)\right] \tag{4.2}$$

where $\bar{k}_o^g$ is the geometric mean $\left(\bar{k}_o^g = \exp\left(E\left[\ln\left(k_o(\vec{x})\right)\right]\right)\right)$ of the point-support permeability k_o (i.e., associated with an infinitely small sample volume), σ_o is the corresponding variance $\left(\sigma_o = Var\left[\ln\left(k_o(\vec{x})\right)\right]\right)$, and g_{xx} is a constant accounting for the spatial anisotropy of the natural-log permeability field. According to the semivariogram analysis presented above and inspection of the sampled block face, the spatial correlation of the permeability field can be characterized by $\lambda_x >> \lambda_z$, where the subscript x is taken parallel to stratification, and z normal. For this case we find $g_{xx} \cong 0$ from Figure 4.4 of Gelhar and Axness [1983]. Note that for $g_{xx} = 0$ the right-hand-side of Equation 4.2 is simply the arithmetic average of $k_o(\vec{x})$, which is a reasonable result considering our assumption of uniform flow oriented parallel to stratification.

As $\bar{k}_o^g$ and σ_o (which are associated with the point support) have not been measured, a direct calculation of $\bar{k}_{xx}$ is not possible. However, we can expect that the mean permeability measured with the largest tip seal $\bar{k}_{1.27}^g$ to be less than or equal to $\bar{k}_{xx}$ and likewise $\bar{k}_o^g \le \bar{k}_{0.15}^g$. Thus, we can write

$$\frac{\bar{k}_{1.27}^g}{\bar{k}_{0.15}^g} \le \frac{\bar{k}_{xx}}{\bar{k}_o^g} = \exp\left[0.5\sigma_o\right] \tag{4.3}$$

Substituting values for $\bar{k}_{0.15}^g$ (2.98×10^{-13} m^2) and $\bar{k}_{1.27}^g$ (4.68×10^{-13} m^2) into Equation 4.3 we find that $\sigma_o \ge 0.9$. This suggests that the point-support variance must be much larger (19

times) than that measured with the smallest tip (Table 4.1) to achieve a close fit between the model and data.

We now employ the restriction of non-uniform flow and investigate its effect on the predicted behavior of the mean upscaling. Permeability upscaling, under conditions of non-uniform flow, has been the subject of a series of studies. In each case this issue has only been explored within the context of theoretical modeling and/or numerical simulation. The analyses have largely been restricted to radially-convergent mean flows in heterogeneous/isotropic domains [Dagan, 1989; Neuman and Orr, 1993; Sanchez-Vila, 1997], one exception being Indelman and Abramovich [1994] who also investigated the case of spherical flow to a point sink in an infinite three-dimensional, isotropic domain. The key implication of these works is that under non-uniform flow conditions it is not possible to define a single effective permeability value that depends only on the statistical properties of the permeability field.

For the purpose of this study we define an apparent effective permeability, $\bar{k}_e$, as the homogeneous permeability value that provides, on average, the same discharge as the heterogeneous formation under the same boundary conditions. In this way, $\bar{k}_e$ is directly comparable to the permeability values calculated from the gas flow and pressure data measured with the MSP. Unfortunately, only a few non-uniform flow studies treat the effective permeability in a similar context (i.e., as $\bar{k}_e$). Using stochastic perturbation methods Matheron [1967] formulated an expression for the apparent effective permeability assuming radial flow to a well located in an isotropic domain. Ababou and Wood [1990] modified Matheron's result, treating the second-order approximation as a truncated exponential series expansion

$$\bar{k}_e = \bar{k}_o^g \exp\left\{\frac{\sigma_o}{2}\left|\frac{2\left[1+\left(\ln(r_w/\lambda_o)\right)^2\right]}{\left[\ln(r_c/r_w)\right]^2}-1\right|\right\} \tag{4.4}$$

where r_w is the well radius and r_c is the effective radius of the cone of depression. Consistent with Matheron they found that for fixed λ_o, $\bar{k}_e$ increases toward $\bar{k}_o^a$ as $r_w/\lambda_o \to 0$, and decreases and asymptotically approaches $\bar{k}_o^h$ (i.e., ensemble harmonic average of $k_o(\vec{x})$) as $r_c/\lambda_o \to \infty$. For similar flow conditions, Desbarats [1992b] modeled $\bar{k}_e$ as a weighted spatial geometric average where the log permeabilities were weighed by the inverse square of their distance from the well. He found $\bar{k}_e$ to decrease from $\bar{k}_o^a$ toward $\bar{k}_o^g$ as the field size becomes large compared to λ_o. According to these models, which assume non-uniform flow, the mean permeability should follow a decreasing trend as the sample support increases relative to λ_o. Although the difference between their assumed flow geometry (radial) and the actual flow conditions beneath the minipermeameter tip seal (approximately hemispherical) will influence the behavior of the mean upscaling, it should not effect the sense (decreasing) of the trend. Beyond predicting a decreasing trend for the mean upscaling, these models also predict that the absolute change in the mean permeability will be relatively small. According to these models the maximum change the mean could experience is bound by $\bar{k}_o^a$ and $\bar{k}_o^h$. Although we do not have data to calculate $\bar{k}_o^a$ or $\bar{k}_o^h$ we do know $\bar{k}_{0.15}^a/\bar{k}_{0.15}^h = 1.05$, which is much smaller than the measured change in the mean permeability (i.e., $k_{0.15}^a/k_{1.27}^a = 1.54$).

Discussion

Theoretical models of radial flow predict that the mean permeability should decrease as the sample support becomes large compared to λ_o, while a theoretical model for infinite uniform flow predicts that the mean remains constant (arithmetic average). In contrast, the

measured mean upscaling follows a deliberate, increasing trend. More important, the measured change in the mean far exceeds that theoretically anticipated for a medium with such low variance. Reasons for the discrepancy between the models and data lie in the experimental violation of assumptions on which the theoretical models are predicated. We now explore some of these assumptions in efforts to interpret the controls on the permeability upscaling measured on the Berea Sandstone.

One possible cause for the increasing mean permeability, which is not represented in the models, is that the depth and lateral dimensions of the sampling domain increases as the tip seal size increases. What if the permeability of the Berea Sandstone sample were to increase with depth into the block (i.e., normal to Face 3)? As the tip seal size is increased measurements penetrate deeper into the rock accessing zones of higher permeability, thus causing the mean permeability to increase with increasing sample support. However, this explanation seems unlikely given that all six faces of the Berea Sandstone yield a strongly increasing trend in the mean with increasing tip seal size. Similar arguments can be made concerning the increasing lateral dimensions of the sampling domain. The permeability at points around the perimeter of the sampling grid could increase with tip seal size due to increased accessibility of high permeability zones or due to increased interaction with the boundaries of the rock block. Again, this does not explain the measured upscaling as the perimeter nodes can be excluded from the larger tip seal data sets with imperceptible effect on the calculated statistics.

Another potential cause for the poor fit between the data and models may be the limited size of the sampling domain with respect to $\vec{\lambda}_o$, the correlation length scale of the Berea Sandstone (i.e., lack an infinite medium, see Figure 4.4). The limited domain size could bias the sample means associated with the different tip seals; however, because each

data set is equally subject to the same bias (since each is measured on the same grid) this effect does not explain the difference between the model and the data.

It could be argued that the measured upscaling is the result of discrete high-permeability pathways (the presence of which would violate key assumptions of the models) that are widely distributed across the rock face. That is, measurements made with the larger tip seals more often sample the high-permeability features leading to an increasing mean. Inspection of the sampled rock face and permeability maps (Figure 4.1) suggests the presence of such pathways oriented along select laminae. We expect the anisotropic structure of the rock, which gives rise to the spatially continuous "high" permeability pathways, to play an important role in the measured permeability upscaling; however, we currently do not feel that the anisotropy alone explains the upscaling. We support this opinion with three pieces of evidence. First, the mean permeability for the 1.27 cm tip seal is larger than 96% (all but 23 values) of the permeability values measured with the 0.31 cm tip seal, thus there are not enough "high" permeability values to explain the measured upscaling. Considering that the 0.31 cm tip seal provides full coverage of the sampling domain, using the conservative criteria that $r_{eff} = r_o$, it is very unlikely that we simply failed to sample such pathways. Second, indicator semivariograms [e.g., Deutsch and Journel, 1997] calculated from the measured permeability data sets do not support this explanation. Indicator semivariograms were calculated using cutoff values corresponding to the 25th, 50th, 75th, and 90th percentiles of the permeability distribution. Results do not reveal any discernible differences in the range values between the different permeability classes. Third, the calculated spatial weighting (filter) functions given in Chapter 3 did not discern significant anisotropy that would be diagnostic of preferred flow paths along the laminae.

These models, as well as most effective media theory, assume that there exists a point-support permeability that is homogeneous, isotropic, and independent of its

conditions of measurement. However, the point-support, which is associated with a fictitious, infinitely small sample support, is not a measurable quantity. In practice the local support (i.e., smallest sample support for which permeability data are available) is taken to represent the point support, sometimes subject to minor modifications [e.g., Clark, 1977]. However, under non-uniform flow conditions and where heterogeneity occurs on the scale of the measurement, such treatment can be dangerous. Consider the divergent flow geometry (Figure 4.6) associated with a minipermeameter tip seal measurement. Now, superimpose the sample support associated with a smaller tip seal (i.e., a local support) on the flow field. If the local support is centered on the larger measurement then the local support will principally experience uniform one-dimensional flow oriented vertically into the rock surface. If the local support is moved to a position under the rubber seal, gas flow will be predominately radial and oriented parallel to the rock surface. Finally, if the local support is moved well away from the outer perimeter of the rubber seal, gas flow will again be nearly uniform and one-dimensional but oriented toward the surface of the rock. In each of these three cases the local support experiences a very different gas flow geometry depending on its position in the larger flow field. More importantly, these geometries are very different from the divergent flow geometry under which the local support is measured. Where anisotropy occurs on the scale of the local support, effective permeabilities will differ depending on the dimensionality of the gas flow and its orientation with respect to the anisotropy. Evidence for such anisotropy in the Berea Sandstone is expressed in the semivariogram transects (Figure 4.4) calculated for each tip seal data set.

From these arguments we conclude that the primary factors influencing the upscaling measured on the Berea Sandstone sample are the non-uniform flow imposed by the minipermeameter coupled with permeability anisotropy, which occurs at scales comparable to that of the measurements. The poor fit between the data and the theoretical

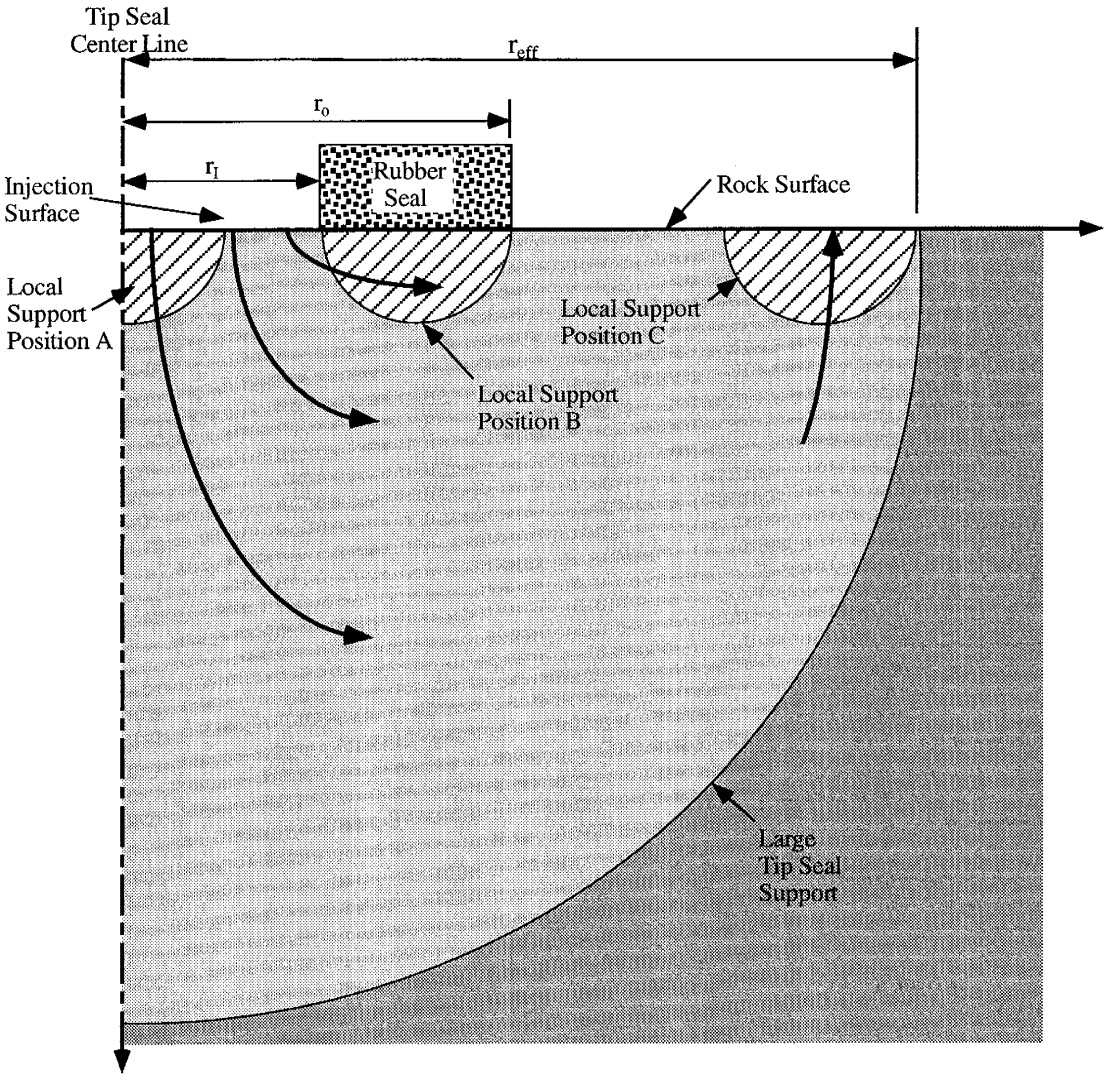

Figure 4.6. Schematic of the gas flow field imposed by a minipermeameter measurement. Superimposed on the flow field is the sample support associated with a smaller tip seal measurement (i.e., local support). The local support is shown in three positions to demonstrate the differences in flow conditions that it experiences depending on its location within the larger measurement. The relative sizes of the two sample supports are intended to represent that of the 1.27 cm and the 0.15 cm tip seals.

models results largely from the fact that our local-scale permeability data, which we are forced to treat as point-support, are inconsistent with the conditions assumed in the models; specifically, that the point-support permeability is isotropic and independent of its measurement conditions. We recognize that a rigorous, quantitative analysis of these coupled effects is needed; however, much effort will be required to develop the analytical and/or numerical tools with which to analyze the upscaling of non-uniform flows subject to locally-heterogeneous, anisotropic permeability distributions.

A key implication of this work is that local-scale permeability values are not a intrinsic characteristic of the porous medium from which they are measured. Where non-uniform flows are an issue and/or the scale of heterogeneity approaches that of the sample support, explicit consideration of the measurement characteristics and/or media characteristics may be required in defining the point-support permeability from local-scale values. These local-scale effects can have significant influence on the mean upscaling as evidenced by the comparisons drawn here. As computational capabilities continue to improve the desire to incorporate finer-scale detail into geologic simulations will follow. Thus, as the gap between the local scale and the desired scale of analysis is narrowed, precise treatment of local-scale effects will play a role of increasing importance in the modeling and upscaling of heterogeneous porous formations. However, additional work is needed to develop a proper theoretical foundation and the complimentary tools for addressing local-scale processes.

4.5. Conclusions

There are few data sets, collected under controlled experimental conditions, that clearly document the upscaling of permeability measurements collected from natural geologic materials. Here, we present the results of physical upscaling experiments performed on a block of Berea Sandstone. Using a computer automated minipermeameter

test system we measured 2304 permeability values with four different sample supports (sample volumes). The data sets are unique in that measurements made at different sample supports were subject to consistent boundary conditions and flow geometries, all measurements were made on the same physical sample, and high-resolution (sub-centimeter resolution) sampling was employed at each sample support. Results show the calculated permeability statistics (i.e., permeability maps, semivariograms) to be strongly correlated with the stratified structural features visible in the sandstone sample. The summary statistics calculated from the data show clear and consistent trends with changing sample support (i.e., upscaling): among these are an increasing mean, decreasing variance, and increasing semivariogram range with increasing sample support.

To help interpret the measured upscaling we compared the observed trend in the mean permeability to predictions from two published theoretical models based, respectively, on uniform and non-uniform flow assumptions. In each case the models were found to significantly under predict the measured upscaling. Discrepancies between the data and models were used to identify the basic controls on the measured permeability upscaling. Non-uniform flow imposed by the minipermeameter coupled with local-scale (i.e., smallest sample support for which data are available) anisotropy in the permeability were found to be the primary factors influencing the measured upscaling. The non-uniform flow theories did not predict the measured mean upscaling largely because of their treatment of the local-scale permeability. These models, as well as most effective media theories, assume the local-scale permeability is isotropic and independent of the mode of measurement, which are inappropriate assumptions for our experimental data.

These results demonstrate both the important role of non-uniform flow on permeability upscaling and the care that must be exercised when conditioning upscaling models on local-scale data. Implications of our results are not limited to minipermeameters,

but rather to any instrument that imposes non-uniform flow conditions (e.g., slug, pump, and tracer tests). Unfortunately, there is an apparent the lack of theory and complimentary tools for formulating local-scale permeabilities and predicting permeability upscaling under non-uniform flow conditions.

Acknowledgments: We would like to thank Justin Von Doemming and Mark Bailey for help in collecting the presented data and Allan Gutjahr, Robert Glass, and Fred Phillips for providing constructive advice. We also gratefully acknowledge the helpful reviews of Sean McKenna, Peter Davies, and two anonymous reviewers. This work was supported by the U.S. Department of Energy, Office of Basic Energy Science, Geoscience Research Program, under contracts DE-AC04-94AL85000 and DE-F303-96ER14589/A000. Sandia is a multiprogram laboratory operated by Sandia Corporation, a Lockheed Martin Company, for the United States Department of Energy.

4.6. References

Ababou, R. and E.F. Wood, Comment on "Effective groundwater model parameter values: Influence of spatial variability of hydraulic conductivity, leakance, and recharge by J.J. Gomez-Hernandez and S.M. Gorelick," *Water Resour. Res.*, 26(8), 1843-1846, 1990.

Bear, J. and Y. Bachmat, *Introduction to Modeling of Transport Phenomena in Porous Media*, 553 pp., Kluwer Academic Publishers, Boston, 1990.

Bracewell, R.N., *The Fourier Transform and Its Applications*, 474 pp., McGraw-Hill, New York, 1986.

Clark, I., Regularization of a semi-variogram, *Computers and Geosciences*, 3, 341-346, 1977.

Cushman, J.H., On unifying the concepts of scale, instrumentation, and stochastics in the development of multiphase transport theory, *Water Resour. Res.*, 20(11), 1668-1676, 1984.

Dagan, G., Analysis of flow through heterogeneous random aquifers by the method of embedding matrix 1. Steady flow, *Water Resour. Res.*, 17(1), 107-121, 1981.

Dagan, G., *Flow and Transport in Porous Formations*, 465 pp., Springer-Verlag, New York, 1989.

Desbarats, A.J., Spatial averaging of hydraulic conductivity in three-dimensional heterogeneous porous media, *Math. Geol.*, 24(3), 249-267, 1992a.

Desbarats, A.J., Spatial averaging of transmissivity in heterogeneous fields with flow toward a well, *Water Resour. Res.*, 28(3), 757-767, 1992b.

Deutsch, C.V. and A.G. Journel, *GSLIB: Geostatistical Software Library and User's Guide*, 368 pp., Oxford University Press, New York, 1997.

Deutsch, C.V., Calculating effective absolute permeability in sandstone/shale sequences, *SPE Form. Eval.*, 4(3), 343-348, 1989.

Durlofsky, L.J., Numerical calculation of equivalent grid block permeability tensors for heterogeneous porous media, *Water Resour. Res.*, 27(5), 699-708, 1991.

Gelhar, L.W. and C.L. Axness, Three-dimensional stochastic analysis of macrodispersion in aquifers, *Water Resour. Res.*, 19(1), 161-180, 1983.

Goggin, D. J., R. L. Thrasher, and L. W. Lake, A theoretical and experimental analysis of minipermeameter response including gas slippage and high velocity flow effects, *In Situ*, 12(1-2), 79-116, 1988.

Gutjahr, A.L., L.W. Gelhar, A.A. Bakr, and J.R. Macmillan, Stochastic analysis of spatial variability in subsurface flows, 2. Evaluation and application, *Water Resour. Res.*, 14(5), 953-960, 1978.

Indelman, P. and B. Abramovich, Nonlocal properties of nonuniform averaged flows in heterogeneous media, *Water Resour. Res.*, 30(12), 3385-3393, 1994.

Journel, A G. and C.J. Huijbregts, *Mining Geostatistics*, 600 pp., Academic Press, New York, 1978.

Kitanidis, P.K., Effective hydraulic conductivity for gradually varying flow, *Water Resour. Res.*, 26(6), 1197-1208, 1990.

Kossack, C.A., J.O. Aasen, and S.T. Opdal, Scaling up heterogeneities with pseudofunctions, *SPE Form. Eval.*, 5(3), 226-232, 1990.

Marle, C.-M., Ecoulements monophasiques en milieu poreux, *Rev. Inst. Fr. Petrol.*, 22, 1471-1509, 1967.

Matheron, G., *Elements pour une theorie des milieux poreux*, 166 pp., Maisson et Cie, Paris, 1967.

Neuman, S. P., Generalized scaling of permeabilities: Validation and effect of support scale, *Geophys. Res. Lett.*, 21(5), 349-353, 1994.

Neuman, S.P. and S. Orr, Prediction of steady state flow in nonuniform geologic media by conditional moments: Exact nonlocal formalism, effective conductivities, and weak approximation, *Water Resour. Res.*, 29(2), 341-364, 1993.

Pepper, J.F., W. De Witt, Jr., and D.F. Demarest, Geology of the Bedford Shale and Berea Sandstone in the Appalachian Basin, *Geological Survey Professional Paper 259*, U.S. Geological Survey, 1954.

Rubin, Y. and J.J. Gomez-Hernandez, A stochastic approach to the problem of upscaling of conductivity in disordered media: Theory and unconditional numerical simulations, *Water Resour. Res.*, 26(4), 691-701, 1990.

Sanchez-Vila, X., Radially convergent flow in heterogeneous porous media, *Water Resour. Res.*, 33(7), 1633-1641, 1997.

White, C.D. and R.N. Horne, Computing absolute transmissivity in the presence of fine-scale heterogeneity, SPE 16011, paper presented at the SPE Symposium on Reservoir Simulation, San Antonio, Tex., 1987.

CHAPTER 5: PERMEABILITY UPSCALING: RESULTS FOR A BLOCK OF MASSILLON SANDSTONE EXHIBITING NESTED SCALES OF HETEROGENEITY[4]

5.1. Abstract

Over 75,000 permeability measurements were collected with five different sample supports (i.e., sample volumes) from a meter-scale block of Massillon Sandstone, characterized by conspicuous cross-bedding that forms two distinct nested-scales of heterogeneity. This extensive data set provides a unique opportunity to physically investigate the relationship between the multi-scale cross-stratified attributes of the sandstone and the corresponding statistical characteristics of the permeability. More importantly, the data provide quantitative physical information concerning the permeability upscaling of a complex heterogeneous medium. Here, we analyze a subset of the data taken from a single block face cut normal to stratification. Results indicate a strong correlation between the calculated summary statistics and the cross-stratified structural features visibly evident in the sandstone sample. In particular, the permeability maps and semivariograms are characterized by two distinct nested scales of heterogeneity; including, a low-frequency structure defined by the cross-stratified sets (delineated by distinct bounding surfaces) and a high-frequency structure defined by the low-angle cross-stratification comprising each set. The measured permeability data also provide clear evidence of upscaling. That is, each calculated summary statistics exhibits distinct and consistent trends with increasing sample

[4] Tidwell, V.C. and J.L. Wilson, to be submitted to Water Resources Research or other journal, 1999.

support. Among the noted trends are an increasing mean, decreasing variance, and a linearly increasing semivariogram range. Also, comparisons of the permeability maps and semivariograms measured with tip seals of increasing size reveal that the high-frequency structural feature is preferentially filtered from the data, while the low-frequency structural feature remains virtually unchanged. Comparison of the statistical characteristics and permeability upscaling between cross-stratified sets shows considerable consistency; however, subtle differences are noted that are likely the result of minor variations in sediment load/flow conditions between depositional events. Minor differences are also found between the statistics characterizing the individual cross-stratified sets and those corresponding to the integrated coset (i.e., sampled block face).

5.2. Introduction

Permeability data are rarely acquired at the scale of their intended use, thus necessitating upscaling. Although there are many factors that affect permeability upscaling, one of the more closely studied is media heterogeneity. A common tenet of these studies is that the heterogeneity is structured according to a discrete and disparate hierarchy of scales. For example, the hierarchical models proposed by Dagan [1986] and Haldorsen [1986] conveniently classify heterogeneities according to the pore, laboratory, formation, and regional scales. This assumed disparity in scales allows permeability variations occurring at scales smaller than the modeled flow/transport process to be spatially averaged to form an effective media property [Warren and Price, 1961; Kirkpatrick, 1973; Gutjahr et al., 1978; Deutsch, 1989; King, 1989] while large-scale variations are treated as a simple deterministic trend [Gelhar, 1986; Rajaram and McLaughlin, 1990]. Owing to the complex processes responsible for their deposition and lithification, natural media are not always characterized by a large disparity in scales as assumed above [Rubin, 1995]. In other cases, an infinite number of scales may coexist [Hewett, 1986; Neuman, 1994; Di Federico and

Neuman, 1997; Liu and Molz, 1997], leading to a fractal geometry or continuous hierarchy of scales [Cushman, 1990].

Clastic sedimentary formations have long been described in terms of the hierarchy of bedforms specific to a particular depositonal environment. The hierarchical bedform assemblages largely dictate the spatial permeability patterns characterizing these formations. Two empirical examples include the Page Sandstone, an eolian deposit [Goggin et al., 1986; Chandler et al., 1989], and the Rannoch Formation, a storm-dominated shoreface sandstone [Corbett and Jensen, 1993]. Detailed simulation of the full hierarchy of bedforms is rarely an option, due to computational constraints. However, experimental observation [Robertson and Caudle, 1971] and numerical studies [Kortekaas, 1985; Van De Graaff and Ealey, 1989; Ringrose et al., 1993] suggest that even the smallest-scale heterogeneities can significantly influence flow and transport processes for a number of important engineering problems. Representing these small-scale complexities in upscaled parameters is complicated by the tendency of directional permeabilities to vary among bedforms. For this reason, upscaling must generally be pursued numerically with the large-scale effective block permeabilities determined from the output of fine-scale simulations. This process is performed in a step-wise manner starting at the smallest scale of heterogeneity and progressing from one discrete scale of heterogeneity to the next until the desired scale of analysis is achieved. This is referred to as upscaling by grid-block averaging [Bierkens and Weerts, 1994] or psuedofunctions [Kyte and Berry, 1975; Lasseter et al., 1986; Kossack et al., 1990]. Kasap and Lake [1990] offer an analytical alternative for calculating the full effective block permeability tensor.

Although the issue of scale, as it pertains to complexly structured media like cross-stratified sandstones, has received considerable attention, detailed physical data characterizing the permeability upscaling of such systems is lacking. To meet this need, we

have adapted a minipermeameter test system to acquire permeability data over a series of discrete sample supports (i.e., sample volumes). With this technique, spatially exhaustive, multi-support measurements are made subject to consistent flow geometries and boundary conditions by simply varying the size of the minpermeameter tip seal. These methods have been employed to test a block of Massillon Sandstone that exhibits two nested-scales of heterogeneity: a high-frequency feature defined by ubiquitous low-angle cross stratification and a low-frequency feature defined by the bounding surfaces delineating the individual cross-stratified sets. Here, we present a subset of the over 75,000 permeability measurements taken from this meter-scale block of rock. Analyses are performed to address the following questions:

- can correlations be drawn between the measured permeability characteristics and the visual aspects of the sampled block face?
- does the permeability upscale in a consistent and quantifiable manner?
- do the different scales of heterogeneity exhibit different upscaling behavior?
- do the permeabilities measured in different cross-stratified sets exhibit similar statistical characteristics and upscaling behavior, and are they similar to that of the integrated coset (i.e., sampled block face)?

5.3. Methods and Materials

Multi-Support Permeameter (MSP)

The collection of spatially exhaustive data from multiple, discrete sample supports is key to our investigation of permeability upscaling. The acquired data are uniquely qualified for investigating upscaling processes as: 1) all measurements, regardless of sample support, are made subject to consistent boundary conditions and flow geometries; 2) measurements are non-destructive thus allowing all data to be collected from the same physical sample; 3) dense sampling grids are employed to provide detailed spatial

information on the permeability field; and, 4) measurements are precise, subject to small and consistent measurement error. By acquiring data in this manner, sampling artifacts that hinder the quantification of permeability upscaling are minimized or eliminated.

We employ a specially designed minipermeameter [Dykstra and Parsons, 1950; Eijpe and Weber, 1971; Goggin et al., 1988] test system, which we term the Multi-Support Permeameter (MSP) (see Chapter 2). Permeability is measured by simply compressing a tip seal against a flat, fresh rock surface while injecting gas at a constant pressure. Using information on the seal geometry, gas flow rate, gas injection pressure, and barometric pressure, the permeability is calculated using a modified form of Darcy's Law [Goggin et al., 1988]. This process is automated by coupling a minipermeameter with an x-y positioner and computer control system. The minipermeameter functions as the measurement device of the MSP and consists of four electronic mass-flow meters (0-50, 0-500, 0-2000, and 0-20,000 cm^3/min. at standard conditions), a pressure transducer (0-100 kPa gauge), a barometer, and a gas temperature sensor that are all connected to a regulated source of compressed nitrogen. Measurements are made according to a user specified sampling grid programmed into the x-y positioner. Along with locating the tip seal for sampling, the positioner also compresses the tip seal squarely against the rock surface with a consistent and constant force. The electronic minipermeameter and x-y positioner are configured with a computer control system to govern the data acquisition process and provide unattended operation of the MSP. A full description and analysis of the MSP is given in Chapter 2.

MSP Tip Seals and the Sample Support

Measurements are made at different sample supports subject to consistent boundary conditions and flow geometries by simply varying the radius of the tip seal. Tip seals, specifically designed for this program, consist of a rigid aluminum housing to which a molded silicone rubber ring is affixed. A series of such tip seals have been built with inner

radii (r_1) of 0.15, 0.31, 0.63, 1.27, and 2.54 cm, and an outer radii measuring twice the inner. A consistent and known tip seal geometry under compressed conditions is critical to precise measurement. For this reason, each of the tip seals is equipped with an internal spring-driven guide to maintain a constant inner seal diameter. For the 0.63 cm and smaller tip seals, which experience considerable deformation on compression, an immobile outer guide is also employed.

It is important to note that the ring-shaped tip seal imposes a strongly divergent flow geometry on the test medium. The resulting non-uniform flow field not only has important implications relative to the measured permeability upscaling [Matheron, 1967; Desbarats, 1992; Indelman and Abramovich, 1994] but also raises questions concerning what the MSP actually measures. To address this latter issue, we empirically investigated the measurement characteristics of the MSP by way of linear filter analysis (see Chapter 3). Results, as given by the empirical spatial weighting functions, indicate that the sample support is approximately hemispherical (even for the samples characterized by permeability anisotropy) consistent with the symmetry of the tip seal. Heterogeneities located near the center of the tip seal influence the measurement more than those located further away, consistent with the divergent flow field imposed by the MSP. Also, as the tip seal size increases the effective radius, r_{eff}, of measurement increases. Although additional work is needed to fully quantify the sample support associated with each tip seal, we and others [e.g., Goggin et al., 1988] believe that the r_{eff} is roughly proportional to r_1, hence the volumetric sample support increases by a power of 8 for each doubling of r_1.

Massillon Sandstone Sample

Permeability data were acquired from a 0.94 by 0.96 by 1.01 m block of Massillon Sandstone acquired from the Briar Hill Stone Company in Glenmont, Ohio. The Massillon Sandstone, of Pennsylvanian age, outcrops through much of northeastern Ohio and is an

important commercial source of dimensional stone. Based on thin section analysis, this sample can be classified as a moderately well-sorted, medium-grained quartz sandstone. Diagenetic alterations affecting the sandstone have occurred as evidenced by the presence of hydrous iron oxide precipitates and quartz overgrowths.

The fabric of the sandstone sample is characterized by a series of sub-horizontal bounding surfaces spaced approximately 16-22 cm apart (Figure 5.1a). The bounding surfaces are planar with locally undulatory interfaces. Between the bounding surfaces low-angle cross stratification is evident with individual laminae spaced approximately 2-4 cm apart. In each of the cross-stratified sets (delineated by the bounding surfaces), the laminae are unidirectionally oriented with an apparent dip varying from 10° to 22°. Tangential contacts between the cross beds and bounding surface are common. The degree of disruption of the cross stratification at the bounding surface interface also varies among the different sets.

The composition, sorting, and structure of the formation suggest that the Massillon Sandstone was water lain under relatively energetic conditions. However, there is some uncertainty concerning the actual mode of deposition, with both fluvial [Schmidley, 1987] and tidal environments [Gray, 1956] having been suggested.

5.4. Results

Over 75,000 permeability measurements were collected from the six block faces of the Massillon Sandstone sample. Measurements were made on the exact same grid using the 0.15, 0.31, 0.63, 1.27, and 2.54 cm r_t tip seals. The sample grid contained 2500 measurement points organized on a square 50 by 50 lattice on 1.27 cm centers. To avoid boundary effects on the measurement, the 62.2 by 62.2 cm grid was centered on the block

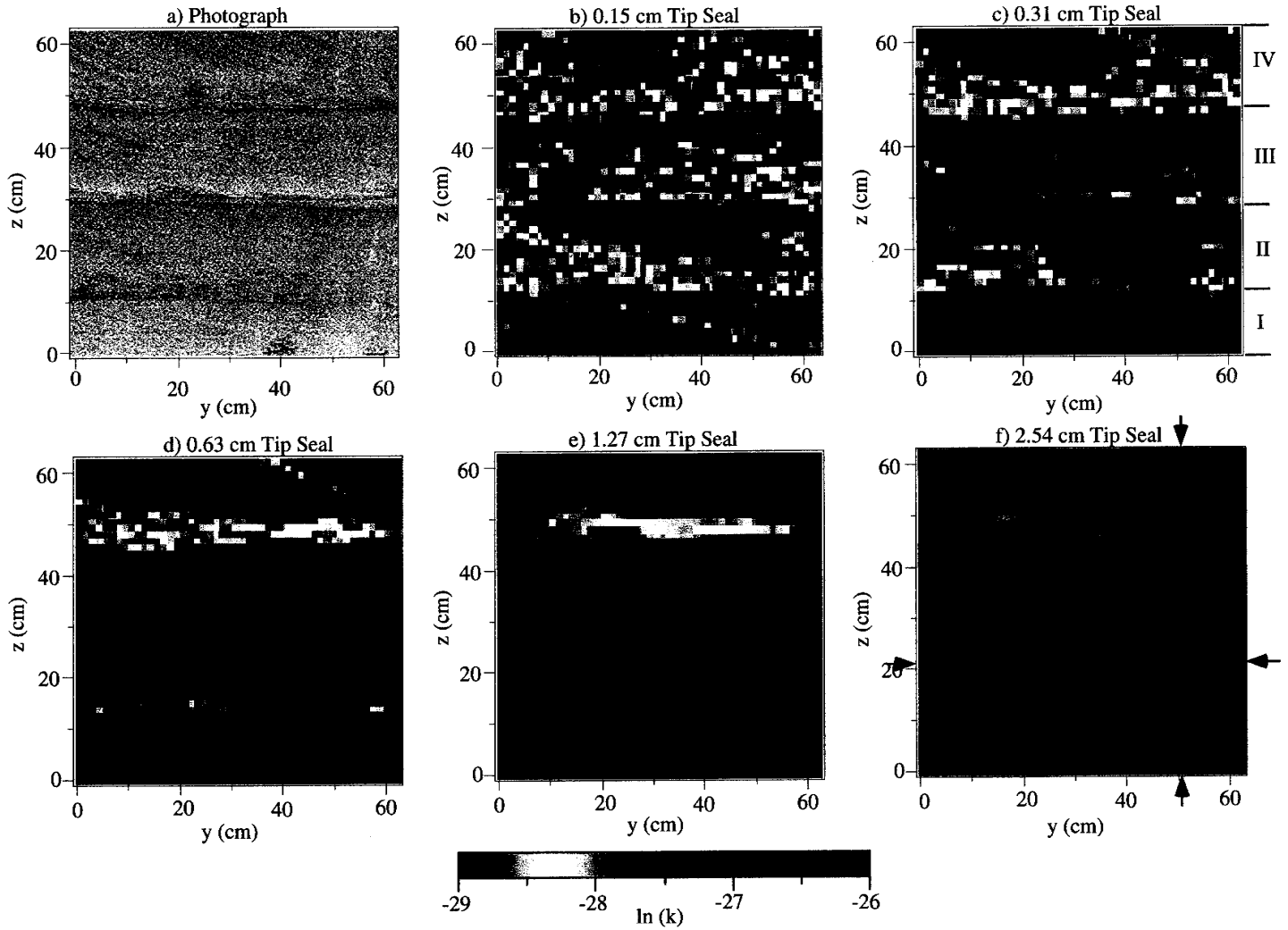

Figure 5.1. Photograph a) of Face 4 of the Massillon Sandstone sample showing the area sampled with the MSP. The corresponding natural-log permeability fields (where k is in m^2) measured with the b) 0.15, c) 0.31, d) 0.63, e) 1.27, and f) 2.54 cm r_1 tip seals are also given. Data were collected from a 50 by 50 point grid on 1.27 cm centers. Also shown are c) the inferred bounds for each of the cross-stratified sets (Table 5.1), and f) locations for the permeability transects given in Figure 5.2.

face providing a buffer of over 16 cm between the grid and edge of the block. Although all six block faces were sampled, we limit our attention here to data from a single block face cut normal to the cross stratification (we term Face 4). Data from the other face block faces are not presented, in part, to maintain a manageable length to this paper. More importantly, all six block faces exhibit similar statistical and upscaling characteristics. Thus, for purposes of this paper, presentation of results for all six block faces would be redundant.

It should be noted that each face of the Massillon Sandstone block is marked by a small number of narrow voids. These voids appear to be the mold of some feature that has subsequently weathered from the rock. MSP measurements made directly on or very near these voids have no real meaning because unrestrained gas flow occurred. As the voids are few and disconnected, the measured, meaningless, permeability values were replaced with values representative of those near the feature. The missing values were replaced via ordinary kriging [Deutsch and Journel, 1997] using the retained permeability data (i.e., values measured away from the voids) and corresponding semivariograms (see below). On Face 4, a total of 15, 14, 14, 39, and 86 permeability values were replaced for the 0.15, 0.31, 0.63, 1.27 and 2.54 cm tip seals, respectively. Thus, only 168 out of 12,500 measurements required replacement for this block face. Differences between summary statistics and semivariograms calculated with and without the replaced permeability values are almost indistinguishable. The adjustments are reflected in the data presented below.

Raw Permeability Data

The natural-log permeability fields ($\ln[k(y,z)]$ where k is in m^2, y is parallel to the bounding surfaces, and z normal) measured with the 0.15, 0.31, 0.63, 1.27 and 2.54 cm r_t tip seals are given in Figure 5.1b-f. Comparison of the permeability fields and photograph (Figure 5.1a) reveal a remarkable correlation between the structural features visible in the rock face and the spatial patterns characterizing the two-dimensional

permeability fields. Four well-defined sets of cross stratification, which we designate as Sets I-IV (see Table 5.1 and Figure 5.1c), are delineated by three bounding surfaces. These bounding surfaces are marked by zones of distinctly lower permeability that vary from 3-6 cm in thickness and fully span the width of the sampling domain. Between these bounding surfaces permeabilities are clearly higher and structured, exhibiting bands of alternating permeability, corresponding to the low-angle cross stratification.

According to this comparison it is apparent that the measured variations in permeability correlate with the textural (e.g., grain size, sorting, packing) changes in the rock. Textural changes are most pronounced at the bounding surfaces and at the interface between individual cross strata. Inspection of Figure 5.1 reveals that a corresponding contrast in permeability accompanies these textural interfaces. In addition, iron oxide cements (distinguished by its dark color in the photograph) appear to be concentrated at the textural interfaces. Although beyond the scope of the current paper, detailed thin-section analysis is being performed to quantify the relationships between the permeability, texture, degree of lithification, and upscaling [Chapin et al., 1998].

Striking differences are evident between the permeability maps measured with the different size tip seals, the most obvious being the distinct smoothing that accompanies increasing tip seal size. However, the same basic structural features are retained in each of the permeability maps. All three bounding surfaces and evidence of the low-angle cross stratification are clearly visible in each of the permeability maps. It is apparent that the smoothing reflects the filtering of the finer-scale heterogeneity by the sequentially increasing sample support (i.e., tip seal size).

Table 5.1. Bounding limits for the cross-stratified sets evident in Face 4 of the Massillon Sandstone sample.

	Lower Bound	Upper Bound
Set I	z=0.0 cm	z=11.43 cm
Set II	z=12.7 cm	z=29.21 cm
Set III	z=30.48 cm	z=45.72 cm
Set IV	z=46.99 cm	z=63.5 cm

This sequential filtering of the fine-scale heterogeneity is particularly evident if we explore the permeability along transects extracted from each of the two-dimensional maps given in Figure 5.1. Permeability transects oriented parallel (centered on z=20.32 cm, see Figure 5.1f) and normal to the bounding surfaces (centered on y=50.8 cm) are plotted in Figure 5.2. To facilitate comparison the permeabilities for each tip seal have been rescaled according to the mean log permeability of the transect. In both cases the 0.15 cm tip seal transect is characterized by a relatively smooth low-frequency component on which a higher-frequency (noisier) feature is superimposed. As the tip seal size is increased the higher-frequency feature is sequentially filtered while the lower-frequency component remains almost unchanged. Closer inspection suggests that the window size of the filter is roughly equal to the outer diameter of the tip seal. For a more thorough analysis of the spatial filtering characteristics of the MSP see Chapter 3.

The high- and low-frequency components evident in the transects can be easily related to the cross-stratified features visible in the sampled block face. Normal to the bounding surfaces (Figure 5.2b) a low-frequency component, with a period of approximately 18 cm, and high-frequency feature, with a period of approximately 3 cm, are evident. The low-frequency feature exhibits three distinct cycles, each corresponding to a

set of cross stratification. This cyclical behavior occurs because each cross-stratified set is characterized by a distinct bounding surface (the bounding surface associated with Set *I* was excluded by the sampling grid) followed by a coarsening upward trend. The associated high-frequency component is ubiquitous and appears to be a product of the cross stratification comprising each set. Parallel to the bounding surfaces (Figure 5.2a) both high- and low-frequency components are evident. The high-frequency component is of similar amplitude but of slightly lower frequency than that found in the orthogonal transect. Again, the high-frequency component appears related to permeability variations arising from the cross stratification. The low-frequency component has a slightly lower amplitude than its orthogonal compliment and a larger period (~60 cm). This feature is not associated with a bounding surface but rather is believed to be the result of changes in the sediment source coincident with the progradation of the bedform. It is also likely that each of the aforementioned permeability features are in some way influenced by the distribution of cementing agents, which, in turn, appear to be related to the textural variations in the rock sample.

Cumulative Distribution Functions

The cumulative distribution functions (CDFs) for the natural-log permeability data measured with the five different tip seals are given in Figure 5.3. The permeability range spanned by the individual CDFs varies by over two orders of magnitude for the 0.15 cm tip to less than one order of magnitude for the 2.54 cm tip. Each of the CDFs is characterized by a distinct negative skew. The skewness is largely a product of the bands of lower permeability associated with the bounding surfaces, particularly the one associated with Set IV. Given the distinct negative skew we conclude that the permeability is not log-normally distributed.

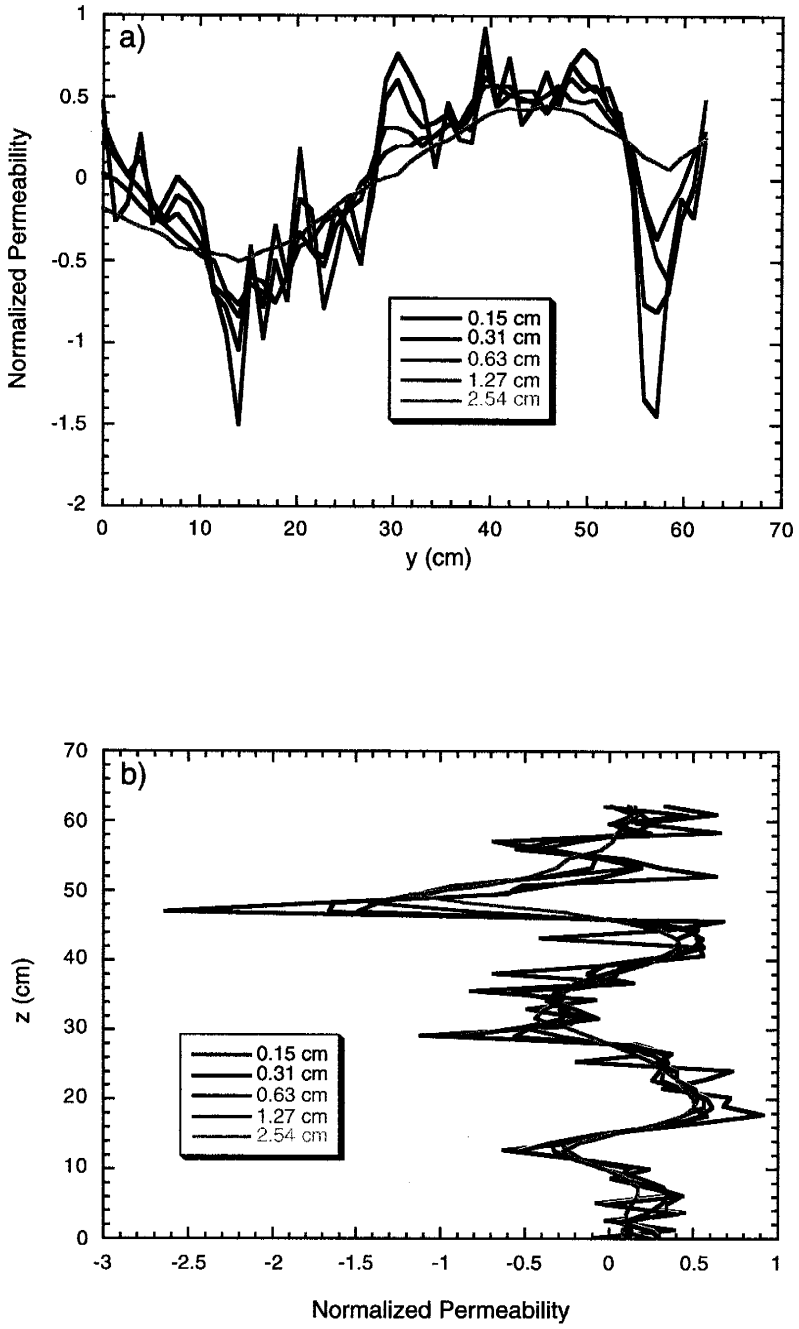

Figure 5.2. Permeability transects measured with each of the five MSP tip seals. Shown are transects oriented a) parallel to stratification centered on z=20.32 cm (see Figure 5.1f), and b) normal to stratification centered on y=50.8 cm. To facilitate comparison, each transect has been normalized by its mean permeability. As tip seal size increases note the distinct filtering of the high-frequency feature while the low-frequency component remains virtually unchanged.

Several changes in the CDFs are noted with increasing tip seal size. Subtle differences are noted across the entire distribution; however, the most significant changes occur in the lower tail. As the tip seal size increases there is a decrease in the skew. Rather than the distribution becoming symmetric, a bimodal structure appears. The two modes are distinguishable in the CDFs for 1.27 and 2.54 cm tip seals by the offset evident between the 1st to 5th percentiles. This trend toward a weak bimodal distribution reflects the organization of the permeability field into alternating bands of "high-" and "low-permeability" (see Figure 5.1); that is, the high-frequency variability is filtered from the permeability field leaving a simple layered system (i.e., the low-frequency structure). Other important changes in the CDFs correspond to the mean and variance of the distribution. Specifically, the sample mean increases with increasing sample support while the sample variance decreases (see below).

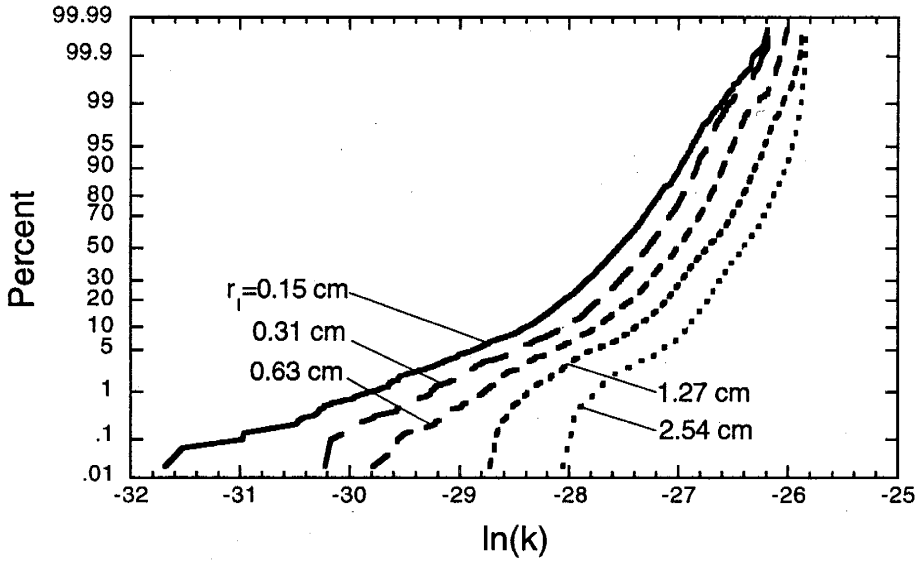

Figure 5.3. Cumulative distribution functions for the natural-log permeability data sets given in Figure 5.1. Each curve represents 2500 permeability values.

Comparisons are also drawn between the CDFs calculated for individual sets of cross stratification. The CDFs for the natural-log permeability values measured in Sets II and IV are given in Figure 5.4. The CDFs for the individual sets consistently exhibit an upper log permeability range of between -26.4 and -25.8, a negative skew that decreases with increasing sample support, and an increasing mean and decreasing variance with increasing tip seal size. Where the CDFs tend to differ is in the minimum range of the distribution and in the detailed shape of the distribution. The noted similarities in the CDFs occur because the same depositonal process formed each cross-stratified set. Alternatively, differences in the CDFs among the individual sets reflect variations in flow velocity, flow direction, and/or sediment load between the events responsible for depositing each particular cross-stratified set.

In comparing the CDFs for individual cross-stratified sets (Figure 5.4) with that of the integrated coset (for the entire sampled block face as shown in Figure 5.3) similarities in the upper log permeability range, general shape, and trends in the mean and variance are evident. Differences are primarily noted within the lower log permeability range and the detailed shape of the distribution. These differences arise because the lower tail of the coset CDF is defined by the "extreme" low permeability values which happen to be concentrated in Set IV, while the central region (~5th to 95th percentile) of the coset CDF reflects the average behavior of the individual sets and not the subtle differences.

Spatial Structure

The spatial correlation of the acquired permeability data was also investigated. Full two-dimensional semivariograms were calculated for each of the five tip seal data sets using Fourier analysis (via Fast Fourier Transforms, see Bracewell, 1986 and Section 3.3). The two-dimensional semivariogram for the 0.15 cm tip seal is given in Figure 5.5 for reference. In addition, transects oriented parallel and normal to the bounding surfaces, and

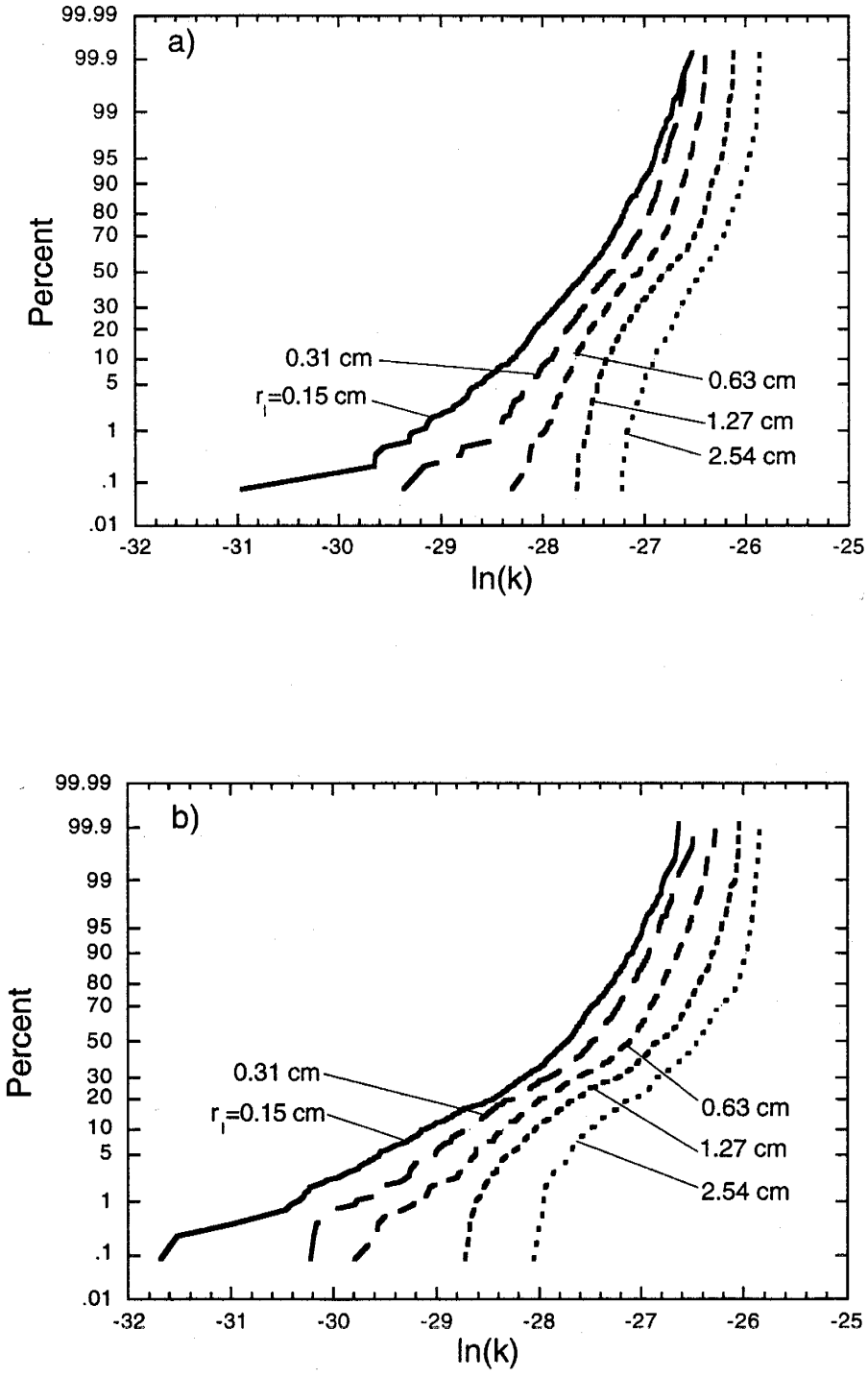

Figure 5.4. Cumulative distribution functions for individual sets of cross stratification. Shown are the CDFs for a) Set II and b) Set IV (see Figure 5.1 and Table 5.1).

taken through the center of the two-dimensional semivariograms, are plotted in Figure 5.6. To quantify the spatial structure, semivariogram models were fit to each of the transects (Figure 5.6). Two nested anisotropic exponential models coupled with a cosine hole-effect model (applied only in the z direction) closely fit the sample semivariograms. The composite fitted model γ is given by

$$\gamma(\vec{s}) = \sigma_1\left(1-\exp\left[-\left(\frac{(3\vec{s})^2}{\vec{\lambda}_1^2}\right)^{1/2}\right]\right)+\sigma_2\left(1-\exp\left[-\left(\frac{(3\vec{s})^2}{\vec{\lambda}_2^2}\right)^{1/2}\right]\right)+\sigma_3\left(1-\cos\left[\frac{2\pi s_z}{T_z}\right]\right) \quad (5.1)$$

where σ_i the variance component for the ith model $(i = 1,2,3)$, $\vec{\lambda}_i$ the semivariogram range (cm) in the principal directions $\left(\vec{\lambda} = \left(\lambda_y, \lambda_z\right)\right)$ for the i th model, T_z (cm) the period of the hole-effect feature, and $\vec{s} = \left(s_y, s_z\right)$ is the separation vector (cm) in the principal directions. The fitted models are given in Figure 5.6 by the solid lines while the corresponding parameters are presented in Table 5.2.

The structural characteristics of the semivariograms are strongly correlated with the spatial features visible in the sampled block face (Figure 5.1a). The semivariograms reveal a strong degree of anisotropy reflecting the stratified structure of the Massillon Sandstone sample. Long-range spatial correlation is apparent parallel to the bounding surfaces while shorter-range correlation, dominated by a strong hole-effect feature, is exhibited normal to the bounding surfaces (Figure 5.6). The distinct hole-effect reflects the presence of multiple cross-stratified sets, each of relatively similar thickness and permeability characteristics. The semivariogram transects also indicate the presence of two nested structural features, a low-frequency feature defined by the distance between bounding surfaces and a high-frequency feature defined by the intervening cross stratification. The low-frequency feature

exhibits a range of 18 cm normal to the bounding surfaces and extends beyond the length of the semivariogram (30 cm) parallel to the bounding surfaces. The high-frequency feature shows only slight anisotropy and is defined by a range of approximately 2-3 cm. The low-frequency feature parallel to the bounding surfaces (associated with the inferred changes in the sediment source), evident in the permeability maps (Figure 5.1) and transects (Figure 5.2b), is not resolved by the semivariograms as its period exceeds the length of the semivariogram.

Several upscaling trends are evident among the fitted semivariograms. First, the sill of the semivariogram decreases with increasing sample support, reflecting the behavior of the sample variance (discussed below). Second, the semivariogram range increases with

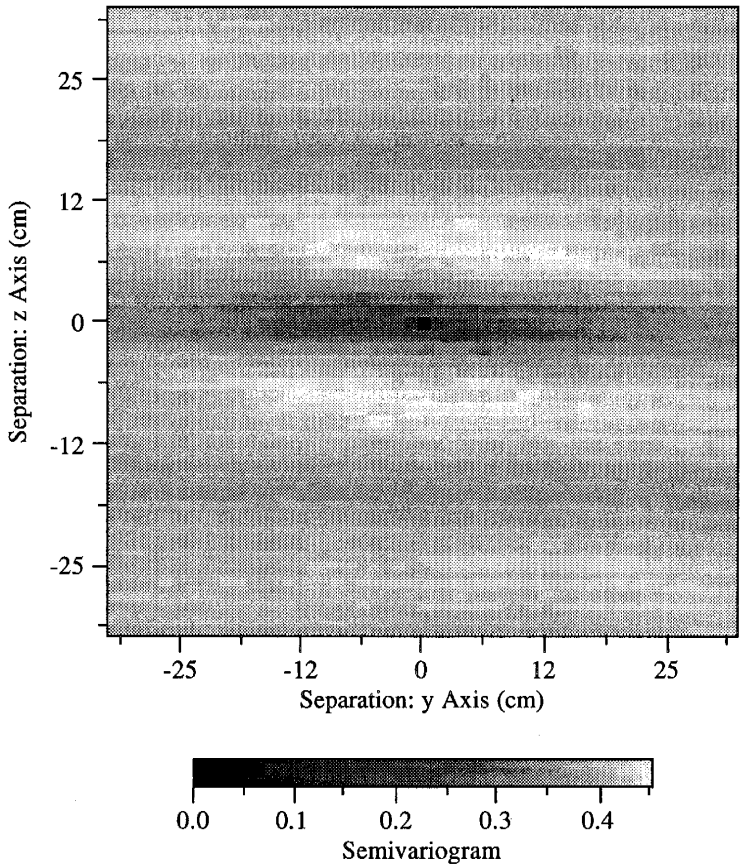

Figure 5.5. Two-dimensional semivariogram calculated from the natural-log permeability data collected with the 0.15 cm r_1 tip seal on Face 4 of the Massillon Sandstone sample.

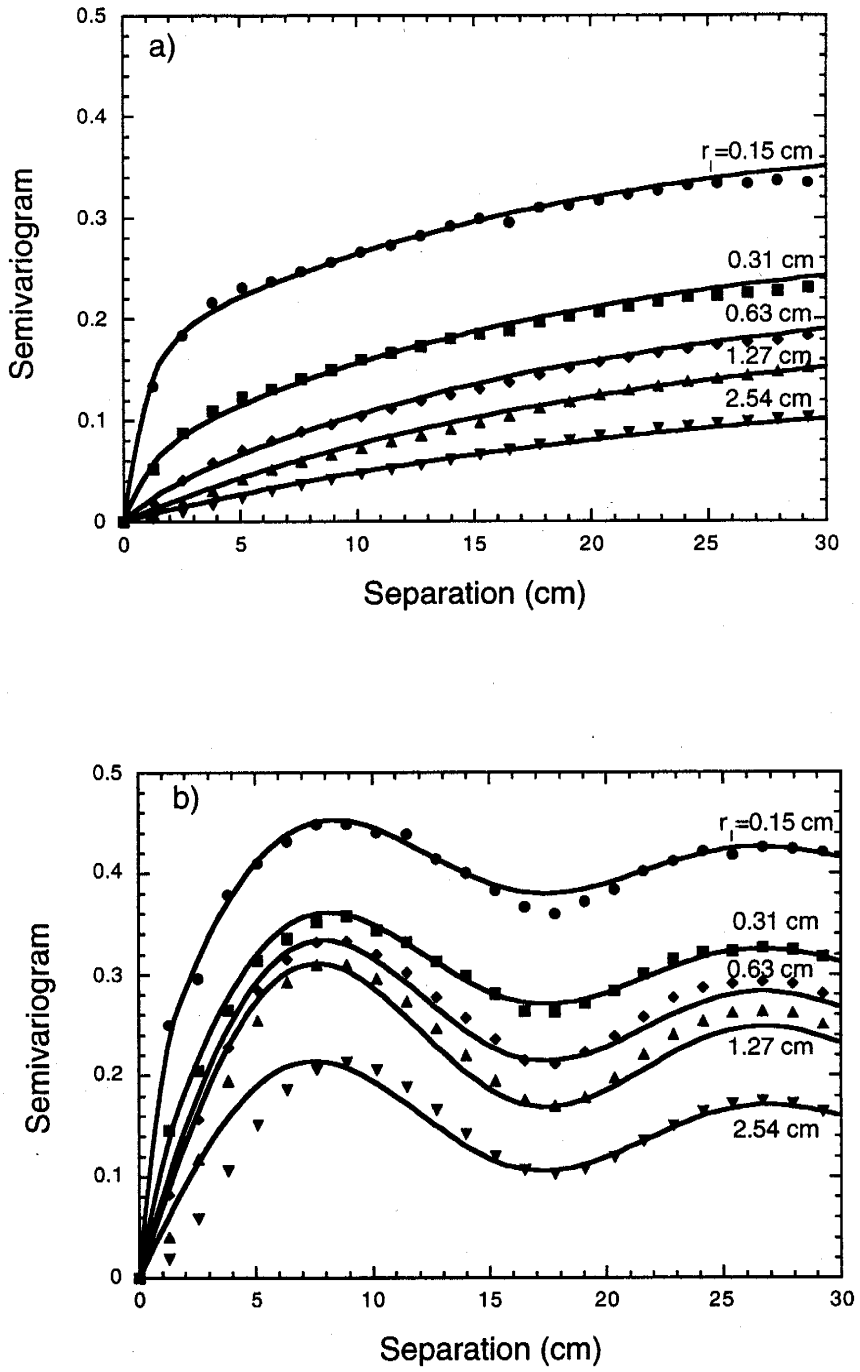

Figure 5.6. Semivariogram transects (symbols) for the natural-log permeability data sets measured with each of the five different-size tip seals on Face 4 of the Massillon Sandstone sample. Orientation is a) parallel (y axis) and b) normal (z axis) to the bounding surfaces. The fitted semivariogram models (Equation 5.1) are given by solid lines.

Table 5.2. Parameter values for the semivariogram models fitted to the data given in Figure 5.6.

	High-Frequency Structure			Low-Frequency Structure			Hole-Effect Structure	
Tip	σ_1	λ_y(cm)	λ_z(cm)	σ_2	λ_y(cm)	λ_z(cm)	σ_3	T_z(cm)
0.15 cm	0.17	2.7	1.5	0.23	33.0	18	0.055	18.0
0.31 cm	0.06	3.3	2.1	0.23	34.8	19.5	0.065	18.0
0.63 cm	0.02	4.5	3.3	0.22	57.0	22.5	0.080	18.0
1.27 cm	-	-	-	0.20	63.0	28.5	0.090	18.0
2.54 cm	-	-	-	0.15	75.0	40.5	0.068	18.0

increasing tip seal size. In fact, there is evidence that the range increases as a linear function of tip seal size, thus suggesting a direct relation between the value of the fitted range and the tip seal radius with which it was measured [Clark, 1977; Journel and Huijbregts, 1978]. However, the estimated range values must be viewed with some caution as the fitted model (Equation 5.1) is only mildly sensitive to this parameter. Although a number of trends are noted among the fitted parameters, the general semivariogram model (Equation 5.1) remains essentially unaffected by changing sample support. It is important to note that the 1.27 and 2.54 cm tip seals fail to resolve the high-frequency structural feature (i.e., associated with the low-angle cross stratification). This suggests that as the size of the tip seal becomes large with respect to a feature, that structure is effectively filtered from the permeability field. This is exactly what we see in the permeability transects given in Figure 5.2.

It is interesting to note that the qualitative upscaling trends exhibited by the semivariograms are consistent with that predicted by semivariogram regularization theory

[Clark, 1977; Journel and Huijbregts, 1978]. This is a bit surprising given that the permeability does not upscale according to a simple arithmetic averaging process, as demonstrated by the distinct increase in the mean permeability with increasing sample support (see below). Given the non-linear volume averaging characterizing the permeability upscaling, quantitative comparisons drawn between our data and semivariogram regularization theory is expected to meet with less success. Such comparisons will be the subject of future analyses.

Two-dimensional semivariograms were also calculated for each of the individual cross-stratified sets. The semivariograms for the 0.15 and 1.27 cm tip seals are plotted in Figure 5.7 for sets II and IV. Both cross-stratified sets exhibit distinct anisotropy with the principal axes oriented at an inclined angle to the horizontal. Both sets also exhibit similar upscaling trends, characterized by a decreasing semivariogram sill, increasing range, and a consistent semivariogram structure with increasing tip seal size. A notable difference between the two cross-stratified sets is the orientation of the principal permeability axes, and hence the orientation of the cross stratification. Set II is inclined at an angle of 10° while set IV is inclined at an angle of 22°, consistent with the orientation of the cross stratification visibly evident in the sampled block face (Figure 5.1a). This difference is likely the result of changes in the sediment load/flow conditions between depositional events.

Comparisons are also drawn between the semivariograms calculated for the individual sets (Figure 5.7) and that calculated for the integrated coset (e.g., Figure 5.5). By combining the sets an additional scale of heterogeneity is realized that provides information on the geometric configuration of the sets. However, by combining the sets it

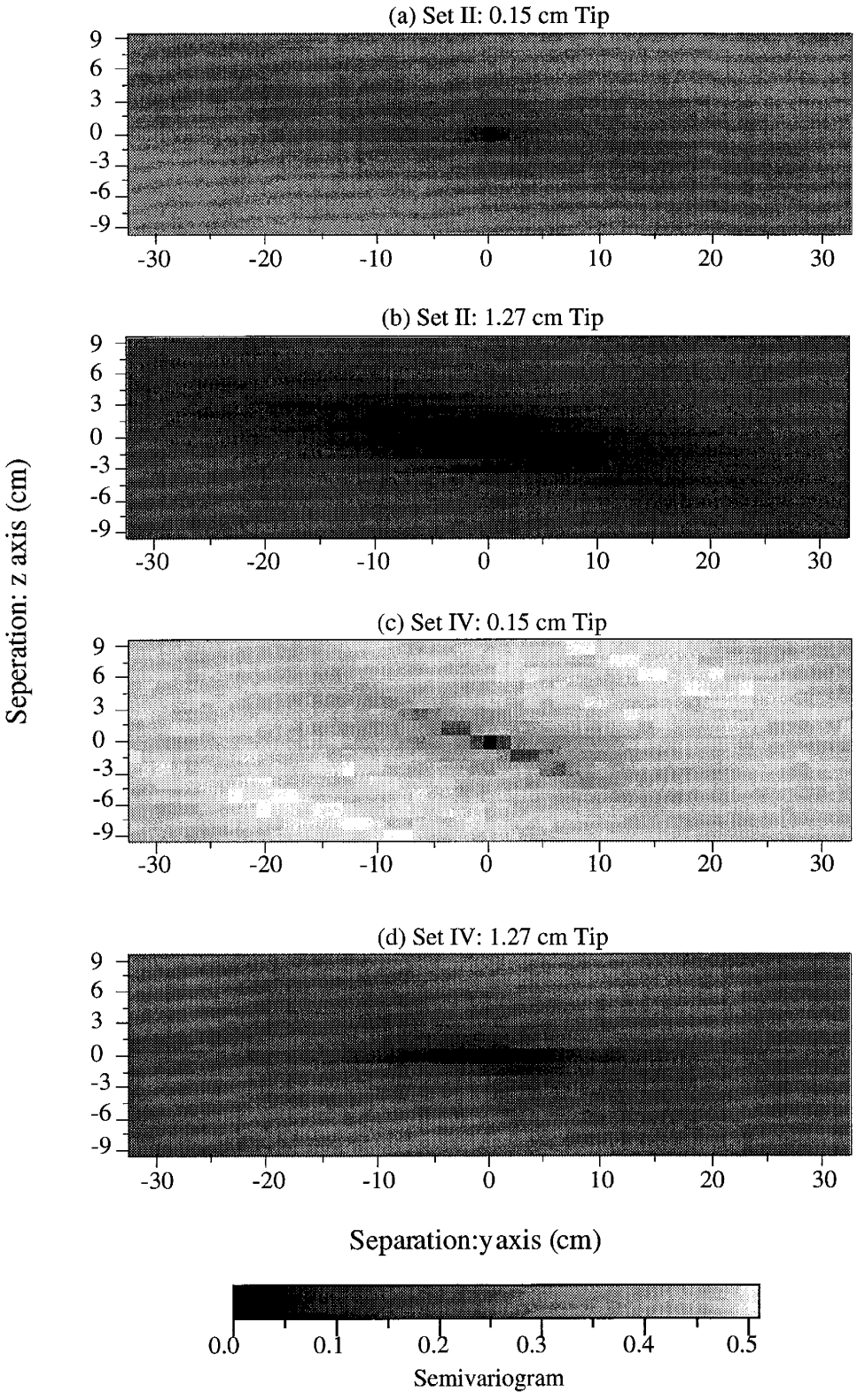

Figure 5.7. Two-dimensional semivariograms calculated for individual sets of cross stratification. Shown are the semivariograms for the a) 0.15 and b) 1.27 cm tip seals from Set II, and the c) 0.15 and d) 1.27 cm tip seals from Set IV.

becomes difficult to distinguish the inclined orientation of the high-frequency structural feature (i.e., low-angle cross stratification). To the extent that it can be measured, we find its the orientation to be limited to an average of the individual sets (approximately 14° in the semivariograms calculated for the integrated coset).

Sample Mean and Variance

In Figure 5.8, the mean and variance of the natural-log permeabilities are plotted as a function of the characteristic length of measurement, which we take to be equal to the outer tip seal diameter (i.e., $4r_l$). In the case of the mean, we also plot the value of a single permeability measurement made with a large tip seal (7.62 cm r_l) centered on the sampling grid (inset in Figure 5.8). The 7.62 cm tip seal provides a single effective permeability value that integrates over much of the sampling domain.

As with the other statistical measures given above, the sample mean and variance exhibit distinct upscaling trends. Specifically, the mean exhibits a consistent increasing trend with increasing sample support (i.e., sample volume). This increasing trend is believed to be a product of the divergent (non-uniform) flow imparted by the MSP coupled with the strong anisotropy in permeability, which spans all scales of measurement. For a more detailed analysis of the mean upscaling under such conditions see Chapter 4. Alternatively, the variance exhibits a consistent decreasing trend with increasing tip seal size. This trend simply reflects the fact that as the tip seal size increases its measurement integrates over more heterogeneity resulting in a "smoothed" permeability. This smoothing is particularly evident in the permeability maps (Figure 5.1) and the transects given in Figure 5.2.

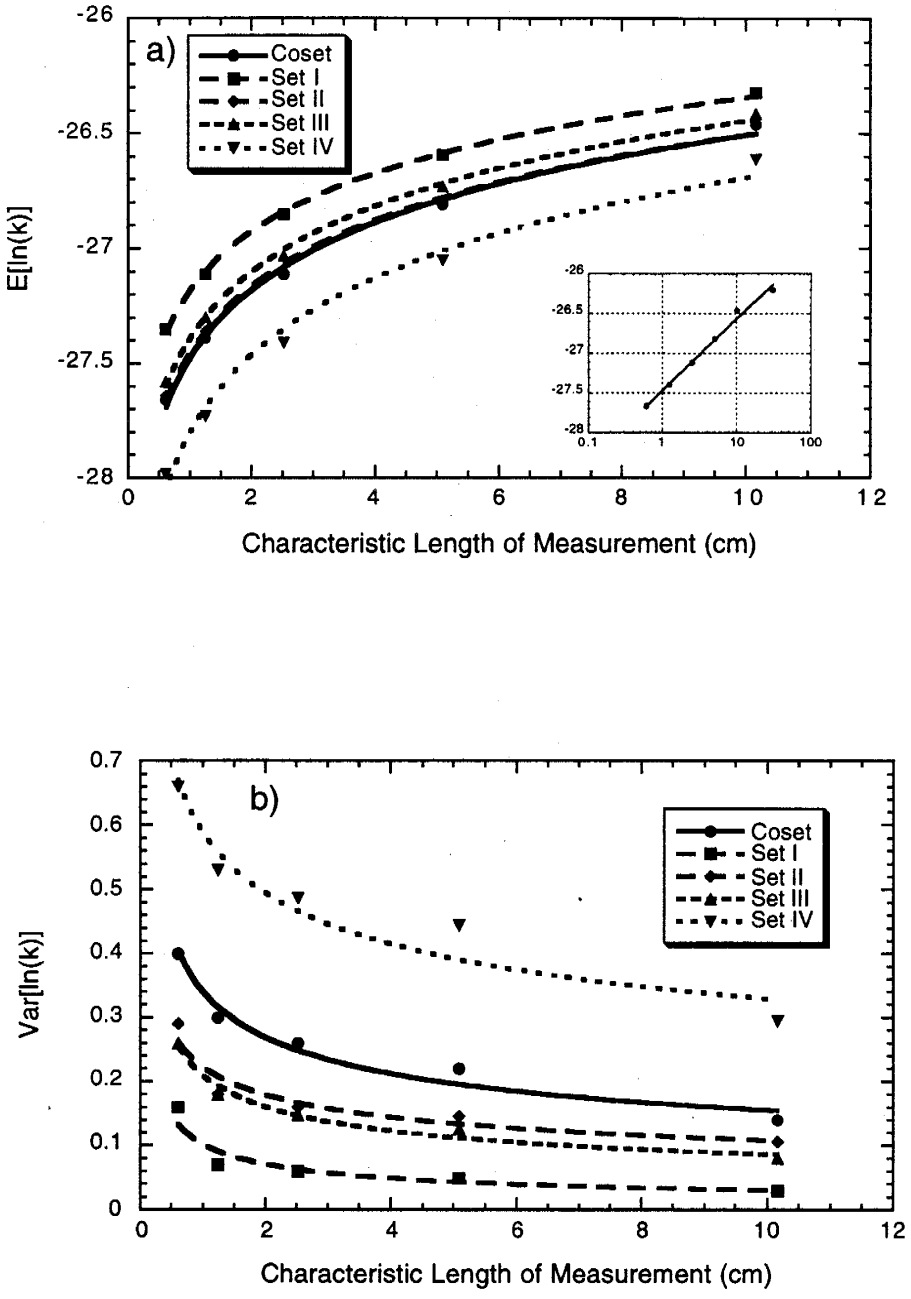

Figure 5.8. Mean a) and variance b) upscaling measured on Face 4 of the Massillon Sandstone versus the characteristic measurement length (i.e., outer tip seal diameter). Shown are the upscaling trends for each individual set of cross stratification and for the integrated coset. In each case a power-law model (Equation 5.2 and Table 5.3) is fit to the calculated statistic (symbols). The inset in (a) shows log-log plot of the mean upscaling for the integrated block face with the addition of a single measurement made with the 7.62 cm r_1 tip seal.

Both the mean and variance upscaling trends display a power-law behavior

$$A(d) = cd^{\alpha} \tag{5.2}$$

where A is either the mean or variance, c is a constant, d is the outer tip seal diameter (cm), and α is the power coefficient (see Table 5.3 for the fitted parameter values). The mean (variance) increases (decreases) rapidly at first and then follows a more gradual change as tip seal size increases. In both cases the upscaling trends exhibit the sharpest transition at about 2-4 cm, which is the point where the size of the tip seal approaches the characteristic length of the low-angle cross stratification. Neither the mean nor the variance appear to have reached an asymptotic limit suggesting that the low-frequency structure extends beyond the boundaries of the sampling domain.

Also plotted are the mean and variance upscaling for each of the individual cross-stratified sets (Figure 5.8). A power-law relation has been fit to each to facilitate comparison (see Table 5.3 for the fitted parameter values). The mean upscaling exhibited by each of the sets and the integrated coset (i.e., sampled block face) follow almost identical trends as is evidenced by similarity in the fitted α values. Similar results are achieved for the variance. However, a distinct offset in the absolute magnitudes of the mean and variance are evident (see the constant c). The offsets are most significant for sets I and IV. Set I exhibits a high mean and low variance relative to the others because its bounding surface was truncated from the analysis by the position of the sampling grid. Set IV exhibits a low mean and high variance relative to the others because the lowest permeabilities are concentrated in this cross-stratified set.

Table 5.3. Power-law coefficients (Equation 5.2) fitted to the mean and variance upscaling plotted in Figure 5.8.

	Mean		Variance	
	c	α	c	α
Coset	-27.47	-0.015	0.34	-0.34
Set I	-27.18	-0.013	0.10	-0.52
Set II	-27.45	-0.015	0.22	-0.31
Set III	-27.38	-0.015	0.21	-0.38
Set IV	-27.79	-0.017	0.59	-0.25

The variance upscaling associated with each of the structural features identified in the semivariograms is also explored. The variances corresponding to the high-frequency feature, the low-frequency feature, and the hole-effect feature were determined from the semivariogram model parameters ($i = 1,2,3$ in Equation 5.1, respectively) fitted to the transects in Figure 5.6 (see Table 5.2). These variances are plotted as a function of outer tip seal diameter in Figure 5.9. In each case the variances follow smooth but different upscaling trends. The greatest loss of variance is associated with the high-frequency structural feature and tip seals smaller than 1.27 cm. The variance for the low-frequency feature exhibits a gradual decline that accelerates with increasing tip seal size. Thus, the variability associated with structures smaller than the tip seals (i.e., high-frequency) is quickly filtered from the data while the variability associated with structures larger than the tip seals (i.e., low-frequency) experience relatively little change. The variance associated with the hole-effect structure exhibits a shallow convex trend with a maximum centered at about 5 cm. The initial rise is believed to be caused by the filtering of the high-frequency structure thus sharpening the contrast between the bounding surfaces and the cross stratification. The eventual decline observed for the 2.54 cm tip seal occurs because the size

of the tip seal has become large enough to begin filtering the features distinguishing individual cross-stratified sets.

5.5. Discussion and Conclusions

We believe that the results presented above represent the most comprehensive data set ever compiled (75,000 permeability measurements with over 12,000 shown here) characterizing the permeability upscaling of a porous medium exhibiting nested scales of heterogeneity. These upscaling studies were made possible through the use of a novel experimental system that we term the Multi-Support Permeameter (MSP) (see Chapter 2). Detailed permeability measurements were acquired from a meter-scale block of Massillon Sandstone. This sample was selected for testing because of its visually striking cross-stratified features. Here, we review the results presented above and put them in context with the questions raised in the introduction to this paper.

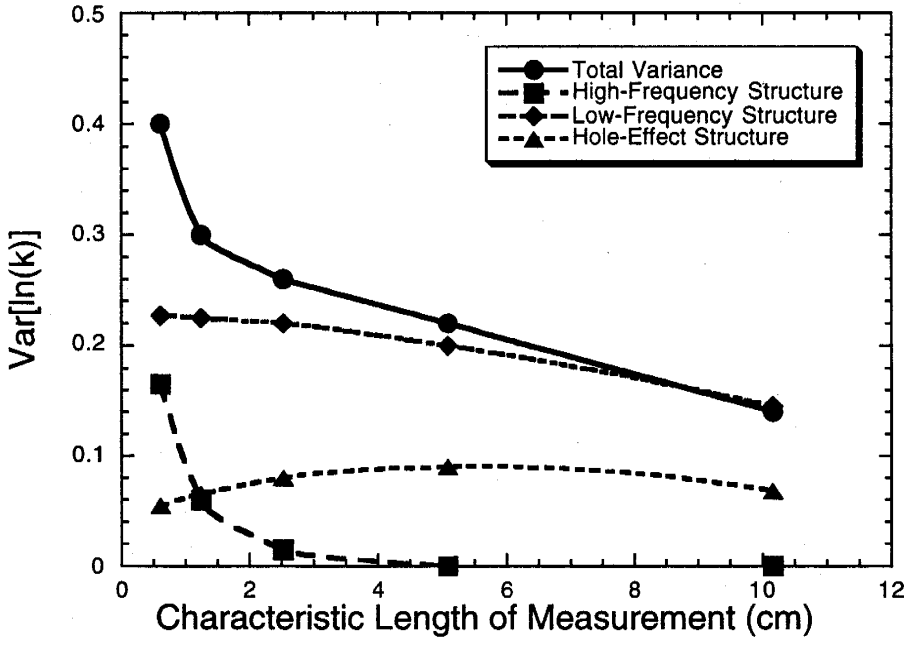

Figure 5.9. Variance upscaling associated with each semivariogram structural feature (Equation 5.1 and Table 5.2).

Permeability is strongly correlated with the "geology"

One of the most striking features of the acquired data is the correlation between the spatial characteristics of the measured permeability (Figure 5.1b-f) and the physical features visible in the sampled block face (Figure 5.1a). Each of the bounding surfaces are marked by zones of distinctly lower permeability while alternating bands of permeability, inclined with respect to the horizontal, mark the presence of low-angle cross stratification. In the corresponding semivariograms (Figures 5.5 and 5.6) two distinct scales of heterogeneity are evident: a high-frequency structure associated with the low-angle cross stratification, and a low-frequency feature that is defined by the distance between the bounding surfaces. Characteristic length scales associated with the fitted semivariogram models (Equation 5.1 and Table 5.2) are entirely consistent with the physical geometry of the bounding surfaces and cross stratification. On the basis of this body of evidence we conclude, unsurprisingly, that the permeability is intimately related to the physical attributes of the rock sample. Whether these variations in the permeability reflect changes in the rock's texture (e.g., grain size, sorting, packing), degree of lithification (presence of iron oxide and silica cements), or both is a subject of current research by the authors.

Permeability exhibits clear trends with increasing sample support (i.e., upscaling)

Spatially exhaustive permeability data sets were collected at each of five different sample supports (i.e., sample volumes) by simply varying the size the minpermeameter tip seal. In this way, all measurements, regardless of sample support, were made subject to the same flow geometry and boundary conditions. According to these careful and detailed measurements, permeability upscaling is evident in the two-dimensional permeability maps by the distinct smoothing that occurs as the tip seal size is increased (Figure 5.1). Likewise, the associated summary statistics show clear and consistent trends with changing sample support. As the sample support increases the mean increases and variance decreases according to a power-law relation, the correlation length scales increase linearly, while the

general structure of the semivariogram (anisotropic, exponential model with coupled hole-effect) remains relatively unchanged. Similar trends have been found for the other block faces and for other statistical measures but are not reported here.

We have also performed physical upscaling studies on other rock samples, with each exhibiting clear upscaling trends. Of particular interest are the results from a block of Berea Sandstone that is of a fluvio-deltaic origin. It exhibits an anisotropic spatial structure but only a single scale of heterogeneity. Nevertheless very similar statistical characteristics and upscaling behavior were measured (see Chapter 4). In contrast, the results for a block of volcanic tuff show considerably different statistical and spatial characteristics and likewise different upscaling behavior (see Chapter 6). This provides encouraging physical evidence that rocks of similar genetic origin upscale similarly while rocks of different origin upscale differently.

Nested scales of heterogeneity upscale differently

There is a distinct difference in the manner with which the high- and low-frequency structural features upscale. As the tip seal size increases the high-frequency structure is filtered from the data while the low-frequency component remains virtually unchanged. The associated filter appears to scale in proportion to the increasing outer diameter of the tip seal. This difference in upscaling between structural scales is evident in the permeability maps, transects, and semivariograms. In the permeability maps and transects (Figures 5.1 and 5.2) the high-frequency variability, corresponding the low-angle cross stratification, is sequentially filtered from the data sets. What remains are the low-frequency features associated with the bounding surfaces, and the large-scale trend in the y direction. In the semivariograms (Figures 5.6) the difference in upscaling is demonstrated by the disappearance of the high-frequency structural feature from the 1.27 cm and larger tip seal data sets. The high-frequency feature is filtered from the semivariogram at the point where the outer diameter of the tip seal exceeds the characteristic length of the low-angle cross

stratification. The preferential filtering of the high-frequency feature is also clearly demonstrated in the upscaling behavior of the variance. Specifically, the variance associated with the high-frequency structural feature is completely filtered from the data (Figure 5.9), while the variance associated with the low-frequency and hole-effect features exhibit considerably less change.

Similarities and differences characterize the relationship between individual cross-stratified sets and the integrated coset

In general, each cross-stratified set exhibits similar statistical and spatial characteristics as well as upscaling behavior. Each exhibits a non-Gaussian, negatively skewed permeability distribution whose mean increases and variance decreases with increasing sample support. Each set is characterized by an anisotropic semivariogram in which the principal permeability axes are inclined with respect to the horizontal. As the sample support increases the sill of the semivariogram decreases, the range increases, while the structural model remains consistent. Finally, the mean and variance upscaling trends consistently follow a power-law relation with relatively little variation in the power coefficient α, respectively (Equation 5.2). This suggests that consistency in depositional process results in consistent statistical and spatial permeability characteristics and consistent upscaling behavior. Nevertheless relatively subtle differences do exist between the different cross-stratified sets that are manifest in the detailed shape of the CDFs, the inclination of the cross strata, and the absolute values of the mean permeability and variance. These differences likely reflect changes in the conditions from one depositonal event to another. Such changes might include flow velocity, flow orientation, sediment load, and/or size distribution of the sediment.

Given the similarity in the statistical, spatial, and upscaling characteristics between the individual cross-stratified sets, it is no wonder that the same general characteristics are reflected in the integrated coset. However, some notable differences exist, in the lower tails

of the CDFs, the detailed shape of the CDFs (Figures 5.3 and 5.4), and in the directional characteristics of the low-angle cross stratification as inferred from the semivariograms (Figures 5.5 and 5.7). Probably of more importance are differences in the absolute means and variances of the log permeabilities (Figure 5.8). While the integrated coset statistics provide valuable information on the average behavior of the combined sets and on their geometric configuration (semivariogram), the subtle and not-so-subtle differences between the individual sets is sacrificed. For certain applications variations in the mean, variance, and/or inclination of cross stratification between sets, or the presence of zones of concentrated high or low permeability (e.g., low permeability bounding surface associate with Set IV) may have significant effect on the integrated behavior of the system. Thus, analyses of both the integrated coset and individual sets is generally warranted, if for no other reason than to identify the differences.

Acknowledgments. The authors wish to thank Mark Bailey for his help in data collection and Allan Gutjahr, Robert Glass, and Fred Phillips for providing constructive advice throughout this effort. We also recognize the critical reviews of this manuscript provided by Mike Chapin, Peter Davies, and Robert Holt. This work was supported by the U.S. Department of Energy, Office of Basic Energy Science, Geoscience Research Program, under contracts DE-AC04-94AL85000 and DE-F303-96ER14589/A000. Sandia is a multiprogram laboratory operated by Sandia Corporation, a Lockheed Martin Company, for the United States Department of Energy.

5.6. References

Bierkens, M.F.P. and H.J.T. Weerts, Block hydraulic conductivity of cross-bedded fluvial sediments, *Water Resour. Res.*, 30(10), 2665-2678, 1994.

Bracewell, R.N., *The Fourier Transform and Its Applications*, 474 pp., McGraw-Hill, New York, 1986.

Cushman, J.H., An introduction to hierarchical porous media, in *Dynamics of Fluids in Hierarchical Porous Media*, ed. by J.H. Cushman, Academic Press, New York, 1-6, 1990.

Chandler, M.A., G. Kocurek, D.J. Goggin, and L.W. Lake, Effects of stratigraphic heterogeneity on permeability in eolian sandstone sequence, Page Sandstone, Northern Arizona, *AAPG Bull.*, 73(5), 658-668, 1989.

Chapin, M., Jr., V.C. Tidwell, P. Mozley, and J.L. Wilson, Primary and secondary controls on permeability at a variety of scales in a cross-stratified sandstone, *1977 Annual Meeting of the GSA*, Salt Lake City, October, 1997.

Clark, I., Regularization of a semi-variogram, *Computers and Geosciences*, 3, 341-346, 1977.

Corbett, P.W.M. and J.L. Jensen, Application of probe permeametry to the prediction of two-phase flow performance in laminated sandstones (lower Bent Group, North Sea), *Marine and Pet. Geol.,* 10, 335-346, 1993.

Dagan, G., Statistical theory of groundwater flow and transport : Pore to laboratory, laboratory to formation, and formation to regional scale, *Water Resour. Res.*, 22(9), 120S-134S, 1986.

Desbarats, A.J., Spatial averaging of transmissivity in heterogeneous fields with flow toward a well, *Water Resour. Res.*, 28(3), 757-767, 1992.

Deutsch, C.V., Calculating effective absolute permeability in sandstone/shale sequences, *SPE Form. Eval.*, 4(3), 343-348, 1989.

Deutsch, C.V. and A.G. Journel, *GSLIB: Geostatistical Software Library and User's Guide*, 368 pp., Oxford University Press, New York, 1997.

Dykstra, H. and R.L. Parsons, The prediction of oil recovery by water flood, in *Secondary Recovery of Oil in the United States*, 2nd ed., American Petroleum Institute, New York, pp. 160-174, 1950.

Di Federico, V. and S.P. Neuman, Scaling of random fields by means of truncated power variograms and associated spectra, *Water Resour. Res.*, 33(5), 1075-1085, 1997.

Eijpe, R. and K.J. Weber, Mini-permeameters for consolidated rock and unconsolidated sand, *AAPG Bull.*, 55(2), 307-309, 1971.

Gelhar, L.W., Stochastic subsurface hydrology from theory to applications, *Water Resour. Res.*, 22(9), 135S-145S, 1986.

Goggin, D. J., R. L. Thrasher, and L. W. Lake, A theoretical and experimental analysis of minipermeameter response including gas slippage and high velocity flow effects, *In Situ*, 12(1-2), 79-116, 1988.

Goggin, D.J., M.A. Chandler, G.A. Kocurek, and L.W. Lake, Patterns of permeability in eolian deposits: Page Sandstone (Jurassic), Northeastern Arizona, *SPE Form. Eval.*, 3, 297-306, 1986.

Gray, H.H., Petrology of the Massillon sandstone at the type locality, The Ohio Journal of Science, 56(3), 138-146, 1956.

Gutjahr, A.L., L.W. Gelhar, A.A. Bakr, and J.R. Macmillan, Stochastic analysis of spatial variability in subsurface flows, 2, Evaluation and application, *Water Resour. Res.*, 14(5), 953-960, 1978.

Haldorsen, H.H., Simulator parameter assignment and the problem of scale in reservoir engineering, in *Reservoir Characterization*, ed. by L.W. Lake and H.B. Carroll, Jr., Academic, San Diego, 293-340, 1986.

Hewett, T.A., Fractal distributions of reservoir heterogeneity and their influence on fluid transport, SPE 15386, in 61st Annual Technical Conference and Exhibition, Soc. of Pet. Eng., New Orleans, La., Oct. 5-8, 1986.

Indelman, P. and B. Abramovich, Nonlocal properties of nonuniform averaged flows in heterogeneous media, *Water Resour. Res.*, 30(12), 3385-3393, 1994.

Journel, A G. and C.J. Huijbregts, *Mining Geostatistics*, 600 pp., Academic Press, New York, 1978.

Kasap, E. and L.W. Lake, Calculating the effective permeability tensor of a gridblock, *SPE Form. Eval.*, 5(2), 192-200, 1990.

King, P.R., The use of renormalization for calculating effective permeability, *Trans. in Porous Media*, 4(1), 37-58, 1989.

Kirkpatrick, S., Percolation and conduction, *Rev. Mod. Phys.*, 45(4), 574-588, 1973.

Kortekaas, T.F.M., Water-oil displacement characteristics in cross-bedded reservoir zones, *SPEJ*, 25, 917-926, 1985.

Kossack, C.A., J.O. Aasen, and S.T. Opdal, Scaling up heterogeneities with pseudofunctions, *SPE Form. Eval.*, 5(3), 226-232, 1990.

Kyte, J.R. and D.W. Berry, New pseudofunctions to control numerical dispersion, *SPEJ*, 15, 269-276, 1975.

Lasseter, T.J., J.R. Waggoner, and L.W. Lake, Reservoir heterogeneities and their influence on ultimate recovery, in *Reservoir Characterization*, ed. by L.W. Lake and H.B. Carroll, Jr., Academic Press, New York, 545-560, 1986.

Liu, H.H. and F.J. Molz, Multifractal analyses of hydraulic conductivity distributions, *Water Resour. Res.*, 33(11), 2483-2488, 1997.

Matheron, G., *Elements pour une theorie des milieux poreux*, 166 pp., Maisson et Cie, Paris, 1967.

Neuman, S. P., Generalized scaling of permeabilities: Validation and effect of support scale, *Geophys. Res. Lett.*, 21(5), 349-353, 1994.

Rajaram, H. and D. McLaughlin, Identification of large-scale spatial trends in hydrologic data, *Water Resour. Res.*, 26(10), 2411-2423, 1990.

Ringrose, P.S., K.S. Sorbie, F.A. Feghi, G.E. Pickup, and J.L. Jensen, Relevant reservoir characterization: Recovery process, geometry, and scale, *In Situ*, 17(1), 55-82, 1993.

Robertson, R.W. and B.H. Caudle, Permeability continuity of laminae in the Calvin Sandstone, *J. Petrol. Technol.*, 23, 661-670, 1971.

Rubin, Y., Flow and transport in bimodal heterogeneous formations, *Water Resour. Res.*, 31(10), 2461-2468, 1995.

Schmidley, E.B., *The sedimentology, paleogeography and tectonic setting of the Pennsylvanian Massillon Sandstone in east-central Ohio*, University of Akron, MS Thesis, 1987.

Van De Graaff, W.J.E. and P.J. Ealey, Geological modeling for simulation studies, *AAPG Bull.*, 73(11), 1436-1444, 1989.

Warren, J.E. and H.S. Price, Flow in heterogeneous porous media, *SPE J.*, 1, 153-169, 1961.

CHAPTER 6: UPSCALING EXPERIMENTS CONDUCTED ON A BLOCK OF VOLCANIC TUFF: RESULTS FOR A BIMODAL PERMEABILITY DISTRIBUTION[5]

6.1. Abstract

Permeability upscaling is physically investigated by making over 31,000 permeability measurements on a meter-scale block of volcanic tuff. The experiments are made possible by a specially adapted minipermeameter test system. Here we present and analyze 5185 permeability values, corresponding to five different sample supports (i.e., sample volumes), collected from one of the block faces. Results show the measured spatial permeability patterns, bimodal permeability distribution, and semivariogram structure/length scales to be closely related to the strong textural contrast characterizing the tuff sample (i.e., highly porous pumice fragments embedded in a tight rock matrix). Each of the summary statistics investigated show distinct and consistent trends with increasing sample support (i.e., upscaling). As the sample support increases the mean and variance decrease according to a power-law relation, the semivariogram range increases linearly, while the general structure of the semivariogram (isotropic, spherical model) remains unchanged. Interpretation of these results is pursued according to two very different points of view; one concerns upscaling of the ensemble statistics (i.e., integrated over the entire sampling domain), while the second concerns upscaling from a local or point-wise perspective. According to our analysis of the ensemble statistics we find that the measured

[5] V.C. Tidwell and J.L. Wilson, submitted to Water Resources Research, 1998.

upscaling is not only dependent on the bimodal characteristics of the tuff sample but also depends on the non-uniform flow conditions imposed by the minipermeameter. The local analysis reveals strong variability in permeability upscaling from point to point throughout the sampling domain. Specifically, the permeability upscaling exhibited by zones rich in pumice is very different from that for zones dominated by matrix.

6.2. Introduction

Upscaling models are required where permeability data are measured at one scale but utilized in analyses conducted over much larger scales. Unfortunately, the upscaling of permeability data is a non-trivial task requiring careful consideration of the characteristics of the geologic medium and the measurement. Given the pervasiveness of the upscaling problem, significant efforts have been made to formulate predictive models. One case receiving particular attention is the upscaling of permeabilities corresponding to bimodal systems. Two important examples include sand-shale sequences [Fogg, 1986; Bachu and Cuthiell, 1990] and fractured reservoirs/aquifers [Schulze-Makuch and Cherkauer, 1997; Gavrilenki and Gueguen, 1998].

A number of models have been developed to investigate and predict the upscaling of bimodal systems. Some of the first efforts employed percolation theory [Kirkpatrick, 1973; Batchelor, 1974]. In this approach bimodal systems were conceptualized as a network of conducting sites (nodes) and bonds (links between sites) from which sites or bonds were randomly excluded to represent the non-conducting media. Flow simulations performed on the networks revealed that the effective conductance or permeability was sensitive to the volume fraction of the conducting media and the dimensions of the problem. Near the percolation threshold (critical volume fraction at which the conducting media spans the network and flow is established) the effective conductance was also found to depend on the geometry (size and shape) of non-conducting zones. Empirically based upscaling models

were proposed for conditions near the percolation threshold, while effective media theory was found to yield satisfactory results outside this limit [Kirkpatrick, 1973].

Haldorsen and Lake [1984] employed the stream-tube method to investigate the effective permeabilities of sand-shale systems. Monte Carlo simulation was used to randomly position shale bodies of prescribed geometry within a homogeneous and isotropic sand matrix. Horizontal and vertical effective permeabilities were then calculated using simple Darcy flux calculations applied to the resulting torturous stream tubes. The anisotropy introduced by elongate shale bodies was found to cause a large reduction in the vertical effective permeability but have minimal impact on the horizontal effective permeability. Begg and King [1985] extended this method by incorporating statistics of shale size and abundance into the stream tube formulation, thus removing the need to simulate the sand-shale sequence. Begg et al. [1985] further refined this approach by allowing consideration of multiple layers in which anisotropy of the sand matrix, shale fraction, and shale body geometry were allowed to vary from layer to layer. However, the authors note that the model is limited to cases involving simple shale body configurations and relatively low shale fractions.

Desbarats [1987] investigated the effective permeability of bimodal systems by coupling the geostatistical simulation of sand-shale sequences with the numerical modeling of flow. In this way, explicit consideration of the spatial correlation in the position of the shale bodies was possible. Desbarats [1987] found the effective permeability to depend on the shale fraction, spatial correlation structure, and the dimension of flow. Using a similar numerical approach as Desbarats, but assuming the shale bodies to be distributed independently, Deutsch [1989] investigated the upscaling of bimodal sand-shale sequences. He employed a spatial power-average model to quantify the effects of shale-body geometry and flow-field orientation on the upscaling process. Although the spatial power-average

model provides a convenient means of describing upscaling behavior, there is no theoretical basis for predicting the power coefficient (principal model parameter governing upscaling) from site specific information.

Desbarats [1990] and Rubin and Journel [1991] proposed an alternative approach for modeling bimodal systems. The distinguishing feature of their work is that each mode is defined by a multivariate probability density function, rather than a single value. Rubin [1995] determined the effective permeability, according to a perturbation expansion, for bimodal systems modeled in this way. He found the effective permeability to compare well with numerical simulations except where the volume fraction of low-permeability material was small. Under such conditions better results were obtained using the "self-consistent model" of Dagan [1979].

A unique opportunity to physically investigate permeability upscaling has recently been realized with the development of a specially adapted minipermeameter test system, which we call the Multi-Support Permeameter (MSP). This system allows the collection of spatially exhaustive permeability data over a range of different sample supports (i.e., sample volumes) subject to consistent measurement conditions. Here, we apply this novel technology to investigate permeability upscaling for a block of volcanic tuff. The sample is characterized by a bimodal permeability distribution arising from the presence of highly porous pumice fragments that are dispersed in a tight rock matrix. In this paper we present results for the upscaling experiment and interpret these results in light of the experimental conditions. In particular, we consider how the bimodal characteristics of the tuff sample and measurement characteristics of the MSP influence the upscaling results. Our analysis is approach from two disparate points of view; one concerning the upscaling of ensemble statistics (integrated over the entire sampling domain), while the second concerns upscaling from a local perspective (discrete zones distributed throughout the sampling domain).

6.3. Methods

Multi-Support Permeameter (MSP)

Physical investigation of permeability upscaling is approached by collecting large suites of data at several different sample supports. Considerable effort is made to isolate our experiments from many of the problems that impede and/or preclude unique quantification of permeability upscaling: specifically, incomplete knowledge of the permeability distribution, and inconsistencies in measurements made over different sample supports. To avoid these problems: 1) permeability data are acquired according to a spatially exhaustive sampling grid, 2) each measurement, regardless of the sample support, is made subject to the same boundary conditions and flow geometry, 3) measurements are non-destructive, and 4) measurement error is minimized.

Permeability data are acquired with a specially adapted minipermeameter test system, which we call the Multi-Support Permeameter (MSP). With this system permeability measurements are made by simply compressing a tip seal against a flat, fresh rock surface while injecting gas at a constant pressure. Using information on the seal geometry, gas flow rate, gas injection pressure, and barometric pressure, the permeability is calculated using a modified form of Darcy's Law [Goggin et al., 1988]. This process is automated by coupling a minipermeameter with an x-y positioner and computer control system. The minipermeameter functions as the measurement device of the MSP and consists of four electronic mass-flow meters (0-50, 0-500, 0-2000, and 0-20,000 cm^3/min. at standard conditions), a pressure transducer (0-100 kPa gauge), a barometer, and a gas temperature sensor that are all connected to a regulated source of compressed nitrogen. Measurements are made according to a user specified sampling grid programmed into the x-y positioner. Along with locating the tip seal for sampling, the positioner also compresses

the tip seal squarely against the rock surface with a consistent and constant force. The electronic permeameter and x-y positioner are configured with a computer control system to govern the data acquisition process and provide unattended operation. A full description and analysis of the MSP is given in Chapter 2.

Tip Seals and Sample Support

Key to this experimental program are the tip seals that direct gas flow into the rock sample. By simply varying the radius of the tip seal, measurements are made over different sample supports subject to consistent boundary conditions and flow geometry. Tip seals are made of a rigid aluminum housing to which a molded silicone rubber ring is affixed. A series of such tip seals were built with inner radii (r_1) of 0.15, 0.31, 0.63, 1.27, and 7.62 cm and outer radii measuring twice the inner. Critical to precise measurement is a consistent and known tip seal geometry under compressed conditions. For this reason, each of the tip seals is equipped with an internal spring-driven guide to maintain a constant inner seal diameter (the guide is unnecessary for the large 7.62 cm seal). For the 0.63 cm and smaller tip seals, which experience considerable deformation on compression, an immobile outer guide is also employed.

It is important to note that the ring-shaped tip seal imposes a divergent flow field during testing. The resulting non-uniform flow field not only has important implications relative to the measured permeability upscaling [Matheron, 1967; Desbarats, 1992a; Indelman and Abramovich, 1994], but also raises questions concerning what the MSP actually measures. To address this latter issue, we empirically investigated the measurement characteristics of the MSP by way of linear filter analysis (see Chapter 3). Results, as given by the calculated spatial weighting functions, indicate that the sample support is approximately hemispherical consistent with the symmetry of the tip seal. Heterogeneities located near the center of the tip seal influence the measurement more than those located

further away, consistent with the divergent flow field imposed by the MSP. Also, as the tip seal size increases the effective radius, r_{eff}, of measurement increases. Although additional work is needed to fully quantify the sample support associated with each tip seal, we and others [e.g., Goggin et al., 1988] believe that the r_{eff} is roughly proportional to r_l, hence the volumetric sample support increases by a power of 8 for each doubling of r_l.

Tuff Sample and Sampling Grid

Permeability data were acquired from a 81 by 74 by 63 cm block of moderately welded, devitrified ash flow tuff. The tuff sample is from the Miocene age, Topopah Spring Tuff Member of the Paintbrush Tuff Group [Sawyer et al., 1994]. The sample originated as a boulder collected from Fran Ridge on the Nevada Test Site, located approximately 100 km northwest of Las Vegas, Nevada. Preparation of the sample involved its shipment to a quarry where it was shaped into a block with a diamond-impregnated wireline saw. The rock sample is characterized by an aphanitic fabric with conspicuous pumice and lithic fragments (Figure 6.1a). The pumice fragments are easily distinguished from the matrix on the basis of textural and color contrast. The pumice fragments are characterized by an open, porous texture, reflecting alteration (i.e., devitrification) of the tuff, and a lighter or darker color than the matrix (Figure 6.1a). The pumice exhibit an oblate (~2:1 ratio) shape, owing to the compaction of the fragments during lithification. On average the pumice fragments measure <1 cm in diameter and comprise approximately 23% of the rock sample. However, each face is populated with a number of larger fragments (>3 cm dia.). Lithic fragments, of similar texture to that of the matrix, account for another 2-3% of the rock; however, their diameter rarely exceeds 1 cm.

Measurements were collected from all six faces of the tuff sample. For each face, measurements were made on the exact same grid using the 0.15, 0.31, 0.63, and 1.27 cm

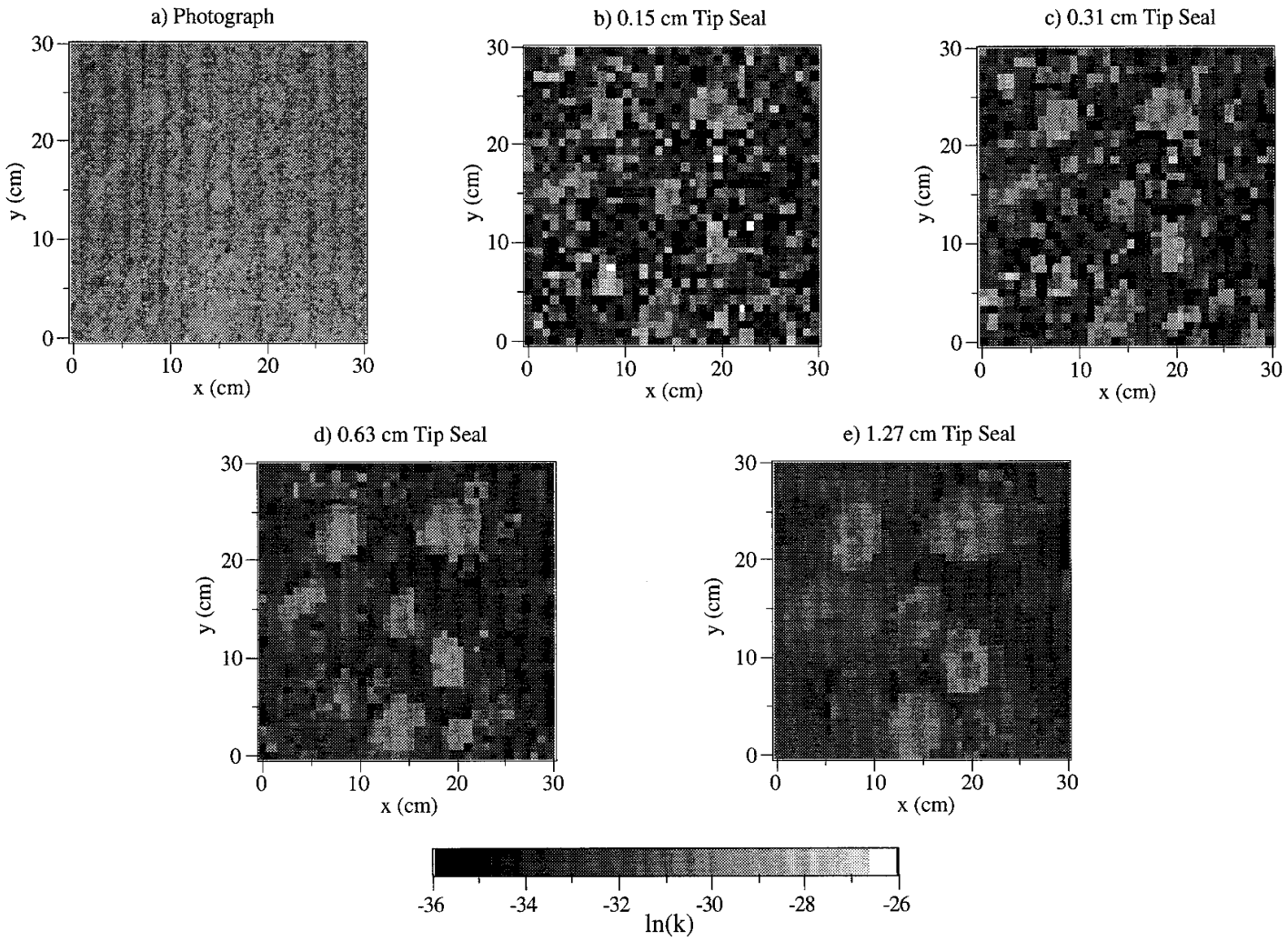

Figure 6.1. Photograph a) of Face 1 of the Topopah Spring Tuff sample that shows the area sampled with the MSP and the corresponding natural-log permeability fields (where k is in m^2) measured with the b) 0.15, c) 0.31, d) 0.63, and e) 1.27 cm r_I tip seals. Data were collected on a 36 by 36 point grid with 0.85 cm centers.

r_1 tip seals with no movement of the MSP or rock sample for the duration of sampling. The grid was centered on the block to avoid interference of the block edges with the measurements. The sampling grid contained 1296 measurement points organized on a square 36 by 36 lattice on 0.85 cm centers. The total size of the grid was 29.75 by 29.75 cm. In addition, a single measurement centered on the sampling grid was collected with the 7.62 cm tip seal. Sampling with the five tip seals yielded 5185 permeability measurements on each face; a total of 31,110 measurements over the entire block. As results for all five block faces are quite similar, we limit our attention here to a single block face, termed Face 1, oriented parallel to compaction foliation.

6.4. Results

The natural-log permeability fields ($\ln[k(\vec{x})]$ where k is in units of m^2) measured with the 0.15, 0.31, 0.63 and 1.27 cm r_1 tip seals on Face 1 of the Topopah Spring Tuff sample are shown in Figure 6.1. Comparisons drawn between the permeability fields and photograph (Figure 6.1a) reveal a strong correlation between the permeability and the spatial patterns visible in the sampled block face. Areas of high permeability are associated with pumice fragments, while the supporting rock matrix is marked by significantly lower permeability. Comparison of the permeability maps also reveals upscaling. As the tip seal size increases a distinct smoothing of the permeability field occurs; however, the signature of the larger pumice fragments is reproduced in each map.

The natural-log permeability distributions measured with the four tip seals are presented in Figure 6.2. The structure of the distributions is consistent with the strong textural contrast exhibited by the tuff sample. Each distribution is characterized by a bimodal structure with one mode associated with the low-permeability matrix and the other

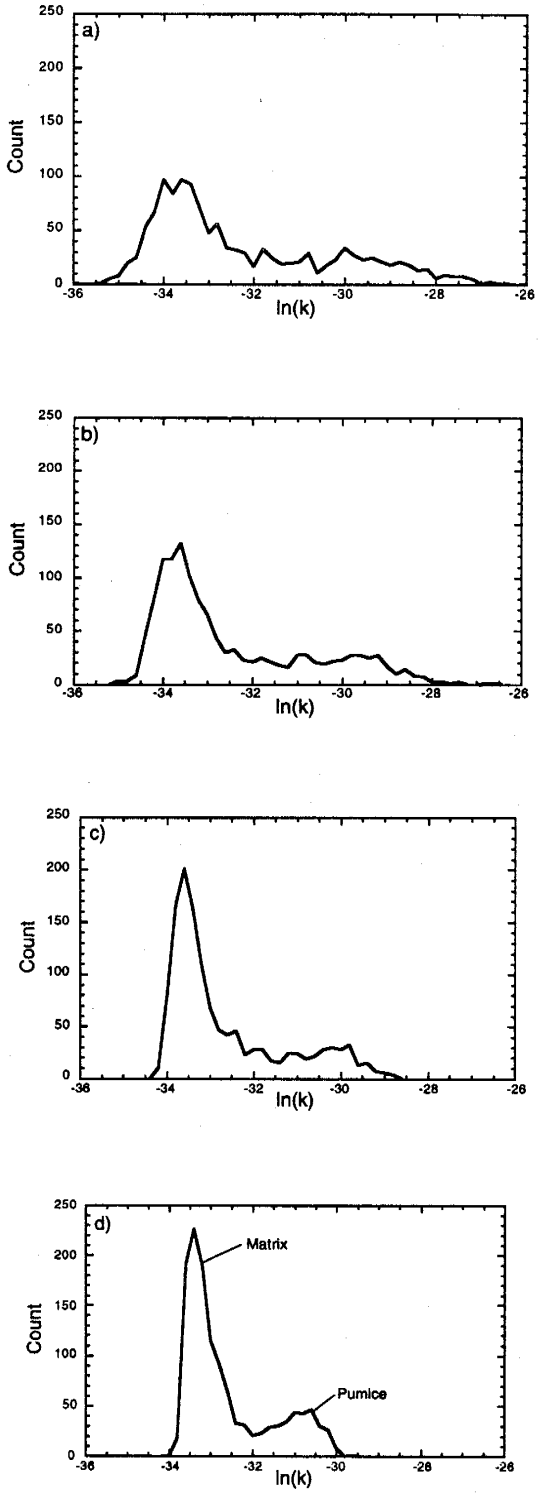

Figure 6.2. Natural-log permeability distributions measured with the a) 0.15, b) 0.31, c) 0.63, and d) 1.27 cm r_t tip seals on Face 1 of the Topopah Spring Tuff sample. Each distribution is comprised of 1296 values.

the high-permeability pumice. The strong textural contrast is also evidenced by the relatively large range and variance characterizing the distributions. Upscaling is evident in the shape, mean, and variance of the distributions. As the tip seal size increases the low-permeability mode associated with the matrix shifts slightly to the right (toward higher permeability), the high-permeability mode associated with the pumice shifts to the left, while the sample mean and sample variance (natural-log permeability) decrease according to a power-law relation (Figure 6.3).

To investigate the spatial correlation of the permeability, two-dimensional semivariograms were calculated using Fourier analysis (via Fast Fourier Transforms, see Bracewell, 1986; Section 3.3). Calculations were made using the natural-log permeability data sets acquired with each of the four tip seals. The semivariograms indicate that the permeability is isotropically correlated with relatively short-range correlation. Transects taken through the two-dimensional semivariograms (oriented along the x and y axes shown in Figure 6.1) are presented in Figure 6.4 and are fitted with a spherical semivariogram model

$$\gamma(s) = \begin{cases} C_o + \sigma\left[1.5\left(\frac{s}{\lambda}\right) - 0.5\left(\frac{s}{\lambda}\right)^3\right] & \text{where } s \le \lambda \\ C_o + \sigma & \text{where } s > \lambda \end{cases} \qquad (6.1)$$

where s is the separation distance, C_o is the nugget, σ is the variance, and λ is the semivariogram range. Values for the fitted semivariogram model parameters are given in Table 6.1. Comparison of the semivariogram transects (Figure 6.4), rock face photograph (Figure 6.1a), and the permeability maps (Figure 6.1b-e) reveals a strong correlation

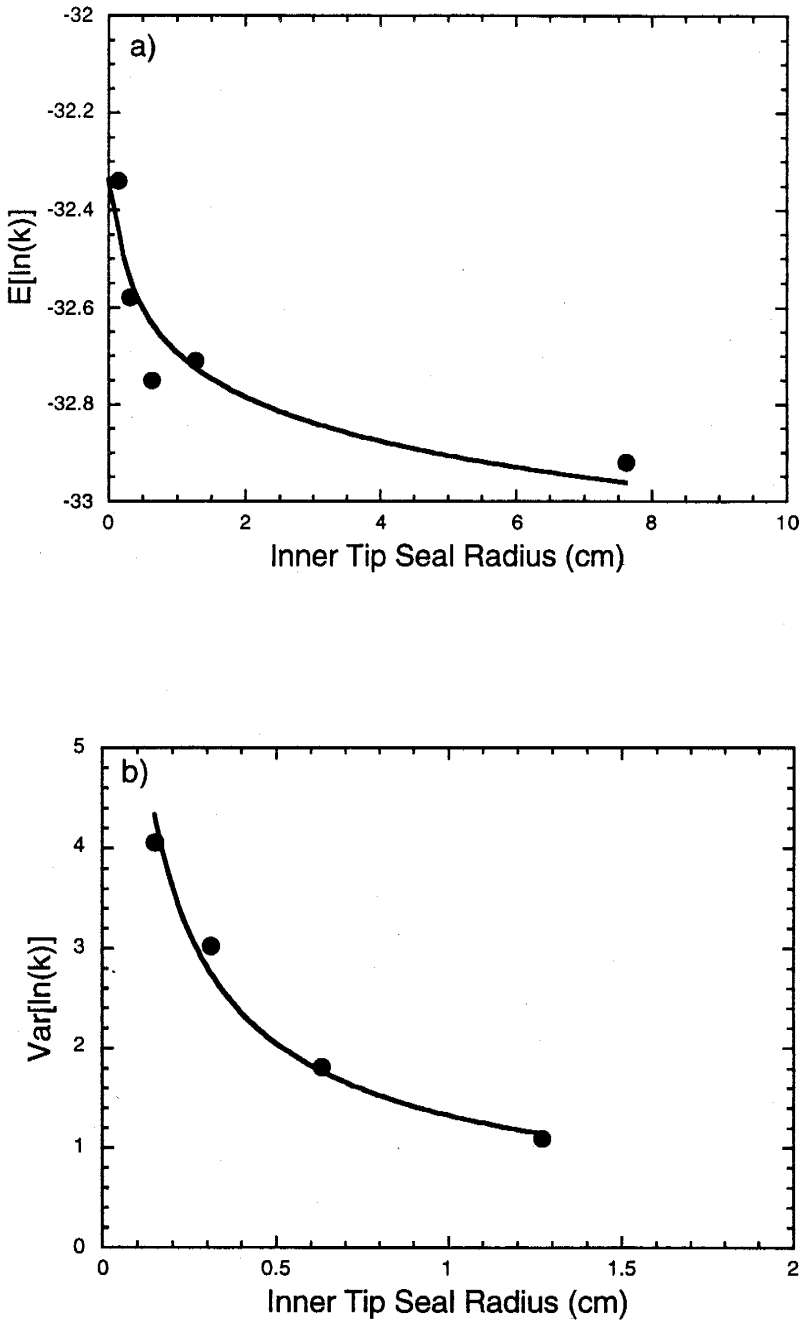

Figure 6.3. Mean upscaling (a) for the natural-log permeability measured on Face 1 of the Topopah Spring Tuff sample. Each value was calculated from a data set comprised of 1296 points, except for the last value which is associated with the single measurement made with the 7.62 cm tip. The variance upscaling for the natural-log permeability is given in (b) below. A power-law model was fit to the data for comparison (solid line).

between the spatial patterns exhibited by the rock and the structural features of the semivariogram. The relatively high nugget values reflect the strong spatial variability in permeability that occurs over very small separation distances. This short range variability is due to the presence of small, but high-permeability pumice fragments. The spatial correlation results from the few relatively large pumice fragments that are scattered throughout the sampling domain. In fact, the correlation length scale inferred from the semivariograms (~3.5 cm) is consistent with the nominal diameter, 3-5 cm, of the larger pumice fragments. For the other block faces (not shown) orthogonal to Face 1, slight anisotropy (2:1) is observed in the semivariograms, consistent with the "compacted" shape of the pumice fragments in these faces.

As with the other statistics investigated, several distinct upscaling trends are evident among the semivariograms. As the sample support increases the semivariogram sill and

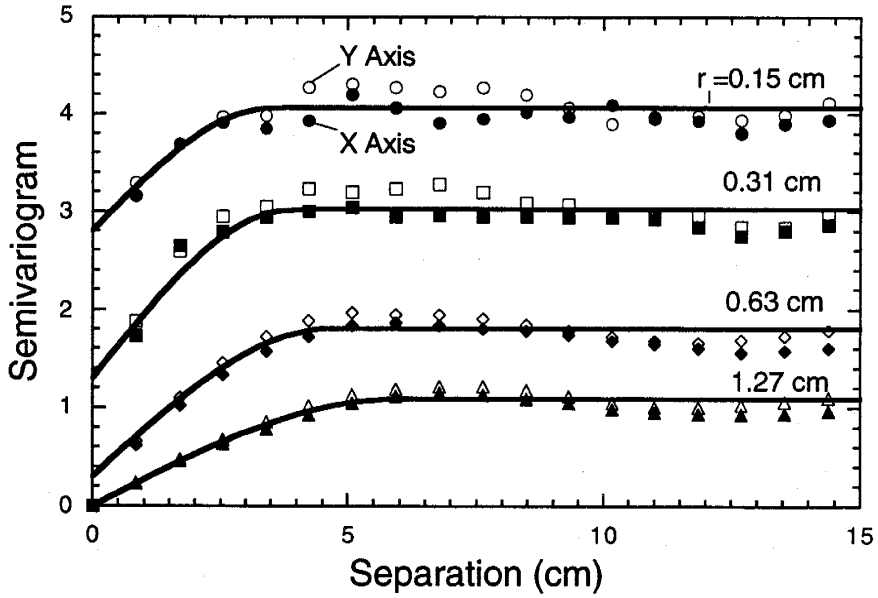

Figure 6.4. Transects extracted from the two-dimensional semivariograms calculated from the four tip seal data sets (natural-log permeabilities) measured on Face 1 of the Topopah Spring Tuff sample (filled symbols for the x-axis, open for the y-axis, see Figure 6.1). The solid lines are the fitted spherical semivariogram model (Equation 6.1).

Table 6.1. Model parameters (Equation 6.1) fitted to the semivariogram transects shown in Figure 6.3.

Tip	C_o	σ	λ (cm)
0.15	2.80	1.26	3.5
0.31	1.30	1.72	3.9
0.63	0.30	1.51	4.7
1.27	0.00	1.09	6.0

nugget decrease, while the fitted semivariogram range values increase linearly. Although the model parameter values vary with increasing sample support, the semivariogram maintains a spherical, isotropic spatial structure (Figure 6.4).

Two important conclusions can be drawn from the results presented above. First, the physical characteristics of the rock sample (i.e., strong textural contrast) has a significant and predictable influence on the permeability statistics (i.e., spatial permeability patterns, bimodal permeability distribution, and semivariogram structure/range). Second, each of the summary statistics investigated show distinct and consistent trends with increasing sample support (i.e., upscaling). As the sample support increased the mean and variance decreased according to a power-law relation, the semivariogram range increased linearly, while the general structure of the semivariogram (isotropic, spherical model) remained unchanged. Although not show, similar results were observed for the other five block faces.

6.5. Discussion

The results presented above show clear evidence of permeability upscaling. We now wish to interpret these results. Our interpretation is pursued according to two very

different paths of analysis; one focused on upscaling of the ensemble statistics and the other focused on upscaling from a local perspective. In each case our analysis is structured around comparisons drawn between the measured data and that predicted by theoretical upscaling models. Our goal is to gain a better understanding of the controls on permeability upscaling.

Upscaling of the Ensemble Statistics

Here, we explore the permeability upscaling as measured for the integrated sampling domain. Our analysis is focused on the trends exhibited by the ensemble statistics calculated from the spatially-exhaustive natural-log permeability data sets (i.e., all 1296 values). With this analysis we identify some of the basic controls on our permeability upscaling results. Specifically, we investigate the influence of the bimodal characteristics of the tuff sample and the measurement characteristics of the MSP on upscaling.

As the basis of our analysis, we compare the measured behavior in the mean permeability with that predicted by the self-consistent model of Dagan [1979]. Note that our intent is not to test the model, but rather to interpret our data; particularly, determine whether the mean upscaling can be explained on the basis of the bimodal characteristics of the tuff sample alone. Dagan [1979] approaches modeling of the effective permeability, k_{eff}, by sequentially isolating inclusions of permeability k within an embedding homogeneous matrix of unknown permeability, k_o, that extends to infinity. The self-consistent approximation is invoked by assuming that k_o is equal to k_{eff} (i.e., the matrix has the same k_{eff} as the composite system). The self-consistent approximation yields,

$$k_{eff} = \frac{1}{m}\left[\int \frac{f(k)dk}{(m-1)k_{eff} + k}\right]^{-1} \tag{6.2}$$

where $f(k)$ is the frequency distribution of the permeability and m is the dimension of flow.

This particular model was adopted for comparison with our data because its basis of formulation is consistent with the media characteristics exhibited by the Topopah Spring Tuff sample. The concept of embedding inclusions of one permeability within a matrix of different permeability is conceptually equivalent to the pumice/matrix system of the Topopah Spring Tuff. Also, the self-consistent model has application to any frequency distribution, including bimodal systems. Finally, the self-consistent model is not limited to systems characterized by low variance.

Recognizing that our MSP measurements are three-dimensional and that the measured permeability distributions are discrete, we tailor the self-consistent model to our application. For simplicity we discretized the permeability distribution (Figure 6.2) into 40 bins, each spanning 0.25 natural-log units. We note that resolving the distribution into more than 40 bins has negligible effect on the calculations. Rewriting Equation 6.2 to reflect these changes yields

$$k_{eff} = \frac{1}{3}\left[\sum_{j=1}^{40} \frac{f(k_j)}{2k_{eff} + k_j}\right]^{-1} \tag{6.3}$$

In this way, k_{eff} for the sampled block face is calculated from k_j and $f(k_j)$ data taken from the measured permeability distribution.

In Table 6.2 we present the k_{eff} values calculated from Equation 6.3 using the permeability distribution (Figure 6.2) measured with the 0.15 cm tip seal. Results are

presented for Face 1 as well as the other five block faces (i.e., Faces 2-6). We draw comparisons between the calculated k_{eff} values and that measured with the 7.62 cm tip seal, $k_{7.62}$, both of which represent an integrated measure over the entire sampling domain. Although we are relying heavily on the measurement made with the 7.62 cm tip seal for our comparison (i.e., one measurement per face), we have confidence in this data. We note that for each block face the $k_{7.62}$ measurement is consistent with the upscaling trend exhibited by the means calculated from the other tip seal data sets (e.g., Figure 6.3) and we are able to reproduce the $k_{7.62}$ measurement to $\pm 1\%$. In comparing k_{eff} and $k_{7.62}$ we find the self-consistent model always under predicts $k_{7.62}$. The disparity, as represented by the ratio of $k_{eff}/k_{7.62}$, ranges between 1.4 and 3.0. We also calculated k_{eff} using data from the other tip seals (i.e., 0.31-1.27 cm, not shown). These too under predicted $k_{7.62}$ but to a slightly lesser degree, likely reflecting the narrower permeability distribution over which the calculations were made.

Discrepancies between the model and the mean upscaling (i.e., k_{eff} and $k_{7.62}$) are largely the result of experimental conditions which differ from that assumed in the self-consistent model. In efforts to identify potential controls on the mean upscaling we examine the experimental conditions in light of the assumptions on which the self-consistent model is predicated. Modeling assumptions include: infinite medium, isotropic spatial correlation, neighboring measurements are uncorrelated, the flow field and sampling domain are of similar dimensions, and uniform flow conditions.

The only assumption of concern appears to be that of uniform flow. We note that the sampling domain encompasses 8 to 9 correlation length scales, which is usually sufficient for treatment as an infinite medium. The relatively weak spatial correlation (Figure 6.4) and anisotropy exhibited by the permeability is not expected to significantly

Table 6.2. Comparison of the mean upscaling measured on the Topopah Spring Tuff sample with that predicted by the self-consistent model of Dagan [1979] (see Equation 6.3).

Face	$k_{7.62}$ m^2	k_{eff} m^2	$k_{eff}/k_{7.62}$
1	5.2×10^{-15}	1.3×10^{-14}	2.5
2	9.1×10^{-15}	2.0×10^{-14}	2.2
3	1.4×10^{-14}	2.0×10^{-14}	1.4
4	7.6×10^{-15}	2.3×10^{-14}	3.0
5	5.7×10^{-15}	1.5×10^{-14}	2.6
6	3.5×10^{-15}	4.8×10^{-15}	1.4

effect results. This is supported by the fact that no distinct differences in results (Table 6.2) are evident between faces characterized by anisotropy (Face 2-5) and those characterized by isotropy (Faces 1 and 6). Also, the inconsistency between our two-dimensional sampling statistics and the three-dimensional flow imparted by the MSP (i.e., the 7.62 cm tip seal measurement penetrates deeper into the rock than the other tip seal measurements) does not appear to explain the discrepancy between the model and data. This is because a decreasing trend in permeability with depth into the rock is inconsistent with the semivariograms calculated for each block face. This explanation is even more unlikely given that all six block faces exhibit similar mean upscaling and similar differences with the self-consistent model (Table 6.2).

We conclude that the critical assumption violated by our test conditions results from the non-uniform flow imparted by the MSP. This implies that the mean upscaling depends not only on the statistical characteristics of the tuff sample but also on the characteristics of the MSP measurement. This result is supported by similar findings for MSP upscaling

experiments conducted on a block of Berea Sandstone (see Chapter 4), characterized by planar cross stratification. Although the scales and patterns of heterogeneity differ significantly between the tuff and sandstone samples, the measured mean upscaling is consistently under predicted by theory based solely on media characteristics. Unfortunately, further analysis of the mean upscaling is limited as there are no published analytical or numerical studies supporting hemispherical flow in strongly heterogeneous medium. The development of such theories are well beyond the scope of the current paper, but is an area of active research by the authors.

Local Analysis

Now we explore the permeability upscaling from a local or point-wise perspective. Of interest is the spatial variability in the upscaling process. Specifically, we wish to determine whether zones rich in pumice upscale differently than zones dominated by matrix. To facilitate the analysis we employ the spatial power-average model [e.g., Korvin, 1981; Deutsch, 1989; Desbarats, 1992]. It provides a simple, quantitative basis for investigating permeability upscaling within the local context, and allows comparison with simple bounding models of permeability upscaling. In this model the upscaled permeability k_i is represented as a spatial power-average of the permeabilities measured at a smaller support k_j and located within the neighborhood V_i about k_i

$$k_i^{\omega}(\bar{x}) = \frac{1}{V_i}\int_{V_i} k_j^{\omega}(\bar{x})d\bar{x} \quad \text{for } \omega \neq 0 \tag{6.4a}$$

$$\ln k_i(\bar{x}) = \frac{1}{V_i}\int_{V_i} \ln k_j(\bar{x})d\bar{x} \quad \text{for } \omega = 0 \tag{6.4b}$$

where ω is the power coefficient. According to this formulation a harmonic average is represented by $\omega = -1$, geometric average by $\omega = 0$, and an arithmetic average by $\omega = 1$. These simple averages correspond to important limiting cases within the context of

permeability upscaling. The harmonic average provides an estimate of the effective permeability for uniform flow oriented normal to a perfectly layered medium, the arithmetic average for uniform flow oriented parallel to layering, and the geometric average for uniform flow in a spatially uncorrelated medium.

Our local investigation is pursued by applying the spatial power-average model (Equation 6.4) to discrete neighborhoods of data to empirically determine local values of ω and thus spatially characterize the upscaling process. The permeability values measured with a small tip seal (k_j) and within the neighborhood V_i are averaged together and compared to the corresponding larger tip seal measurement (k_i). The averages are computed using values for ω that are systematically varied (without constraint) until the difference between the spatial power-average and k_i is minimized. For this simple case, V_i is taken as any grid point within four-times the inner tip seal radius of k_i ($r_{eff} = 4r_i$ [Goggin et al., 1988] where r_i denotes the inner tip seal radius of the *i*th tip seal). Treatment of r_{eff} and its effect on ω are investigated below. Local values of ω are determined for each point in the sampling grid that is a distance of at least $4r_i$ from the grid boundary.

To evaluate the effects of V_i on the local analysis, ω values characterizing the upscaling of permeabilities measured with the 0.15 cm tip seal (k_j) to that of the 1.27 cm tip seal (k_i) were determined for three different local neighborhoods. CDFs for these three cases are given in Figure 6.5. We first investigated the cases where V_i was defined by a uniform spatial weighting with an $r_{eff} = 3r_i$ and $r_{eff} = 4r_i$. Results indicate that almost no difference in ω is realized when the neighborhood size is changed by a modest amount. Calculations were also performed assuming a non-uniform spatial weighting of the permeabilities populating the averaging neighborhood. A simple two-dimensional, isotropic

Gaussian model was used as the weighting function, consistent with the results of previous linear filtering studies performed for the MSP (see Chapter 3). Again, little difference is noted (Figure 6.5), suggesting that ω is relatively insensitive to minor changes in V_i.

Also of interest is the change in the ω distribution for different tip seal pairs. To illustrate this change, the CDF for ω characterizing the upscaling of permeabilities measured with the 0.15 cm tip seal (k_j) to that of the 0.63 cm tip seal (k_i) is presented in Figure 6.5. ω values for the 0.15-1.27 cm tip seal pair (i.e., $r_{eff} = 4r_i$) encompass a much narrower range than that of the 0.15-0.63 cm pair. In fact, we consistently find that the range in ω decreases as the difference in tip seal size (i.e., $\Delta r = r_i - r_j$) increases. This occurs because the k_i distribution becomes smoother as r_i increases (increasing Δr, as in Figure 6.5) and/or the k_j distribution becomes more variable as r_j decreases (again, increasing Δr).

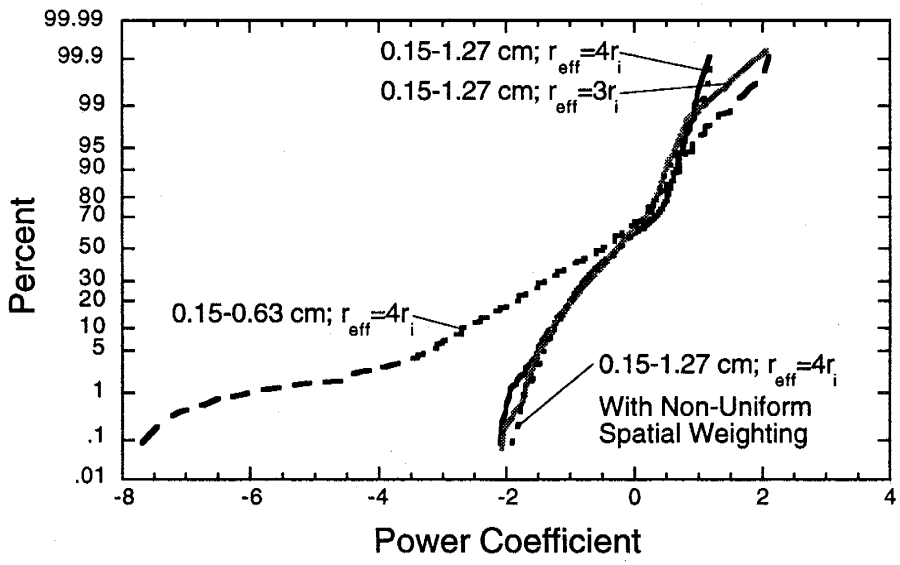

Figure 6.5. CDFs for calculated power coefficients ω (Equation 6.4). Comparisons are drawn between the CDFs for different pairs of tip seals and CDFs for the same tip seal pair but for different averaging neighborhoods.

Figure 6.6 presents a two-dimensional map of estimated ω values for Face 1 of the tuff sample. These ω values characterize the spatial power-average required to upscale data measured with the 0.15 cm tip seal (k_j) to that measured with the 1.27 cm tip seal (k_i) (see the CDF in Figure 6.5). This map reveals a surprising degree of spatial variability in the permeability upscaling process. A clear relationship between ω, the physical attributes of the tuff sample (Figure 6.1a), and the permeability (Figure 6.1b-e) is evident. High ω values tend to be distributed around the margins of the larger pumice fragments while the lower ω values are found near the center of the large fragments and in areas dominated by the low permeability rock matrix. Another important characteristic of the upscaling is the very broad range of calculated ω values that, in this unconstrained analysis, extend from <-1 to >1.

From Figures 6.5 and 6.6 it is apparent that permeability upscaling varies spatially across the sampled block face. Zones rich in pumice (i.e., points where the k_i measurement is spanned by a pumice fragment) exhibit distinctly different upscaling than zones dominated by matrix. Specifically, upscaling of the matrix dominated zones is characterized by a power-averaging coefficient (Equation 6.4) less than zero, $\omega<0$, while zones rich in pumice upscale according to a power-average coefficient greater than zero, $\omega>0$. That is, the matrix dominated zones experience a much more rapid decline in permeability than the pumice rich zones.

The disparity in permeability upscaling exhibited between the pumice and matrix is likely intensified by the measurement characteristics of the MSP. That is, the MSP is particularly sensitive to conditions directly underneath the tip seal. Thus, the divergent flow conditions tend to disproportionately weight (relative to other flow geometries) high permeability features spanning the sample support. These non-uniform flow effects may in

part explain the ω values that are smaller than -1 (harmonic spatial average) and greater than 1 (arithmetic spatial average).

The quantitative aspects of the local analysis presented above must be viewed with some caution. There are several limitation of the spatial power-average model (Equation 6.4) as it pertains to our experiments. Two potentially important inconsistencies include: 1) the multi-support permeability data are measured on two-dimensional rock faces while the

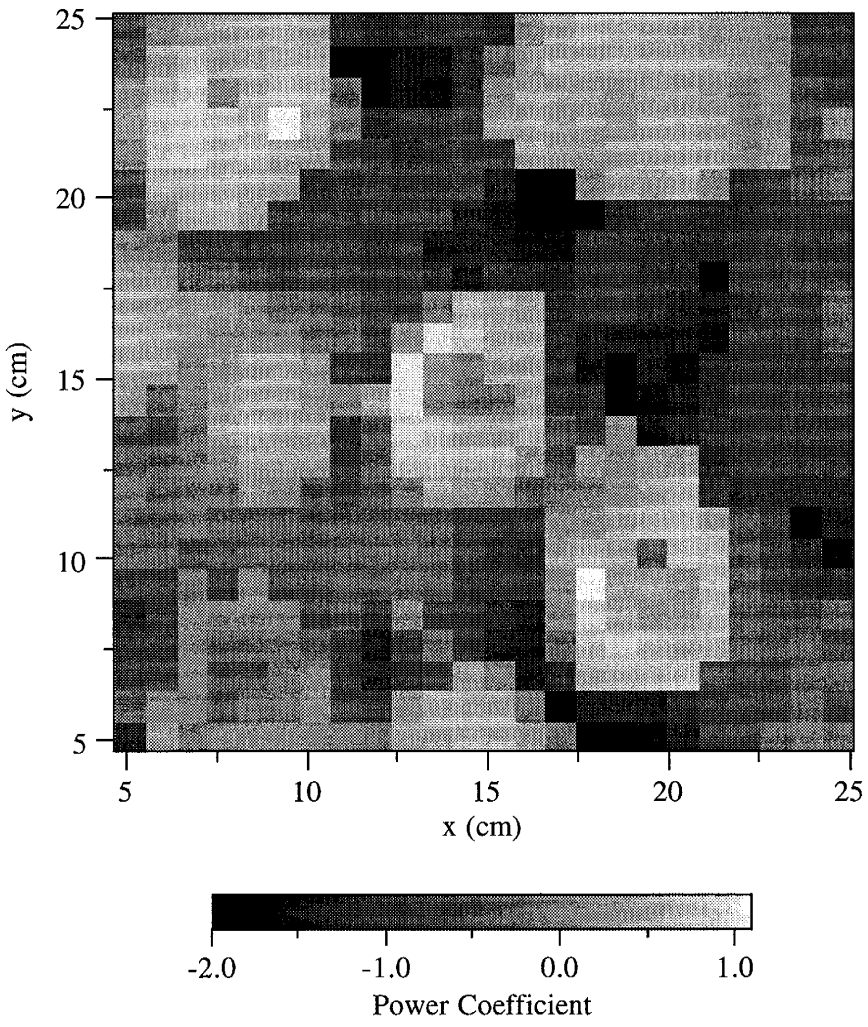

Figure 6.6. Two-dimensional map of calculated power coefficients ω for Face 1 of the Tuff sample $\left(r_{eff} = 4r_i\right)$. The ω values characterize the spatial power-average (Equation 6.4) required to locally upscale permeability data measured with the 0.15 cm tip seal to that measured with the 1.27 cm tip seal. If we constrained ω to lie within the range (-1, +1) then the same plot results with all values out of this range assigned to be -1 or +1, as appropriate.

corresponding calculations are necessarily three-dimensional in nature, and 2) we have largely ignored the role of the spatial weighting function (e.g., see Equation 3.14) on the measured upscaling. Although we may not have much confidence in the quantitative ω values, we do feel that the strong variability in ω and their correlation with the spatial features visible in the sampled block face provide ample evidence concerning the spatial variability in the local permeability upscaling.

6.6. Conclusions

Permeability upscaling experiments were conducted on a meter-scale block of volcanic tuff characterized by numerous porous pumice fragments isolated in an otherwise tight rock matrix. Upscaling experiments were conducted by collecting 5185 permeability measurements, corresponding to five different sample supports (sample volumes), from each block face. The spatially exhaustive data sets were collected with a specially adapted minipermeameter system. With this system measurement were made over different sample supports, subject to consistent flow geometries and boundary conditions by simply varying the size of the minipermeameter tip seal.

Data were presented and analyzed for a single block face. Results show a direct relationship between the calculated permeability statistics and the strong textural contrast characterizing the tuff sample. Specifically, the spatial permeability patterns, bimodal permeability distribution, and the semivariogram structure/range are easily related to the spatial patterns visible in the sampled block face. For each statistic investigated distinct and consistent trends with increasing sample support were observed (i.e., upscaling). As the sample support increased small-scale features were filtered from the permeability field, while the larger-scale features were preserved. Also, the sample mean, variance, semivariogram sill and nugget decreased with increasing support, while the semivariogram

range increased linearly. Although not show, similar results were observed for the other five block faces.

Interpretation of the results was approached along two separate paths of analysis; one focused on upscaling of the ensemble statistics (calculated over the entire sampling domain) and the second focused on the local or point-wise upscaling. In each case interpretation of the data was pursued by comparing measured results with theoretical models of permeability upscaling. According to our analysis of the ensemble statistics we find that the measured upscaling is not only dependent on the bimodal characteristics of the tuff sample but also depends on the non-uniform flow conditions imposed by the minipermeameter. As many other hydraulic instruments are subject to non-uniform flow conditions (e.g., pump and slug tests) these results mark the need for expanded tools and theory for treating upscaling under such conditions. Results of the local analyses show distinct spatial variability in the permeability upscaling. Specifically, the permeability upscaling exhibited by the pumice rich zones is very different from that exhibited by zones dominated by rock matrix. Our local results have important implications for the parameterization of numerical simulations where the grid block dimensions are of similar magnitude to the correlation length scale of the medium.

Acknowledgments. We would like to thank Mark Bailey and Nick Teske for help in collecting the reported data, and Allan Gutjahr, Robert Glass, and Fred Phillips for their advice concerning the conduct of these studies. This work was supported by the U.S. Department of Energy, Office of Basic Energy Science, Geoscience Research Program, under contract DE-AC04-94AL85000 and DE-F303-96ER14589/A000. Sandia is a multiprogram laboratory operated by Sandia Corporation, a Lockheed Martin Company, for the United States Department of Energy.

6.7. References

Bachu, S. and D. Cuthiell, Effects of core-scale heterogeneity on steady state and transient fluid flow in porous media: Numerical analysis, *Water Resour. Res.*, 26(5), 863-874, 1990.

Batchelor, G.K., Transport properties of two-phase materials with random structure, *Ann. Rev. Fluid Dyn.*, 6, 227-255, 1974.

Begg, S.H. and P.R. King, Modeling the effects of shales on reservoir performance: Calculation of effective vertical permeability, SPE 13529, presented at Reservoir Simulation Symposium, Soc. of Pet. Eng., Dallas, TX, Feb. 10-13, 1985.

Begg, S.H., D.M. Chang, and H.H. Haldorsen, A simple statistical method for calculating the effective vertical permeability of a reservoir containing discontinuous shales, SPE 14271, presented at the 60th Annual Technical Conference, Soc. of Pet. Eng., Las Vegas, NV, Sept. 22-25, 1985.

Bracewell, R.N., *The Fourier Transform and Its Applications*, 474 pp., McGraw-Hill, New York, 1986.

Clark, I., Regularization of a semi-variogram, *Computers and Geosciences*, 3, 341-346, 1977.

Dagan, G., Models of groundwater flow in statistically homogeneous porous formations, *Water Resour. Res.*, 15(1), 47-63, 1979.

Desbarats, A.J., Numerical estimation of effective permeability in sand-shale formations, *Water Resour. Res.*, 23(2), 273-286, 1987.

Desbarats, A.J., Macrodispersion in sand-shale sequences, *Water Resour. Res.*, 26(1), 153-163, 1990.

Desbarats, A.J., Spatial averaging of transmissivity in heterogeneous fields with flow toward a well, *Water Resour. Res.*, 28(3), 757-767, 1992a.

Desbarats, A.J., Spatial averaging of hydraulic conductivity in three-dimensional heterogeneous porous media, *Math. Geol.*, 24(3), 249-267, 1992b.

Deutsch, C.V., Calculating effective absolute permeability in sandstone/shale sequences, *SPE Form. Eval.*, 4(3), 343-348, 1989.

Fogg, G.E., Groundwater flow and sand body interconnectedness in a thick, multiple-aquifer system, *Water Resour. Res.*, 22(5), 679-694, 1986.

Gavrilenki, P. and Y. Gueguen, Flow in fractured media: A modified renormalization method, *Water Resour. Res.*, 34(2), 177-191, 1998.

Goggin, D. J., R. L. Thrasher, and L. W. Lake, A theoretical and experimental analysis of minipermeameter response including gas slippage and high velocity flow effects, *In Situ*, 12(1-2), 79-116, 1988.

Haldorsen, H.H. and L.W. Lake, A new approach to shale management in field-scale models, *SPEJ*, 24(4), 447-457, 1984.

Indelman, P. and B. Abramovich, Nonlocal properties of nonuniform averaged flows in heterogeneous media, *Water Resour. Res.*, 30(12), 3385-3393, 1994.

Journel, A.G. and C.J. Huijbregts, *Mining Geostatistics*, 600pp., Academic Press, New York, 1978.

Kirkpatrick, S., Percolation and conduction, *Rev. Mod. Phys.*, 45(4), 574-588, 1973.

Korvin, G., Axiomatic characterization of the general mixture rule, *Geoexploration*, 19, 267-276, 1981.

Matheron, G., *Elements pour une theorie des milieux poreux*, 166 pp., Maisson et Cie, Paris, 1967.

Rubin, Y., Flow and transport in bimodal heterogeneous formations, *Water Resour. Res.*, 31(10), 2461-2468, 1995.

Rubin, Y. and A.G. Journel, Simulation of non-Gaussian space random functions for modeling transport in groundwater, *Water Resour. Res.*, 27(7), 1711-1721, 1991.

Sawyer, D.A, R.J. Fleck, M.A. Lanphere, R.G. Warren, D.E. Broxton, and M.R. Hudson, Episodic caldera volcanism in the Miocene southwestern Nevada volcanic field: Revised stratigraphic framework, $^{40}Ar/^{39}Ar$ geochronology, and implications for magmatism and extension, *GSA Bull.*, 106, 1304-1318, 1994.

Schulze-Makuch, D. and D.S. Cherkauer, Method developed for extrapolating scale behavior, *Eos. Trans. AGU*, 78(1), 3, 1997.

CHAPTER 7: PHYSICAL INVESTIGATION OF PERMEABILITY UPSCALING: A COMPARISON OF RESULTS MEASURED ON FOUR BLOCKS OF HETEROGENEOUS ROCK[6]

7.1. Abstract

Over 150,000 permeability values, corresponding to six different sample supports, have been collected from four blocks of heterogeneous rock: two sandstones and two volcanic tuffs. The distinct contrast in the physical characteristics of these rock samples, particularly between the cross-bedded structure of the sandstones and the binary structure of the tuffs (i.e., aphanitic fabric with isolated high permeability pumice fragments), provide a unique basis for testing. Here, we compare and contrast results to investigate how the spatial patterns visible in each rock sample influence the statistical and upscaling characteristics of the permeability. Comparison of data sets indicate that the permeability maps, cumulative distribution functions, semivariograms, and to a lesser extent the mean and variance are directly related to the spatial patterns characterizing each of the four rock samples. These exhaustive data sets, measured under consistent experimental conditions, also yield compelling empirical evidence of permeability upscaling. By upscaling we mean the change in the mean, variance, semivariogram, etc. as its associated scale of measurement is increased. Permeability upscaling is ubiquitous in our data; that is, consistent trends are evident for each rock sample and each statistic investigated. Although

[6] Tidwell, V.C., J.L. Wilson, and R.J. Glass, to be submitted to Water Resources Research, 1999.

there is a degree of consistency in the manner with which the permeability upscales (e.g., variance always decreases with increasing measurement scale), distinct differences are also evident between the rock samples. The most notable differences are realized in the sample mean where the sandstones exhibit an increasing trend, while the tuffs display a decreasing to invariant trend with increasing measurement scale. Given the controlled nature of the experiments, these differences in upscaling result from differences in the physical characteristics of the rock samples. Closer inspection indicates that the spatial continuity of the "high" permeability fraction (i.e., roughly any permeability value exceeding the mean) and its range of correlation relative to the scale of measurement are the primary features effecting the measured mean upscaling.

7.2. Introduction

There is an extensive body of evidence acquired through physical [Brace, 1984; Parker and Albrecht, 1987; Molz et al., 1990; Clauser, 1992; Hanor, 1993; Schulze-Makuch and Cherkauer, 1997] and numerical [Warren and Price, 1961; Desbarats, 1987; Gomez-Hernandez and Gorelick, 1989; Bachu and Cuthiell, 1990; Durlofsky, 1992] experimentation demonstrating permeability upscaling. By permeability upscaling we mean the change in key summary statistics (e.g., mean, variance) as the scale of measurement increases. Unfortunately, permeability upscaling rarely conforms to simple averaging laws; rather, it is the manifestation of a complex array of physical processes and media characteristics acting on permeability measurements made at different scales. For example, the dimensionality of the flow system [Gutjahr et al., 1978] and the geometry of the imposed flow field (i.e., uniform, radial, spherical) play important roles in defining permeability upscaling [e.g., Matheron, 1967; Desbarats, 1992a; Indelman and Abramovich, 1994]. Even the measurement characteristics of the sampling instrument influence upscaling [Baveye and Sposito, 1984; Cushman, 1984].

Receiving particular attention in the literature has been the relationship between permeability upscaling and the physical characteristics of the porous medium. These studies have generally focused interest on the distributional properties and spatial correlation of permeability. Consider the case of discrete permeability distributions like sand/shale or fracture/matrix systems. Permeability upscaling is governed by the contrast in permeability between the competing phases, the relative phase ratios [Deutsch, 1989], and the lateral continuity/spatial disposition of the poorly conductive phase [Haldorsen and Lake, 1984]. Where the high-permeability phase (e.g., sand bodies, fractures) is spatially well-connected, the corresponding upscaling may be distinguished by an increasing trend in the mean permeability [Fogg, 1986; Silliman and Wright, 1988]. Continuously distributed systems are usually assumed to behave according to a Gaussian model and thus are fully described by their first two statistical moments [e.g., Freeze, 1975]. However, additional information is generally required to model the upscaling; for example, the degree of media anisotropy, orientation of flow [Gelhar and Axness, 1983], steady vs. transient flow [Dagan, 1982], and even the size of the flow domain versus the integral scale of heterogeneity [Desbarats, 1992b].

It is apparent that the relationship between permeability upscaling and media heterogeneity has received considerable attention; however, these studies are based largely on theoretical constructs. Although physical investigation of permeability upscaling has been conducted, the studies are generally limited in scope to one, or at most two, test media. As a result, we lack a coherent set of physical data for investigating this critical relationship.

Here we present results for upscaling experiments conducted on four blocks of heterogeneous rock; two sandstones and two volcanic tuffs. The distinguishing feature of

this work is the controlled and consistent manner with which all data were collected. Exhaustive sampling was employed allowing quantification of the distributional and spatial statistics characterizing each rock sample and each scale of measurement, with a high degree of confidence. Specifically, over 150,000 permeability values corresponding to six different sample supports (i.e., sample volumes) were measured on the four rock samples. Furthermore, all permeability values were measured under the exact same conditions, regardless of the sample support or rock sample. By controlling our experiments in this fashion, we limit the number of factors complicating or even preventing interpretation of the measured upscaling. For all practical purposes, only the physical attributes characterizing the four rock samples contribute to differences in the measured upscaling.

Our interest in this paper is to compare and contrast results. Specifically, we explore how the spatial patterns distinguishing each rock sample influence the statistical and upscaling characteristics of the permeability. By way of this comparison we wish to address three fundamental yet very important questions: (1) are the statistical characteristics of the measured permeability influenced by the physical attributes of the rock sample, (2) does the measured permeability upscale in a coherent and potentially quantifiable manner, and (3) is the measured permeability upscaling influenced by the physical attributes of the rock sample?

7.3. Materials and Methods

Here we describe the materials and methods used to investigate permeability upscaling. Two distinguishing characteristics of this work are: 1) the broad scope of the studies, and 2) the controlled physical experimentation. Upscaling experiments were conducted on four different rock samples, each of which exhibit different spatial patterns owing to differences in their mode of origin. The acquired data provide a unique opportunity to study permeability upscaling as stringent control was maintained over the

experiments. In particular, all measurements, regardless of the sample support, were: 1) made subject to consistent boundary conditions and flow geometries; 2) non-destructive, thus allowing all data to be collected from the same physical sample; and, 3) precise, subject to small and consistent measurement error. The permeability data were also collected at high-spatial resolution (generally <1 cm), allowing quantification of the distributional and spatial statistics characterizing each rock sample (over multiple sample supports) with a high degree of confidence. In this way, we were able to control the variables influencing our experiments, thus facilitating the interpretation of the measured upscaling.

Rock Sample Description

To date, permeability upscaling studies have been conducted on four rock samples, each from different depositional environments exhibiting different physical characteristics. We refer to these samples as the Massillon Sandstone, Berea Sandstone, Topopah Spring Tuff, and the Tiva Canyon Tuff.

The Massillon Sandstone sample (Figure 7.1) measures 0.94 by 0.96 by 1.01 m and was acquired from the Briar Hill Stone Company in Glenmont, Ohio. The Massillon Sandstone, of Pennsylvanian age, outcrops throughout much of northeastern Ohio and is an important commercial source of dimensional stone. Based on thin-section analysis, this sample is classified as a moderately well-sorted, medium-grained quartz sandstone. Diagenetic alterations affecting the sandstone have occurred as evidenced by the presence of hydrous iron oxide precipitates and quartz overgrowths. The fabric of the sandstone sample is characterized by a series of sub-horizontal bounding surfaces spaced approximately 16-22 cm apart (Figure 7.1). The bounding surfaces are planar with locally undulatory interfaces. Between the bounding surfaces planar and low-angle cross stratification (apparent dip of 10° to 22°) is evident with individual laminae spaced approximately

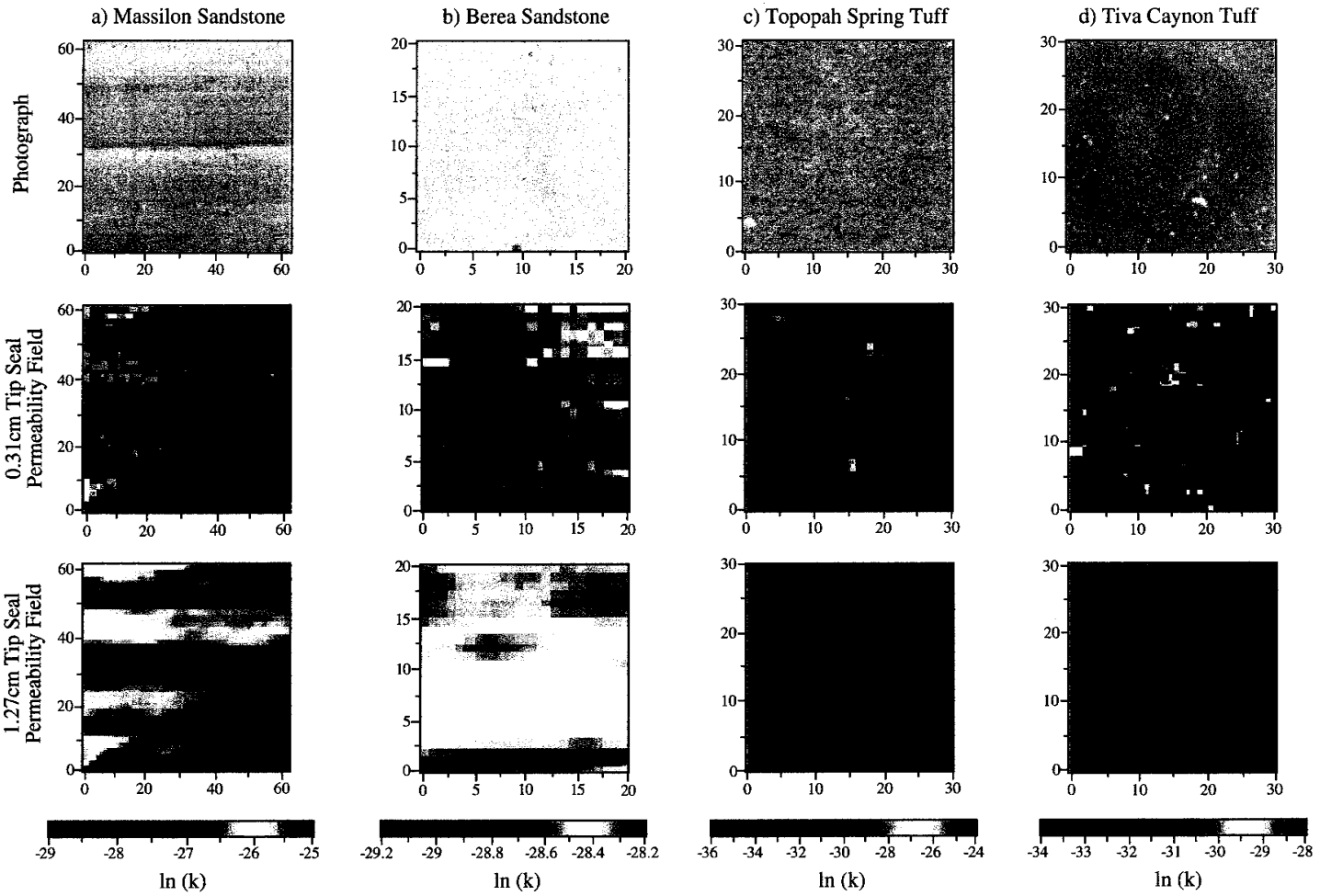

Figure 7.1. Rock sample photograph and corresponding permeability fields. From top to bottom is a photograph of the sampled rock face and the associated two-dimensional natural-log permeability fields measured with the 0.31 and 1.27 cm tip seals, respectively. Presented are data for a) Face 5 of the Massillon Sandstone, b) Face 4 of the Berea Sandstone, c) Face 5 of the Topopah Spring Tuff, and d) Face 6 of the Tiva Canyon Tuff. Note that different color scales are used for each rock sample because of the significant range in permeabilities spanned by the four samples. Likewise, different spatial scales have (grid dimensions are in cm) been employed to facilitate their presentation.

2-4 cm apart. The composition, sorting, and structure of the formation suggest that the Massillon Sandstone was water lain under relatively energetic conditions; however, there is some uncertainty concerning the actual mode of deposition, with both fluvial [Schmidley, 1987] and tidal environments [Gray, 1956] having been suggested.

The Berea Sandstone was selected for testing because of its common use in laboratory studies and its relatively simple physical features (Figure 7.1). The rock block measures 0.3 by 0.3 by 0.3 m and was obtained from Cleveland Quarries in Amherst, Ohio. The Berea Sandstone is presumed to be of Mississippian age with its origins in a low-energy, fluvial-deltaic environment [Pepper et al., 1954]. According to visual inspection, the sample is characterized as a very-fine grained, well-sorted quartz sandstone. The sample is relatively featureless except for faint stratification oriented parallel to the upper and lower faces of the block.

The Topopah Spring Tuff sample (Figure 7.1) is a 0.81 by 0.74 by 0.63 m block of moderately welded, devitrified ash flow tuff. The sample is from the Miocene age, Topopah Spring Tuff of the Paintbrush Group [Sawyer et al., 1994]. The sample originated as a boulder collected from Fran Ridge on the Nevada Test Site, located approximately 100 km northwest of Las Vegas, Nevada. The rock sample is characterized by an aphanitic fabric with conspicuous pumice and lithic fragments. The pumice fragments have an average diameter of <1 cm and comprise approximately 23% of the rock sample. However, each face is populated with a number of larger fragments (>3 cm dia.). The pumice fragments have an oblate shape (ratio of principal axes is approximately 2:2:1) caused by compaction which occurred while the flow cooled. Low permeability lithic fragments account for another 2-3% of the rock; however, their size rarely exceeds 1 cm.

The Tiva Canyon Tuff sample (Figure 7.1) is a 1.18 by 0.63 by 0.39 m block of poorly welded, ash flow tuff. The sample is from the Miocene age, Tiva Canyon Tuff of the Paintbrush Group [Sawyer et al., 1994] and stratigraphically overlies the Topopah Spring Tuff. The sample was collected from Yucca Mountain, which is also located on the Nevada Test Site. The rock sample exhibits an aphanitic fabric with sparse pumice fragments. The pumice fragments, which comprise from 5-10% of the rock sample, are predominately smaller than 0.5 cm in diameter but on rare occasions reach sizes of up to 3 cm in diameter.

This suite of rock blocks provides us with two sets of samples that are of very different genetic origin; one set that results from sedimentary processes while the second set is the result of extrusive volcanic processes. The spatial patterns exhibited by these rocks likewise differ with the sandstones characterized by distinct stratification while the tuffs are characterized by an aphanitic fabric with pumice and lithic fragments. However, within the genetically related sets, differences between the rock samples exist. The Massillon Sandstone exhibits nested scales of heterogeneity and greater spatial contrast than that of the Berea Sandstone. The Topopah Spring Tuff is characterized by larger and more numerous pumice fragments and a tighter matrix than that found in the Tiva Canyon Tuff.

Multi-Support Permeameter (MSP)

Permeability data were acquired with a specially adapted minipermeameter test system, which we call the Multi-Support Permeameter (MSP) (see Chapter 2). With this system permeability measurements were made by simply compressing a tip seal against a flat, fresh rock surface while injecting gas at a constant pressure. Using information on the seal geometry, gas flow rate, gas injection pressure, and barometric pressure, the permeability was calculated using a modified form of Darcy's Law [Goggin et al., 1988]. This process was automated by coupling a minipermeameter with an x-y positioner and computer control system. The minipermeameter functions as the measurement device of the

MSP and consists of four electronic mass-flow meters (0-50, 0-500, 0-2000, and 0-20,000 cm^3/min. at standard conditions), a pressure transducer (0-100 kPa gauge), a barometer, and a gas temperature sensor that are all connected to a regulated source of compressed nitrogen. Measurements were made according to a user specified sampling grid programmed into the x-y positioner. Along with locating the tip seal for sampling, the positioner also compresses the tip seal squarely against the rock surface with a consistent and constant force. The electronic permeameter and x-y positioner are configured with a computer control system to govern the data acquisition process and provide unattended operation. A full description and analysis of the MSP is given in Chapter 2.

The MSP is designed for use with meter-scale blocks of rock. Blocks are preferred because they provide multiple faces for sampling, with each oriented parallel to an inferred principal axis of permeability. Blocks also provide a test medium that is thick relative to the depth of penetration of any minipermeameter measurement.

MSP Tip Seals and the Sample Support

Measurements were made at different sample supports (i.e., sample volumes) by simply varying the radius of the tip seal. Tip seals consist of a rigid aluminum housing to which a molded silicone rubber ring is affixed. Tip seals were built with inner radii, r_1, of 0.15, 0.31, 0.63, 1.27, and 2.54, cm and an outer radii measuring twice the inner. Critical to precise measurement is a consistent and known tip seal geometry under compressed conditions. For this reason, each of the tip seals is equipped with an internal spring-driven guide to maintain a constant inner seal diameter. For the 0.63 cm and smaller tip seals, which experience considerable deformation on compression, an immobile outer guide is also employed.

An additional large tip seal was constructed to provide a means of collecting a single measurement that integrates over most of the sampling domain. The large tip seal has an inner radius, r_1, of 7.62 cm and an outer radius that is twice r_1. Given its large size little deformation of the seal occurs during compression and hence no inner or outer guides are needed. As this large seal exceeds the compression capacity of the x-y positioner, it was secured directly to the rock using nylon hoist straps. A floor jack was expanded between the straps and tip seal to compress it firmly against the rock. A load cell was used to monitor the applied force. Measurements were made when the applied compressive stress was equal to that used to compress the 2.54 cm tip seal. Measurements were also made at other compressive stresses to evaluate sensitivity of the calculated permeability to the applied stress.

It is important to note that the ring-shaped tip seal imposes a strongly divergent flow geometry on the test medium. The resulting non-uniform flow field not only has important implications relative to the measured permeability upscaling [Matheron, 1967; Desbarats, 1992a; Indelman and Abramovich, 1994], as we will see later, but also raises questions concerning what the MSP actually measures. To address this latter issue, we empirically investigated the measurement characteristics of the MSP by way of linear filter analysis (see Chapter 3). Results, as given by the empirical spatial weighting functions, indicate that the sample support is approximately hemispherical (even for the samples characterized by permeability anisotropy) consistent with the symmetry of the tip seal. Heterogeneities located near the center of the tip seal influence the measurement more than those located further away, consistent with the divergent flow field imposed by the MSP. Also, as the tip seal size increases the effective radius, r_{eff}, of measurement increases. Although additional work is needed to fully quantify the sample support associated with each tip seal, we and others [e.g., Goggin et al., 1988] believe that the r_{eff} is roughly

proportional to r_l, hence the volumetric sample support increases by a power of 8 for each doubling of r_l.

Upscaling Experiments

Upscaling experiments were conducted by making hundreds to thousands of permeability measurements on a block face with each tip seal, then flipping the block to another face and repeating the process. Measurements were made with each tip seal according to the same regular grid. To avoid boundary effects on the measurements, the grid was located away from the edges of the block. Where possible, the grid spacing was selected so as to yield exhaustive spatial coverage of the sampling domain with the smallest tip seal while the dimensions of the grid were dictated by the scale of the heterogeneity (including 3-4 correlation length scales where possible).

Over 150,000 permeability values form the basis of our analysis: 75,006 from the Massillon Sandstone, 13,824 from the Berea Sandstone, 31,110 from the Topopah Spring Tuff, and 38,882 from the Tiva Canyon Tuff. Although data were always collected on a square, uniform grid the dimensions, number of sampling points, and grid spacing varied between samples. Specific grid characteristics for each sample are given in Table 7.1. It was not always possible to make measurements with every tip seal on each sample. Specifically, the 2.54 and 7.62 cm tip seal were not used on the Berea Sandstone sample because of the limited size of the block, while the 2.54 cm tip seal was not used on the Topopah Spring Tuff because of difficulties in achieving a satisfactory seal.

Permeability upscaling experiments were conducted on all six block faces of each sample; however, in efforts to convey this information in a concise manner we present data only for a single face of each block. Presented are data for Face 5 of the Massillon

Table 7.1. Sampling grid specifications for the four rock samples.

Rock	Grid Points	Grid Spacing (cm)	Grid Dimensions (cm)
Massillon Sandstone	50 x 50 = 2500	1.27	62.23
Berea Sandstone	24 x 24 = 576	0.85	19.55
Topopah Spring Tuff	36 x 36 = 1296	0.85	29.75
Tiva Canyon Tuff	36 x 36 = 1296	0.85	29.75

Sandstone, oriented normal to cross-stratification; Face 4 of the Berea Sandstone, oriented normal to stratification; Face 3 of the Topopah Spring Tuff, oriented normal to the plane of compaction foliation; and Face 6 of the Tiva Canyon Tuff (no preferred orientation). In general, the upscaling measured on a particular rock sample is quite consistent across its six block faces. As such, the basic conclusions drawn here are independent of the rock faces used in the analysis. Data beyond that given here may be found in Chapter 2 (Berea Sandstone Face 5), Chapter 3 (Berea Sandstone Face 2), Chapter 4 (Berea Sandstone Face 3), Chapter 5 (Massillon Sandstone Face 4), and Chapter 6 (Topopah Spring Tuff Face 1).

7.4. Results

We now explore this unique data set by comparing and contrasting the statistical and upscaling characteristics of the permeability measured on the four different rock samples. Again, our purpose is to explore how the spatial patterns distinguishing each rock sample influence the statistical and upscaling characteristics of the permeability. Although our analysis could encompass many statistical measures, we limit our discussion to select statistics, which were chosen so as to provide a reasonably broad basis for evaluating

upscaling behavior and because of their common use in current theoretical upscaling models.

We begin our analysis with the measured permeability maps and progress to the distribution function, semivariogram, variance, and mean, respectively. In this way we progress from more detailed measures of the permeability distribution to less detailed. For each statistical measure we begin by presenting the data for each rock sample (single rock face). We then explore differences in the statistic in light of differences in the spatial characteristics of the rock samples. Upscaling of the statistic is then explored. By upscaling, we mean the change in the statistic as the sample support (i.e., sample volume or scale of measurement) increases. Finally, we attempt to explain the measured differences in upscaling according to the spatial patterns characterizing each of the four rock samples.

Permeability Maps

We begin our comparison with the natural-log permeability fields ($\ln(k(\vec{x}))$ where k is in m^2) measured with the different size tip seals on the four rock samples. Figure 7.1 presents photographs of the sampled rock faces and the corresponding permeability fields measured with the 0.31 and 1.27 cm tip seals. The color scale used for the permeability maps is organized such that the warm colors correspond to higher permeability and cool colors correspond to lower permeability. Note that different color scales are used for each sample because of the large range in permeability spanned by the four samples. To facilitate presentation, the spatial scales employed also differ between rock samples.

Comparing the permeability fields with the associated photographs (Figure 7.1) reveals a strong correlation between the spatial patterns visible in the sampled rock face and the spatial patterns characterizing the two-dimensional permeability fields. The bounding surfaces that cross-cut the Massillon Sandstone sample are delineated in the permeability

fields by elongate zones of lower permeability, while narrow bands of alternating permeability mark the presence of planar and low-angle cross stratification. Although not as distinct as the Massillon Sandstone, stratification is evident in the permeability fields measured on the Berea Sandstone, consistent with the faint stratification visible in the rock face. In the permeability fields measured on the tuff samples, a strong contrast in permeability is evident between the highly porous pumice fragments and the tight rock matrix. In fact, a one-to-one relation can be established between zones of higher permeability and the presence of a pumice fragment. Unfortunately, it is difficult to distinguish the pumice fragments in the tuff photographs as there is not a distinct and consistent color contrast between the pumice, lithic fragments, and rock matrix.

By comparing permeability maps measured with different size tip seals, distinct upscaling trends are recognized. In fact, all four rock samples exhibit the same general behavior. As the scale of measurement increases (i.e., tip seal size) there is a distinct smoothing of the permeability field that preserves the large-scale structural features. This behavior suggests that the minipermeameter tip seal functions as a low-pass filter. Specifically, high-frequency (small-scale) structural features are preferentially filtered from the data, while the low-frequency (large-scale) structural features remain virtually unchanged. Whether a feature is filtered depends on its size relative to the characteristic length of the measurement.

Cumulative Distribution Functions

The cumulative distribution functions (CDFs) calculated from the natural-log permeability data sets measured with each of the different size tip seals are given in Figure 7.2. The CDFs are presented separately for each of the four rock samples; however, all four graphs are plotted with the same permeability scales. Inspection of the CDFs reveals a distinct difference in the shape of the permeability distributions, particularly in the skewness. These differences are related to the textural contrast characterizing each rock

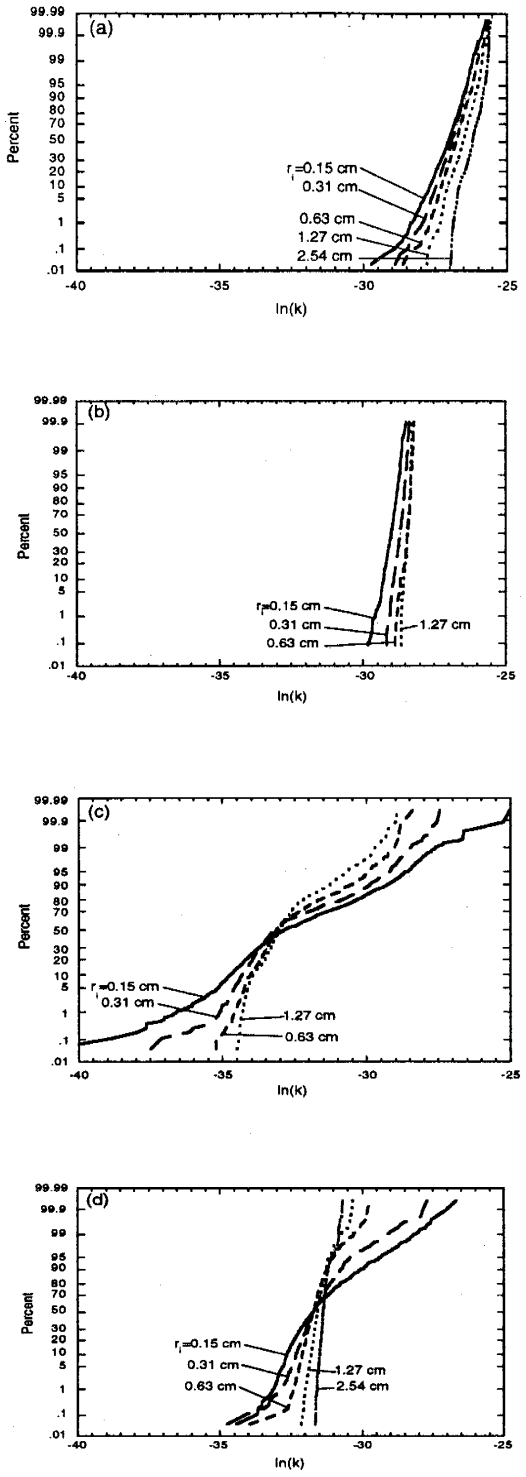

Figure 7.2. Cumulative distribution functions (CDFs) for the natural-log permeabilities measured with different size tip seals on the four rock samples. CDFs are plotted separately for: (a) Face 5 of the Massillon Sandstone, (b) Face 4 of the Berea Sandstone, (c) Face 5 of the Topopah Spring Tuff, and (d) Face 6 of the Tiva Canyon Tuff. All graphs are plotted to the same permeability scale.

sample. The tuff samples are characterized by very sharp textural contrast between the tight rock matrix and the porous pumice fragments, which gives rise to a skewed, bimodal distribution. Alternatively, the textural contrast exhibited by the sandstones is slight, gradually grading from one location to another. The resulting CDFs are characterized by very low skewness.

Upscaling of the CDFs is evident for all four rock samples (Figure 7.2). The upscaling is marked by changes in the shape, slope, and position of the CDF as the tip seal size increases. Here, we focus attention on the shape of the distribution, while upscaling of the slope and position of the CDF, that is the variance and mean of the distribution, respectively, are addressed separately below. Careful inspection of the CDFs for the Massillon Sandstone reveal that the slight negative skew exhibited by the smaller tip seals (i.e., $r_t < 0.63$ cm) dissipates giving rise to a weak, narrow bimodal distribution. Similar behavior, but to a lesser extent, occurs with the Berea Sandstone. This trend toward a weak bimodal distribution reflects the organization of the permeability field into alternating bands of "high-" and "low-permeability" (see Figure 7.1) as tip seal size increases. This occurs because the tip seal acts as low-pass filter, while the characteristic length of the stratification (see below) exceeds that of the largest tip seal, thus preserving the "permeability bands." The CDFs measured on the tuff samples consistently exhibit a positively skewed, bimodal distribution; however, as tip seal size increases the distribution becomes more compact (i.e., less skewed). The change in skewness of the distribution simply reflects the sequential filtering of spatial features (i.e., pumice fragments) smaller than the tip seal from the permeability field. Thus, the rapid change in the Tiva Canyon Tuff CDFs with increasing tip seal size is consistent the relatively small size and frequency of pumice fragments.

Semivariograms

To investigate the spatial correlation of the permeability data, semivariograms were calculated from the natural-log permeability data sets measured with each tip seal on all four rock samples. In each case the full, two-dimensional semivariogram was calculated using Fourier analysis (via Fast Fourier Transforms, see Bracewell, 1986; Section 3.3). To facilitate comparison we have plotted one-dimensional transects, extracted from the two-dimensional semivariograms, oriented along the principal permeability axes (Figure 7.3). Separate graphs are presented for the major and minor permeability axes for the Massillon Sandstone (Figure 7.3a-b), Berea Sandstone (Figure 7.3c-d), and the Topopah Spring Tuff (Figure 7.3e-f) while a single graph is given for the Tiva Canyon Tuff (Figure 7.3g), which exhibits an isotropic structure. In each case, semivariogram models (lines) have been fit to the data (symbols) for the purpose of quantitative comparison.

Comparison of the semivariogram transects (Figure 7.3) reveals distinct differences, with the most apparent differences between the sandstone and tuff samples. These differences can be interpreted on the basis of the spatial patterns distinguishing the individual rock samples. The spatial patterns characterizing the sandstone samples are dominated by numerous subhorizontal layers. In the case of the Berea Sandstone the subhorizontal layers correspond to simple planar cross-stratification whereas for the Massillon Sandstone the layers are comprised of cross-stratified sets (as delineated by the low permeability bounding surfaces). It is this subhorizontal layering that is the cause of the anisotropy in the permeability semivariograms. Specifically, semivariogram transects oriented parallel to the subhorizontal layering are characterized by strong, long-scale correlation that extends beyond the length of the semivariogram. Normal to the subhorizontal layering the semivariogram transects are characterized by much shorter scale correlation. Also, in this orientation the semivariograms for both sandstones exhibit a hole-

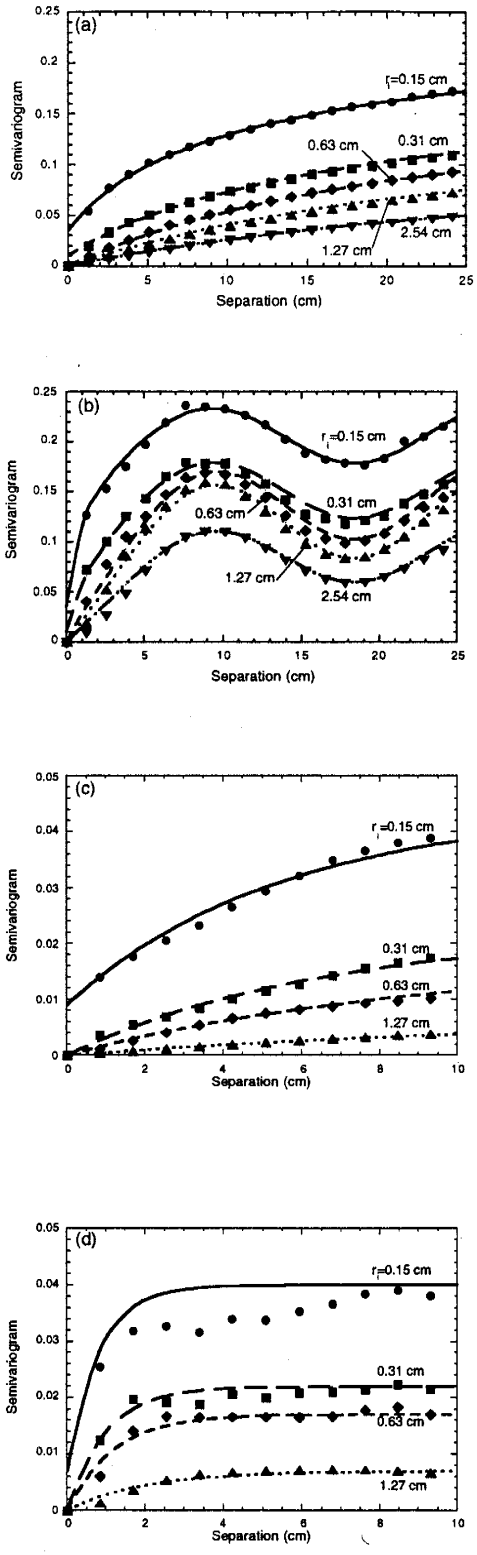

Figure 7.3. Semivariogram transects. See full description on the next page.

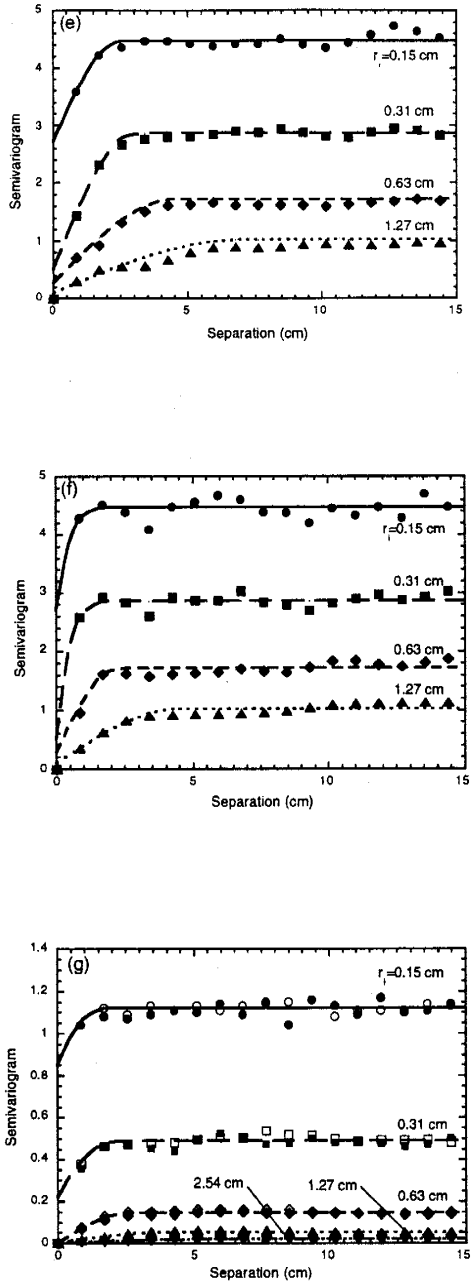

Figure 7.3. Semivariogram transects calculated from the natural-log permeability data sets measured with different size tip seals on the four rock samples. For those rocks exhibiting anisotropy, transects oriented parallel and normal to the primary structure are given. Plotted are the semivariograms for Face 5 of the Massillon Sandstone oriented (a) parallel and (b) normal to the bounding surfaces, Face 4 of the Berea Sandstone oriented (c) parallel and (d) normal to stratification, Face 5 of the Topopah Spring Tuff oriented (e) parallel and (f) normal to the long-axis of the pumice fragments, and (g) Face 6 of the Tiva Canyon Tuff. Note that the symbols mark the calculated semivariogram values while the solid lines are models fit to the data.

effect reflecting the periodic structure of the layers. The hole-effect is very strong in the case of the Massillon Sandstone because of the consistency between the repeated cross-stratified sets.

The spatial patterns characterizing the tuff samples are dominated by the pumice fragments populating the rock blocks. Thus, it is the size, shape, and frequency of the pumice fragments that dictates the characteristics of the semivariogram. The semivariogram transects for the volcanic tuffs exhibit relatively poor (i.e., large nugget), short-scale correlation reflecting the strong contrast in permeability between the pumice and rock matrix and the varied size distribution of the pumice. Slight anisotropy is noted in the case of the Topopah Spring Tuff while the Tiva Canyon Tuff exhibits an isotropic structure. We attribute these differences to the variations in the nominal shape of the pumice fragments comprising the different tuffs. A slight flattening of the pumice fragments is evident in the Topopah Spring Tuff caused by compaction during lithification of the flow. Also, a faint hole-effect is evident in the Topopah Spring Tuff semivariograms corresponding to the frequency at which the pumice fragments are nominally spaced.

The semivariogram range values fitted to the calculated semivariograms (Figure 7.3) are also seen to closely correlate with the spatial patterns visible in the sampled rock faces. Two nested scales of structure are discernible in the Massillon Sandstone. There is a scale of structure associated with the cross-stratified sets (delineated by the sub-horizontal bounding surfaces) and a second scale corresponding to the low-angle and planar cross-stratification appearing within the cross-stratified sets. The short-scale structure with fitted range values of $\lambda_x = 2.5$ cm and $\lambda_z = 1.5$ cm (where x denotes the orientation parallel to subhorizontal layering and z normal) is consistent with the average thickness of the cross-stratification. The anisotropy exhibited is the result of both low-angle and planar cross-stratified features being averaged together. A longer-scale feature with $\lambda_x > 30$ cm and

$\lambda_z = 18$ cm corresponds to the geometry of the cross-stratified sets. The horizontal spatial correlation agrees with the laterally continuous nature of the cross-stratified sets while the vertical spatial correlation reflects the distance between sets. The $\lambda_x > 10$ cm and $\lambda_z = 2.4$ cm fitted to the Berea Sandstone data likewise correlates with the laterally continuous but thin stratification visible in the rock sample. The range values fitted to the semivariograms for the tuff samples are related to the size distribution of the pumice fragments. Their magnitude, $\lambda_x = 2.5$ cm and $\lambda_z = 1.2$ cm for the Topopah Spring Tuff and $\lambda = 1.2$ cm for the Tiva Canyon Tuff, is related to the diameter of the largest pumice fragments in the distribution.

Even the shape (i.e., fitted mathematical model) of the semivariograms can be related to the spatial structure of the different rock samples. The exponential semivariogram structure of the sandstones correlates with their gradual (smooth) variation in permeability. The spherical semivariogram structure of the tuff samples is characteristic of the sharp permeability contrast between the rock matrix and pumice.

As with the other statistics investigated, distinct upscaling trends are evident in the semivariograms calculated from the permeability data measured on the different rock samples (Figure 7.3). Upscaling is manifest by changes in the structure of the semivariogram, the semivariogram range, and the magnitude of the semivariogram as tip seal size increases. Comparison of the semivariograms for the four rock samples shows that each of these attributes upscale according to the same general trends.

The general structure of the semivariogram remains essentially unaffected by changing sample support except over small separation distances. This finding is consistent with the low-pass filtering behavior of the tip seal; that is, as the size of the tip seal becomes large with respect to a particular heterogeneous feature, that feature is filtered from

the permeability field. We see this behavior in the Massillon Sandstone data where the small-scale structural feature (associated with the low-angle and planar cross-stratification) is apparent in the semivariograms for the 0.15 and 0.31 cm tip seals but is absent from the semivariograms associated with the larger tip seals. Similarly, the decreasing nugget effect with increasing tip seal size exhibited by the Berea Sandstone and the two tuff samples is further evidence of this filtering effect. The fact that the large-scale structural features exhibited by the four rock samples remain unchanged confirms that structures larger than the tip seal do not experience the filtering effect.

Closer inspection of the sample semivariograms for each of the four rock samples reveals that the fitted semivariogram range values increase with increasing tip seal size. In fact, the range increases roughly as a linear function of tip seal size (Figure 7.4). The linear (increasing) trend in the semivariogram range simply reflects the increasing effective radius of the tip seal (i.e., r_{eff}), and as r_{eff} increases two measurements must be spaced that added distance apart before they become uncorrelated [Clark, 1977; Journel and Huijbregts, 1978]. Although the range is always an increasing function of sample support the slope of the linear function differs among the rock samples. These differences may stem from effects of media heterogeneity on the geometry of the tip seal sample support, reflect differences in the permeability upscaling between rock samples, or be a combination of these.

Inspection of the semivariograms for the four rock samples also reveals that the sill of the semivariogram always decreases with increasing sample support. This behavior is simply reflecting the reduction in the spatial variability of the permeability as the tip seal size is increased. We address this issue below where we explore upscaling of the sample variance in detail.

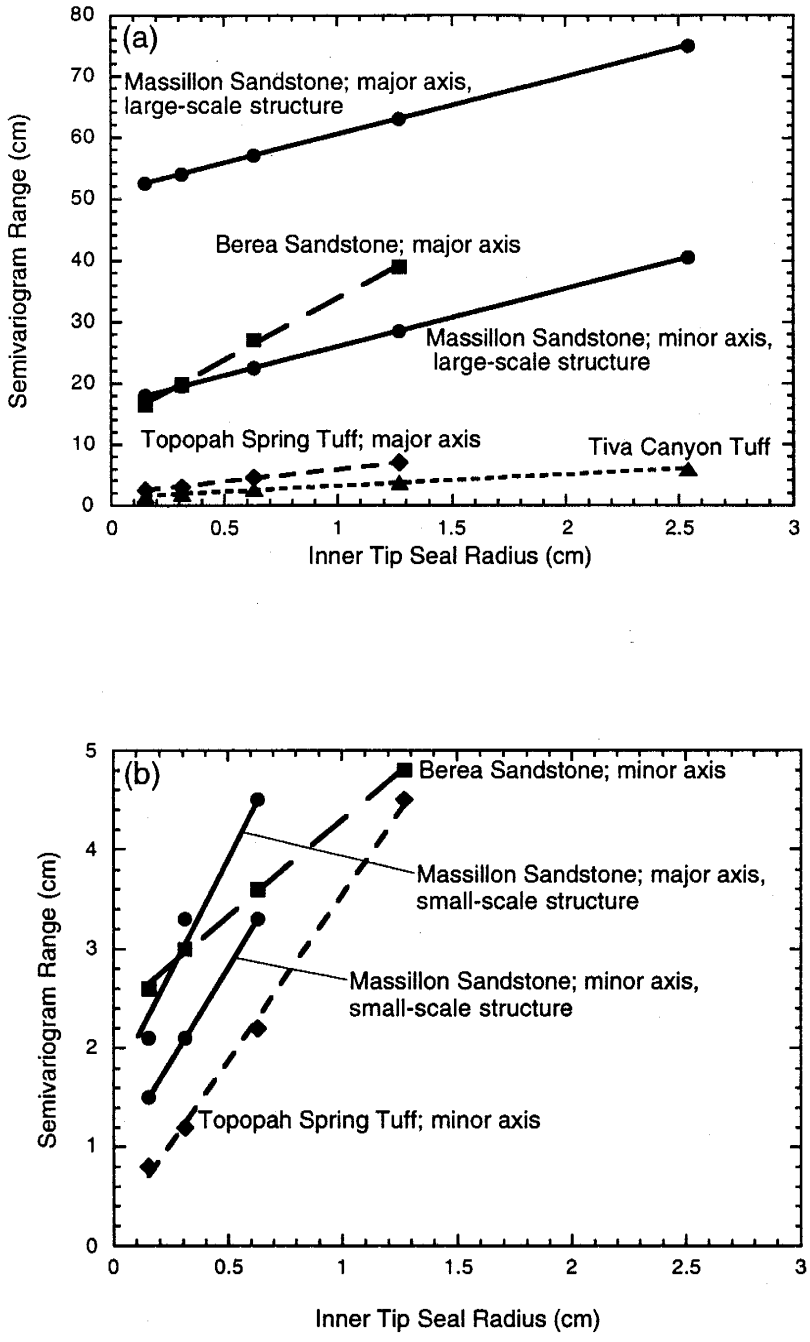

Figure 7.4. Upscaling of the range values fitted to the semivariogram transects (Figure 7.3) calculated for Face 5 of the Massillon Sandstone, Face 4 of the Berea Sandstone, Face 5 of the Topopah Spring Tuff, and Face 6 of the Tiva Canyon Tuff. Two graphs, (a) and (b), are presented because the range values differ by over a magnitude of order.

It is interesting to note that for each rock sample the qualitative upscaling trends exhibited by the semivariograms are consistent with that predicted by semivariogram regularization theory [Clark, 1977; Journel and Huijbregts, 1978]. This is a bit surprising given that the permeability does not upscale according to a simple arithmetic (i.e., linear) averaging process, as demonstrated by the distinct increase in the mean permeability with increasing sample support (see below). Given the non-linear volume averaging characterizing the permeability upscaling, quantitative comparisons drawn between our data and semivariogram regularization theory is expected to meet with less success. In fact, this is evidenced in part by the upscaling of the semivariogram range values, which exhibit different rates of change (i.e., slopes) across the different rock samples and different coordinate directions (Figure 7.4).

Sample Variance

In Figure 7.5, sample variances calculated from the natural-log permeability data sets are plotted as a function of the inner tip seal radius. Note that each plotted value was calculated from data sets comprised of 576 to 2500 data points measured on a single block face of the respective sample. Although not shown, similar trends and relative magnitudes characterize the variances measured on the other block faces.

The four rock samples exhibit a considerable range in variance. There is almost two-orders of magnitude difference in the variance between the four rock samples with the tuff samples exhibiting the highest variance, at least for the smaller tip seal sizes. A relationship between the variance and the spatial characteristics of the rock samples is not as evident as with some of the other statistics already investigated. However, some qualitative estimates of the relative magnitude of the variance can be made by way of the visual contrast exhibited by the rock samples. From this perspective, the Berea Sandstone is expected to have the lowest variance given its uniform appearance, while the Topopah

Spring Tuff should have the highest variance given its strong visual contrast. However, such relative comparisons are not as obvious for the Massillon Sandstone and Tiva Canyon Tuff.

Upscaling of the sample variance is evident. All four rock samples are characterized by a variance that decreases as the sample support increases, following roughly a power-law relation. This trend simply reflects the fact that larger tip seals integrate over more heterogeneity than do smaller tip seals and hence yield "smoother" permeability distributions; again, reflecting the low-pass filtering of the tip seals. The slope of the upscaling trend differs between the rock samples with the Massillon Sandstone exhibiting the slowest rate of change while the Tiva Canyon Tuff exhibits the fastest rate (Figure 7.5b). These trends are consistent with the fact that the Massillon Sandstone is characterized by the longest-range correlation and the Tiva Canyon Tuff the shortest-range correlation among the four rock samples.

Sample Mean

In Figure 7.6 the sample means calculated from the natural-log permeability data sets are plotted as a function of the inner tip seal radius. Values corresponding to the 0.15, 0.31, 0.63, 1.27, and 2.54 cm r_I tip seals represent an average of between 576 and 2500 permeability values, while the value corresponding to the 7.62 cm r_I tip seal represents a single measurement that integrates over most of the sampling domain. In each case these data were acquired from a single block face, and we note that very similar results are achieved regardless of which block face is employed in the analysis. Also, for a point of reference we have plotted the mean upscaling for the simple case of a geometric averaging process (Figure 7.6b).

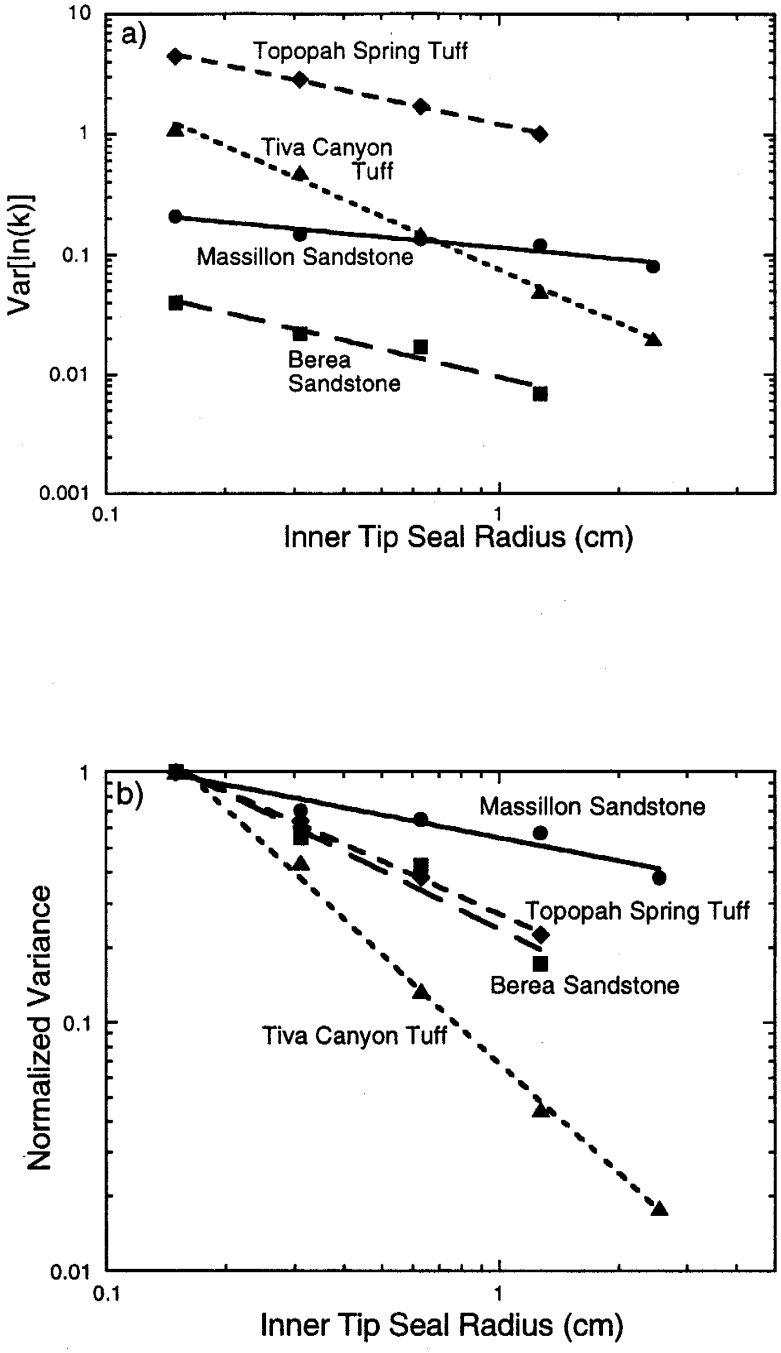

Figure 7.5. Variance upscaling measured on Face 5 of the Massillon Sandstone, Face 4 of the Berea Sandstone, Face 5 of the Topopah Spring Tuff, and Face 6 of the Tiva Canyon Tuff. Results are presented in two different ways: a) variance of the natural-log permeability data, and b) variance of the natural-log permeability data normalized by the sample variance for the 0.15 cm tip seal.

Clear differences are evident in the mean permeabilities calculated for the four rock samples. Specifically, the mean values calculated from the 0.15 cm tip seal data differ by over two orders of magnitude, while those measured with the largest tip seal differ by almost three orders of magnitude (Figure 7.6a). The sandstone samples are characterized by distinctly higher permeability than that exhibited by the tuff samples. Between sandstone samples, the mean permeability is highest for the Massillon Sandstone which has the larger average grain size, while for the tuff samples the permeability decreases as the degree of welding increases. Beyond these gross qualitative assessments it would be difficult to speculate further concerning the relationship between differences in the mean permeability and the physical attributes of the rock sample.

As with the other statistics we have investigated, the mean permeabilities for all four rock samples exhibit distinct trends with increasing sample support. In each case the mean upscaling follows a weak power-law relation; however, the sense (i.e., increasing or decreasing) and rate with which the mean upscales differs considerably. Both sandstone samples exhibit a mean that increases with increasing sample support while the tuff samples are characterized by a mean that is invariant or decreases with increasing tip seal size. Thus, the mean upscaling is unique with respect to the other statistics we have investigated in that the sense of the upscaling differs between rock samples.

These differences in the mean upscaling can in part be explained on the basis of the differing physical attributes of the rock samples. Consider the Tiva Canyon Tuff that exhibits a mean upscaling which closely matches that of a geometric averaging process. This upscaling behavior is consistent with the poor to non-existent spatial correlation of its permeability distribution. The decreasing trend in the mean upscaling for the Topopah Spring Tuff occurs because the pumice fragments are spatially disconnected. Thus, as the

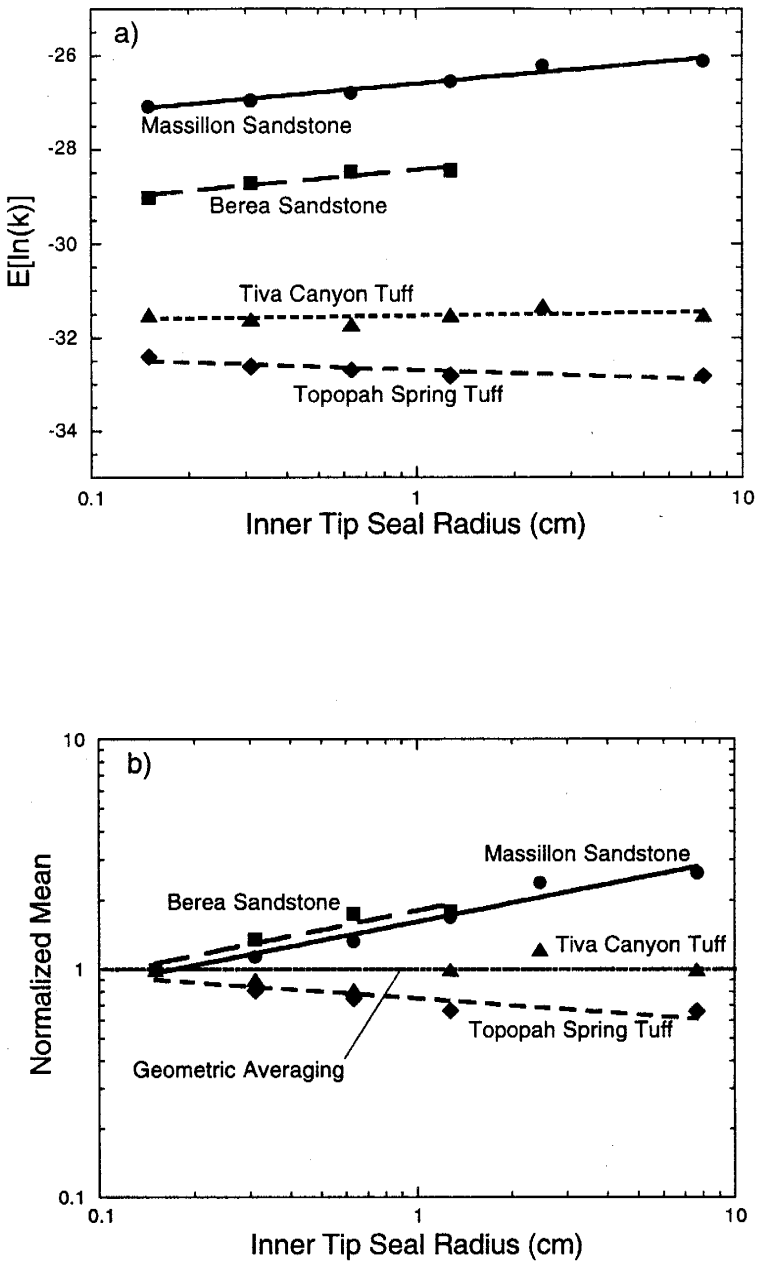

Figure 7.6. Mean upscaling measured on Face 5 of the Massillon Sandstone, Face 4 of the Berea Sandstone, Face 5 of the Topopah Spring Tuff, and Face 6 of the Tiva Canyon Tuff. The results are presented in two different ways, a) mean of the natural-log permeability data, and b) geometric mean $\left(k_g = \exp\left[E\left[\ln\left(k(\vec{x})\right)\right]\right]\right)$ normalized by the geometric mean calculated from the data measured with the 0.15 cm tip seal. For comparison we have plotted the mean upscaling for a geometric averaging process (i.e., invariant with changing sample support).

tip seal size increases fewer pumice span the tip seal forcing more gas through the rock matrix. This causes a reduction in the positive skew of the permeability distribution, and thus a shift in the mean permeability toward that of the rock matrix. In contrast, the subhorizontal layering characterizing the sandstone samples yields numerous well-connected, "high-permeability" pathways (i.e., spatial features that are largely populated by values that exceed the mean permeability) that cross-cut the sample. As the spatial continuity of these pathways exceeds the width of all six tip seals, the mean permeability remains high, reflecting the presence of these preferred flow paths.

According to this simplistic analysis, the general mean upscaling trends exhibited by the four rock samples can be explained. The key physical features distinguishing the behavior in the mean upscaling appear to be the spatial continuity of the "high" permeability fraction and its range of correlation relative to the scale of measurement (i.e., tip seal radius). However, full quantitative assessment of the mean upscaling will require a more detailed accounting of the structure of the porous media as well as consideration of the characteristics of the minipermeameter measurement. According to previous analyses of the mean upscaling for the sandstone samples, heterogeneities occurring at the local scale (i.e., the smallest support for which data is available) and the non-uniform flow conditions imposed by the minipermeameter exert significant influence on the measured upscaling (see Chapter 4).

7.5. Discussion and Conclusions

Here we present a subset of over 150,000 permeability values measures on four different blocks of rock. Beyond the shear volume, these data are unique in that: (1) measurements were made on six different sample supports (i.e., sample volumes) spanning five orders of magnitude on a per volume basis, (2) all data, regardless of sample support or rock sample, were measured in an entirely consistent manner, and (3) the data were

acquired at high-spatial resolution allowing estimation of the associated distributional and spatial statistics with a high degree of confidence. According to these controlled experiments, we present rare empirical evidence of permeability upscaling measured on four blocks of rock, each exhibiting differing physical attributes.

Our purpose is to compare and contrast the permeability upscaling measured on the four blocks of rock. Of particular interest is how the spatial patterns distinguishing each rock sample influence the statistical and upscaling characteristics of the permeability. Toward this end, rock samples of very different genetic origin were selected for testing; two sandstones and two volcanic tuffs. Differences are also explored within a given rock type. The two sandstone samples are distinguished according to the energy of the depositonal environment while the tuffs differ by their degree of welding (i.e., related to cooling history). Below we explore this extensive data set according to the three questions raised in the introduction to this paper.

Permeability Statistics vs. Attributes of the Rock Sample

Although each of the tested rock samples exhibit unique physical features, the most apparent differences are between the sandstones and tuffs. The striking difference in appearance undoubtedly reflects their dissimilar depositonal and diagenetic histories. According to the data presented, these differences in physical appearance are accompanied by distinct differences in the permeability statistics characterizing the four rock samples. Two-dimensional permeability maps reproduce the basic spatial patterns visible in each sampled block face. The permeability patterns measured on the sandstones exhibit a cross-bedded structure, while the tuffs are dominated by scattered high permeability features that correspond to porous pumice fragments isolated in an otherwise tight rock matrix. The cumulative distribution functions reflect the degree of textural contrast in the sampled block face. The sandstones exhibit a narrow distribution with low skewness consistent with the smoothly varying contrast between adjacent strata, while the tuffs exhibit a relatively broad

distribution with strong positive skewness marking the strong textural contrast between pumice and matrix. Likewise, the calculated semivariograms are consistent with the number, geometry, and size of the features populating the sampled block face. The cross-bedded structure of the sandstones gives rise to an anisotropic semivariogram structure with strong spatial correlation parallel to the subhorizontal layering, while the tuff samples are characterized by relatively short range correlation and near isotropic conditions reflecting the dominant role of the subround pumice fragments.

This empirical evidence relating the permeability statistics to the physical attributes of the rock sample has important implications relative to the simulation of heterogeneous geologic formations. Specifically, the visual qualities of the medium provide important qualitative and semi-quantitative information on which to condition the models. Although the physical appearance of the porous media can aid in conditioning the models, it cannot be used as a substitute for good quantitative data. Good data is particularly critical in the case of permeability, as the measured permeability depends not only on the characteristics of the porous medium but on the characteristics of its measurement as well.

Upscaling of Permeability Statistics

The experiments presented here yield clear empirical evidence of permeability upscaling. By upscaling we mean distinct and consistent trends in key summary statistics corresponding to an increase in the scale of measurement. These results are particularly compelling given the exhaustive quantity of data and the controlled manner with which the data were measured. Even more compelling is the ubiquitous nature of the upscaling. Regardless of the statistic or rock type, upscaling was measured. Although the sampled rocks exhibit considerable differences there is a degree of consistency in the manner with which the permeability upscales. Consider the two-dimensional permeability maps. Distinct smoothing of the permeability field is evident with increasing tip seal size, while the large-scale structural features remain essentially unchanged. That is, features that are small

relative to the size of the tip seal are filtered from the permeability field while features larger than the tip seal remain largely unaffected. Similar trends are noted in the structure of the calculated semivariograms. Where the tip seal size becomes large with respect to a feature, that feature is filtered from the semivariogram, while the structure of the semivariogram at scales larger than the tip seal remains essentially unaffected. Other examples of this consistency in upscaling include the semivariogram range which always increases as a linear function of the inner tip seal radius, and the sample variance that always decreases according to a power-law relation.

The nature and consistency of the qualitative upscaling trends noted above come as no real surprise. In fact, each of these trends are qualitatively consistent with one of the simplest models of upscaling, that being volume averaging (e.g., semivariogram regularization). Also of no surprise is the fact that the permeability does not upscale according to a simple linear volume averaging process. This is clearly demonstrated by the increasing/decreasing trends in the mean permeabilities with increasing sample support. Although the non-linear volume averaging behavior characterizing the upscaling comes as no surprise, the origin of the nonlinearity is not so obvious (see below).

Permeability Upscaling vs. Attributes of the Rock Sample

Comparisons drawn between the data measured on the four rock samples suggest that the physical attributes of the porous medium do indeed influence permeability upscaling. Although there is considerable consistency in the manner with which the permeability upscales (as noted above), distinct differences are also evident. These differences are primarily manifest in the rate at which a statistic upscales and in the absolute change in the value of the statistic. However, the most obvious differences are noted in the upscaling of the mean permeability. Specifically, both sandstone samples are characterized by a mean that increases with increasing sample support, while the volcanic tuffs exhibit an invariant to decreasing trend in the mean. As the only variable in the experiments was the

test medium, any difference in upscaling must be the result of differences in the rock samples. Furthermore, we find the most distinct differences in upscaling between rocks of differing genetic origin (i.e., sandstones vs. tuffs), while rocks of similar genetic origin (e.g., sandstones) exhibit the greatest degree of consistency in upscaling.

Thus, it appears that the measured differences in the permeability upscaling can be explained on the basis of differences in the physical attributes of the rock samples. In fact, the spatial continuity of the "high" permeability fraction (i.e., roughly any permeability value exceeding the mean) and its range of correlation relative to the scale of measurement appear to be the primary features effecting the measured mean upscaling. Although our results provide encouraging evidence that the permeability upscales in a potentially quantifiable manner, quantitative modeling of the measured upscaling is not a trivial matter. Not only is the upscaling influenced by the heterogeneous features of the rock sample, as shown here, but is also affected by the characteristics of its measurement (see Chapters 3, 4, and 6). Of particular importance is the non-uniform flow geometry imposed by the MSP, which is an issue that has received relatively little attention in the literature.

Acknowledgments: We would like to thank Justin Von Doemming, Mark Bailey, and Nick Teske for their help in collecting the reported data. We would also like to extend our appreciation to Allan Gutjahr, Fred Phillips, and Peter Mozley for their helpful advice and constructive reviews of this manuscript. This work was supported by the U.S. Department of Energy, Office of Basic Energy Science, Geoscience Research Program, under contracts DE-AC04-94AL85000 and DE-F303-96ER14589/A000. Sandia is a multiprogram laboratory operated by Sandia Corporation, a Lockheed Martin Company, for the United States Department of Energy.

7.6. References

Bachu, S. and D. Cuthiell, Effects of core-scale heterogeneity on steady state and transient fluid flow in porous media: Numerical analysis, *Water Resour. Res.*, 26(5), 863-874, 1990.

Baveye, P. and G. Sposito, The operational significance of the continuum hypothesis in the theory of water movement through soils and aquifers, *Water Resour. Res.*, 20(5), 521-530, 1984.

Brace, W.F., Permeability of crystalline rocks: New in situ measurements, *J. Geophys. Res.*, 89(B6), 4327-4330, 1984.

Bracewell, R.N., *The Fourier Transform and Its Applications*, 474 pp., McGraw-Hill, New York, 1986.

Clark, I., Regularization of a semi-variogram, *Computers and Geosciences*, 3, 341-346, 1977.

Clauser, C., Permeability of crystalline rocks, *Eos. Trans. AGU*, 73(21), 233, 1992.

Cushman, J.H., On unifying the concepts of scale, instrumentation, and stochastics in the development of multiphase transport theory, *Water Resour. Res.*, 20(11), 1668-1676, 1984.

Dagan, G., Analysis of flow through heterogeneous random aquifers 2. Unsteady flow in confined formations, *Water Resour. Res.*, 18(5),1571-1585, 1982.

Desbarats, A.J., Numerical estimation of effective permeability in sand-shale formations, *Water Resour. Res.*, 23(2), 273-286, 1987.

Desbarats, A.J., Spatial averaging of transmissivity in heterogeneous fields with flow toward a well, *Water Resour. Res.*, 28(3), 757-767, 1992a.

Desbarats, A.J., Spatial averaging of hydraulic conductivity in three-dimensional heterogeneous porous media, *Math. Geol.*, 24(3), 249-267, 1992b.

Deutsch, C.V., Calculating effective absolute permeability in sandstone/shale sequences, *SPE Form. Eval.*, 4(3), 343-348, 1989.

Durlofsky, L.J., Representation of grid block permeability in coarse scale models of randomly heterogeneous porous media, *Water Resour. Res.*, 28(7), 1791-1800, 1992.

Freeze, R.A., A stochastic-conceptual analysis of one-dimensional groundwater flow in nonuniform homogeneous media, *Water Resour. Res.*, 11(5), 724-741, 1975.

Fogg, G.E., Groundwater flow and sand body interconnectedness in a thick, multiple-aquifer system, *Water Resour. Res.*, 22(5), 679-694, 1986.

Gelhar, L.W. and C.L. Axness, Three-dimensional stochastic analysis of macrodispersion in aquifers, *Water Resour. Res.*, 19(1), 161-180, 1983.

Goggin, D. J., R. L. Thrasher, and L. W. Lake, A theoretical and experimental analysis of minipermeameter response including gas slippage and high velocity flow effects, *In Situ*, 12(1-2), 79-116, 1988.

Gomez-Hernandez, J.J. and S.M. Gorelick, Effective groundwater model parameter values: Influence of spatial variability of hydraulic conductivity, leakance, and recharge, *Water Resour. Res.*, 25(3), 405-419, 1989.

Gray, H.H., Petrology of the Massillon Sandstone at the type locality, The Ohio Journal of Science, 56(3), 138-146, 1956.

Gutjahr, A.L., L.W. Gelhar, A.A. Bakr, and J.R. Macmillan, Stochastic analysis of spatial variability in subsurface flows, 2, Evaluation and application, *Water Resour. Res.*, 14(5), 953-960, 1978.

Haldorsen, H.H. and L.W. Lake, A new approach to shale management in field-scale models, *SPE J.*, 24(4), 447-457, 1984.

Hanor, J.S., Effective hydraulic conductivity of fractured clay beds at a hazardous waste landfill, Louisiana Gulf Coast, *Water Resour. Res.*, 29(11), 3691-3698, 1993.

Indelman, P. and B. Abramovich, Nonlocal properties of nonuniform averaged flows in heterogeneous media, *Water Resour. Res.*, 30(12), 3385-3393, 1994.

Journel, A G. and C.J. Huijbregts, *Mining Geostatistics*, 600 pp., Academic Press, New York, 1978.

Matheron, G., *Elements pour une theorie des milieux poreux*, 166 pp., Maisson et Cie, Paris, 1967.

Molz, L.J., O. Guven, J.G. Melville, and C. Cardone, Hydraulic conductivity measurement at different scales and contaminant transport modeling, in *Dynamics of Fluids in Hierarchical Porous Media*, edited by J.H. Cushman, Academic Press, New York, pp. 37-59, 1990.

Parker, J.C. and K.A. Albrecht, Sample volume effects on solute transport predictions, *Water Resour. Res.*, 23(12), 2293-2301, 1987.

Pepper, J.F., W. De Witt, Jr., and D.F. Demarest, Geology of the Bedford Shale and Berea Sandstone in the Appalachian Basin, *Geological Survey Professional Paper 259*, U.S. Geological Survey, 1954.

Sawyer, D.A, R.J. Fleck, M.A. Lanphere, R.G. Warren, D.E. Broxton, and M.R. Hudson, Episodic caldera volcanism in the Miocene southwestern Nevada volcanic field: Revised stratigraphic framework, $^{40}Ar/^{39}Ar$ geochronology, and implications for magmatism and extension, *GSA Bull.*, 106, 1304-1318, 1994.

Schmidley, E.B., *The sedimentology, paleogeography and tectonic setting of the Pennsylvanian Massillon Sandstone in east-central Ohio*, University of Akron, MS Thesis, 1987.

Schulze-Makuch, D. and D.S. Cherkauer, Method developed for extrapolating scale behavior, *Eos. Trans. AGU*, 78(1), 3, 1997.

Silliman, S.E. and A.L. Wright, Stochastic analysis of paths of high hydraulic conductivity in porous media, *Water Resour. Res.*, 24(11), 1901-1910, 1988.

Warren, J.E. and H.S. Price, Flow in heterogeneous porous media, *SPE J.*, 1, 153-169, 1961.

CHAPTER 8: CONCLUSIONS

The issue of upscaling, that is the dependency of measured parameters on their corresponding sample support, is encountered in the modeling of a wide range of physical phenomenon. The problem is one of parameterization; specifically, input properties can rarely be measured at the desired scale of analysis. Usually, some averaging or upscaling model is employed to accomplish the parameterization. Where the property depends only on the volume fraction of phase present (i.e., additive property), upscaling simply follows an arithmetic averaging process. Where the property depends both on the characteristics of the media and the modeled process (i.e., constitutive property), upscaling is not so easily determined.

Considerable attention has been paid to the issue of upscaling, which has resulted in numerous conceptual and theoretical models. Because of the difficulty and expense of acquiring large suites of data at different measurement scales, physical investigation of upscaling is sorely lacking. To provide fresh insight we have conceived, developed, and implemented an experimental program to physically investigate upscaling, using permeability as our basis of study. To gain a better understanding of permeability upscaling we explore our data with three questions in mind: 1) does the measured permeability data exhibit clear evidence of upscaling?, if so 2) is the measured permeability upscaling influenced by the physical attributes of the porous medium?, and 3) what media characteristics/physical processes govern the measured permeability upscaling? Below, we

summarize the collective results for this work and where appropriate discuss the implications of the findings. We conclude with recommendations for future studies.

8.1. Results

Novel Method for Physically Investigating Permeability Upscaling

This project required the development of an experimental method for collecting permeability data at different measurement scales. To do this we adapted an established measurement tool, the minipermeameter [Goggin et al., 1988], to meet the special needs of our project. This, in part, involved automation of the data collection procedure to facilitate acquisition of large data sets subject to nominal measurement error. Automation was achieved by integrating a computer-controlled electronic air minipermeameter with an x-y positioning system. We termed the integrated test system the Multi-Support Permeameter (MSP). The unique feature of the MSP is the use of different size tip seals for investigating permeability upscaling. By simply changing the tip seal size, permeability data were acquired in a completely consistent manner over a range of discrete sample supports. We also made numerous improvements to the minipermeameter tip seal design in order to assure consistency in the geometry of the seal under compressed conditions.

The critical design specification for the MSP was that all measurements, regardless of the sample support, be completely consistent. By consistent, we mean that all data were collected from the same physical sample (i.e., non-destructive sampling); sampling was spatially exhaustive, which allows the distributional and spatial permeability statistics to be calculated with a high degree of confidence; measurement error was small and consistent across all tip seals; and measurements were made subject to a consistent flow geometry, and boundary conditions, thus providing a uniform basis for comparison. By maintaining such consistency in measurement, we effectively limited the number of factors influencing

the permeability upscaling, improving our ability to interpret and quantify the measured behavior.

We extensively tested the system. The precision and consistency of measurements made with the MSP were evaluated using a suite of data collected from blocks of three relatively homogeneous materials: Berea Sandstone and two synthetic rocks. Results suggested that measurement error was small (approximately ±1% of the measured permeability) and consistent, and measurements made at different sample supports were free from systematic bias. As part of this testing, extensive characterization of the effects of tip seal compression pressure on the measured permeability was performed. We also investigated the conditions under which the measurements were made; specifically, whether the flow was steady and Darcian and whether the flow was subject to gas slippage effects.

Collection of Unique Data Sets

One of the most important products of this work is the extensive data set that was collected. The scope, quantity, and quality of our data is unparalleled. There are a few published data sets that rival the number of data and spatial resolution contained in any single permeability map presented here; however, we repeated the measurements with three or four additional tip seals. In each case, a second "realization" of the permeability field was measured by sampling the rock face directly opposite the block. Then measurements were made on the other four block faces, providing a full three-dimensional picture of the permeability distribution. Finally, the exhaustive data sets were measured on four different blocks of rock. Complimenting the scope and quantity of data is its quality; specifically, the consistency in measurement maintained across the different sample supports, individual rock faces, and the four rock samples.

The scope, quantity, and quality of the acquired data provide a unique opportunity to physically investigate permeability upscaling. The data yield empirical evidence of permeability upscaling, provide a basis for investigating controls on permeability upscaling, and a physical data set for testing conceptual and theoretical models of upscaling. The data are also useful for investigating issues beyond permeability upscaling. Examples include stochastic simulation of heterogeneous permeability distributions, the role of "geology" in defining permeability characteristics, and the testing of sampling schemes and their effect on calculated summary statistics. These data sets could also be used as natural analogues in numerical flow and transport modeling exercises.

Empirical Spatial Weighting Functions were Calculated from MSP Data

The non-uniform flow geometry imposed by the MSP raises questions concerning what is actually measured by tip seals of different size. By measure we mean the sample support or sample volume associated with the tip seal, as well as the spatial weighting of the heterogeneities comprising that sample support. We empirically addressed this issue with the aid of linear filter theory. Specifically, we calculated spatial weighting (filter) functions, characterizing the minipermeameter measurements, from permeability data sets collected with the MSP. In fact, these weighting functions provide the only physical (i.e., calculated directly from physical data) evidence of a hydraulic instrument functioning as a linear filter.

Results demonstrated that the empirical weighting functions were consistent with the basic physics of the minipermeameter measurement. The weighting functions were centered on the measurement, consistent with the symmetry of the tip seal. Each of the weighting functions decayed according to a nonlinear function of radial distance, consistent with the divergent flow geometry imparted by the minipermeameter. Also, the shape of the weighting function changed in a predictable manner as tip seal size was varied. As the tip

seal size became larger the effective radius of the measurement, and thus the sample support, increased. We further demonstrated, both empirically and theoretically, that non-additive properties like permeability are amenable to linear filter analysis under certain limiting conditions (i.e., small variances). Specifically, the weighing function is independent of the power average employed in its calculation (e.g., arithmetic vs. harmonic average).

Permeability Statistics are Influenced by Attributes of the Rock Sample

Upscaling studies were conducted on four different blocks of rocks, two sandstones and two volcanic tuffs. Specifically, investigations were performed on blocks of: Berea Sandstone, a faintly laminated fluvial-deltaic sandstone; Massillon Sandstone, a conspicuously cross-stratified sandstone from a high-energy fluvial or near-shore environment; Topopah Spring Tuff, a densely-welded devitrified tuff; and Tiva Canyon Tuff, a poorly-welded tuff.

Although each of the tested rock samples exhibit unique physical features, the most apparent differences are between the sandstones and tuffs. The striking difference in appearance undoubtedly reflects their dissimilar depositonal and diagenetic histories. The data presented demonstrate that these differences in physical appearance are accompanied by distinct differences in the permeability statistics characterizing the four rock samples. Two-dimensional permeability maps reproduce the basic spatial patterns visible in each sampled block face. The permeability patterns measured on the sandstones exhibit a cross-bedded structure, while the tuffs are dominated by scattered high permeability features that correspond to porous pumice fragments isolated in an otherwise tight rock matrix. The cumulative distribution functions reflect the degree of textural contrast in the sampled block face. The sandstones exhibit a narrow distribution with low skewness consistent with the smoothly varying contrast between adjacent strata, while the tuffs exhibit a relatively broad

distribution with strong positive skewness marking the strong textural contrast between pumice and matrix. Likewise, the calculated semivariograms are consistent with the number, geometry, and size of the features populating the sampled block face. The cross-bedded structure of the sandstones gives rise to an anisotropic semivariogram structure with strong spatial correlation parallel to the subhorizontal layering, while the tuff samples are characterized by relatively short range correlation and near isotropic conditions reflecting the dominant role of the subround pumice fragments.

This empirical evidence relating the permeability statistics to the physical attributes of the rock sample has important implications for the simulation of permeability distributions corresponding to heterogeneous geologic formations. Specifically, the visual qualities of the medium provide important qualitative and semi-quantitative information on which to condition the models. Although the physical appearance of the porous media can aid in conditioning the models, it cannot be used as a substitute for good quantitative data. Good data is particularly critical in the case of permeability, as the measured permeability depends not only on the characteristics of the porous medium but on the characteristics of its measurement as well.

Empirical Evidence of Permeability Upscaling

The experiments presented here yield clear empirical evidence of permeability upscaling. By upscaling we mean distinct and consistent trends in key summary statistics corresponding to an increase in the scale of measurement. These results are particularly compelling given the exhaustive quantity of data and the controlled manner with which the data were measured. Even more compelling is the ubiquitous nature of the upscaling. Regardless of the statistic or rock type, upscaling was measured. Although the sampled rocks exhibit considerable differences there is a degree of consistency in the manner with which the permeability upscales. Consider the two-dimensional permeability maps. Distinct

smoothing of the permeability field is evident with increasing tip seal size, while the large-scale structural features remain essentially unchanged. That is, features that are small relative to the size of the tip seal are filtered from the permeability field while features larger than the tip seal remain largely unaffected. Similar trends are noted in the structure of the calculated semivariograms. Where the tip seal size becomes large with respect to a feature, that feature is filtered from the semivariogram, while the structure of the semivariogram at scales larger than the tip seal remains essentially unaffected. Other examples of this consistency in upscaling include the semivariogram range which always increases as a linear function of the inner tip seal radius, and the sample variance that always decreases according to a power-law relation.

The nature and consistency of the qualitative upscaling trends noted above come as no real surprise. In fact, each of these trends are qualitatively consistent with one of the simplest models of upscaling, that being volume averaging (e.g., semivariogram regularization). Also of no surprise is the fact that the permeability does not upscale according to a simple linear volume averaging process. This is clearly demonstrated by the increasing/decreasing trends in the mean permeabilities with increasing sample support. Although the non-linear volume averaging behavior characterizing the upscaling comes as no surprise, the origin of the nonlinearity is not so obvious (see below).

Permeability Upscaling is Influenced by Attributes of the Rock Sample

Comparisons drawn between the data measured on the four rock samples suggest that the physical attributes of the porous medium do indeed influence the measured permeability upscaling. Although there is considerable consistency in the manner with which the permeability upscales (as noted above), distinct differences are also evident. These differences are primarily manifest in the rate at which a statistic upscales and in the absolute change in the value of the statistic. However, the most obvious differences are

noted in the upscaling of the mean permeability. Specifically, both sandstone samples are characterized by a mean that increases with increasing sample support, while both volcanic tuffs exhibit a decreasing trend in the mean. As the only variable in the experiments was the test medium, any difference in upscaling must be the result of differences in the rock samples. Furthermore, we find the most distinct differences in upscaling between rocks of differing genetic origin (i.e., sandstones vs. tuffs), while rocks of similar genetic origin (e.g., sandstones) exhibit the greatest degree of consistency in upscaling.

By exploring differences in the behavior of the sample means, we can gain insight into the key porous media controls on the measured upscaling. The Tiva Canyon Tuff upscales according to a geometric averaging process, which is expected given the poor to non-existent spatial correlation characterizing its permeability distribution. The decreasing trend in the mean upscaling for the Topopah Spring Tuff occurs because the pumice fragments, which are larger and more numerous than found in the Tiva Canyon Tuff, are spatially disconnected. Thus, as the tip seal size increases fewer pumice fragments span the tip seal forcing more gas through the rock matrix. This causes a reduction in the positive skew of the permeability distribution, and thus a shift in the mean permeability toward that of the rock matrix. The stratified structure of the sandstone samples gives rise to well-connected zones of relatively high permeability. These "high permeability" features span the full width of the sampled block face. For this reason, the mean permeability remains high, governed by the "high-permeability" pathways which span all tip seals. Thus, the key physical feature controlling the behavior in the mean upscaling appears to be the connectedness of the "high-permeability" fraction and its range of correlation relative to the widths of the tip seals.

Other Controls on Permeability Upscaling Explored

Although a qualitative explanation of the differences in the measured permeability upscaling can be made on the basis of the physical characteristics of the rock samples, a full quantitative description of upscaling is subject to additional controls. In an effort to identify these controls, we compared observed trends in the mean permeability to those predicted by a variety of published theoretical models. The selected models differed according to their assumptions concerning the permeability distribution, spatial structure, and the uniformity of the imposed flow field. Discrepancies between the data and models were used to identify important processes and attributes of the experiments contributing to the measured upscaling. In each case, the non-uniform flow imposed by the minipermeameter coupled with local-scale (i.e., smallest sample support for which data are available) anisotropy in the permeability were the primary factors influencing the measured mean upscaling. Where applied, the non-uniform flow theories did not predict the measured mean upscaling largely because of their treatment of the local-scale permeability. These models, as well as most effective media theories, assume the local-scale permeability is isotropic and independent of the mode of measurement. These are inappropriate assumptions for our tests.

8.2. Recommendations

The studies presented here provide important physical evidence of permeability upscaling and elucidate key controls on upscaling that are not well supported in current theoretical models. However, if these studies only have application over the narrow range of scales investigated here they are of limited value in understanding and quantifying permeability upscaling under conditions relevant to "real world" problems, which in many cases involve scales exceeding hundreds or even thousands of meters.

We strongly believe that permeability upscaling is not intrinsically tied to any particular (absolute) scale, but to the structure of the heterogeneity and to the measurement instrument. That is, permeability upscaling depends on the relative scales of heterogeneity and the flow field, but not on the absolute scale. As the relative scales of heterogeneity and flow vary, the importance of competing processes may change. In a particular aquifer or reservoir absolute scales become important only because the structure of heterogeneity, or the characteristics of the instrument, changes with scale, not because of any intrinsic aspect of the scale itself. Nevertheless, the relevance of the laboratory-scale studies to larger-scale problems needs to be demonstrated. We suggest a four-fold approach:

- Extend selected theoretical upscaling models to the flow geometry of the minipermeameter. Existing stochastic Gaussian models, developed for other flow fields (mostly mean uniform flows, but some radial flows), suggest that the absolute scale of permeability variability is unimportant, only the relative scale. Self-similar fractal models also suggest that permeability studies at one scale can be applied at another. By extending such models to the specialized case of the MSP one can evaluate whether this flow geometry will render the expected (idealized) upscaling behavior dependent on the absolute scale of measurement.

- Employ linear filter theory to empirically and theoretically investigate the relationship between the MSP measurement and the absolute scales of heterogeneity characterizing each rock sample. Extend the current two-dimensional analyses to three-dimensions with the aid of numerical simulation.

- Conduct high resolution three-dimensional numerical simulations of flow through synthetic heterogeneous porous materials that mimic the MSP measurements. In this way one can "numerically experiment" to find qualitative matches with the behavior observed in the minipermeameter measurements (perhaps using formal inverse

procedures). Once accomplished the absolute scales of the problem can be varied to examine their effect on upscaling.

- The most direct approach involves conducting a limited number of controlled upscaling experiments at scales spanning hundreds to thousands of meters. The goal would be to run tests with equivalent "relative scales" to that conducted in the laboratory and look for similarities in response and controls on the upscaling. Such efforts could also be supplemented with existing field-scale data sets published in the literature.

Assuming that relevancy can be confirmed additional laboratory experiments and analyses of the data are justified. The primary purpose would be to further interpret the measured upscaling behavior, develop quantitative models for describing the measured upscaling, and to generalize the results to other instruments and other porous media types. These goals can be achieved by: 1) mining the existing data sets, 2) further theoretical analysis, and 3) additional experimentation.

The upscaling studies conducted on the four different rock samples form a very rich data set. The analyses presented here only begins the process of tapping this extensive resource. Below we list a few additional analyses that should be performed on the existing data sets:

- Quantitatively characterize the pore-scale features of the different rock samples using thin-section analysis. Such analyses would yield information on pore-size distribution, spatial connectedness of the pores, and the presence and distribution of cementing agents in the pore bodies and throats. By comparing these characteristics with the measured permeability, additional insight into the physical controls on the

permeability will be achieved. This work is currently being performed for the Massillon Sandstone sample.

- Compare the permeability statistics measured on different faces of the same block of rock. Relate differences in the statistics to variations in the depositional environment (e.g., direction of flow).
- Compare permeability upscaling measured on different faces of the same block of rock. Interpret differences based on orientation of MSP gas flow relative to the local anisotropy of the rock sample.
- Investigate the statistical dependence/independence of the permeability distributions measured on opposing block faces.
- Characterize the permeability measured on the four rock samples with other statistical measures. Fractals, wavelets, indicator functions are but a few of the potential descriptors. Also, investigate the upscaling of these statistical measures.
- Draw comparisons between theoretical upscaling models and the measured data using statistical measures other than the sample mean. One relatively simple example involves comparing the sample semivariogram (including the sample variance) with semivariogram regularization theory [e.g., Journel and Huijbrets, 1978; Clark, 1977]. Such models should first be modified to incorporate the effects of non-uniform weighting of the sample volume.

Analysis of the measured data suggests the importance of local-scale heterogeneity and non-uniform flow on permeability upscaling; however, there is no existing theory to test our interpretations. Here, we present some ideas on how to use our existing data to address these issues. Note that these tests largely overlap with the modeling exercises proposed for investigating the relevance of the laboratory-scale data.

- The first step would be to develop analytical and/or numerical models for MSP imposed flow in stochastic three-dimensional heterogeneous domains. Verification of

the models would then be approached through comparison with the measured MSP data.

- Employ the developed models to investigate the effects of local-scale heterogeneity and non-uniform flow on permeability upscaling for a broad range of conditions (beyond that possible with physical experimentation). Also, compare results for other flow geometries including radial and uniform flows.
- These models could also be used to develop theoretical spatial weighting functions for homogeneous and heterogeneous domains. These three-dimensional models could then be used to interpret and quantify the two-dimensional empirical spatial weighting functions calculated from the MSP data. Once verified with the MSP data, this general modeling approach could be extended to develop weighting functions for other important hydraulic testing instruments (e.g., slug and pump tests).
- With the aid of the quantitative weighting functions calculated from the MSP data measured on the different rock samples, investigate the effect of media heterogeneity/anisotropy on the shape and effective radius of the measurement.

Although the current data set is quite large, it is still limited in a number of ways. Below we suggest additional experiments that would greatly broaden the scope of the existing data.

- Data are limited to two rock types, sandstones and tuffs. Similar experiments need to be conducted on other rocks from other environments (e.g., carbonates, eolian deposits, intrusive volcanics, mud/siltstones).
- Data are limited to a single flow geometry (spherical). To address this issue resampling of the existing rock samples could be performed with a different instrument. One could take a series of core samples from the rock block and measure their permeability using a Hassler Sleeve permeameter. These could then be compared to a single large permeability measurement made on the entire rock (prior to coring)

by sealing the sides of the rock and passing air through the rock under a constant gradient. One could also measure the permeability in the core holes left in the rock block. In this way, permeability measurements under uniform, radial, and spherical flow conditions could be made and compared.

- Data are limited to a single parameter, permeability. Using the rocks samples that have been characterized for permeability upscaling, investigate the upscaling behavior for another parameter like porosity or relative permeability. One can measure the porosity with the air minipermeameter by making a step change in the applied pressure and observing the response. It may be possible to investigate the relative permeability by carefully wetting the rock and then make measurements with the MSP using sequentially increasing gas pressures.